SYNTHESIS, CHARACTERIZATION AND PROPERTIES OF NOVEL POLYOLEFINS BY SINGLE-SITE CATALYSTS

By

ZHIBIN YE, B. ENG, M. ENG

A Thesis

Submitted to the School of Graduate Studies

in Partial Fulfillment of the Requirements

for the Degree

Doctor of Philosophy

McMaster University

Hamilton, Ontario, Canada

SYNTHESIS, CHARACTERIZATION AND PROPERTIES OF NOVEL POLYOLEFINS BY SINGLE-SITE CATALYSTS

By

ZHIBIN YE

B.ENG, M. ENG

Doctor of Philosophy (2004) McMaster University

(Chemical Engineering) Hamilton, Ontario

TITLE: Synthesis, Characterization and Properties of Novel Polyolefins by Single-Site Catalysts

AUTHOR: Zhibin Ye
B. Eng., M. Eng.
(Zhejiang University, China)
SUPERVISOR: Professor Shiping Zhu

NUMBER OF PAGES: xxvii, 238.

ABSTRACT

Developments in single-site catalysts for olefin polymerization have offered unprecedented freedom in designing new polyolefins, controlling polyolefin structure, and tailoring materials properties. The main theme of this sandwich-style thesis is the synthesis, characterization, and properties of a novel series of polyolefin materials that have unique chain structures and superior materials properties. These polyolefin materials were respectively prepared with a variety of recently developed single-site catalysts.

High-strength polyethylene fibers were *in situ* synthesized via nano-extrusion polymerization of ethylene with a mesoporous particle (MCM-41) supported titanocene catalyst, Cp_2TiCl_2. The unique nanotube structure prevented the conventional folding of growing polymer chains inside the nanotubes and thus led to the formation of polyethylene nanofibrils with unique extended chain crystalline structure. Further aggregation of nanofibrils resulted in macro-scaled polyethylene microfibers. The morphological properties of nascent PE fibrous materials were investigated extensively using ESEM, XRD, and DSC. Tensile mechanical analyses showed that the polyethylene microfibers produced in this nanofabrication process exhibited tensile strength comparable to those of polyethylene fibers fabricated through post-reactor processing methods.

A Ni/α-diimine catalyst, 1,4-bis(2,6-diisopropylphenyl) acenaphthene diimine nickel(II) dibromide, was supported on various mesoporous particles (MCM-41 and MSF) having different nanotube structures to produce short chain branched polyethylenes by ethylene polymerization. The effects of catalyst supporting methods and nanotube structure of the mesoporous particles on the catalyst impregnation were studied. In ethylene polymerization, some active sites of the supported catalysts showed reduced chain walking ability compared to the

homogeneous counterparts. The effects of nanotube structure of mesoporous particles on ethylene polymerization activity, polymer property, and polymer particle morphology were investigated.

A series of branched polyethylenes with various chain topologies were prepared with chain walking Pd- and Ni-diimine catalysts, [(ArN=C(Me)-C(Me)=NAr)Pd(CH_3)(NCMe)]SbF_6 and (ArN=C(An)-C(An)=NAr)$NiBr_2$/MMAO, respectively, under different reaction conditions. In addition to topological characterizations using GPC-VIS and ^{13}C NMR techniques, a rheological study was conducted to investigate their unique rheological behaviors. The high molecular weight polyethylenes prepared under low ethylene pressures (0.2 and 1 atm at 35 °C) with the Pd-diimine catalyst exhibited extremely low viscosity and typical Newtonian flow behavior, suggesting dendritic topological structures. Changing the polymer chain topology by varying reaction conditions and/or changing the catalyst metal center significantly affected polymer rheological properties. These novel dendritic polyethylenes have potential in such applications as lubricants, printing materials, and polymer processing additives.

A one-step polymerization process employing binary tandem catalyst systems, (η^5-$C_5H_4CMe_2C_6H_5$)$TiCl_3$/MMAO coupled with [(η^5-C_5Me_4)$SiMe_2$(^{t}BuN)]$TiCl_2$/MMAO or *rac*-Me_2Si(2-MeBenz[*e*]Ind)$_2ZrCl_2$/MMAO, was applied and investigated for an efficient production of ethylene-1-hexene copolymers with ethylene as the sole monomer. This strategy utilized a tandem action between the two single-site catalysts. During the polymerization, the trimerization catalyst, (η^5-$C_5H_4CMe_2C_6H_5$)$TiCl_3$/MMAO, trimerized ethylene to form 1-hexene, while the other metallocene catalyst component efficiently copolymerized the *in situ* produced 1-hexene with ethylene to form butyl branched polyethylenes. A simple adjustment of the molar ratio of catalyst components, catalyst combination, and reaction conditions effectively regulated

branching density in the copolymers. The branching structure of the copolymers was confirmed and characterized using ^{13}C NMR and DSC. This one-step process has clear advantages over the two-step procedure for linear low density polyethylene (LLDPE) production.

A binary catalyst system, consisting of a bisiminepyridine iron catalyst $[(2\text{-ArN=C(Me)})_2C_5H_3N]FeCl_2$ (Ar = 2,6-$C_6H_3(Me)_2$)/MMAO and a zirconocene catalyst *rac*-$Me_2Si(2\text{-MeBenz}[e]Ind)_2ZrCl_2$/MMAO, was developed to synthesize isotactic polypropylenes grafted with atactic side chains. The iron catalyst *in situ* generated 1-propenyl ended atactic polypropylene macromonomer, while the zirconium catalyst incorporated the macromonomer into the copolymer. The effects of reaction conditions, such as catalyst addition procedure and ratio of the two single-site catalysts on branching frequency were studied. Copolymer samples having branching densities up to 8.6 aPP side chains per 1000 iPP monomer units were obtained.

Novel long chain branched isotactic polypropylenes were produced by propylene copolymerization with a very small amount of non-conjugated diene, 1,7-octadiene or 1,9-decadiene, with a single-site metallocene catalyst, *rac*-$Me_2Si(2\text{-MeBenz}[e]Ind)_2ZrCl_2$/MMAO. By controlling the amount of dienes in the polymerization system, isotactic polypropylenes with different long chain branching densities were effectively produced. Rheological studies showed that the presence of long chain branching significantly enhanced polymer melt strength and improved polymer processibility. This in-reactor method is more effective and convenient than other post-reactor processes used for producing LCBed PP.

ACKNOWLEDGEMENT

I take this opportunity to express my sincere gratitude to those who helped me during my Ph.D. study at McMaster University.

First I would like to thank my supervisor, Professor Shiping Zhu, for his patient guidance, intelligent suggestion, stimulating encouragement, and generous support during my study. His innovative inspiration, commitment for success, and unyielding dedication to research will always stimulate me.

I thank my supervisory committee members, Professor John Vlachopoulos, Professor Daniel S.-C. Yang, and Professor James Dickson, for their constructive advice and remarks. I owe thanks to Professor Jerry Y. S. Lin (Univ. of Cincinnati) for his valuable contributions, suggestions, and help to this thesis.

I am grateful to my colleagues, Dr.Wen-Jun Wang, Leming Gu, Youqing Shen, Sam Zeng, Ed Kolodka, Fahad AlObaidi, and others, for their tremendous help during my study.

My appreciation also goes to Hatem Alsyouri (Univ. of Cincinnati), Paul Gatt, Julie Birch, Gord Slater, Lynn Falkiner, Kathy Showkenik, Justyna Derkach, Doug Keller, and Brian Sayer for their help.

Finally I would like to thank my wife, Tingting Jin, for her constant understanding and solid support for my study at McMaster.

PUBLICATIONS

This Ph.D. thesis is organized in a sandwich style based on the following publications (as of April 16, 2004):

1. Z. Ye, F. AlObaidi, S. Zhu, "Melt rheological properties of branched polyethylenes produced with Pd- and Ni- Diimine catalysts", *Macromolecular Chemistry and Physics*, **2004**, *205*, 897-906.

2. Z. Ye, F. AlObaidi, S. Zhu, "Synthesis and rheological properties of long chain branched isotactic polypropylenes produced by copolymerization of propylene with nonconjugated dienes", *Industrial & Engineering Chemistry Research*, in press.

3. Z. Ye, F. AlObaidi, S. Zhu, "A tandem catalytic system for synthesis of ethylene-1-hexene copolymers from ethylene stock", *Macromolecular Rapid Communication*, **2003**, *25*, 647-652.

4. Z. Ye, S. Zhu, W.-J. Wang, H. Alsyouri, and Y. S. Lin, "Morphological and mechanical properties of nascent polyethylene fibers via ethylene extrusion polymerization with MCM-41 supported metallocene catalyst", *Journal of Polymer Science, Part B, Polymer Physics,* **2003**, *41*, 2433-2443.

5. Z. Ye, W.-J. Wang, S. Zhu, "ESR study on reduction of constrained geometry catalyst systems", *Journal of Applied Polymer Science*, **2003**, *89*, 2474-2482.

6. Z. Ye, S. Zhu, "Newtonian flow behavior of high-molecular-weight hypebranched polyethylenes produced with a Pd-diimine catalyst and its dependence on chain topology", *Macromolecules*, **2003**, *36*, 2194-2197.

7. Z. Ye, S. Zhu, "Synthesis of branched polypropylene with isotactic backbone and atactic side chains by binary iron and zirconium single-site catalysts", *Journal of Polymer Science, Part A, Polymer Chemistry,* **2003**, *41*, 1152-1159.

8. Z. Ye, S. Zhu, H. Alsyouri, and Y. S. Lin, "Catalyst impregnation and ethylene polymerization with mesoporous particle supported Ni-diimine catalysts", *Polymer*, **2003**, *44*, 969-980.

TABLE OF CONTENTS

LIST OF FIGURES

Chapter 4 Page

Chapter 5 Page

Chapter 6 Page

Chapter 7 Page

Appendix Page

LIST OF SCHEMES

Chapter 6 Page

Appendix Page

LIST OF TABLES

NOMENCLATURE

Atm	Atmosphere (s)
CCD	Chemical Composition Distribution
CGC	Constrained Geometry Catalyst
Cp	Cyclopentadienyl
Cp*	Tetramethylcyclopentadienyl
DMA	Dynamic Mechanic Analyzer
DSC	Differential Scanning Calorimeter
DRI	Differential Refractive Index
E_a	Activation Energy (kJ/mol)
EPDM	Ethylene-Propylene-Diene
EPR	Ethylene-Propylene Rubber
ESEM	Environmental Scanning Electron Microscopy
ESR	Electron Spinning Resonance
G'	Storage Modulus (Pa)
G"	Loss Modulus (Pa)
GC	Gas Chromatography
GPC	Gel Permeation Chromatography
GPC-VIS	Gel Permeation Chromatography coupled with on-line Viscometer
HDPE	High Density Polyethylene
ICP-MS	Inductively Coupled Plasma- Mass Spectroscopy
LCB	Long Chain Branching
LCBD	Long Chain Branching Density
LDPE	Low Density Polyethylene
LLDPE	Linear Low Density Polyethylene
MAO	Methylaluminoxane
MCM	Mobile Composition of Matter

MMAO	Modified Methylaluminoxane
M_n	Number Average Molecular Weight
M_w	Weight Average Molecular Weight
MSF	Mesoporous Silica Fiber
MW	Molecular Weight
MWD	Molecular Weight Distribution
^{13}C NMR	Carbon-13 Neutron Magnetic Resonance
PDI	Polydispersity Index
PE	Polyethylene
PP	Polypropylene
SANS	Small Angle Neutron Scattering
SCB	Short Chain Branching
SEC	Size Exclusion Chromatography
SEM	Scanning Electron Microscopy
T_g	Glass Transitional Temperature
T_m	Melting temperature
TCB	1,2,4-trichlorobenzene
TMA	Trimethylaluminum
XRD	X-Ray Diffraction
Z-N	Ziegler-Natta

ω	Angular Frequency
η^*	Dynamic Complex Viscosity
η_0	Zero Shear Viscosity
λ	Relaxation Time in Cross Equation

Chapter 1

Introduction, Research Background and Objectives

1.1 Introduction to Polyolefins

Polyolefins, which include polyethylene (PE), polypropylene (PP), ethylene-propylene rubber (EPR) and etc, play very important roles in our industrial society. Since the year of 2000, the worldwide annual production of polyolefins has been in excess of 70 million tones and the production of polyethylene alone has been in excess of 47 million.[1] Table 1.1 shows the global consumption of PE, PP, and EPDM for 1995-2004. Despite the fact that polyolefins were one of the last types of polymers to be commercialized, they are the fastest growing segment of the polymer industry. In the year 2000 the polyolefin world market share constituted almost 65 % of the total thermoplastic market, whereas it was in fact only around 20 % in the 1960's.[2]

Table 1.1 Global Market for Polyolefins, 1994-2004 (1000 Tons).[1]

Type	1995	1996	1997	1998	1999	2004	1999-2004 (% Growth p.a.)
LDPE	13,892	14,430	14,785	15,416	15,992	19,115	3.6
LLDPE	8,359	9,044	9,662	10,162	10,758	13,795	5.1
HDPE	16,086	17,379	18,134	19,198	20,281	25,870	5.0
Sub-total PE	38,337	40,853	42,581	44,776	47,031	58,780	4.6
PP	19,263	20,699	21,745	23,355	25,035	35,725	7.4
EPDM	726	771	807	857	937	1,129	3.8
Total	58,326	62,323	65,133	68,988	73,003	95,634	5.5

As a general class, polyolefins are noted for their outstanding dielectric properties, chemical resistance to solvents, toughness, good barrier properties, and their relative adaptability to the various fabrication techniques used for processing plastics. Furthermore, these properties can be easily adjusted through tailoring molecular structure and incorporating additives.[3] Today polyolefins have been widely used in a large number of applications, ranging from simple plastic bags to high module high strength fibers.[4]

1.1.1 Polyethylenes

Polyethylenes are the world's largest commodity synthetic polymers. Traditionally, based on manufacturing process and polymer properties, commercial polyethylenes have been classified into three major groups: Low Density (LDPE), High Density (HDPE), and Linear Low Density (LLDPE).

LDPE has a density of between 0.910-0.935 g/ml. It was the first grade of thermoplastic polyethylene available commercially. LDPE is produced through high pressure (200 bar to 300 bar) high temperature (150 to 260 °C) radical processes. Owing to the free radical polymerization mechanism, LDPE is essentially a branched polymer with both short chain branches (SCB) generated by chain backbiting and long chain branches (LCB) generated by chain transfer to polymer, which give LDPE the distinctive combination of clarity, flexibility, impact resistance, and processibility.[1] LDPE has a market share about 30 % among all polyethylenes. LDPE is mainly used in film applications (~ 60 %).[5] It is widely used for making heavy-duty sacks, refuse bags, carrier bags, general packaging, and in building and construction industries.[6] The production of LDPE is expanding not as fast as that of LLDPE because the latter has better mechanical properties of LLDPE films and lower construction and operation costs.[1]

LLDPE has a density of between 0.910-0.925 g/ml. It is a copolymer of ethylene and a small amount of α-olefin, such as 1-butene, 1-hexene, and 1-octene. It is essentially a linear polymer grafted with a controlled amount of short chain branch (SCB). Both LLDPE and HDPE are produced by low pressure (20-30 bar) low temperature (80-120 ˚C) transitional metal catalyzed coordination polymerization processes. LLDPE is the type of polyethylene that attracts most attention in the research of single-site metallocene catalysts and new production technologies. This is because LLDPE offers the highest potential for manufacturing tailor-designed products that can be readily tuned to either mimic existing product grades or to produce completely new materials.[1] LLDPE is replacing LDPE in some film applications due to its higher impact strength, tensile strength, and extensibility, which yield films of lower gage but of the same mechanical performance. However, LLDPE also exhibits some undesirable properties, such as lower gloss, greater haze, and narrow heating sealing range.[6] LLDPE makes around 25 % of share in the polyethylene market and is mainly used for film applications (66 %).[5]

HDPE has a density of 0.940-0.965 g/ml and has been commercially available since the mid 1950's. HDPE is an ethylene homopolymer and it is linear in nature with no or very low levels of short chain branching.[1] Compared to LDPE and LLDPE, HDPE is far more crystalline and consequently has higher density and higher thermal stability. It also has increased tensile strength, stiffness, chemical resistance, and upper temperature range. However, HDPE has reduced low temperature impact strength, elongation, permeability, and resistance to stress cracking.[7] HDPE has a market share of 45 % among all the polyethylenes and it has the broadest envelope of processibility of all the various polyethylenes. HDPE is primarily used in blow molding of bottles and toys (35 %), injection molding of household goods (18 %), and film applications (19 %).[5]

1.1.2 Polypropylenes

Polypropylene is the world's second largest commodity synthetic polymer with a production volume only smaller than polyethylene. It has had the highest growth rate of all the commodity plastics over the past 30 years. World polypropylene consumption has grown from 1.2 million tons in 1970, to 25 million tons in 1999 and is predicted to grow to 36 million tons by 2004. The reasons for the rapid growth in polypropylene applications lie in the great versatility of polypropylene for injected, extruded, and fibrous products.[1]

Depending on the stereoregularity of the polymer chains, polypropylene can be classified into three categories: atactic (random distribution of methyl groups either side of chain), isotactic (all methyl groups lie on one side of the chain), and syndiotactic (methyl groups alternate regularly on both sides of the chain). All three categories of polypropylenes are produced by coordination polymerization processes.

Atactic polypropylene was the only form available before the development of stereospecific Ziegler-Natta catalysts. The material is amorphous and waxy; it is used as an additive or blended with other polymers.

Isotactic polypropylene is a relatively low cost material, especially on a volume basis because of its inherent low density, making it attractive for many packaging, transport, appliance, furniture, and textile applications. It has the lowest density of commercially available thermoplastics (0.905 g/ml).[3] The stiff chain backbone gives isotactic polypropylene a high melting temperature (about 165 °C) and tensile strength, but low impact strength. Propylene is also copolymerized with a very small amount of ethylene to produce random copolymers. The incorporation of 0.5-3 % ethylene into the polymer chain can

produce polymers with improved impact and optic properties, but with reduced melting temperature, crystallinity and tensile modulus.[1] Commercial isotactic polypropylene is also mixed with ethylene-propylene rubbers to prepare impact polypropylene grades.

Syndiotactic polypropylene was developed more recently. It is the development of metallocene catalysts that has enabled a commercially viable route to be devised for syndiotactic polypropylene and it is still at a relatively early stage of its development. Compared to isotactic polypropylene, syndiotactic polypropylene exhibits a lower melting point, lower stiffness, slower crystallization, improved clarity and impact properties. It is largely used as a competing material to clarified random copolymers. The primary focus for syndiotactic polypropylene will be in the packaging sector.[1]

1.2 Historical Developments of Polyolefin Production Technology

1.2.1 Free Radical Processes

Before the discovery of Ziegler-Natta catalysts, polyethylene was only produced with free-radical processes under severe polymerization conditions. The first high molecular weight resinous polyolefin, polyethylene, was discovered in UK by E.W.M Fawcett and R.O. Gibson in 1933 in the laboratories of Imperial Chemical Industries, Ltd. The original discovery was an accidental one – made in the course of an attempt to react ethylene with benzaldehyde in an autoclave. In 1937 a continuous laboratory process was devised and in 1939 full-scale commercial production started in England.[3]

The ICI process is a free radical high pressure process and it stands for the first type of process used for olefin polymerization. The polyethylene produced is essentially LDPE with both SCB and LCB. The polymer melts at about 112 °C and has a broad melting range. However, the free radical process can only be used for ethylene polymerization and is not capable of polymerizing propylene or higher olefins to corresponding high molecular weight polyolefins.[3]

1.2.2 Ziegler-Natta Catalysts

The discovery of Ziegler-Natta catalysts started a new era in polyolefin research and production. The catalysts were first discovered in the laboratories of K. Ziegler in 1953 to produce high density polyethylene under low ethylene pressures and further developed by G. Natta in 1954 to produce isotactic polypropylene. These original discoveries stimulated a worldwide research and development effort that culminated in many new commercial olefin plastics and elastomers, including high density polyethylene, linear low density polyethylene, isotactic polypropylene, isotactic poly-1-butene, isotactic poly-4-methyl-1-pentene, *trans*-1,4-polyisoprene, *cis*-1,4-polybutadiene, *cis*-1,4-polyisoprene, ethylene-propylene copolymers, and polypenteneamers. The Z-N polymerization has joined the ranks of conventional radical, cationic, anionic, condensation polymerizations as one of the major polymerization methods.[8]

In its broad definition, Z-N catalyst is a mixture composed of a transitional metal salt of metals of groups IV to VIII (catalyst) and a metal alkyl of base metal of group I to III (cocatalyst). However, not all of the possible combinations are effective. Many of these combinations are active only for certain monomers and/or under certain conditions. In industry, most Z-N catalysts are based on titanium salts and aluminum alkyls, such as $TiCl_4$ + $AlEt_3$. Z-N catalysts have been used in soluble or insoluble forms in reaction medium for olefin

polymerization. In commercial applications, most Z-N catalysts are used in insoluble/supported heterogeneous form.[8] Various polymerization processes, including solution, slurry, and gas phase, have been developed and applied in commercial production.[9]

Table 1.2 Performance of the different catalyst generations for PP production.[2]

Generation	Composition and structure	Prod.[a]	II[b] (wt%)	Technology control	Process requirements
1st (1957-1970)	$TiCl_3/AlEt_2Cl$	0.8-1.2	88-91	Irregular powder	Purification. Atactic removal
2nd (1970-1978)	$TiCl_3/AlEt_2Cl$/Lewis base	3-5	95	Irregular powder	Purification. Atactic removal
3rd (1978-1980)	$TiCl_4$/Ester/$MgCl_2$+ $AlEt_3$/Ester	5-15	98	Regular or irregular powder	No purification. No removal
4th Reactor Granule Technology (1980)	$TiCl_4$/Diester/$MgCl_2$+ $AlEt_3$/Silane three-dimensional catalyst granule architecture	20-60	99	Particle with regular shape and adjustable size and PSD. Designed distribution of different products inside each particle.	No purification. No atactic removal. No pelletization.
	$TiCl_4$/Diester/$MgCl_2$+ $AlEt_3$ three-dimensional catalyst granule architecture	50-120	99	Particle with regular shape and adjustable size and PSD. Designed distribution of different products inside each particle.	No purification. No atactic removal. No pelletization.

[a] Productivity in kg PP/g Catalyst.

[b] wt% insoluble polymer in boiling heptane, which correlates to the degree of stereoregularity.

Since their first introduction, Z-N catalysts have experienced several major evolutions with four generations recognized.[2] Table 1.2 illustrates the development of Z-N catalysts for polypropylene production. Each generation exhibits a considerable improvement in both catalyst productivity and stereochemical control. In 1953 Ziegler discovered that the binary mixture of metal alkyl with transitional metal salts, such as $AlEt_3$ + $TiCl_4$, had high activity for ethylene polymerization at moderate pressure and temperature, but could only produce mainly atactic, low molecular weight polypropylene. Natta discovered in 1954 that solid transitional metal halides in lower valence states, $TiCl_3$, could produce more isotactic polypropylene than Ziegler's formulation (1^{st} generation catalysts). It was later found that the addition of certain Lewis bases could increase both stereospecificity and productivity of propylene polymerization (2^{nd} generation catalysts). It was also recognized that productivity of the catalysts could be significantly improved by supporting them onto inorganic supports, such as $MgCl_2$ (3^{rd} generation catalysts). Due to the improved catalyst productivity and polymer isotacticity, the 3^{rd} generation catalysts precluded the need of removals of catalyst residue and atactic PP materials, which were usually required for the 1^{st} and 2^{nd} generation catalysts. Since 1980, developments in the catalyst technology have been targeted at further controlling polymer particle size and morphology to avoid the pelletization process, in addition to further improving catalyst productivity and stereospecificity.[2]

Polymers produced with Z-N catalysts invariably have a common property: a broad molecular weight distribution (MWD) and, in the case of copolymers, a broad chemical composition distribution (CCD). Z-N catalysts are usually multi-site type catalysts with transitional metal active sites of different oxidation states and in various ligand environments. Polymer chains produced at different sites have different average molecular weight, comonomer composition, and stereoregularity. Therefore, polymers produced with Z-N catalysts are

essentially mixtures of different polymer fractions with broad MWD and CCD. Although some conventional soluble Z-N catalysts can produce polymers with narrow MWD and CCD, these soluble catalysts usually have low activity and yield polymers with poor particle morphology and low stereoregularity in the case of isotactic polypropylene production. Hence, these soluble catalysts have been mainly studied for academic purpose and are not used on commercial production.[8]

1.2.3 Metallocene Catalysts

Since the 1980's, polyolefins have been in the epoch of metallocene catalysts. Metallocene catalysts are a new generation of Z-N catalysts that offer unprecedented control over polymer structure and property and are poised to revolutionize the polyolefin industry.[10]

Early in the 1950's metallocene catalysts, bis(cyclopentadienyl) titanium derivatives, had been used together with alkylaluminum for ethylene polymerization under mild conditions. These original metallocene catalyst systems, however, had low activities and stabilities for ethylene polymerization and produced only low molecular weight polymers. Moreover, they were inactive for propylene polymerization.[4] Until the late 1970's these metallocene catalyst systems had been mainly used for theoretical studies. The breakthrough came in the late 1970's when Kaminsky et al. noticed that the activity of metallocene/alkylaluminum catalysts could be significantly increased by adding a trace amount of water to the polymerization reactor.[4] This enhanced activity was attributed to the reaction between water and alkylaluminum to form alkylaluminoxane, which is an effective cocatalyst for metallocene catalysts. This discovery led to the development of an entirely new generation of soluble Z-N catalytic systems: the metallocene/aluminoxane catalysts. Since then, tremendous

interests and efforts in both academia and industry have been applied to investigate this novel generation of catalyst systems.[4]

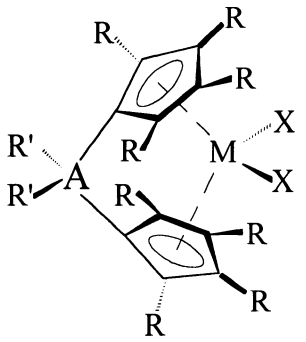

Scheme 1.1 Generic structure of metallocene catalysts.

Metallocene catalysts are soluble in their reaction medium. The typical chemical structure of a metallocene catalyst consists of a transition metal atom sandwiched between π-carbocyclic ligands such as cyclopentadienyl, fluorenyl, indenyl, or their substituted structures. It is schematically shown in Scheme 1.1 where M is a transition metal of Group IV, normally Zr, Ti, and Hf; A is an optional bridging group alkylene, alkyl radical, and hetero atoms usually Si or C atom; R and R' are ring substituents such as H, alkyl, or other hydrocarbon groups; and X is either chlorine, another halogen, or an alkyl group. By varying the ligand type, bridging ligands, ligand substituents and bridges to alter the steric and electronic surrounding of the active center, and transitional metal type, metallocene catalysts can be tailored to almost an unlimited number of site types to control polymerization behavior and structure and properties of polymers produced.[11]

Cocatalyst is the other important part of metallocene catalytic system. Alkylaluminoxane, especially methylaluminoxane (MAO), remains the most often used cocatalyst in metallocene polymerization. Despite its significant influence on catalytic performance, the exact roles of the aluminoxane component are not known. They are generally thought to act as alkylation agents that facilitate the formation of electron-deficient/coordinatively unsaturated "cationic" alkyl species. They also serve as impurity scavengers.[12] The exact structure of aluminoxane is still a matter of controversy. They are mixtures of different cyclic or linear oligomers with various degrees of oligomerizatin varying from 6 to 20. The structures of methylaluminoxane are shown in Scheme 1.2.[11] Recently some experimental studies have suggested that MAO can also have a three-dimensional open cage structure.[12]

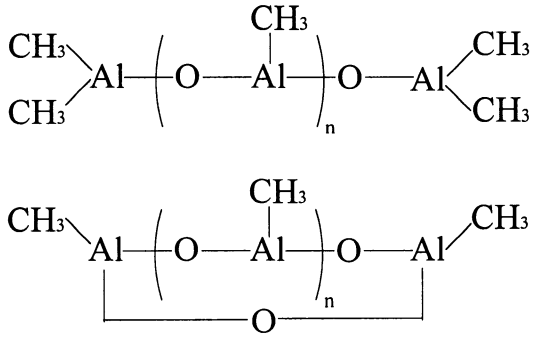

Scheme 1.2 Linear and cyclic structures proposed for MAO.[11]

One of the major disadvantages of metallocene catalyst is the high amount of MAO required to achieve sufficient activities, with aluminum/catalyst molar ratios of 1000 to 20000 commonly reported. Aluminoxanes are difficult to synthesize and to handle and are therefore extremely expensive.[12]

With the progress made in understanding the function of the cocatalyst, recently a new type of borate cocatalysts have been developed.[12] Borates with strong Lewis acidity, such as tris(pentafluorophenyl)borane and other borane compounds, have been used as cocatalysts for metallocene catalysts.[12] Compared to complicated and intractable species produced by MAO-activated metallocene systems, the reaction of Group 4 dialkyl metallocenes with stoichiometric amounts of perfluoroaryl boranes or borates can yield isolable and characterizable catalysts. Many studies, such as computational, synthetic, structural, and polymerization investigations, on the isolated complexes have provided much insight into the highly efficient catalytic systems, especially for ethylene and α-olefin copolymerizations.[12] Scheme 1.3 shows the structure of tris(pentafluorophenyl)borane cocatalyst.

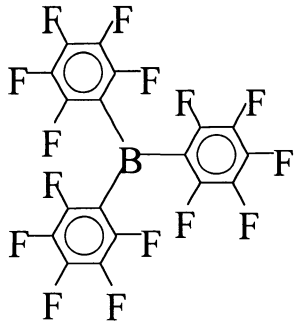

Scheme 1.3 Structure of the tris(pentafluorophenyl)borane cocatalyst.

Metallocene catalysts, which are considered as the 5th generation Z-N catalysts used for polyolefin production, revolutionized polyolefin industry.[2] The application of metallocene catalysts greatly expands the possibilities of olefin polymerization and the properties of resulting polyolefin materials. The main advantages of metallocene catalysts are that they offer extremely high

productivity and allow unprecedented control over polyolefin microstructure. The well-defined and controllable homogeneous catalysts can be hundreds times more active and have better comonomer incorporation ability than conventional Z-N catalysts. They allow the formation of unique single active site type compared to multi-site Z-N catalysts. They enable the production of polymers with narrow MWD and more uniform α-olefin comonomer distribution in polymer backbone, which gives LLDPE improved clarity, strength, and lower hexane-extractables. By designing metallocenes with different stereoselectivity, various stereospecific poly(α-olefin)s, such as isotactic, syndiotactic, hemitactic polypropylenes, can be efficiently synthesized. In addition, these catalysts provide new approaches for homo- and copolymerization of cyclic olefins, cyclopolymerization of dienes, and even functionalized polyolefins, which greatly expand the range and versatility of polyolefin materials. More uniquely, these homogeneous catalysts, owing to their homogeneous and open active site structure, can produce long chain branched (LCBed) polyolefins by copolymerizing olefins with *in situ* produced or externally added long chain α-olefin macromonomers.[4,10,11,13]

Owing to their unique feature, metallocene catalyst systems are now used commercially in the manufacture of several families of new and improved polymers for both specialty and commodity polyolefin markets. It is predicted that metallocene products will reach a market volume of around 6 million tons by 2004.[1]

1.2.4 Single-Site Late Transitional Metal Catalysts

Early transitional metal (Ti, Zr, V, and Cr) based Z-N and metallocene catalysts exhibit high oxophilicity, which causes them to be poisoned by most functionalized olefins, particularly commercially available polar comonomers. Due to this inefficiency, copolymers of functionalized olefins with ethylene are

still produced commercially by free-radical polymerizations. Compared to early metals, the lower oxophilicity and presumably greater functional-group tolerance of late transitional metals make them likely targets for the development of catalysts for the copolymerization of ethylene with polar monomers under mild conditions.[14] Stimulated by this initiative, research interests during the first half of the 1990s grew in developing a new generation of late transitional metal catalysts to explore their potential for olefin polymerization.[14-16]

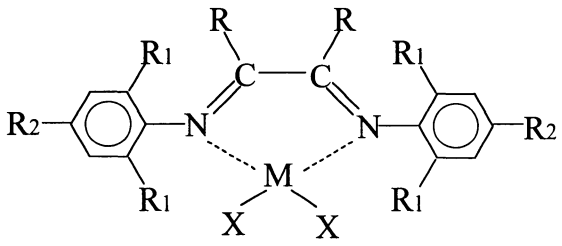

Scheme 1.4 Generic structure of Ni(II)/Pd(II) α-Diimine catalysts.

One very important breakthrough was the discovery of a family of highly active α-diimine based Ni(II) and Pd(II) catalysts by Brookhart and his group.[14,17] Scheme 1.4 shows the generic structure of these catalysts. This series of catalysts are also single-site type catalysts. When activated by cocatalysts, such as MAO and borate, these catalysts polymerize ethylene and α-olefins to high molecular weight polymers with activities comparable to those of metallocene catalyst systems. But dramatic differences in microstructure and polymer properties were observed between polymers made with the Ni/Pd-based catalysts and those made with conventional Z-N and metallocene technologies. Polyethylenes prepared with Ni(II)- or Pd(II)-based catalysts can vary from highly branched to linear, and their properties vary from viscous oil to soft elastomers to rigid plastics

accordingly. The polymer structure and properties greatly depend on reaction conditions, ligand structure, and the metal.[14,17,18]

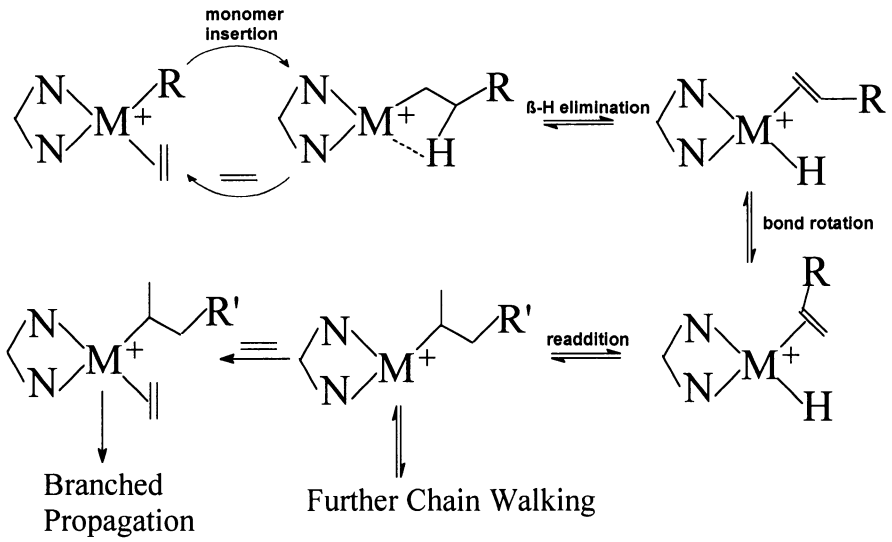

Scheme 1.5 Mechanism for ethylene polymerization and polymer branching formation with Ni/Pd α-Diimine complexes.

The unique feature of these catalysts is the chain walking mechanism. Different from the early metal Z-N and metallocene catalyst systems, the active growing site in the Ni and Pd α-diimine polymerization system isomerizes to internal position on polymer backbone during monomer propagation, so the next monomer unit can be assembled onto the backbone instead of the end. This chain isomerization is completed through β-H elimination followed by bond rotation and then re-addition of the resulted coordinated vinyl-ended chain to the metal hydride.[14] Scheme 1.5 shows the mechanism for the polymer branch formation. Instead of introducing branches by monomer structure, branching in this system is introduced by a catalyst that can uniquely control the position of the next monomer addition. This nonlinear fashion of chain propagation leads to the

formation of novel branched and hyperbranched polymers.[19] Changing polymerization conditions, ligand structure and metal type can adjust the competition between chain walking and monomer insertion processes to tailor polymer chain topology and branching density.[18,19]

Another unique feature of this series of catalysts is their unprecedented functional group tolerance. With cationic Pd-diimine catalysts, ethylene polymerization can be carried out in the presence of ethers, organic esters, and acids. Polymerizations have been even conducted in the presence of air and in the presence of an aqueous phase. Aqueous emulsion and suspension polymerization and polymerization in supercritical CO_2 with Pd-diimine catalysts have also been investigated. The tolerance to functional group extends to comonomer types that have polar moieties. Copolymerizations of ethylene and α-olefin with polar monomers such as acrylates with Pd-diimine catalysts can yield high molecular weight, random copolymers under mild conditions.[14]

Another representative series of late transitional metal catalysts are the pyridyl bis-imine based Co(II) and Fe(II) catalysts.[14-16] Scheme 1.6 shows the generic structure of this series of catalysts. When activated with MAO, this series of single-site catalysts show ethylene polymerization activity comparable or even higher than those found for Group IV metallocene catalysts under analogous conditions. The molecular weight of polyethylene materials strongly depends on the aryl substitution pattern, which affects chain transfer reactions. Aryl substituents with only one small *ortho* substituent give highly active ethylene oligomerization catalysts with exceptionally high selectivity for the production of α-olefins. Increasing the size of this substituent to *t*Bu, or placing substituents in both of the *ortho* positions, result in the formation of high molecular weight linear polyethylenes. In addition to β-H transfer, the chain termination mechanism of this series of catalysts also includes chain transfer to aluminum cocatalyst. By

controlling the amount of MAO or alkylaluminum in reaction system, polymers with bimodal MWD can be obtained.[14-16,20]

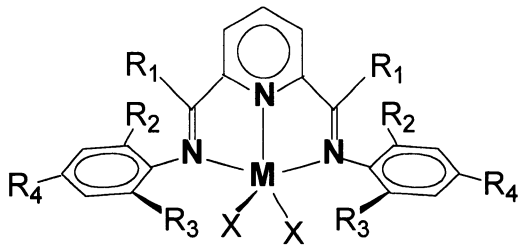

M = Fe, Co;
R_1 = H, Me;
R_2,R_3 = iPr, R_4 = H;
R_2,R_3 = Me, R_4 = H, Me;
R_2, R_4 = Me, R_3 = H.

Scheme 1.6 Generic structure of pyridyl bis-imine based Co(II) and Fe(II) catalysts.[15]

The late transitional metal catalysts are likely to provide fertile grounds for future development. The greater functional group tolerance of this series of single-site catalysts makes them very attractive and promising in commercial copolymerization of olefin with polar monomers. A relatively small amount of functionality incorporation in polyolefins can dramatically enhance adhesion and wetability properties of polymer materials; more heavily functionalized products offer the prospect of materials with totally new properties and performance parameters.[15]

1.3 Novel Polyolefins Design Using Single-Site Catalyst Technology

Although it has been more than half a century since the first commercialization of polyethylenes, polyolefins still remain highly technology-driven. Developing novel advanced polyolefin materials with unique and tailor-made properties for new applications is the major and constant topic in polyolefin

research.[14] The developments in homogeneous single-site catalysts have provided polymer scientists with unprecedented freedom in controlling polymer chain structure and tailoring polymer properties.[4] A wide range of novel polyolefins with advanced materials properties have been developed utilizing single-site catalyst technology.

1.3.1 Long Chain Branched Polyolefins

Polymers produced with single-site catalysts have comparatively narrow molecular weight distribution (theoretically polydispersity = 2). This narrow distribution leads to superior mechanical properties, but meanwhile worsens materials processibility because of the lack of shear thinning. Although polymers produced with Z-N catalysts have lower mechanical properties, they have excellent materials processibility, i.e. significant shear thinning, due to broad polymer MWD generated from multiple active sites. The processing pressure and subsequent capital and energy expenditures required to process metallocene polymers are therefore higher than those for Z-N polymers.

An ideal way to resolve the processing deficiency of metallocene polymers is to introduce long chain branches (LCB) to the narrowly distributed polymers. A long chain branch is defined as a branch whose length is comparable to or longer than a critical entanglement length (correspond to the critical entanglement molecular weight M_c). This critical entanglement molecular weight is polymer specific and for PE it is approximately 3800 g/mol. The influence of long chain branching on melt rheological properties of polymers can be tremendous. It can significantly increase polymer melt relaxation time, enhance polymer melt strength at low shear rate, and improve shear thinning behavior.[21,22]

LCB in LDPE is introduced by a chain transfer to polymer reaction. However, HDPE and LLDPE produced with Z-N catalysts are essentially linear. Metallocene catalysts, unlike heterogeneous Z-N catalysts, have been shown to produce polymers with long chain branching. Due to their homogeneous nature and open structure, single-site metallocene catalysts have unprecedented abilities to copolymerize *in situ* produced or externally added vinyl-ended macromonomers to form LCBed polymers. This unique feature, owing to its practical significance, has led to numerous investigations in both industry and academia.[23-47]

1.3.1.1 LCBed Polyethylenes

Metallocene catalyst systems have been shown to be able to produce LCBed polyethylenes by incorporating *in situ* generated polyethylene macromonomers. During ethylene polymerization, vinyl-ended polyethylenes can be *in situ* generated by chain termination processes through β-H elimination and chain transfer to monomer. Some of these in situ generated long chain macromonomers can be further incorporated during chain propagation processes. Scheme 1.7 shows the mechanism of *in situ* long chain branching.

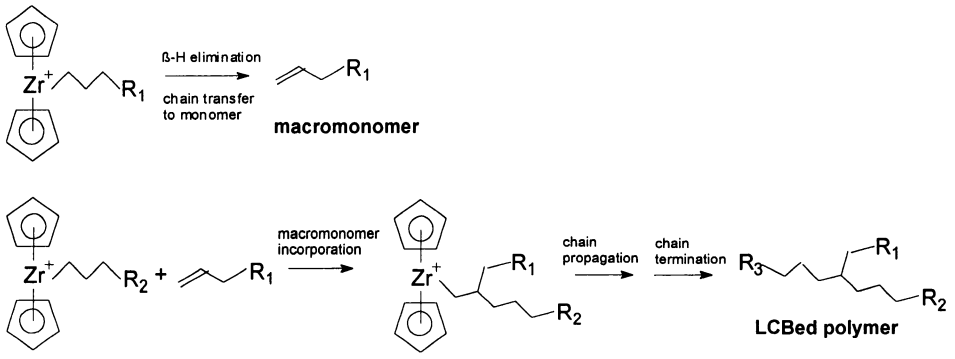

Scheme 1.7 Mechanism for *in situ* LCB formation.

The constrained geometry catalyst (CGC) systems, $[C_5Me_4(SiMe_2N^tBu)]TiMe_2/B(C_6F_5)_3$ or $[C_5Me_4(SiMe_2N^tBu)]TiCl_2/MAO$, developed by Dow and Exxon researchers, have been claimed to offer the best capability in producing LCBed polyethylenes due to their relatively open configuration compared to conventional metallocene catalysts.[23-27] The CGC incorporates small amounts of LCB (about 3.0 LCB/10,000 carbons) in polyethylene chains, which can significantly affect polymer rheological properties and improve polymer processibility.[28] Other metallocene systems, such as $Et[Ind]_2ZrCl_2/MAO$, *rac*-$Et[IndH_4]_2ZrCl_2/MAO$, and Cp_2ZrCl_2/MAO, have also been reported for the *in situ* production of LCBed polyethylenes in slurry processes.[33-35]

In addition to the above *in situ* processes, LCBed polyethylenes can also be produced through a two-step polymerization process. Soga et al. first produced oligoethylene with vinyl-end group using Cp_2ZrCl_2/MAO. Ethylene was then copolymerized with the oligoethylenes with $[C_5Me_4(SiMe_2N^tBu)]TiCl_2/MAO$ in the second step.[37] Shiono et al. synthesized LCBed polyethylenes by ethylene copolymerization with atactic polypropylene macromonomers, which were initially produced by propylene polymerization with $Cp^*_2ZrCl_2/MAO$ catalyst.[38] Kolodka et al. synthesized ethylene-propylene copolymers containing vinyl chain ends with $[C_5Me_4(SiMe_2N^tBu)]TiMe_2/B(C_6F_5)_3$ in a continuous solution process and subsequently the EP copolymers were copolymerized with ethylene to form LCBed polyethylenes again using $[C_5Me_4(SiMe_2N^tBu)]TiMe_2/B(C_6F_5)_3$.[39] Compared to the *in situ* process, the two-step process by externally adding initially synthesized macromonomers can produce polymers with more and controllable LCB.

LCBed polyethylenes have also been synthesized by ethylene copolymerization with non-conjugated α,ω-dienes. Diene monomers

copolymerize with ethylene or propylene and become pendant vinyl moieties that are further incorporated into growing chains to form H-type LCBed polymers. A very small amount of diene can introduce a significant level of LCBs.[40]

1.3.1.2 LCBed Polypropylenes

Isotactic polypropylene has excellent materials properties, including high melting point, high tensile strength, stiffness, and excellent chemical resistance.[48] However, in spite of their desirable properties, linear isotactic polypropylenes exhibit relatively low polymer melt strength, which limits their applications in some important processes, such as thermoforming, foaming, extrusion coating, and blow molding. In addition, the processibility is also an important issue for linear metallocene polypropylenes of narrow MWD. LCB has long been recognized as an ideal solution to improving PP melt strength and processibility while maintaining other desirable properties.

With metallocene technology LCBed isotactic polypropylenes have been produced. But different from ethylene polymerization, complicated chain insertion (including 1,2-insertion and 2,1-insertion) and chain termination (β-H elimination, β-CH_3 elimination, chain transfer to H_2 and aluminum) mechanisms in propylene polymerization can lead to polymers with various chain ends, while only the vinyl chain end is effective for LCB formation.[49] Therefore, it is quite difficult to find a catalyst system to *in situ* generate significant amounts of vinyl-ended polymers and further incorporate them. So far only one catalyst system, *rac*-Me_2Si(2-MeBenz[*e*]Ind)$_2ZrCl_2$ /MAO, has been reported to be able to *in situ* produce LCBed PP through propylene homopolymerization.[31] During the polymerization this catalyst produces vinyl-ended polypropylene macromonomer through 1,2-insertion pattern followed by chain termination through β-CH_3 elimination.[31]

Several two-step processes have been reported for the synthesis of LCBed PP. Shiono et al. reported the synthesis of isotactic polypropylene grafted with atactic polypropylene side chains by the copolymerization of propylene and atactic polypropylene macromonomer which was previously synthesized with $Cp^*_2ZrCl_2$/MAO catalyst system.[29] Weng et al. explored the copolymerization of propylene with isotactic polypropylene and polyethylene macromonomers prepared in a previous reactor.[30] Recently, Kolodka et al. reported the use of poly(ethylene-co-propylene) macromonomers with tailored molecular weight for the copolymerization.[36]

1.3.2 Production of LLDPE by Ethylene Homopolymerization

LLDPE is conventionally produced by ethylene copolymerization with α-olefin comonomers, such as 1-butene, 1-hexene, and 1-octene, with classical Ziegler-Natta catalysts and/or recently developed single-site type catalysts. This conventional route is a two-stage operation, i.e., ethylene oligomerization to produce α-olefin followed by ethylene copolymerization with the α-olefin comonomer. Recently there has been a significant amount of interest in producing LLDPE with ethylene as the sole monomer stock via the utilization of tandem catalytic systems.[50] This novel approach employs the tandem action between two different catalysts: one catalyst oligomerizes ethylene into 1-alkene, while the other catalyst simultaneously copolymerizes the *in situ* generated 1-alkene with ethylene to produce LLDPE. Through selecting a suitable oligomerization catalyst and adjusting its concentration, LLDPEs with different branch lengths and densities can be effectively produced.[50] Compared to the conventional copolymerization approach, this tandem catalytic approach shows its advantage in using ethylene as the only monomer, which avoids the use of comonomers in LLDPE production.

Some tandem catalytic systems using heterogeneous Z-N and Chromium catalysts have been reported earlier in the literature.[51] Recently several different homogeneous tandem catalytic systems consisting of single-site ethylene polymerization and oligomerization catalysts were introduced for the production of branched PEs.[52,53] Bazan et al. [52a] demonstrated the synthesis of butene-ethylene and hexene-butene-ethylene copolymers by the use of a binary tandem system composed of $\{[(\eta^5\text{-}C_5Me_4)SiMe_2(^tBuN)]TiMe\}\{MeB(C_6F_5)_3\}/[(C_6H_5)_2PC_6H_4C(OB(C_6F_5)_3)O\text{-}\kappa^2P,O]Ni(\eta^3\text{-}CH_2CMeCH_2)$, in which the single site Ni catalyst produced 1-butene and 1-hexene by ethylene dimerization and trimerization, while the Ti catalyst copolymerized ethylene with *in situ* produced 1-butene and/or 1-hexene. Other systems producing branched polyethylenes with various branch lengths were also reported. Bazan et al. reported the production of branched polyethylenes with tandem catalyst combinations such as $(C_5H_5BOEt)_2ZrCl_2$/MAO with $[(\eta^5\text{-}C_5Me_4)SiMe_2(^tBuN)]TiCl_2$/MAO, and $[(2\text{-}ArN{=}C(Me))_2C_5H_3N]FeCl_2$/MAO coupled with either $Me_2SiInd_2ZrCl_2$/MAO or $EtInd_2ZrCl_2$/MAO.[52b,52c] In more recent work,[52d] they reported a triple tandem catalyst system, comprising of $\{[(\eta^5\text{-}C_5Me_4)SiMe_2(^tBuN)]TiMe\}\{MeB(C_6F_5)_3\}$, $[(C_6H_5)_2PC_6H_4C(OB(C_6F_5)_3)O\text{-}\kappa^2P,O]Ni(\eta^3\text{-}CH_2C_6H_5)$, and $\{(H_3C)C[N(C_6H_5)]\text{-}C[O\text{-}B(C_6F_5)_3][N(C_6H_5)]\text{-}\kappa^2N,N\}Ni(\eta^3\text{-}CH_2C_6H_5)$. Dupont researchers [54] have also reported in several patents the production of branched PE with binary systems consisting of the tridentate bisiminepyridine iron and metallocene catalysts.

1.3.3 Polyethylenes with Controlled Chain Topology

In addition to the SCB, LCB, and chain stereoregularity, the topology of polymers is another important molecular parameter determining the physical properties and applications of polymer materials.[55] Control of polymer chain topology and architecture is currently an important theme in polymer science with

a target to prepare polymer materials with novel properties. In the past two decades, many new concepts and unique synthetic strategies have been developed to prepare polymers with various chain topology and architectures, such as dendrimers,[56] hyperbranched,[57] and supramolecular polymers.[58] In spite of the beauty and success of these approaches, most of them involve sophisticated but complicated multi-step organic syntheses and are only limited to specially designed monomers to suit each synthesis step.[59] It has not been possible to prepare polyethylenes with different chain topologies from a simple and inexpensive monomer such as ethylene, using these approaches.

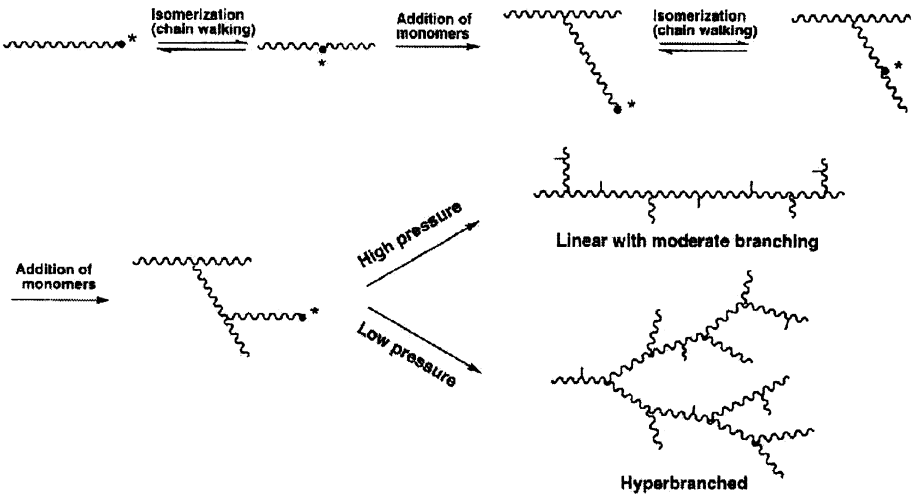

Scheme 1.8 Chain topology control with chain walking catalysts in ethylene polymerization.[19]

The advent of the unique chain-walking catalysts, Pd α-diimine catalysts, has led to for the first time the successful preparation of polyethylenes with various chain topologies.[19] By taking advantage of the chain walking mechanism and by regulating the competition between elementary chain walking and chain

propagation steps, polyethylenes with chain topologies ranging from dendritic to linear structures can be effectively prepared through ethylene polymerization. At polymerization conditions that favor insertion more than chain walking, such as high ethylene pressures and/or low reaction temperatures, the catalyst cannot walk too far after each insertion, therefore, PE with a relatively linear topology will be formed. On the other hand, if chain walking is very competitive, for instances, at low pressure and/or high temperature, the catalyst will walk extensively on polymer chain after each insertion, which will result in a hyperbranched or dendritic polymers.[19,59] Scheme 1.8 shows the mechanism for the control of polymer chain topology.[19]

The topological difference among polymers synthesized at different conditions has been verified by polymer characterizations utilizing size exclusion chromatography (SEC) coupled with multi-angle laser light scattering (MALLS) and small angle neutron scattering (SANS).[19,59,60] It has been shown that polymers synthesized at pressures low enough (e.g., 0.1 atm at 35 °C for catalyst [(ArN=C(Me)-C(Me)=NAr)Pd(CH_2)$_3$C(O)OMe]BAF (Ar = 2, 6-(iPr)$_2$$C_6H_3$)) exhibit a topology similar to that of dendritic polymers.[59,60]

1.3.4 Polyethylenes with Controlled Crystal Structure — Novel PE Fiber from Ethylene Extrusion Polymerization

With the homogeneous single-site catalysts described above, sophisticated controls over polymer structures and architectures, such as molecular weight and distribution, comonomer sequence and distribution, steroregularity, long chain branching, and chain topology can be finally realized to tailor the physical properties of polymer materials. However, for polymers to be used as commodity materials, polymer chain orientation (crystal structure), or polymer particle morphology, or both, must also be controlled.[61]

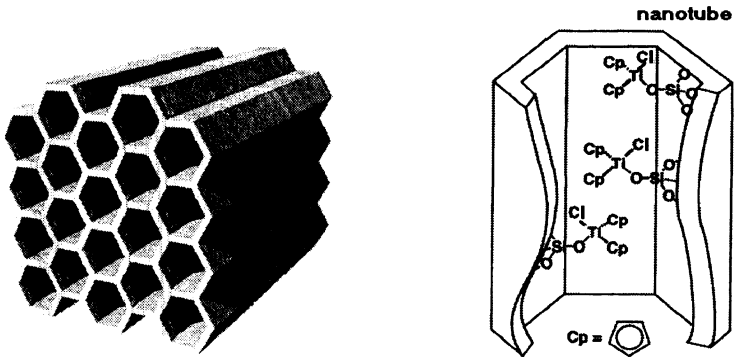

(a) (b)

Scheme 1.9 Schematic representation of the structure of (a) mesoporous particles and (b) nanotubes coated with Cp_2TiCl_2 catalyst.

With the application of spherical fourth generation Z-N catalysts or metallocene catalysts supported on spherical silica, excellent polymer particle morphology control can be conveniently achieved by the reactor granule technology, brought to perfection in Himont's *Spheripol* process in Italy.[62] However, control over the crystal structure of polyolefin is not an easy task. Expensive polymer post-processing steps, such as extrusion or gel spinning, are usually required to fabricate ultrahigh strength polyethylene fibers, which posses extended chain crystalline structure.[63] These additional expensive post-processing steps make the ultra-strength polyethylene much more expensive than commodity HDPE.

Recently, Aida et al. demonstrated a new concept, ethylene extrusion polymerization, for *in situ* production of polyethylene fibers with extended chain crystalline structure directly from polymerization reactor.[61] They supported a titanocene catalyst, Cp_2TiCl_2, onto nanotubes of mesoporous silica particles (such as mesoporous silica fiber (MSF) and MCM-41), which have honeycomb-shaped

nanotube (nanotube diamter ~ 2 nm) structures (see Scheme 1.9). The mesoporous particle supported metallocene catalyst was then used for ethylene polymerization. During the polymerization, polyethylene chains are formed inside the nanotubes. These nascent polymer chains cannot fold within the narrow reaction channels and therefore grow out of the porous framework before they assemble to form extended-chain crystalline fibers (see Scheme 1.10).[61] By using the regularly arranged nanoscale one-dimensional polymerization reactors, the oriented growth of polyethylene macromolecules that normally require post-processing steps can be therefore achieved *in situ*.

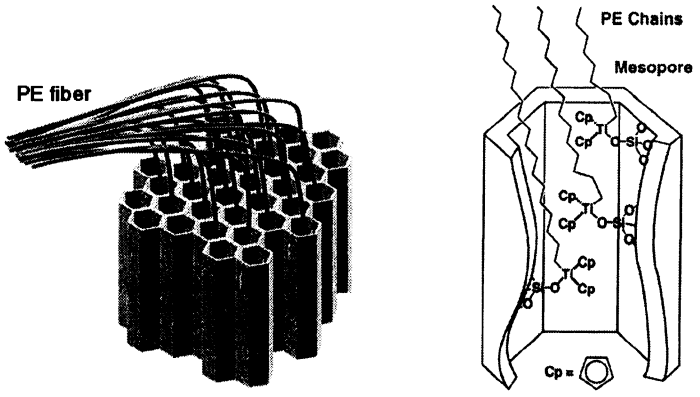

Scheme 1.10 Conceptual scheme for the ethylene extrusion polymerization.[61]

This nanofabrication technique demonstrates that conceptually new engineering materials with controlled crystal structure can result from combining the rational design of organometallic catalysts with nanotechnology.[62]

1.4 Thesis Research Objectives and Outlines

Following the vast developments in polyolefin areas and utilizing the newly-discovered single-site catalyst systems, the overall objectives of this thesis research are: (1) to design and synthesize new polyolefin materials; (2) to develop new processes for olefin polymerizations; and (3) to characterize the new polyolefin macromolecular structures and establish their relationships with materials properties.

In Chapter 2, the nanofabrication technique, ethylene extrusion polymerization, was applied for production of high strength polyethylene fibers. The hierarchical morphological properties and crystal structures of this series of fibers were identified using ESEM, XRD, and DSC techniques. Tensile mechanical properties of the fibers were determined and compared with fibers prepared by post-processing procedures.

In Chapter 3, mesoporous particles with different internal nanotube structures were applied to support a Ni α-diimine catalyst for ethylene polymerization. The effects of catalyst supporting methods and nanotube structures on catalyst impregnation were investigated. The polymerization activity, polymer properties, and polymer particle morphology were investigated to understand the effects of mesoporous particle supports on catalysts.

In Chapter 4, tandem catalytic systems were developed for synthesis of ethylene-1-hexene copolymers directly with ethylene as the only monomer. The effectiveness of this approach and the properties of produced copolymers were evaluated.

In Chapter 5, unique rheological properties of a new series of branched polyethylenes prepared with Ni and Pd α-diimine catalysts were examined in detail. Studies were aimed at finding correlations between chain topology and

rheological properties and also verifying or elucidating polymer topologies from the means of rheology.

In Chapter 6, a new series of branched isotactic polypropylenes were prepared using combinations of bisiminepyridine iron and zirconocene catalysts. The branched polymers have isotactic polypropylene backbones grafted with atactic polypropylene side chains. It is expected that the presence of soft side segments on rigid backbone can improve the materials impact strength.

In Chapter 7, novel long chain branched isotactic polypropylenes were synthesized by propylene copolymerization with a small amount of non-conjugated diene. The molecular structure of produced polymers was investigated using ^{13}C NMR, DSC, and GPC. A detailed study on rheological properties of LCBed polymers was carried out using small amplitude dynamic oscillation.

In Appendix, an on-line electron spinning resonance (ESR) technique was applied to study the *in situ* reduction of constrained geometry catalyst systems. The effects of solvent, temperature, cocatalyst type, and cocatalyst to catalyst ratios on the reduction process were studied. It provides some useful information related to active centers and catalyst activation process.

1.5 Reference

1. IAL Consultants *Advanced Polyolefins – The Competitive Position*, London, Feb. 2000.
2. Galli, P.; Vecellio, G. *Prog. Polym. Sci.* **2001**, *26*, 1287.

3. Sittig, M. *Polyolefin Production Processes, Latest Developments*, Noyes Data Corporation, New Jersey, 1976.
4. Kaminsky, W. *Macromol. Chem. Phys.* **1996**, *197*, 3907.
5. Ross, J. F.; MacAdams, J. L. *Polymeric Materials Encyclopedia, Volume 8*, Ed. Salamone, J. C., CRC Press, 1996, pp 5953-5965.
6. Al-Sammerrai, D.; Al-Nidawy, N. K. *Handbook of Polymer Science and Technology, Volume 2: Performance Properties of Plastics and Elastomers*, Ed. Cheremisinoff, N. P., Marcel Dekker: New York, 1989, pp341-365.
7. Odian, G. Principles of Polymerization, John Wiley & Sons, Inc., New York, 1991.
8. Boor, J. *Ziegler-Natta Catalysts and Polymerization*, Academic Press, New York, 1979.
9. Choi, K.-Y.; Ray, W. H. *J. Macromol. Sci., Rev. Macromol. Chem. Phys.*, **1985**, *C25(1)*, 1.
10. Resconi, L.; Cavallo, L.; Fait, A.; Piemontesi, F. *Chem. Rev.* **2000**, *100*, 1253.
11. Hamielec, A. E.; Soares, J. B. P. *Prog. Polym. Sci.* **1996**, *21*, 651.
12. Chen, E. Y.-X.; Marks, T. J. *Chem. Rev.* **2000**, *100*, 3913.
13. Alt, H. G.; Köppl, A. *Chem. Rev.* **2000**, *100*, 1205.
14. Ittel, S. D.; Johnson, L. K.; Brookhart, M. *Chem. Rev.* **2000**, *100*, 1169.
15. Britovsek, G. J. P.; Gibson, V. C.; Wass, D. F. *Angew. Chem. Int. Ed.* **1999**, *38*, 428.
16. Gibson, V. C.; Spitzmesser, S. K. *Chem. Rev.* **2003**, *103*, 283.
17. Johnson, L. K.; Killian, C. M.; Brookhart, M. *J. Am. Chem. Soc.* **1995**, *117*, 6414.
18. Gates, D. P.; Svejda, S. A.; Onate, E.; Killian, C. M.; Johnson, L. K.; White, P. S.; Brookhart, M. *Macromolecules* **2000**, *33*, 2320.
19. Guan, Z.; Cotts, P. M.; McCord, E. F.; McLain, S. J. *Science* **1999**, *283*, 2059.

20. Small, B. L.; Brookhart, M.; Bennett, A. M. A. *J. Am. Chem. Soc.* **1998**, *120*, 4049.
21. Small, P. A. *Adv. Polym. Sci.* **1975**, *18*, 1.
22. Gahleitner, M. *Prog. Polym. Sci.* **2001**, *26*, 895.
23. Brant, P.; Canich, J. A. M.; Merrill, N. A. US Patent 5, 444,145, 1995.
24. Brant, P.; Canich, J. A. M. US Patent 5, 475,075, 1995.
25. Lai, S. Y.; Wilson, J. R.; Knight, G. W.; Stevens, J. C.; Chum, P. W. S. US Patent 5, 272, 236, 1993.
26. Chum, P. S.; Kruper, W. J.; Guest, M. J. *Adv. Mater.* **2000**, *12*, 1759.
27. Wang, W.-J.; Yan, D.; Zhu, S.; Hamielec, A. E. *Macromolecules* **1998**, *31*, 8677.
28. Yan, D.; Wang, W.-J.; Zhu, S. *Polymer* **1999**, *40*, 1737.
29. Shiono, T.; Azad, S. M.; Ikeda, T. Macromolecules 1999, *32*, 5723.
30. Weng, W.; Markel, E. J.; Dekmezian, A. H. *Macromol. Rapid Commun.* **2001**, *22*, 1488.
31. Weng, W.; Hu, W.; Dekmezian, A. H.; Ruff, C. J. *Macromolecules* **2002**, *35*, 3838.
32. Carella, J. M.; Gotro, J. T.; Graessley, W. W. *Macromolecules* **1986**, *19*, 659.
33. Malmberg, A.; Kokko, E.; Lehmus, P.; Lőfgren. B.; Seppälä, J. V. *Macromolecules* **1998**, *31*, 8448.
34. Malmberg, A.; Liimatta, J.; Lehtinen, A.; Lőfgren. B. *Macromolecules* **1999**, *32*, 6687.
35. Kolodka, E.; Wang, W.-J.; Charpentier, P. A.; Zhu, S.; Hamielec, A. E. *Polymer*, **2000**, *41*, 3985.
36. Kolokda, E.; Wang, W.-J.; Zhu, S.; Hamielec, A. E. *Macromolecules* **2002**, *35*, 10062.
37. Soga, K.; Uozumi, T.; Nakamura, S.; Toneri, T.; Teranishi, T.; Sano, T.; Arai, T. *Macromol. Chem. Phys.* **1996**, *197*, 4237.

38. Shiono, T.; Moriki, Y.; Ikeda, T. *Macromol. Chem. Phys.* **1997**, *198*, 3229.
39. Kolodka, E.; Zhu, S.; Hamielec, A. E. *Macromol. Rapid Commun.* **2003**, *24*, 311.
40. Kokko, E.; Pietikäinen, P.; Koivunen, J.; Seppälä, J. V. *J. Polym. Sci., Part A: Polym. Chem.* **2001**, *39*, 3805.
41. Wood-Adams, P.; Costeux, S. *Macromolecules* **2001**, *34*, 6281.
42. Wood-Adams, P. M.; Dealy, J. M. *Macromolecules* **2000**, *33*, 7481.
43. Shroff, R. N.; Mavridis, H. *Macromolecules* **2001**, *34*, 7362.
44. Garcia-Franco, C. A.; Srinivas, S.; Lohse, D. J.; Brant, P. *Macromolecules* **2001**, *34*, 3115.
45. Hadjichristidis, N.; Xenidou, M.; Iatrou, H.; Pitsikalis, M.; Poulos, Y.; Avgeropoulos, A.; Sioula, S.; Paraskeva, S.; Velis, G.; Lohse, D. J.; Schulz, D. N.; Fetters, L. J.; Wright, P. J.; Mendelson, R. A.; Garcia-Franco, C. A.; Sun, T.; Ruff, C. J. *Macromolecules* **2000**, *33*, 2424.
46. Villar, M. A.; Failla, M. D.; Quijada, R.; Mauler, R. S.; Vallés, E. M.; Galland, G. B.; Quinzani, L. M. *Polymer* **2001**, *42*, 9269.
47. Walter, P.; Trinkle, S.; Suhm, J.; Mäder, D.; Friedrich, C.; Műlhaupt, R. *Macromol. Chem. Phys.* **2000**, *201*, 604.
48. Moore, Jr., E. P.; Larson, G. A. In *Polypropylene Handbook*; Moore, Jr., E. P., Ed.; Hanser: Munich, 1996.
49. Weng, W.; Markel, E. J.; Dekmezian, A. H. *Macromol. Rapid Commun.* **2000**, *21*, 1103.
50. Komon, Z. J. A.; Bazan, G. C. *Macromol. Rapid Commun.* **2001**, *22*, 467.
51. (a) Beach, D. L.; Kissin, Y. V. *J. Polym. Sci., Polym. Chem. Ed.* **1984**, *22*, 3027. (b) Beach, D. L.; Kissin, Y. V. *J. Polym. Sci., Polym. Chem. Ed.* **1986**, *24*, 1069. (c) Pettijohn, T. M.; Reagan, W. K.; Martin, S. J. US Patent 531070, 1994. (d) Benham, E. A.; Smith, P. D.; McDaniel, M. P. *Polym. Eng. Sci.* **1988**, *28*, 1469. (e) Ostoja-Starzewski, A. K.-H.; Witte, J.; Bartl, H. Ger Patent 3228865, 1984.

52. (a) Komon, Z. J. A.; Bu, X.; Bazan, G. C. *J. Am. Chem. Soc.* **2000**, *122*, 1830. (b) Barnhart, R. W.; Bazan, G. C. *J. Am. Chem. Soc.* **1998**, *120*, 1082. (c) Quijada, R.; Rojas, R.; Bazan, G.; Komon, Z. J. A.; Mauler, R. S.; Galland, G. B. *Macromolecules* **2001**, *34*, 2411. (d) Komon, Z. J. A.; Diamond, G. M.; Leclerc, M. K.; Murphy, V.; Okazaki, M.; Bazan, G. C. *J. Am. Chem. Soc.* **2002**, *124*, 15280. (4e) Galland, G. B.; Quijada, R.; Rojas, R.; Bazan, G.; Komon, Z. J. A. *Macromolecules* **2002**, *35*, 339.

53. (a) Abramo, G. P.; Li, L.; Marks, T. J. *J. Am. Chem. Soc.* **2002**, *124*, 13966. (5b) Li, L.; Metz, M. V.; Li, H.; Chen, M.-C.; Marks, T. J.; Liable-Sands, L.; Rheingold, A. L. *J. Am. Chem. Soc.* **2002**, *124*, 12725.

54. (a) Bennett, A. M. A. US Patent Application 729305, 2000. (b) Bennett, A. M. A. US Patent Application 729286, 2000. (c) Bennett, A. M. A.; Coughlin, E. B.; Citron, J. D.; Wang, L. US Patent Application 945861, 2001.

55. Edgecombe, B. D.; Stein, J. A.; Frechet, J. M. J.; Xu, Z.; Kramer, E. J. *Macromolecules* **1998**, *31*, 1292.

56. Fischer, M.; Vőgtle, F. *Angew. Chem. Int. Ed.* **1999**, *38*, 884.

57. Hult, A.; Johansson, M.; Malmstrőm, E. *Adv. Polym. Sci.* **1999**, *143*, 1.

58. Brunsveld, L.; Folmer, B. J. B.; Meijer, E. W.; Sijbesma, R. P. *Chem. Rev.* **2001**, *101*, 4071.

59. Guan, Z. *Chem. Eur. J.* **2002**, *8*, 3087.

60. Cotts, P. M.; Guan, Z.; McCord, E.; McLain, S. *Macromolecules*, **2000**, *33*, 6945.

61. Kageyama, K.; Tamazawa, J.; Aida, T. *Science* **1999**, *285*, 2113.

62. Lehmus, P.; Rieger, B. *Science* **1999**, *285*, 2081.

63. Peacock, A. J. in *Handbook of Polyethylene: Structures, Properties, and Applications*, Marcel Dekker: New York, 2000.

Chapter 2

Synthesis and Characterization of Nascent Polyethylene Fibers Produced via Ethylene Extrusion Polymerization with MCM-41 Particle Supported Metallocene Catalyst

This chapter is organized based on the paper published in *Journal of Polymer Science, Part B, Polymer Physics*, **2003**, *41*, 2433-2443 by Z. Ye, S. Zhu, W.-J. Wang, H. Alsyouri, and Y. S. Lin.

2.1 Abstract

Polyethylene fibers were prepared using ethylene extrusion polymerization with MCM-41 supported titanocene catalyst. The unique morphological and mechanical properties of these nascent PE fibers were investigated in detail using ESEM, XRD, and tensile mechanical analyses. Three levels of hierarchical fibrous morphologies were identified in the fiber samples through an extensive scanning electron microscopy study. The extended chain crystalline structure featured PE nanofibrils with diameters about 60 nm are the major morphological units present in the fiber structure. The nanofibrils are parallel-packed into individual microfibers with diameters about 1 ~ 30 μm. The microfibers are further aggregated irregularly into fiber aggregates/bundles. XRD studies proved the presence of extended chain crystalline structures along the axial direction in the microfibers. Compared to commercial PE fibers and data reported in literatures, the individual microfibers produced *in situ* via ethylene extrusion polymerization without postprocessing exhibit high tensile strength (0.3 ~ 1.0 GPa), low tensile modulus (3.0 ~ 7.0 GPa), and high elongation at breakage

(8.5 ~ 20 %) at 35 °C. The defects in the alignment of nanofibrils are believed to be the major reason for the low modulus values. It was also found that a slight tensile drawing could increase the microfiber strength and modulus.

Keywords: nascent polyethylene fiber, nanofabrication, ethylene extrusion polymerization, extended chain crystalline structure, supported metallocene catalyst, MCM-41, fiber morphology, mechanical property, tensile strength, tensile modulus.

2.2 Introduction

The production of high strength polyethylene fibers is a theme that has captured the imaginations of many researchers and led to a large number of investigations.[1] One important parameter in polyethylene fiber fabrication is the polymer chain orientation and extension, which strongly affects fiber properties. When polymer chains are perfectly aligned in one dimension, polyethylene fiber exhibits ultra high tensile modulus and strength that are even greater than those of steel materials on a weight basis. A variety of fabrication methods, such as gel spinning,[2] solid state ultradrawing,[3] shear force induced fiber formation,[4] and etc, have been developed and some of them have been used in commercial practice. All these methods involve a series of sophisticated and costly post-reactor processing procedures, aiming at introducing chain orientation for improved fiber properties. Ultrahigh strength and modulus (tensile strength ~ 5.0 GPa and modulus ~ 100 GPa) polyethylene fibers have been produced using these methods.[3] However, the production of ultrahigh strength and modulus nascent polyethylene fibers directly from a polymerization reactor without costly post-processing steps still remains as a great challenge for polymer scientists.

Recently, Aida et al.[5] demonstrated a new nanofabrication technique, termed as extrusion polymerization, to produce nascent polyethylene with novel fibrous morphology. In this technique, titanocene catalysts are impregnated onto nanotubes of mesoporous honeycomb-shaped silica particles (MSF, MCM-41). The nanotubes serve both as nanoscale ethylene polymerization reactors and as polyethylene nanoextruders. During polymerization, these one-dimensional nano-scaled reactors prevent polyethylene chains from being folded into conventional crystalline/amorphous lamellar structures. The polymer chains thus grow out of the nanotubes and assemble into long-range ordered polyethylene nanofibers (fiber diameters: 30 ~ 50nm) featured with extended chain crystalline structure.

Fibrous morphologies have been widely observed in nascent polyolefins prepared with Ziegler-Natta catalysts. Extensive investigations on morphologies of nascent polyethylenes were carried out in 1960's and 1970's.[6] It was found that fibers of extended chain and/or folded chain crystal are the basic units of morphological structure in nascent powders produced with heterogeneous catalysts. The fibers are further irregularly attached and connected to form globules.[7] The formation of the fibrous structure depend on catalyst surface, solvent type, polymerization temperature, stirring and many other factors.[8] There have been several models proposed to explain how polymer chains are assembled into larger morphological structures. Such models include extended chain fibril model by Schindler [9] and Marchessault,[10] folded chain model by St John Manley,[11] flow-induced fibril formation model by Keller,[12] and other fibril formation models by Guillet [13] and Wristers,[7] respectively. The work by Aida et al.[5] revitalized the research in this area. Moreover, different from the previous models, Aida et al. introduced an extrusion polymerization model to describe the production of extended chain crystal PE with the nanotube particle supported metallocene catalysts.

The nanofibers in Aida's experiments were in the form of a porous cocoon-like assembly that makes difficult for the materials to be mechanically characterized and thus to be exploited for potential commercial uses. Recently, we synthesized polyethylene fibers using the ethylene extrusion polymerization technology with a MCM-41 supported Cp_2TiCl_2 catalyst system. The nanofibrils (diameters ~ 60 nm) are closely packed in parallel and assembled into individual microfibers having diameters about 1 ~ 30 μm. The unique morphological and mechanical properties of these novel polyethylene fibers were reported in this work.

2.3 Experimental Part

2.3.1 Materials

All manipulations involving air and/or water sensitive compounds were performed in dry nitrogen glove box or under nitrogen protection. Titanocene dichloride (Cp_2TiCl_2) was purchased from Strem Chemicals. Modified methylaluminoxane (MMAO-3A) was provided by Akzo-Nobel Corp. as 7.25 wt% aluminum in toluene. Both Cp_2TiCl_2 and MMAO were used as received. Polymerization-grade ethylene (from Matheson Gas) was purified by passing it through CuO, Ascarite, and 5A molecular sieves. Toluene (anhydrous grade, from Aldrich) was refluxed over sodium with benzophenone as indicator and distilled under nitrogen atmosphere prior to use.

2.3.2 Preparation of MCM-41 supported Cp_2TiCl_2 catalyst

In this work, MCM-41 particles were used as support for Cp_2TiCl_2 catalyst. The MCM-41 particles were silicate-based and were synthesized

according to the procedures published in literature.[14] The particles were calcinated in air at 550 °C for 6 hours for the removal of surfactants. X-ray diffraction (Bruker D8 Advance diffractometer) and nitrogen adsorption-desorption isotherm (Micrometritics ASAP 2010) were used to characterize internal pore structures of the calcinated particles. The characterizations showed that the particles have nanotube diameter of 22.7 Å, pore wall thickness of 22.2 Å, specific surface area of 743.5 m^2/g, and pore volume of 0.63 ml/g. Figure 2.1 shows SEM micrograph of the MCM-41 samples, taken with an Electroscan ESEM 2020 facility. The figure shows that the MCM-41 particles have curved tubular structure of about 10 ~ 50 μm in length (equivalent to nanotube length) and about 10 μm in diameter (each particle consists of thousands to millions nanotubes).

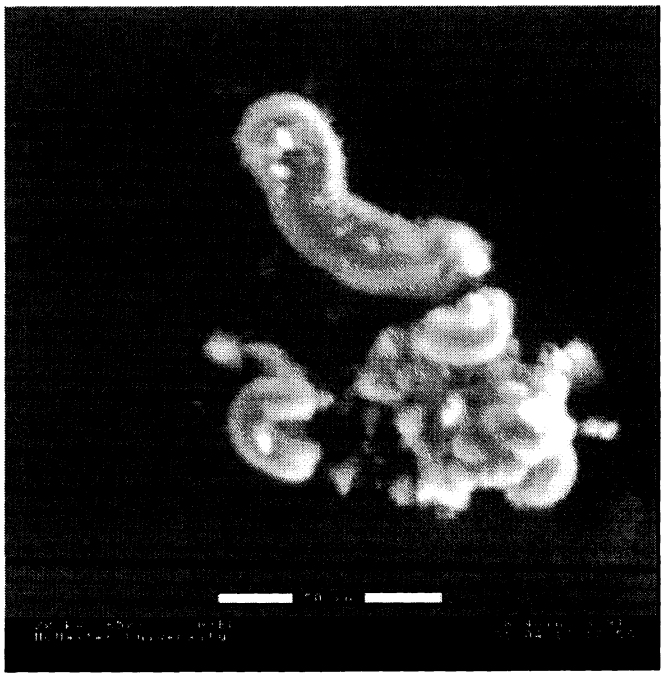

Figure 2.1 SEM micrograph of MCM-41 particles used in this work.

1.0 g of the calcinated MCM-41 particle was mixed with 1.0 mmol Cp_2TiCl_2 catalyst in 60 ml toluene. After stirred for 20 hours at room temperature, the slurry was filtered; the solid was collected and washed with a large amount of fresh toluene and then with 100 ml anhydrous pentane. The supported catalyst was then dried under vacuum at room temperature overnight. An ICP-MS analysis gave the supported Ti amount of 0.11 mmolTi/(g supported catalyst).

2.3.3 Ethylene extrusion polymerization

The extrusion polymerizations of ethylene with the MCM-41 supported Cp_2TiCl_2 catalyst were conducted in a one-liter Autoclave stainless steel reactor equipped with an air-activated mechanical stirrer. The reactor was carefully cleaned and purged before reaction. 400 ml toluene and the required amount of MMAO solution were added to the reactor under nitrogen protection. The mixture was stirred for ten minutes and meanwhile the reactor was heated to establish polymerization temperature. The catalyst suspension was then added, the system was stirred for ten minutes, and then pressurized to the desired ethylene pressure to start the polymerization. A stirring speed of 1000 rpm was kept throughout the reaction. The reactor temperature was maintained by water/ethylene glycol cool circulator through an internal cooling coil. The polymerization was stopped by venting the reactor. The fibrous polymer product was washed with a large amount of methanol acidified with 0.2 % HCl and then dried overnight.

2.3.4 PE fiber characterization

The DSC analysis was carried out using TA Instruments Thermal Analysis 2910 MDSC in the standard DSC mode. UHP N_2 gas with a flow rate of 30

ml/min was purged through the calorimeter. A refrigerated cooling system (RCS) with the cooling capacity to 220 K was attached to the DSC cell. The temperature and heat capacity of the instrument were calibrated with indium standard at the heating rate of 10 °C/min. The polyethylene sample (about 5 mg) was first heated to 180 °C at the rate of 10 °C/min. It was then cooled down to 20 °C at 10 °C/min. Subsequently, a second heating cycle was conducted at the heating rate of 10 °C/min. The polymer molecular weights (MW) and molecular weight distributions (MWD) were measured at 140 °C in 1,2,4-trichlorobenzene using Waters Alliance GPCV 2000 with DRI detector coupled with an in-line capillary viscometer. The polymer molecular weight data were calculated using polystyrene-based universal calibration curve. The X-ray diffraction spectra of the polymers were recorded on Bruker D8 Advance diffractometer. The morphological study on the PE fibers was conducted on Electroscan ESEM (Environmental Scanning Electronic Microscope) 2020 facility that requires no gold coating on samples.

The mechanical properties of the fibers were measured using a calibrated TA Instrument DMA 2980 Dynamic Mechanical Analyzer with tensile clamps. The tensile measurement could only been carried out in the controlled force mode for this instrument. The instrument requires a minimum fiber length about 5 mm and allows for minimum and maximum tensile forces of 0.001 N and 18 N, respectively. All the tensile measurements were conducted at 35 °C. The microfiber samples were carefully mounted onto the tensile clamps. A preload force of 0.005 N and a ramping rate of 0.05 N/min were chosen for the tests. The fiber cross-sectional area, needed for the tensile stress calculation, was obtained using ESEM.

2.4 Results and Discussion

Two batches of polyethylene fibers were synthesized in this work with the MCM-41 supported Cp_2TiCl_2/MMAO catalyst system. Table 2.1 lists the polymerization reaction conditions, polymer molecular weight data, and the DSC results of the fiber samples. Both samples have high unimodal melting temperatures (T_m = 140 °C) compared to melt-crystallized HDPEs (T_m = 133 - 135 °C), indicating the presence of extended chain crystals.[15] Once melted and recrystallized, the PE samples have significant lower melting temperature and melting enthalpy due to the formation of the folded-chain lamellar crystal structure. The melting enthalpy data suggest that the crystallinities (based on ΔH_m = 290 J/g for a perfect PE crystal) reach 82.7 % and 75.9 %, respectively, for the two fiber samples.

Table 2.1 Ethylene extrusion polymerizations with MCM-41 supported Cp_2TiCl_2 catalyst and PE fiber MW data and DSC characterization results.[a]

Run	Pressure (atm)	Temp (°C)	Activity[b]	M_w ($\times 10^4$)	PDI	T_m(°C)[c]		ΔH_m(J/g)	
						1st scan	2nd scan	1st scan	2nd scan
1	20	40	918	202	2.5	140	134	240	172
2	20	85	1262	62	4.5	140	136	220	158

[a] Other reaction conditions: solvent, toluene 400ml; supported catalyst amount, 0.1g (equivalent to 11μmol Ti); Al/Ti molar ratio, 2000; polymerization time, 1hr.
[b] Activity in kg PE/(molTi hr).
[c] T_m refers to the peak temperature in the thermogram.

A detailed morphological investigation was conducted on the nascent PE fiber samples. Three levels of fiber morphology, i.e. nanofibrils, microfibers, and fiber aggregates/bundles, were identified under SEM. Figure 2.2(a) shows the SEM micrographs of the fiber aggregates produced in Run 1. A large number of PE microfibers having diameters ranging from 1 to 30 μm entangled and agglomerated together to form porous fiber aggregates. The aggregation and

orientation of the microfibers in the aggregates are very irregular and random in nature. In addition to the microfiber aggregates, loosely and compactly packed bundles of individual PE microfibers were also observed as shown in Figures 2.2(b) and 2.2(c), respectively. As from Figure 2.2(c), the compactly packed microfiber bundles exhibit a smooth surface with observable striations of individual microfibers. There are no observable voids and/or gaps between the packed microfibers. A certain level of microfiber orientation can be seen inside the bundles. At a macroscopic scale, these fiber aggregates and bundles represent the major morphological feature of the nascent PE samples.

The microfiber bundle shown in Figure 2.2(c) shows a crack position, which was probably formed in the polymerization reactor due to the strong mechanical stirring applied. The crack permitted a close examination on the morphology of the fiber bundle's cross-section. Figure 2.2(d) shows the magnified SEM micrograph of the crack position. A great number of uniformly oriented PE nanofibrils can be identified. The nanofibril diameters are about 60 nm. Similar morphologies were observed with all other fiber bundles with cracks.

Figures 2.3(a) and 2.3(b) show two SEM micrographs with different magnifications taken on an individual microfiber surface. Parallel nanofibril striations can be clearly seen. The diameters of these nanofibrils are about 60 nm. The nanofibrils are closely packed to form the microfiber. Also seen in the figures are fine powders of < 1 μm, which are probably the fragments of MCM-41 particles. To further examine the fiber morphology, the microfiber was intentionally cleaved along the axial direction by mechanical forces with a clamp. Figures 2.3(c) and 2.3(d) show the SEM micrographs on the cleaved position at different magnifications. The PE nanofibrils with diameters about 60 nm can be clearly identified.

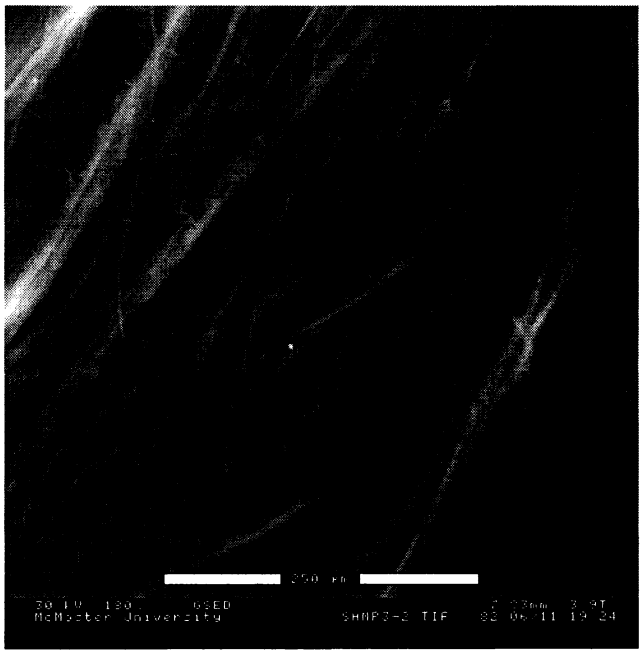

(a)

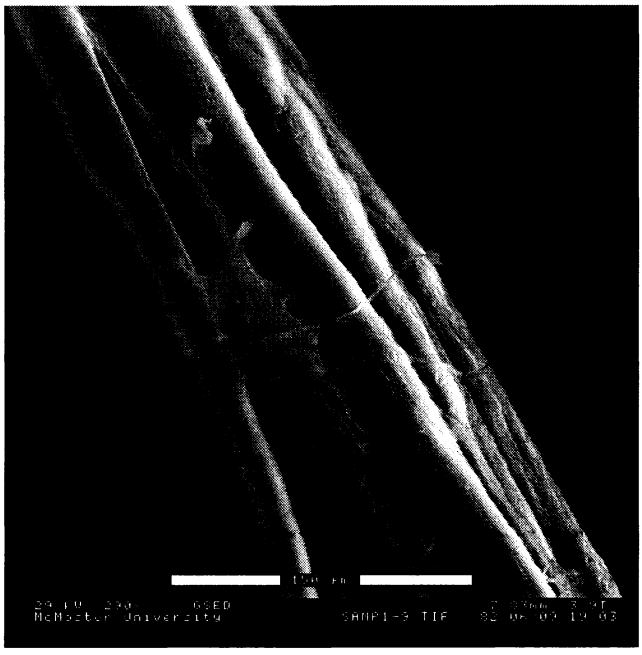

(b)

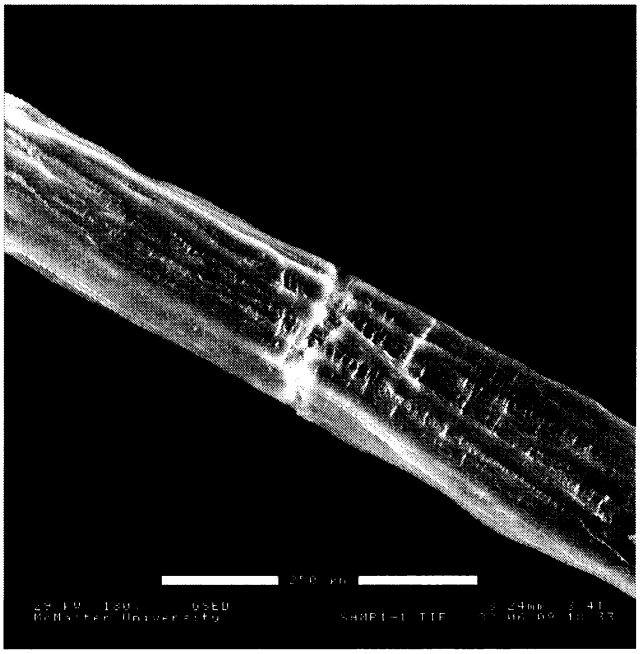

(c)

(d)

Figure 2.2 SEM micrographs of PE sample produced in Run 1: (a) an aggregate of PE microfibers; (b) a loosely packed bundle of PE microfibers; (c) a compactly packed bundle of PE microfibers; (d) magnified image of the crack position shown in (c).

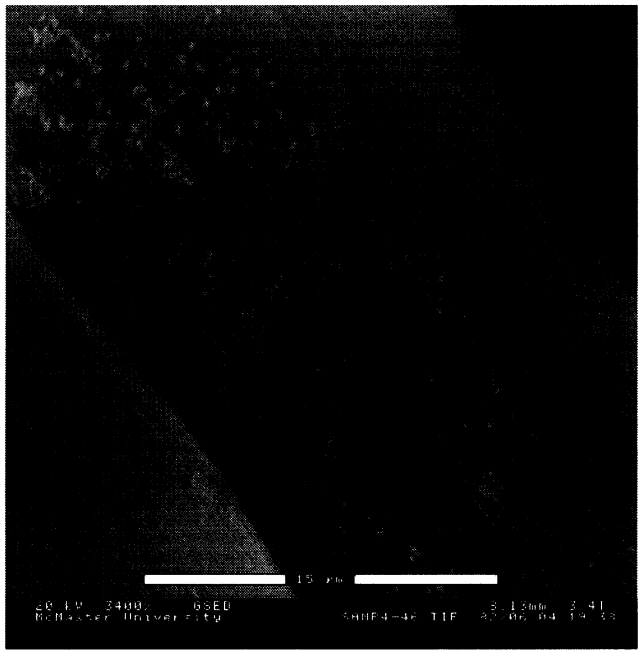

(a)

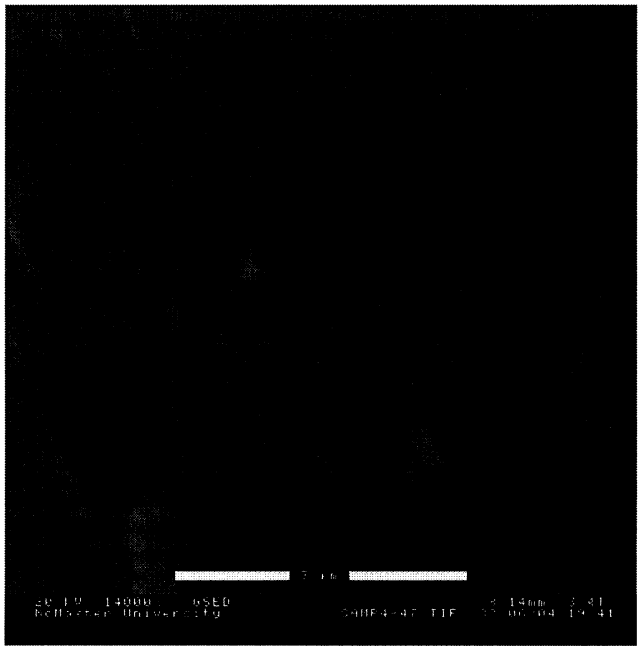

(b)

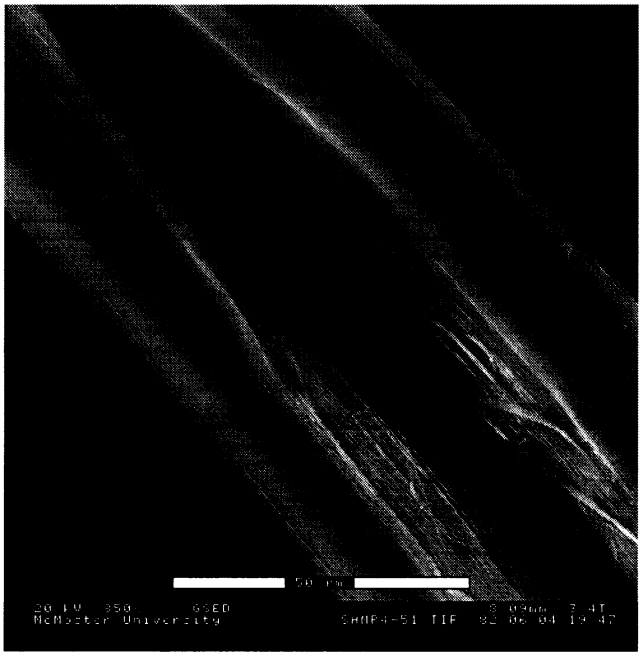

(c)

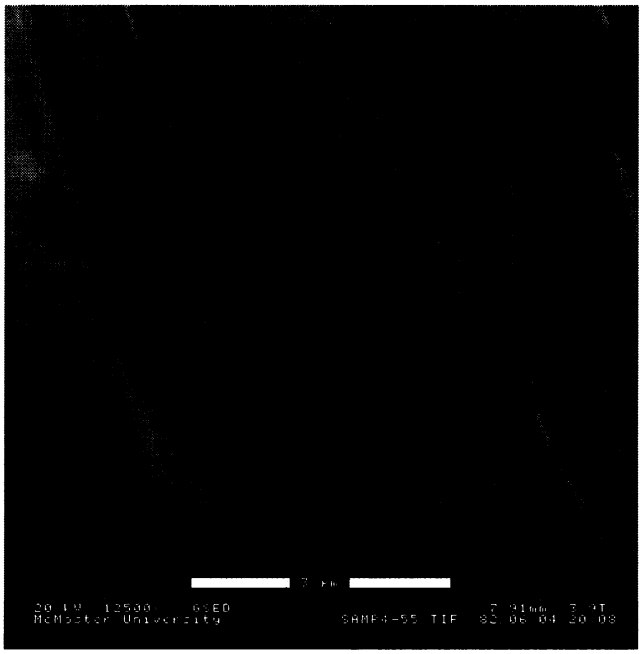

(d)

Figure 2.3 (a) and (b) SEM micrographs of PE a microfiber surface at two different magnifications showing nanofribrils; (c) and (d) SEM micrographs of the cleaved position of the microfiber at two different magnifications also showing nanofibrils.


250 nm
20 kV 175 GSED
McMaster University
FBUND1-5 TIF 02 06 25 20 16

(a)

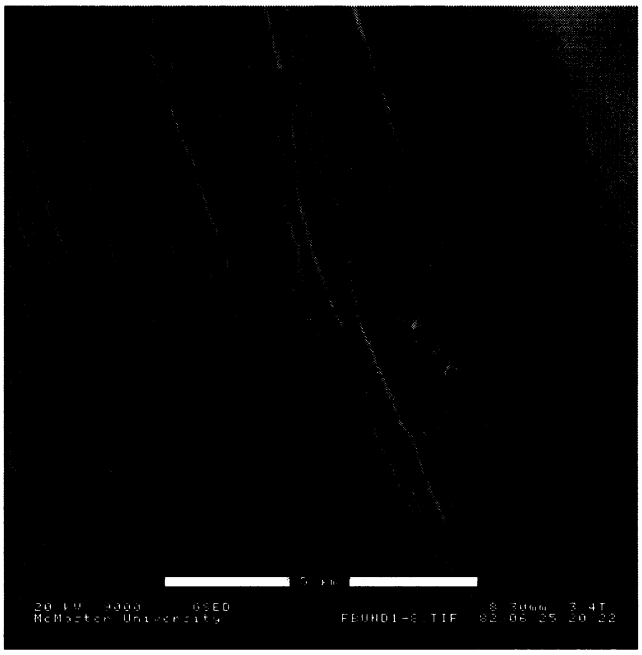
5 nm
20 kV 4000 GSED
McMaster University
FBUND1-6 TIF 02 06 25 20 22

(b)

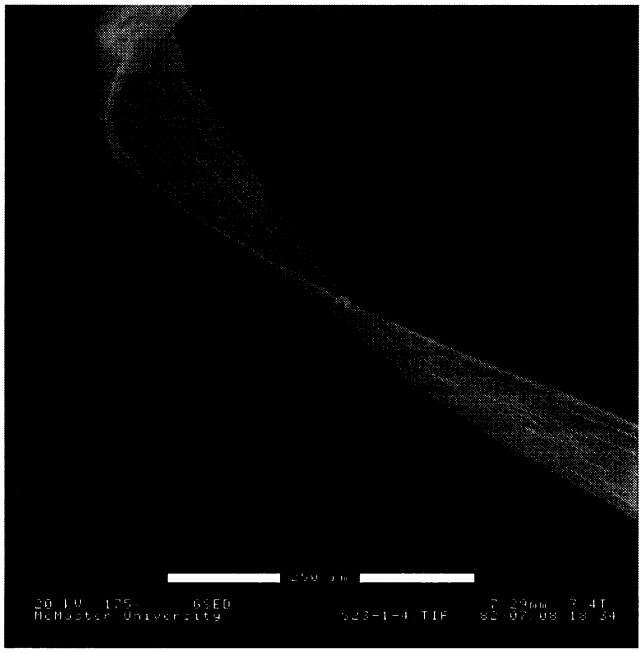

(c)

(d)

Figure 2.4 SEM micrographs of (a) a microfiber bundle produced in Run 2 and (b) its surface morphology. SEM images of (c) a tape-like microfiber produced in Run 2 and (d) its surface morphology.

Similar fiber morphologies were also observed with the PE samples produced in Run 2. Figure 2.4(a) shows a microfiber bundle and Figure 2.4(b) shows its surface morphology. There are also some tape-like microfibers as shown in Figure 2.4(c) with its surface morphology shown in Figure 2.4(d). Uniform and regular nanofibril striations with nanofibril diameters about 60 nm on the microfiber surface could be identified in the SEM images. In addition to the fibrous products, small parts of the PE samples produced in both runs have particle morphology probably due to the fragmentation of MCM-41 supports during polymerization and the loss of control over oriented polymer growth.

An XRD study was conducted to examine crystal structure and morphology of the fibrous materials. From the wide-angle XRD analyses, different diffraction patterns were observed for the three types of fibrous materials with various hierarchical morphologies: microfibers, microfiber aggregates, and microfiber bundles. Figure 2.5(a) shows the X-ray diffraction pattern for a microfiber produced in Run 1. From the figure, the microfiber exhibits a diffraction pattern typical for single crystal. Only diffraction spots could be observed with no isotropic diffraction rings shown up. Moreover, all diffraction spots are symmetrically located on a straight line, which is perpendicular to the sample alignment direction. This result proves that the microfiber has a typical extended chain crystalline structure along the fiber axial direction and also suggests that the nanofibrils are packed in parallel. Randomly distributed lamellar crystalline structure is absent from the absence of diffraction rings. Very similar diffraction pattern was also found in other microfibers investigated.

In comparison, Figure 2.5(b) shows the diffraction pattern for a microfiber aggregate prepared in Run 1. Only isotropic diffraction rings were identified.

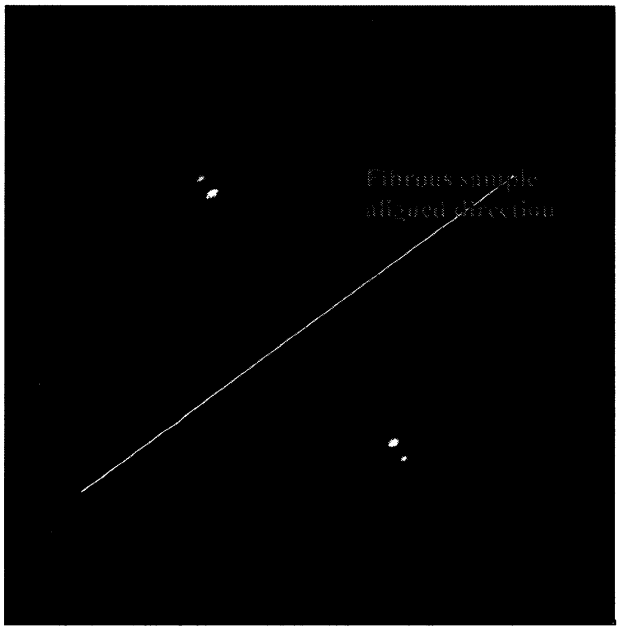
Fibrous sample
aligned direction

(a)

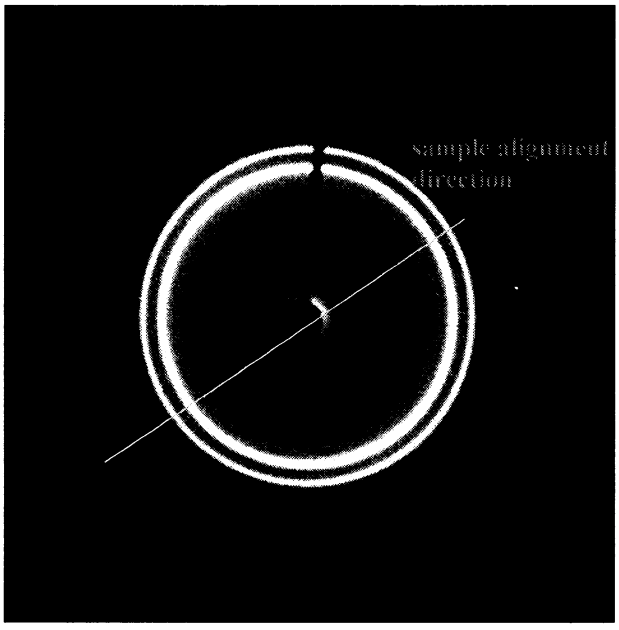
sample alignment
direction

(b)

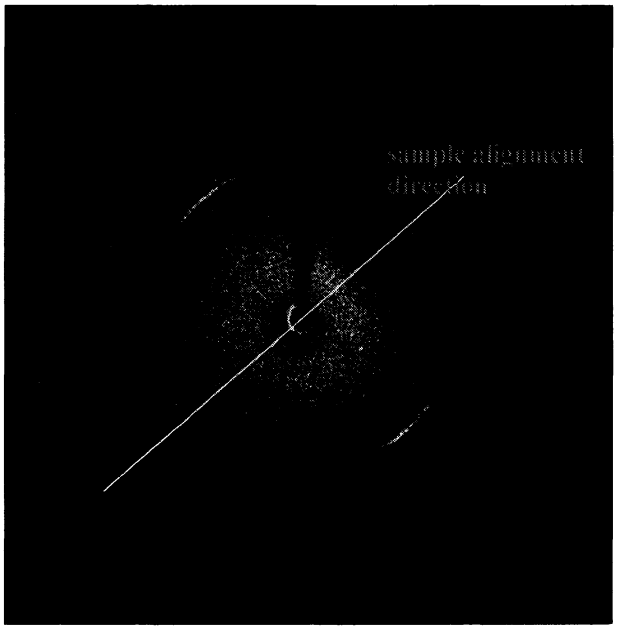

(c)

Figure 2.5 X-Ray diffraction pattern for fibrous materials prepared in Run 1: (a) a single microfiber; (b) a microfiber aggregate; and (c) a microfiber bundle.

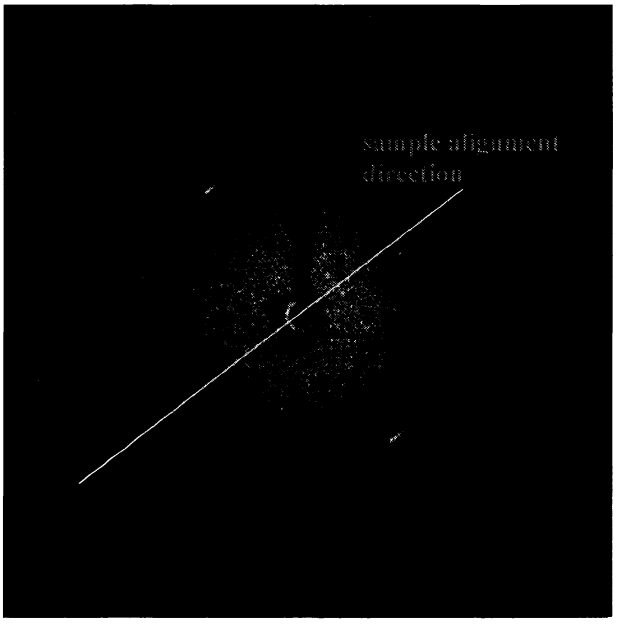

Figure 2.6 X-Ray diffraction for a single microfiber prepared in Run 2.

Compared to the pattern in Figure 2.5(a) for individual microfibers, this pattern suggests that the aggregation of constituting microfibers in microfiber aggregates is random. There is no preferred alignment direction for the microfibers.

Figure 2.5(c) shows the diffraction pattern for a microfiber bundle. Interestingly, its diffraction pattern shows both diffraction spots and rings. The diffraction is quite isotropic in all areas except in the direction perpendicular to the sample alignment direction, where the diffraction is much stronger. The result suggests that there is a certain level of extended chain crystalline structure existing along the fiber axial direction. But at the same time, some non-oriented microfiber aggregations or randomly distributed lamellar crystal structures are present from the isotropic diffraction rings.

Similar diffraction patterns were also observed for fibrous materials produced in Run 2. Representatively in Figure 2.6, the diffraction pattern for a single tape-like microfiber is shown, suggesting extended chain crystalline structure along fiber axial direction from the sole presence of diffraction spots in the direction perpendicular to sample alignment direction.

Although different diffraction patterns could be observed, the fibrous materials, including microfibers, microfiber aggregates and bundles, all exhibit the same orthorhombic crystal cell unit with [110] and [200] reflections at the angle of 21.6 ° and 23.8 °, respectively. Typically Figure 2.7 shows the XRD spectra for the microfiber aggregates produced respectively in Run 1 and Run 2. The amorphous halo, which is around 19.6°, is negligibly small, indicating high crystallinity of the samples.

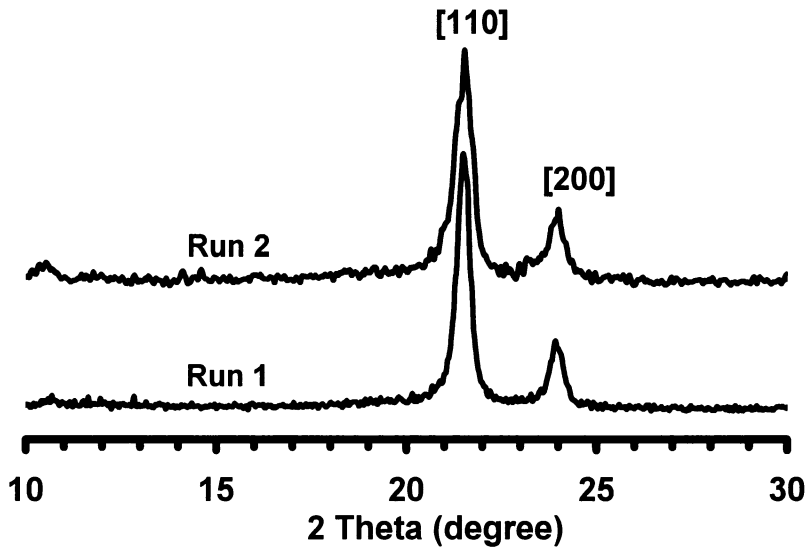

Figure 2.7 XRD spectra of the PE microfiber aggregates.

It is evident from the above SEM morphological study and XRD crystal structure analyses that PE nanofibrils are the major morphological units in the PE samples. These nanofibrils were formed during ethylene extrusion polymerization, in which polymer chains grew out of the honeycomb nanotubes, crystallized, and formed extended-chain-crystal nanofibrils. Furthermore, bunches of nanofibrils were closely and parallel packed together along the nanofibril axial direction to form individual PE microfibers, as shown in Scheme 2.1. Probably due to the strong mechanic stirring involved in the polymerization reactor, the microfibers tended to further agglomerate to form fiber aggregates and bundles. The PE nanofibrils with diameters of 30 ~ 50 nm were reported in Aida's work.[5] Contrary to this work, no parallel nanofibril aggregation was reported in their work. The discrepancy might be due to the differences in reactor systems and polymerization conditions. In Aida's work, MSF particles, which have different nanotube organization pattern compared to MCM-41 used in this work,[17] were used as catalyst supports. The different polymerization conditions in their work (e.g., ethylene pressure of 10 atm and temperature of 40 °C) might

also lead to different fiber morphologies. In addition, in this work, a strong mechanical stirring was applied during polymerization and the added shear stress might help the orientation and aggregation of nanofibrils.

From the micrographs as shown in Figures 2.3(b), 2.4(b) and 2.4(d), this nanofibril morphology is different from the shish-kebab morphology found in fibers produced with shear-induced crystallization technique [4] and in some nascent samples synthesized with Z-N catalysts.[11b] These micrographs combined with the single-crystal XRD pattern of microfibers and unimodal high T_m of the polymers suggest the extended chain crystal structure in the nanofibrils.

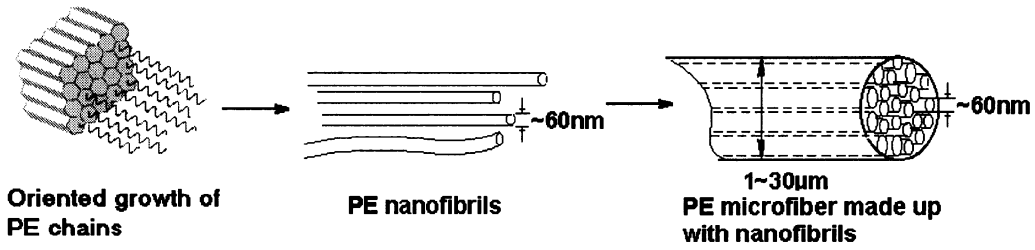

Scheme 2.1 Proposed formation of the hierarchal morphological structure.

The tensile mechanical property characterization was carried out on the microfibers produced in Run 2 due to their relative more aligned fibrillar structure compared to fiber aggregates and bundles. These microfibers generally had a tape-like shape of 30 ~ 90 μm in width, 2 ~ 20 μm in thickness, and 8 ~ 25 mm in length. Their effective cylindrical diameters (d_{eff}) were in the range of 10 ~ 40 μm. Figure 2.4(c) shows a typical image for these microfibers. All the tensile characterizations were carried out along the fiber axial direction. No

characterization could be conducted on the microfiber samples produced in Run 1 due to short fiber lengths (< 5 mm).

Figure 2.8 shows some typical stress-strain curves for these nascent PE microfibers. Different from the linear-like stress-strain behaviors of ultrahigh-strength PE fibers made from post-processing technologies, the tensile stress-strain profiles are curved for all the nascent PE microfibers tested in this work. Typically, the nascent PE fiber exhibits a secant tensile modulus (5 % strain) of 3.0 ~ 7.0 GPa, tensile strength at breakage of 0.3 ~ 1.0 GPa, and elongation at breakage of 8.5 ~ 20 %. Table 2.2 compares the tensile properties of the nascent PE fibers with commercially available PE fiber samples and literature reported data. Although different mechanical testing conditions and methods were used for these different samples, which may affect the tensile testing results, the table does provide us with some valuable comparisons. Compared to those commercial fibers and reported data in literatures, the nascent PE microfibers produced by the extrusion polymerization exhibited some unique tensile properties: low modulus (a little better than the isotropic injection-molded HDPE sample), high tensile strength (comparable to the fibers produced by shear-induced crystallization and by drawing melt-crystallized HDPE), and much higher elongation at breakage.

The high ductility of this nascent PE fiber should be the major cause of its low tensile modulus. As shown in Figure 2.4(d), the orientation and packing of the nanofibrils in the microfiber is not perfect and the constituting nanofibrils are in a rather relaxed than fully extended state. When under tensile strength, these non-fully extended nanofibrils will slip between each other and re-orientate along the tensile direction, which will elongate the microfiber and decrease the fiber modulus significantly. However, the high tensile strength of these fiber samples indicates that once the nanofibrils are in a rather extended state at a certain high

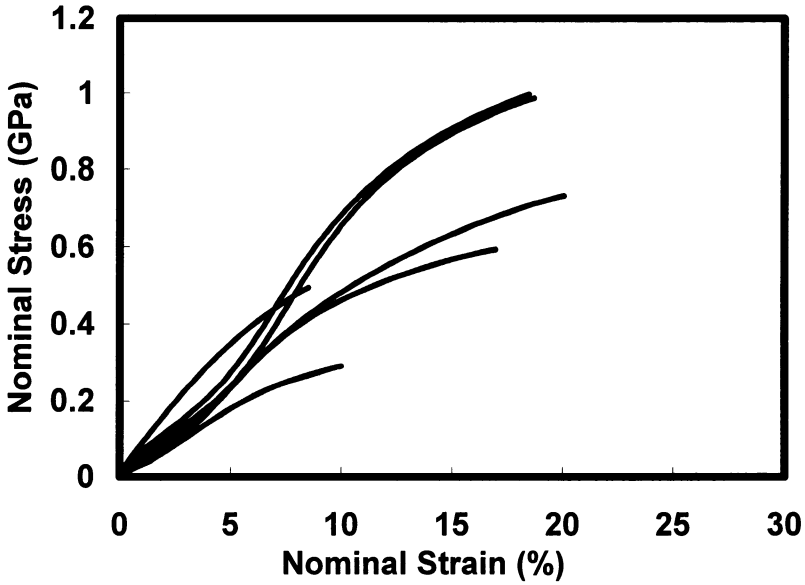

Figure 2.8 Typical tensile stress-strain curves for tape-like nascent PE microfibers produced in Run 2. Test condition: preload force, 0.005 N; force ramping rate, 0.05 N/min; testing temperature, 35 °C.

Table 2.2 Tensile properties of as-synthesized nascent PE fibers and comparison with commercial product and literature data.

PE fiber/sample	Tensile strength (GPa)	Tensile modulus (GPa)	Elongation at breakage (%)
Nascent microfiber produced in Run 2	0.3 ~ 1.0	3.0 ~ 7.0	8.5 ~ 20.0
Injection-molded HDPE [1]	< 0.05	~ 1.0	-
Fiber produced by Shear induced Crystallization [4]	0.026 ~ 1.0	0.22 ~ 27	6.0 ~ 12
Fiber by drawing melt-crystallized HDPE (draw ratio of 15 and 20) [18]	0.8 ~ 1.3	30 ~ 50	-
DSM UHMWPE-Fiber Dyneema SK65 110 dTex [19]	3.3	100	3.6

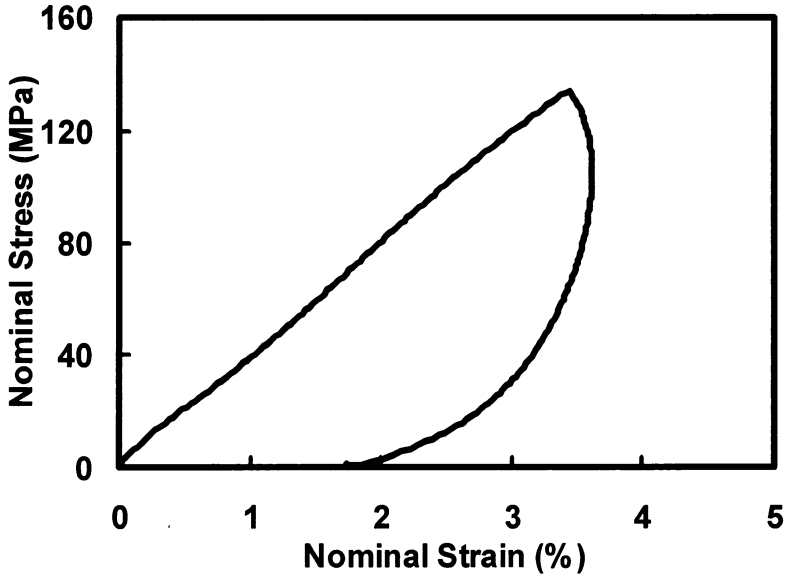

Figure 2.9 Tensile hysteresis curve for a microfiber produced in Run 2. Test conditions: preload force, 0.005 N; force ramping rate, 0.05 N/min; temperature, 35 °C.

Figure 2.10 SEM micrograph of a broken specimen of nascent PE microfiber produced in Run 2 during tensile test.

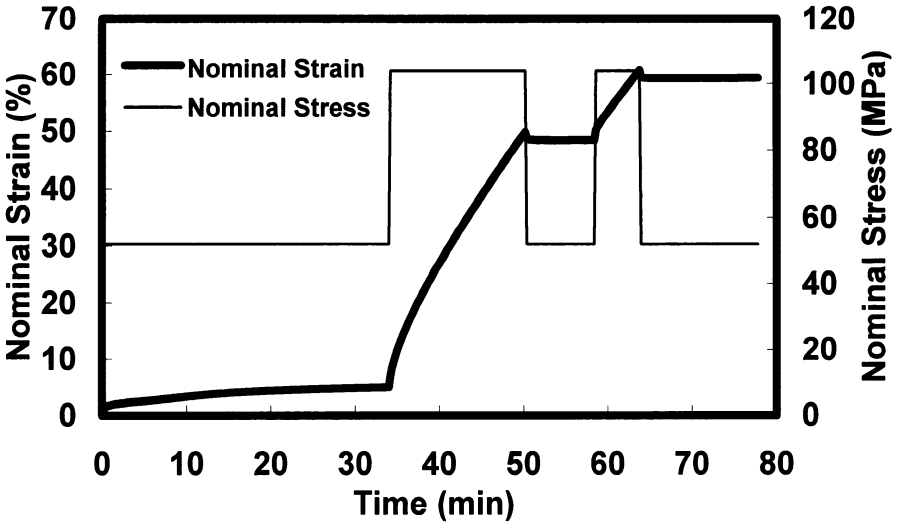

(a)

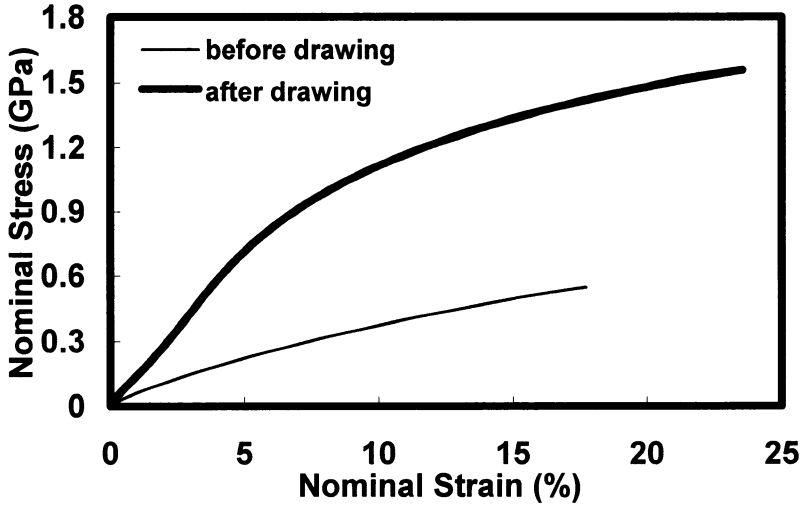

(b)

Figure 2.11 Effect of drawing on fiber tensile properties: (a) strain as a function of time for a PE microfiber (initial fiber diameter $d_{eff,0}$ = 35.0 μm, initial fiber length L_0 = 9.81 mm) produced in Run 2 under programmed stress. Drawing temperature 80 °C. Final drawing ratio 1.6. (b) Comparison of tensile stress-strain curves for the microfiber before and after tensile drawing. The diameter of the drawn microfiber is calculated according to the diameter before drawing and the drawing ratio: $d_{eff} = d_{eff,0}/(\text{draw ratio})^{0.5}$. Testing condition: preload force, 0.005 N; force ramping rate: 0.05 N/min; temperature, 35 °C.

strain, the microfiber can sustain high tensile loading owing to the extended chain crystal structure present in the nanofibrils.

Figure 2.9 shows a tensile hysteresis curve for a microfiber sample. After one cycle with the highest strain of 3.6 %, the sample retained a permanent strain of 1.7 %, showing a significant irreversible change in the fiber dimension even after slight stretching.

The fiber fractures were also examined for the samples after the tensile test. Figure 2.10 shows an SEM micrograph of a typical fiber fracture. In contrast to straight-fracture surface exhibited in isotropic polymeric materials after tensile testing, an irregular rupture with fibril fragments of different lengths could be observed, indicating the presence of epitaxial fibrous structure.

We also investigated the effects of drawing on the fiber strength and modulus. After initial tensile tests, the PE microfibers were subject to a slight tensile drawing. A small and programmed tensile stress was applied during tensile drawing to avoid fiber breakage. The drawing process was carried out at 80 °C. Typically, Figure 2.11(a) shows the fiber strain as function of time under programmed drawing stress. Significant irreversible changes in fiber dimension could be observed in the drawing process, due to the re-orientation of nanofibrils. After a final drawing ratio of 1.6 was reached, a subsequent tensile test was carried out on this drawn microfiber sample. Figure 2.11(b) compares the stress-strain behaviors for a microfiber before and after drawing. The drawing with a small drawing ratio of 1.6 increased both tensile modulus (from 4.4 GPa to 14.4 GPa, 5 % secant modulus) and tensile strength (from 0.55 GPa to 1.6 GPa). Generally, after drawing with drawing ratio of 1.5 ~ 1.6, the tested microfibers exhibited improved tensile modulus of 6.0 ~ 15.0 GPa and tensile strength of 0.6 ~ 1.6 GPa.

2.5 Conclusion

Nascent polyethylene fibers with unique fibrous morphology were synthesized in this work with MCM-41 supported titanocene catalysts via ethylene extrusion polymerization. An extensive SEM investigation revealed three levels of fibrous morphologies in the as-synthesized PE samples. PE nanofibrils (diameters of ~ 60 nm) with extended chain crystal structure were produced by the extrusion polymerization. These nanofibrils aggregated to form PE microfibers with diameters of 1 ~ 30 μm. The individual microfibers entangled and aggregated to form fiber aggregates and/or bundles. XRD study shows the microfibers possess extended chain crystalline structure along the fiber axial direction. Tensile mechanical tests on the microfiber samples gave low modulus (3.0 ~ 7.0 GPa), high tensile strength (0.3 ~ 1.0 GPa), and high elongation (8.5 ~ 20 %) compared to a commercial PE fiber sample and data reported in literatures. It was also found that slight tensile drawing could improve the fiber mechanical properties.

2.6 Reference

1. Peacock, A. J. *Handbook of Polyethylene: Structures, Properties, and Applications*, Marcel Dekker, New York, 2000.
2. Smith, P.; Lemstra, P. J. *J. Mater. Sci.* **1980**, *15*, 505.
3. (a) Smith, P.; Chanzy, H. D.; Rotzinger, B. P. *J. Mater. Sci.* **1987**, *22*, 523; (b) Smith, P.; Chanzy, H. D.; Rotzinger, B. P. *Polym. Commun.* **1985**, *26*, 258.
4. Pennings, A. J.; Schouteten, C. J. H.; Kiel, A. M. *J. Polym. Sci. Polym. Lett.* **1972**, *38*, 167.
5. Kageyama, K.; Tamazawa, J.; Aida, T. *Science* **1999**, *285*, 2113.

6. Boor, J. in *Ziegler-Natta Catalysts and Polymerization*, Academic Press: New York, 1979.
7. Wristers, J. *J. Polym. Sci., Polym. Phys. Ed.* **1973**, *11*, 1601.
8. Wunderlich, B. *Adv. Polym. Sci.* **1968**, *5*, 568.
9. Ingram, P.; Schindler, A. *Makromol. Chem.* **1968**, *111*, 267.
10. Chanzy, H. D.; Day, A.; Marchessault, R. H. *Polymer* **1967**, *8*, 567.
11. (a) Blais, P.; St. John Manley, R. *Science* **1966**, *153*, 539. (b) Blais, P.; St. John Manley, R. *J. Polym. Sci., Part A-1* **1968**, *6*, 291.
12. Keller, A.; Willmouth, F. M. *Makromol. Chem.* **1969**, *121*, 42.
13. Guttman, J. Y.; Guillet, J. E. *Am. Chem. Soc., Div. Org. Coat. Plast. Chem., Pap.* **1970**, *30*, No.1, 177.
14. Mokaya, R.; Zhou, W.; Jones, W. *Chem. Commun.* **1999**, 51.
15. Chanzy, H. D.; Bonjour, E.; Marchessault, R. H. *Colloid & Polym. Sci.* **1974**, *252*, 8.
16. Krimm, S.; Tobolsky. A. V. *J. Polym. Sci.* **1951**, *7*, 57.
17. Ye, Z.; Alsyouri, H.; Zhu, S.; Lin, Y. S. *Polymer* **2003**, *44*, 969.
18. Hallam, M. A.; Cansfield, D. L. M.; Ward, I. M.; Pollard, G. *J. Mater. Sci.* **1986**, *21*, 4199.
19. Product data sheet for DSM ultrahigh molecular weight polyethylene (UHMWPE) fiber: Dyneema SK65 110 dTex

Chapter 3

Catalyst Impregnation and Ethylene Polymerization with Mesoporous Particle Supported Nickel-Diimine Catalysts

This chapter is organized based on the paper published in *Polymer*, **2003**, *44*, 969-980 by Z. Ye, H. Alsyouri, S. Zhu, and Y. S. Lin.

3.1 Abstract

A Ni-Diimine catalyst (1,4-bis(2,6-diisopropylphenyl) acenaphthene diimine nickel(II) dibromide, DMN) was supported on mesoporous particles having parallel hexagonal nanotube pore structure (MCM-41 and MSF) for ethylene polymerization. The effects of supporting methods and particle morphological parameters, such as pore size and length, on the catalyst impregnation were systematically investigated. Pretreating the supports with methylaluminoxane (MAO) followed by DMN impregnation gave much higher catalyst loading and higher catalytic activity than the direct impregnation of DMN. The particle structure significantly affected the catalyst impregnation and this effect was explained with a semi-quantitative molecular diffusion model. Compared to homogeneous catalysts, significant reduction in activity was observed with the supported systems in ethylene polymerization. Extraction of active sites from the supports during polymerization was observed. The mesoporous supports exerted steric effects on unleached active sites, lowering chain walking ability, and producing polymers having lower short chain branch density. Replication of the particle morphology was observed in some polymer samples.

Keywords: ethylene polymerization, catalyst impregnation, mesoporous particle support, Ni-Diimine catalyst, short chain branch, chain walking mechanism.

3.2 Introduction

Metallocene catalysts have a tremendous impact on polyolefin industries. Compared to classical multi-sited Ziegler-Natta catalysts, these single-site type catalysts offer unprecedented control over polymer chain structure and materials properties.[1] In addition to metallocene catalysts, a recent milestone in the area of transitional metal catalyzed olefin polymerization is the discovery of the α-Diimine derived late transitional metal (Ni or Pd) catalysts by Brookhart and coworkers.[2] Different from metallocenes, these catalysts can produce polyethylene with branch structures without comonomer incorporation due to a chain walking mechanism.[2~4] Control over the catalyst structures (diimine ligand and metal center), cocatalyst, and polymerization conditions (ethylene pressure, reaction temperature, etc) allows one to readily produce polyethylene grades from highly branched, completely amorphous materials to linear, semicrystalline, high-density materials by adjusting the competition between chain walking and chain propagation processes.[2~5]

Supported metallocene catalysts have been widely investigated in industry and academia owing to the advantages in control of polymer particle morphology and applicability in gas-phase reactor technologies.[6] The most commonly used supports are spherical amorphous silica, alumina, and $MgCl_2$. Recently, new types of silicate and/or aluminosilicate-based mesoporous particles, i.e., MCM-41 and MSF (mesoporous silica fiber),[7,8] have been applied as supports for metallocene and other catalysts for olefin polymerization.[6,9~15] The geometrical constraints of the nanotube pore structure of these particles as polymerization

reactors affect the pattern of monomer insertion and chain growth processes, and thus offer a possible new route to control polymer chain structure and crystal morphology in olefin polymerization.[9~15] The synthesis of fully extended chain crystal (ECC) polyethylene nanofibers with MSF and MCM-41 supported Cp_2TiCl_2 catalysts through ethylene extrusion polymerization demonstrated the good potential of using nanotube reactors for the control of chain structure and material morphology.[13] Moreover, in co-oligomerization of ethylene and propylene, MAO-grafted MCM-41, generated by *in situ* hydrolysis of TMA in MCM-41 nanotube pores, was used for supporting $[C_2H_4(1\text{-Ind})_2]Zr(CH_3)_2$ catalysts.[11a] The polymerization results showed that the MCM-41-supported catalysts were even more active than the corresponding silica-supported or homogeneous systems and the polymer molecular weight increased with the decrease of MCM-41 pore size. Studies on isotactic polypropylene with MCM-41-supported *rac*-$Et(Ind)_2ZrCl_2$ [9a] and syndiotactic polypropylene with MCM-41-supported $[Me_2C(Cp)(Flu)]ZrCl_2$ [15] also showed that the resulted polymers had higher stereoregularity and melting point than homogeneous or silica-supported systems. The polymerization behaviors were also very different. More recently, ethylene copolymerizations with α-olefins was conducted using $Et(Ind)_2ZrCl_2$ catalysts supported on MCM-41, showing significant effects of the nanotube structure on comonomer incorporation and polymerization behavior.[9b]

There are numerous studies on the Ni-Diimine catalysts impregnated on inorganic supports [16~18], such as silica, clay, and polymeric supports [19]. However, nanotube particle-supported Ni-Diimine catalysts have not been reported. The unique characteristic of the controllable nanotube diameter and particle morphology may provide a good model system to study the effects of support morphology on catalyst impregnation and polymerization. The nanotube structure may influence the Ni-Diimine catalyst performance, such as chain walking, during polymerization.

In this chapter, we used the mesoporous particles with different morphological parameters as support for a Ni-Diimine catalyst (DMN, 1,4-bis(2,6-diisopropylphenyl) acenaphthene diimine nickel(II) dibromide). The supported catalysts were used for slurry polymerization of ethylene. The objectives of this experimental work are to evaluate the effects of such parameters as pore diameter and particle size on the catalyst impregnation, and to elucidate the effects of nanotube geometric constraints on chain walking process, polymer structure and polymerization behavior.

3.3 Experimental Part

3.3.1 Materials

All manipulations involving air and/or water sensitive compounds were performed in dry nitrogen glove box or under nitrogen protection. The α-Diimine ligand (ArN=C(An)-C(An)=NAr, An=acenaphthene, Ar=2,6-(i-Pr)$_2$C$_6$H$_3$) and the dibromide Ni-Diimine catalyst (DMN, (ArN=C(An)-C(An)=NAr)NiBr$_2$) were synthesized following the procedures reported in literatures [2b]. Modified methylaluminoxane aluminum (MMAO-3A) was provided by Akzo-Nobel Corporation as 7.25 wt% aluminum in toluene. Polymerization-grade ethylene (from Matheson Gas) was purified by passing it through CuO, Ascarite, and 5A molecular sieves. Toluene (anhydrous grade, from Aldrich) was refluxed over sodium with benzophenone as indicator and distilled under nitrogen atmosphere prior to use.

3.3.2 Synthesis and Characterization of MCM-41 and MSF Particles

Three MCM-41 particles with different pore sizes and particle sizes and one MSF particle were synthesized and used as supports for this work. These particles were all silicate-based and were synthesized according to the literature procedures.[8a,20a,20b] The particles were all calcinated in air at 550 °C for 6 hours for the removal of surfactants.

X-ray diffraction (XRD) and nitrogen adsorption-desorption isotherm were used to characterize internal structure of the calcinated particles. The X-ray powder diffraction spectra were recorded on a Bruker D8 Advance diffractometer. Nitrogen adsorption–desorption isotherms were measured at 77 K using an ASAP 2010 volumetric adsorption apparatus from Micrometritics. Prior to the analysis, the samples were degassed under vacuum at 200 °C for 2 hours. The specific surface areas of the samples were obtained based on the standard BET method. The average pore diameter was calculated using BJH method. An Electroscan ESEM 2020 was used for investigating the particle morphology.

3.3.3 Preparation of Supported Catalysts

Two supporting methods were used in this work for the impregnation of DMN on the nanotube particles. Method (a): 1.0 g of calcinated particles was heated at 200 °C under vacuum for 8 hours. It was then directly mixed with 60 ml toluene solution of 0.6 mmol DMN. After stirred for 12 hours at room temperature, the slurry was filtered; the solid was collected and washed seven times with 70 ml toluene and once with 70 ml anhydrous pentane. The supported catalyst was then dried under vacuum at room temperature for overnight. Method (b): 1.0 g of calcinated particles was heated at 200 °C under vacuum for 8 hours. It was then mixed with 50 ml toluene solution of 6 mmol Al of MMAO. The slurry was stirred overnight at room temperature. The solid was filtered, washed five times with 100 ml of toluene and once with 70 ml of pentane, and then dried

under vacuum at room temperature. Subsequently the MMAO-pretreated particle was mixed with 60 ml toluene solution of 0.6 mmol DMN. After stirred for 12 hours at room temperature, the solid was collected by filtration, washed seven times with 70 ml of toluene and one time with 70 ml pentane, and then dried overnight under vacuum at room temperature.

The ICP-MS analysis was used to determine the supported Al and Ni amounts on the particles. About 10 mg of the supported catalysts was dissolved with HF and HNO_3 acid on a hotplate. After a complete dissolution, the solution was diluted with distilled water and used for the ICP-MS analysis.

3.3.4 Ethylene Polymerizations

The high-pressure ethylene slurry polymerizations with homogeneous or supported DMN catalysts were conducted in a 1-liter Autoclave stainless steel reactor. The reactor was carefully cleaned with acetone, heated to 140 °C under vacuum for two hours, purged five times with UHP nitrogen, and then cooled down to room temperature. 400 ml toluene and required amount of MMAO solution were added into the reactor under nitrogen protection. The mixture was stirred for ten minutes while being heated up to the reaction temperature. The catalyst solution or suspension was then injected into the reactor; the system was stirred for ten minutes, and then pressurized to the desired ethylene pressure to start the polymerization. The reactor temperature was controlled at a set temperature within ±0.5 °C by water/ethylene glycol cool circulator. The reaction was stopped by venting the reactor and adding 20 ml of acetone. The polymer produced was filtered, washed with a large amount of methanol and then dried under vacuum at 50 °C overnight.

Polymerization with homogeneous DMN catalyst at 1 atm ethylene pressure was conducted in a 500 ml glass flask. 200 ml of toluene was added to the flame-dried flask under 1 atm of ethylene pressure at the set temperature maintained by an oil bath. Then a desired amount of MMAO (Al/Ni (mol) = 2000) solution was added under stirring. The polymerization was started by injecting the catalyst solution, and was terminated by venting the system and adding 20 ml of acetone. The polymer was precipitated, washed with methanol, and dried overnight at 50 °C under vacuum.

3.3.5 Polymer Characterizations

The DSC analysis was conducted using Thermal Analysis 2910 MDSC from TA Instruments in the standard DSC mode. UHP N_2 gas at a flow rate of 30 ml/min was purged through the calorimeter. A refrigerated cooling system (RCS) with the cooling capacity to 220 K was attached to the DSC cell. The temperature and heat capacity for the instrument were initially calibrated with indium standard at the heating rate of 10 °C/min. The polymer sample (about 5 mg) was first heated to 180 °C at the rate of 10 °C/min to remove thermal history. It was then cooled down to 0 °C at 5 °C/min. A second heating cycle was used for the acquisition of the DSC thermogram at the scanning rate of 10 °C/min. Polymer molecular weight (MW) and molecular weight distribution (MWD) were measured at 135 °C in 1,2,4-trichlorobenzene using Waters Alliance GPCV 2000 with DRI detector coupled with an in-line capillary viscometer. The polymer molecular weight was calculated according to a universal calibration curve based on polystyrene standards. 75.4 MHz ^{13}C NMR analysis was conducted on a Bruker AV300 pulsed NMR spectrometer with Waltz-supercycle proton decoupling at 120 °C. The polymer sample was dissolved in 1,2,4-trichlorobenzene and deuterated o-dichlorobenzene mixture in 10 mm NMR tubes with concentration about 20 wt%. At least 4000 scans were applied for each

acquisition to obtain a good signal-to-noise ratio. SEM study on polymer morphology was carried out on an Electroscan ESEM 2020 facility. EDX-TEM study on microtomed polymer samples was carried out on a JEOL 1200EX facility.

3.4 Results and Discussion

3.4.1 Characterization of the Mesoporous Particles

Three MCM-41 particles (MCM-41-A, MCM-41-B, MCM-41-C) and one MSF particle, different in nanopore size, particle size and morphology, were used as supports for the DMN catalyst in this work. Figure 3.1 shows the XRD spectra for the calcinated particles. Table 3.1 summarizes the particle morphological parameters, including specific surface area, average pore diameter, pore volume, and pore wall thickness, from the nitrogen adsorption-desorption and XRD analyses. All the particles have very high specific surface area (> 700 m^2/g), high pore volume (0.63 ~ 1.01 ml/g) and nano-range average pore diameter (2.1 ~ 4.5 nm). MCM-41-A, MCM-41-B and MSF have similar average pore diameters. However, the pore size of MCM-41-C is much bigger. All the particles have similar pore wall thickness. The XRD spectra show that these particles have quite uniform long-range ordered hexagonal nanotube structures. In addition to the main [100] diffraction, the higher order [110] and [200] diffractions are observable. Compared to the other three particles, MCM-41-A has a broader distribution of [100] diffraction, showing a broader pore size distribution.

The particles are also distinctively different from each other in particle size and morphology. Figure 3.2 shows their SEM photographs. MCM-41-A has

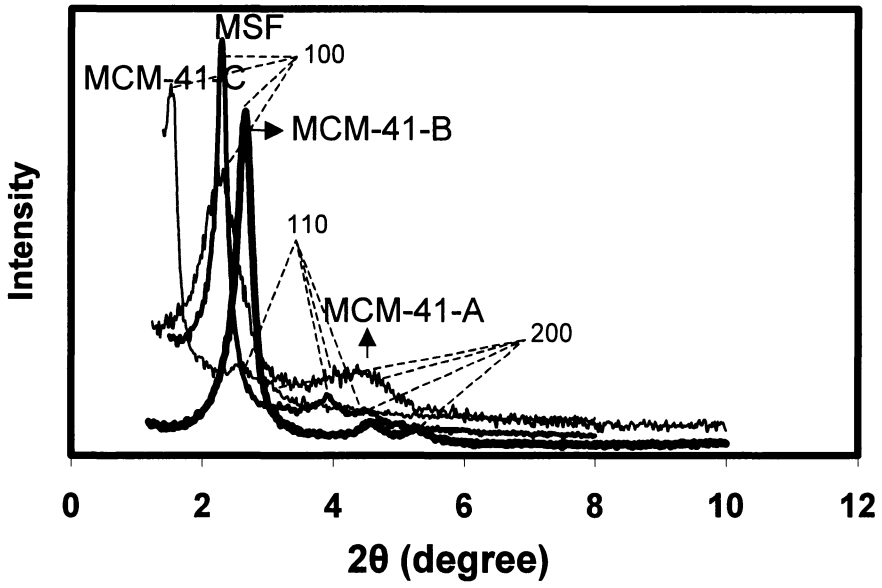

Figure 3.1 XRD spectra of the mesoporous particle samples used in this work as catalyst supports.

Table 3.1 Structural parameters for the mesoporous particles.

Support	S_{BET} (m^2/g)	d_p (Å)	V_p (ml/g)	d_{100} (Å)	a (Å)	b (Å)	Lc (μm)	Preparation Method
MCM-41-A	743.5	22.7	0.63	38.9	44.9	22.2	30	Ref. 20a
MCM-41-B	1231.6	21.4	1.01	33.3	38.5	16.8	1	Ref. 20b
MCM-41-C	829.0	45.1	0.95	55.9	64.5	19.4	15	Ref. 20c
MSF	952.3	27.0	0.80	38.4	44.3	17.3	350	Ref. 8a

S_{BET}: BET specific pore surface area.
d_p: average pore diameter, obtained from BJH adsorption data.
V_p: volume of pores.
d_{100}: XRD interplanar spacing.
a: distance between neighboring pore centers, $a = 2d_{100}/3^{1/2}$.
b: pore wall thickness, $b = a - d_p$.
Lc: characteristic nanotube length from SEM.

(a)

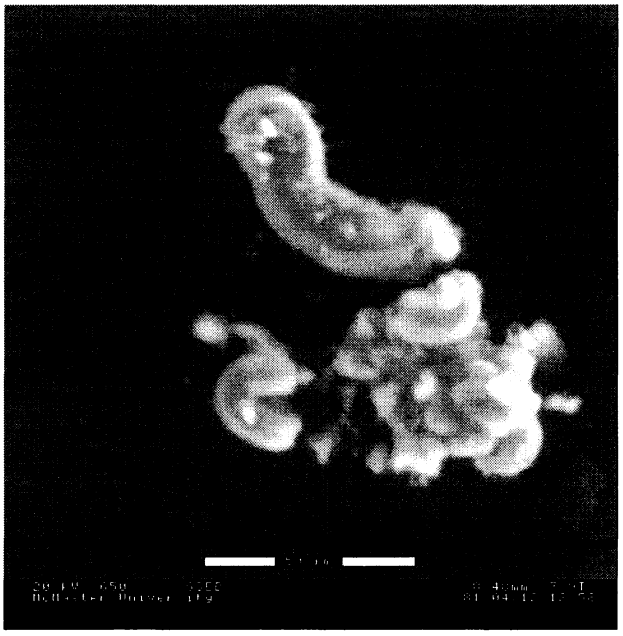

(b)

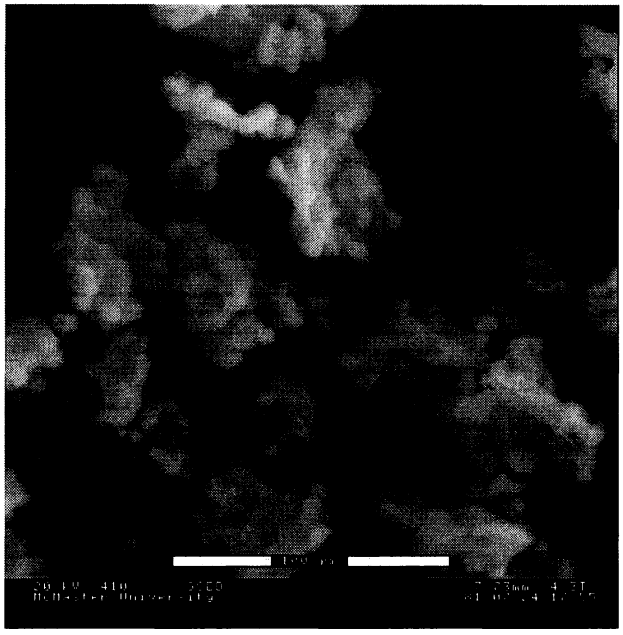

(c)

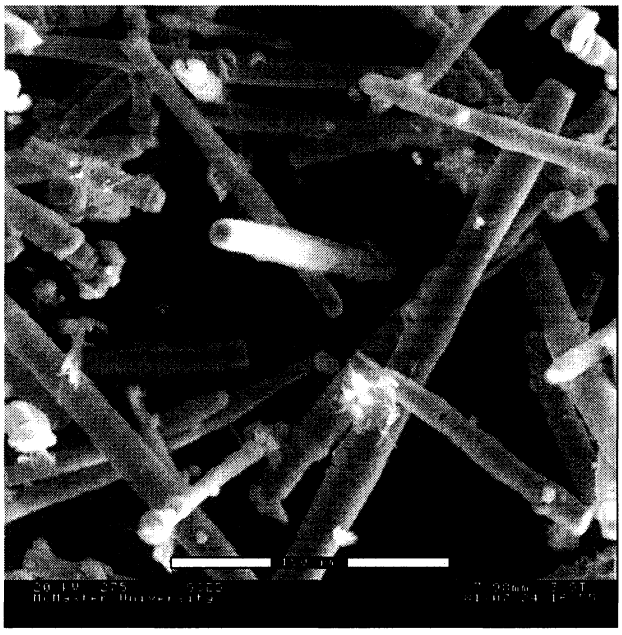

(d)

Figure 3.2 SEM photographs of the mesoporous particles: (a) MCM-41-A (scale bar: 50 μm); (b) MCM-41-B (scale bar: 15 μm); (c) MCM-41-C (scale bar: 100 μm); (d) MSF (scale bar: 150 μm).

curved tubular structure of about 10 ~ 50 μm in length (equivalent to nanotube length) and about 10 μm in diameter (each particle consists of thousands to millions nanotubes). MCM-41-B particles are loose agglomerates of about 15 μm consisting of many small tubular particles of about 1 μm diameter. Like MCM-41-B, MCM-41-C is also agglomerates of particles with sizes of about 15 μm. MSF has long-range highly ordered fiber structure with fiber lengths about 150 ~ 500 μm and fiber diameters in the range of 10 ~ 30 μm. The characteristic tube lengths for these materials are also summarized in Table 3.1. These long-range ordered fibers were demonstrated for applications as waveguide and laser materials.[8a,8b] A recent study on the internal structure of MSF showed that nanotubes inside the fiber were wound in a helical manner along the fiber axial direction.[8c] On the other side, the MCM-41 nanotubes run parallel to the axis.

3.4.2 Effect of Supporting Method on DMN Catalyst Impregnation

The supporting method has a significant effect on catalyst immobilization and characteristics of supported catalysts. There are three major supporting methods applicable for the immobilization of metallocene and other homogeneous catalysts.[6] They are: (a) direct impregnation of catalysts to support, (b) pretreatment of support with MAO or alkylaluminium followed by reaction with catalyst, and (c) immobilization of catalyst ligand on support followed by an addition of transitional metal salt. Different methods give supported catalysts different features due to different steric interaction between catalyst molecules and support surface. The effects of supporting methods on metallocene catalyst properties have been reviewed by Ribeiro et al.[6a] However, the effect of supporting method on Ni-Diimine catalyst impregnation has not yet been reported.

In this work, Methods (a) and (b) were employed and compared for the impregnation of DMN onto MCM-41-B. In MCM-Ni-a, DMN was directly impregnated on MCM-41-B. In MCM-Ni-b, MCM-41-B was pretreated with MMAO prior to the DMN impregnation. For comparison purposes, a metallocene catalyst, Cp_2TiCl_2, was also supported onto MCM-41-B by Method (a). Table 3.2 reports the ICP-MS results of for the supported catalysts. A much higher level (over ten times) of loaded DMN catalyst was obtained with Method (b) than with (a). Compared to Cp_2TiCl_2, the catalyst loading for MCM-Ni-a was also much lower.

Table 3.2 Effect of supporting method on the impregnation of DMN catalysts to MCM-41-B.

Catalyst system	Catalyst	Support	Ni or Ti load [a]	Al load [a]	Support method	Catalyst activity [b]
MCM-Ni-a	DMN	MCM-41-B	0.0184	-	A	41
MCM-Ni-b	DMN	MCM-41-B	0.217	2.71	B	8.0×10^3
MCM-Ti-a	Cp_2TiCl_2	MCM-41-B	0.143	-	A	-

[a] Loaded amounts of Ni or Ti and Al are in mmol of metal per gram of the supported catalyst system (including catalyst and support).

[b] Catalyst activity is in kg PE produced per mol-Ni per hour.
The polymerization conditions are: ethylene pressure, 200 psig; reaction temperature, 35 °C; reaction time, 1 hour; amount of supported catalyst system (including catalyst and support), MCM-Ni-a 0.11 g, MCM-Ni-b 0.017g, equivalent to the Ni contents of 2.0 μmol and 3.7 μmol, respectively; in 400 ml toluene; Al/Ni ratio, 2000 (molar).

The significant differences in the loaded amount are attributed to the different reactivities of DMN with the support surface. In Method (a), the supporting mechanism is believed to be through the reaction of DMN with residual hydroxyl groups on the dehydroxylated silica support surface. For metallocene catalysts, studies have shown that, in Method (a), metallocene reacts with hydroxyl on silica surface to form $=Si\text{-}OMClCp_2$, which is converted to a

catalytic species upon reacting with MAO. It has also been shown that the supported metallocene reactivity changes with metal center type in the order of $Cp_2HfCl_2 > Cp_2ZrCl_2 > Cp_2TiCl_2$.[21] The result of this work suggests that DMN has lower reactivity with hydroxyl on silica surface than Cp_2TiCl_2. For the MAO-mediated support system in Method (b), it was proposed that MAO molecules were chemically bonded to surface by reacting with hydroxyl groups.[22] This MAO-coated surface has a stronger Lewis acidity than the dehydroxylated surface and thus is more reactive toward DMN, resulting in the higher catalyst-loading amount on the support.

The supporting method not only affected the loading but also changed the characteristics of catalytic active centers. Ethylene polymerizations at 35 °C and ethylene pressure of 200 psig were conducted with both MCM-Ni-a and MCM-Ni-b catalysts. Significant differences in the catalyst activity were observed (see Table 3.2). MCM-Ni-a had a very low activity, accounting only 0.5 % of that of MCM-Ni-b. This extremely low activity of MCM-Ni-a reflects that the reaction of DMN with hydroxyl groups on support surface yielded active sites with much lower ethylene incorporation ability, possibly due to steric and/or electronic effects exerted by the surface. However, for MCM-Ni-b, the active sites more likely floated over MAO-coated surface with less surface constraints and exhibited more similarity to a homogeneous system, as suggested by Chien et al for zirconocene catalysts supported on MAO-treated silica.[23]

3.4.3 Effect of Particle Structure on Catalyst Impregnation

The parallel nanotube structure with uniform and controllable pore size makes the particle an excellent model system to study the effects of particle structure, such as nanotube diameter and length, on catalyst impregnation. In this work, the DMN catalyst was impregnated onto the four mesoporous supports with

Method (b). Table 3.3 compares the ICP-MS data of the Ni and Al loading amounts for these supported catalysts. The result shows a strong dependence of the catalyst and MMAO impregnation on the support structure. A significantly higher amount of MMAO loading was observed with the MCM-41-C. The MMAO loading increased in the order of MCM-41-A < MCM-41-B < MSF < MCM-41-C. However, a much lower DMN loading was found with MSF. The DMN loading increased in the order of MSF < MCM-41-A < MCM-41-C < MCM-41-B.

The different loading amounts of MMAO and DMN in the four supports can be related to diffusion limitations during the catalyst impregnation that is a molecular diffusion process inside the nanotubes. Different tube diameters and lengths yield different levels of diffusion resistance. Larger diameter and shorter length favor diffusion and thus favor the impregnation of MMAO and DMN. The nanotube channels of the MCM-41 and MSF particles are one-dimensional. The impregnation process of the MMAO and DMN molecules in these channels can be considered as diffusion into a planar substrate with the channel length (i.e., particle size for MCM-41 and fiber length for MSF) as the characteristic length L_c. The diffusion resistance is inversely proportional to D/L_c, where D is an effective molecular diffusivity.[24] For a molecule of diameter d_m inside a mesopore of diameter d_p in liquid, D is related to the ratio $\lambda = d_m/d_p$ and the molecular diffusivity in bulk liquid D_m such as $D/D_m = \exp(-4.6\lambda)$.[24]

Based on the reported crystallographic studies on the molecular structures of some Ni-Diimine complexes [2d, 25], we estimate the molecular diameter of DMN about 1 nm. The effective diffusivity for DMN in the nanotube can be calculated by $D/D_m = \exp(-4.6\lambda)$.[24] MMAO has a more complicated oligomeric structure. Studies on the structure of MAO, $[\text{-Al(Me)-O-}]_n$, suggested that the MAO molecules could be one-dimensional linear chains or cyclic ring three-

dimensional cage structure with n ≈ 5-20 [26]. Based on the work by Sano and co-workers on the adsorptive separation of MAO by MCM-41 [27], we estimate the molecular diameter of MMAO approximately 2 nm. For the molecules having sizes in this range, their effective diffusivities in mesopores are more accurately described by $D/D_m = 0.984((1-\lambda)/\lambda)^{5/2}$.[24]

Table 3.3 Effect of particle structure on the impregnation of DMN catalysts with Method (b).[a]

Catalyst system	Support	Ni Load [b]	Al Load [c]	Al/Ni molar ratio [d]
MCM-Ni-1	MCM-41-A	0.156±0.010	1.76±0.23	11.3
MCM-Ni-2	MCM-41-B	0.200±0.020	2.55±0.16	12.8
MCM-Ni-3	MCM-41-C	0.165±0.012	4.56±0.17	27.6
MSF-Ni	MSF	0.0643±0.014	2.93±0.14	45.6

[a] Two impregnation runs were repeated for each support.
[b] Loaded Ni amount in [mmol/(g supported catalyst system)].
[c] Loaded Al amount in [mmol/(g supported catalyst system)].
The supported catalyst system includes supported catalyst and the MMAO-treated support.
[d] Calculated based on the average Ni and Al loads.

Table 3.4 Effect of support structure on diffusion parameters of MMAO and DMN.

supports	d_p (nm)	L_c (μm)	MMAO, d_m = 2 nm			DMN, d_m = 1 nm		
			λ (d_m/d_p)	D/D_m [a]	$(D/D_m)/L_c$ (μm^{-1})	λ (d_m/d_p)	D/D_m [b]	$(D/D_m)/L_c$ (μm^{-1})
MCM-41-A	2.27	30	0.881	0.00660	0.00022	0.441	0.132	0.00440
MCM-41-B	2.14	1	0.935	0.00125	0.00125	0.467	0.117	0.117
MCM-41-C	4.51	15	0.443	1.74	0.116	0.221	0.361	0.024
MSF	2.70	350	0.741	0.0711	0.000203	0.370	0.182	0.00052

[a] Calculated according to $D/D_m = 0.984((1-\lambda)/\lambda)^{5/2}$.
[b] Calculated according to $D/D_m = \exp(-4.6\lambda)$.

Table 3.4 shows the diffusion resistance parameter $(D/D_m)/L_c$ for the MMAO and DMN molecules in the four different supports. This model provides good explanation for the high MMAO loading on MCM-41-C and the low DMN loading on MSF. The diffusion resistance for DMN increases in the order of MCM-41-B < MCM-41-C < MCM-41-A < MSF, which is consistent with the amount of DMN loaded on the supports. However, the order of diffusion resistance for MMAO is MCM-41-C < MCM-41-B < MCM-41-A ~ MSF, which does not fully agree with the MMAO loading, particularly for MSF probably due to the complicated molecular structure and broad molecular size distribution of MMAO.

3.4.4 Effect of Support on Ethylene Polymerization Activity

To evaluate the performance of supported catalysts and to provide a reference to show the effect of support on the polymerization behavior and polymer chain structure, ethylene polymerizations using homogeneous DMN catalysts were conducted under various reaction conditions. Table 3.5 shows the polymerization results and polymer properties. The catalyst activity at low ethylene pressure was comparable to the literature data; however, it was lower at high pressure.[2d] The melting points were very close to those reported in the literature.[2d] With the increase of ethylene pressure and decrease of reaction temperature, the melting point tended to increase, exhibiting a trend of the reduction of short chain branches due to the competition between chain walking and chain propagation processes. There was no clear trend in the change of polyethylene molecular weight with ethylene pressure. Increase in temperature decreased the catalyst activity due to deactivation as reported by Brookhart et al.[2d] The polymer molecular weight also decreased at high temperature, due to higher chain transfer rates.

Table 3.5 Ethylene polymerization using homogeneous Ni-Diimine catalysts.[a]

Run	Catalyst (Ni-μmol)	Pressure (psig)	Temp (°C)	Time (min)	Activity [b]	Mn (kg/mol)	PDI	Tm (°C)
1	1.6	15	35	30	4.56	155.2	2.0	-
2	2.0	50	35	20	8.25	131.4	3.1	80
3	1.0	100	35	10	14.8	178.2	2.4	85
4	1.1	100	45	30	23.1	123.4	2.4	76
5	2.0	100	55	30	12.5	103.7	2.4	61
6	1.0	200	35	10	29.5	254.8	2.4	111
7	1.0	200	45	10	26.4	166.3	2.6	99
8	1.0	200	55	10	6.48	137.1	2.4	85
9	1.1	400	35	10	59.3	181.8	2.3	121

[a] Al(MMAO)/Ni molar ratio, 3500; solvent, toluene 400 ml.
[b] In 10^3 kgPE/(mol-Ni hr).

Table 3.6 presents the ethylene polymerization results with DMN supported on the nanotube particles. Compared to the homogeneous catalyst counterparts, significant reductions in the catalyst activity were observed for all the supported systems under the same reaction conditions. The activity for a supported catalyst system was about 10 ~ 30 % of that of the corresponding homogeneous system. The significant activity reduction is a common phenomenon for supported catalyst systems and is believed to be due to steric effects exerted by support on catalyst active centers, which limit the monomer incorporation ability. The activity ratios between the supported and homogeneous systems are very similar to those of metallocene systems. Like the homogeneous system, an increase in temperature lowered the polymerization activity for the supported catalysts due to deactivation.

Figure 3.3 compares the polymerization activities for the four supported catalysts at 35 °C and various ethylene pressures. There was no obvious activity difference between the big pore sized MCM-Ni-3 and the small pore sized MCM-

Ni-1 and MCM-Ni-2 samples, indicating that the nanopore size had no significant effect on the diffusion limitations of small ethylene molecules inside the nanopores. Surprisingly, a much lower activity, about half of those observed in the MCM-41 supported catalyst systems, was found for the MSF supported catalysts. This significant activity drop is believed to be due to ethylene diffusion limitations in the much longer MSF nanotubes, where the produced polymer chains might block ethylene diffusion. In addition, the much higher Al/Ni ratio in this supported catalyst (Table 3.3) may influence the catalyst activity and leads to pore blocking by MMAO.

Table 3.6 Ethylene polymerization using supported catalysts.[a]

Run	Catalyst and charge	P (psig)	T (°C)	t (min)	Activity [b]	Mn (kg/mol)	PDI	Tm (°C)
1	MCM-Ni-1, 31.3 mg	50	35	30	2.04	133.7	3.1	82, 118
2		100	35	30	3.66	162.0	2.9	99
3		100	55	30	2.19	96.9	3.2	63, 128
4		200	35	60	5.34	179.9	2.8	111, 117
5		200	55	30	2.19	140.9	2.5	82, 116
6		400	35	30	5.40	320.4	2.8	121
7	MCM-Ni-2, 17 mg	50	35	60	1.74	150.2	2.3	76
8		100	35	60	3.64	182.6	3.0	96
9		100	55	30	3.30	106.9	2.2	64
10		200	35	60	8.00	264.3	2.4	111
11		200	55	30	2.13	132.4	2.3	82
12		400	35	30	7.53	232.1	2.6	121
13	MCM-Ni-3, 31.7 mg	50	35	30	2.32	139.0	3.2	73
14		100	35	30	4.39	175.0	2.6	100
15		100	55	30	1.80	118.3	2.7	62
16		200	35	30	5.67	174.5	4.9	111
17		200	55	30	1.98	131.6	2.9	82
18	MSF-Ni, 0.102 g	50	35	30	1.02	161.2	3.0	85, 113
19		100	35	30	1.98	197.1	3.3	99, 115
20		100	55	30	0.568	108.0	2.5	62, 117
21		200	35	30	3.57	199.8	4.0	110
22		200	55	30	0.744	205.9	5.2	82, 121

[a] Al(MMAO)/Ni molar ratio, 2000; solvent, toluene 400 ml.
[b] In 10^3 kgPE/(mol Ni*hr).

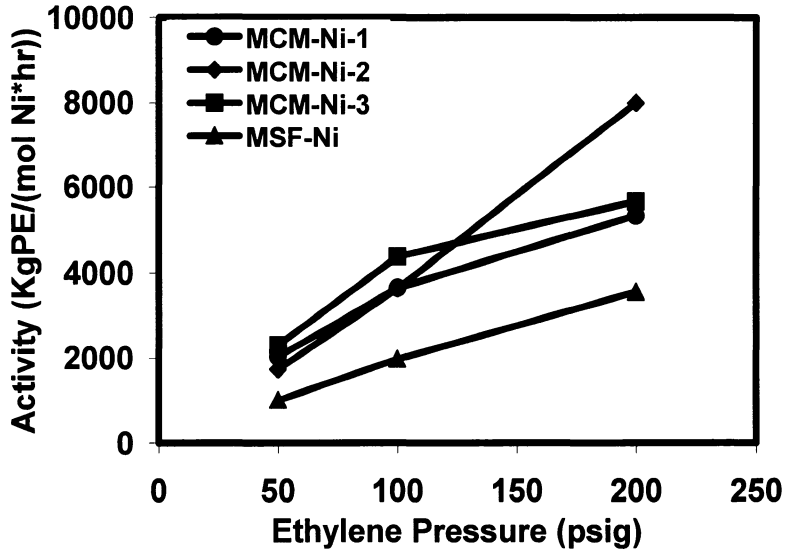

Figure 3.3 Ethylene polymerization activity with the mesoporous particle-supported DMN catalysts at 35 °C and different ethylene pressures. Refer to Table 3.4 for the polymerization conditions.

3.4.5 Effects of Support on Polymer Properties

In a recent patent by Exxon [16c] on ethylene polymerization using silica-supported Ni-Diimine catalysts, the reduction in polymer molecular weight was observed. However, in this work, as shown in Table 3.6, there was no clear trend of change in molecular weight compared to the homogeneous systems. However, broadening of the molecular weight distributions was evident with the supported catalyst systems. A PDI of 5.7 was observed in the MSF supported system.

The chain walking mechanism appeared to be present in the supported systems. Similar to the homogeneous catalysts, the melting points of the polymers produced with the supported systems increased with the increase of ethylene pressure and the decrease of reaction temperature through the competition of propagation versus chain walking. However, the melting

behaviors were very different. Figure 3.4 compares the DSC thermograms of the polyethylene samples prepared at ethylene pressure of 100 psig and temperature of 55 °C. Interestingly, a bimodal melting behavior was observed in the thermograms for the polymers produced with MCM-Ni-1 and MSF-Ni systems. The melting point data are presented in Table 3.6. The melting temperature is related to the short chain branch density. Increasing short chain branch density decreases lamellar thickness of crystal structure and thus lowers melting temperature.

The bimodal melting behavior shows that the polymer sample was a mixture of two chain populations having different short chain branch densities. In the MCM-Ni-1 polymer, the lower melting temperature region centered at 63 °C, being very close to the melting point (61 °C) of the polymers produced with the homogeneous DMN catalyst. These are the chains having high short chain branch densities. The higher melting region centered at 128 °C, corresponding to the chains having much fewer short-chain branches (as a reference, Tm = 121° C for the polymer sample produced with the homogeneous catalyst system at 400 psig and 35 °C). However, the mass fraction of the high Tm chains was small. There were no significant differences in the short chain branch densities among the samples prepared with MCM-Ni-1, MSF-Ni, and homogeneous DMN catalysts. Table 3.7 presents the short chain branch distributions of the samples.

The bimodal melting behavior was also observed in the polymers produced under some other reaction conditions (see Figures 3.5 and 3.6) with MCM-Ni-1 and MSF-Ni supported catalysts. A common feature was that the lower melting temperature in the bimodal thermogram was always similar to that of the homogeneous catalyst under the same polymerization conditions. This

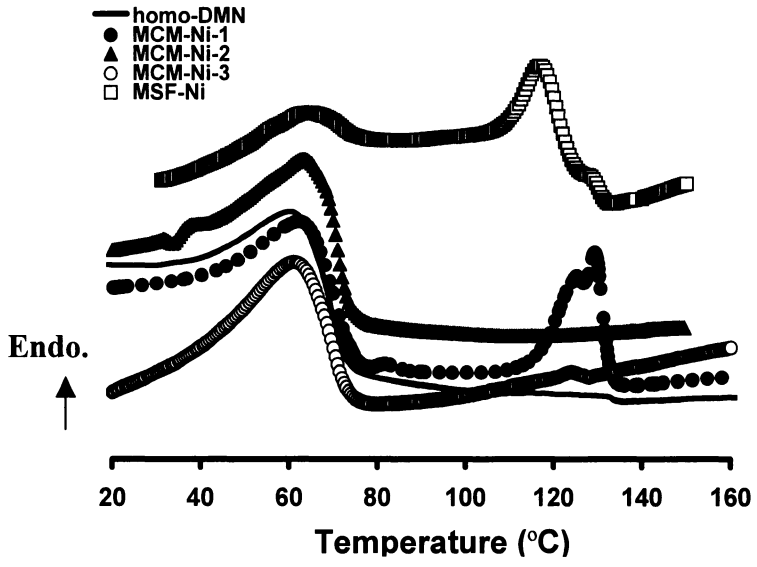

Figure 3.4 DSC thermograms for the polymers produced with homogeneous and supported catalysts at ethylene pressure of 100 psig and reaction temperature of 55 °C.

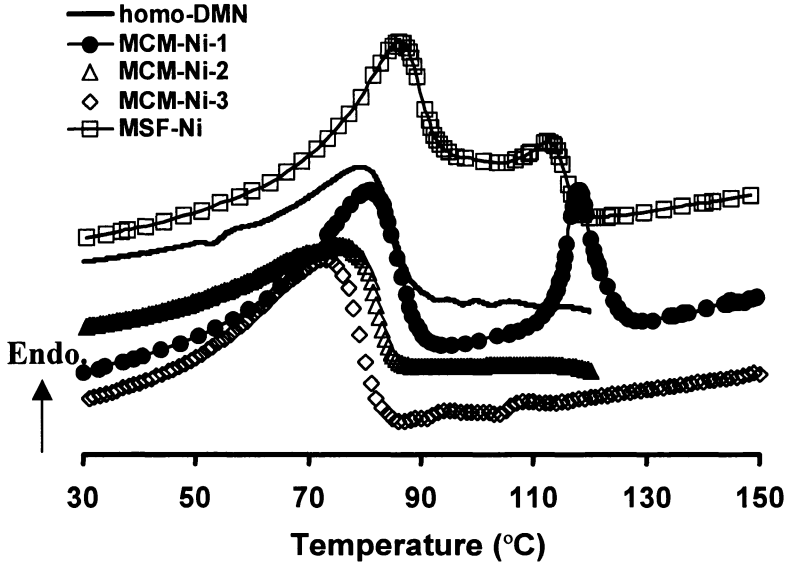

Figure 3.5 DSC thermograms for the polymers produced with homogeneous and supported catalysts at ethylene pressure of 50 psig and reaction temperature of 35 °C.

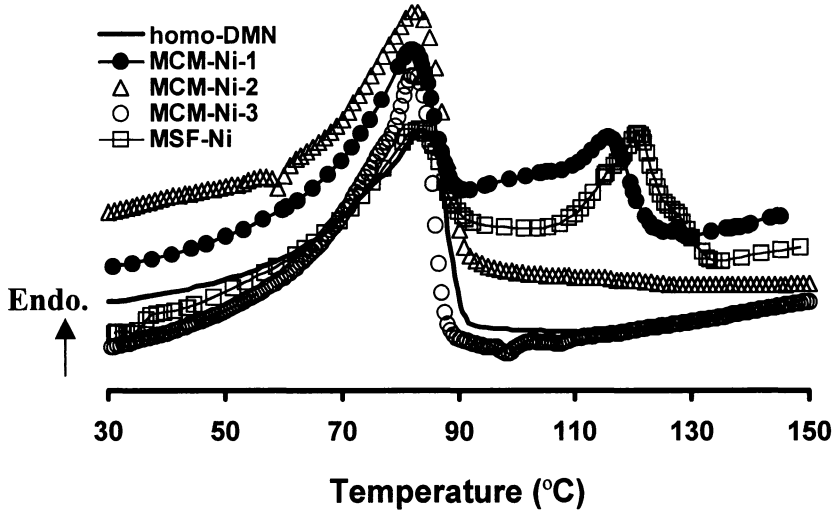

Figure 3.6 DSC thermograms of the polymers produced with homogeneous and supported catalysts at ethylene pressure of 200 psig and reaction temperature of 55 °C.

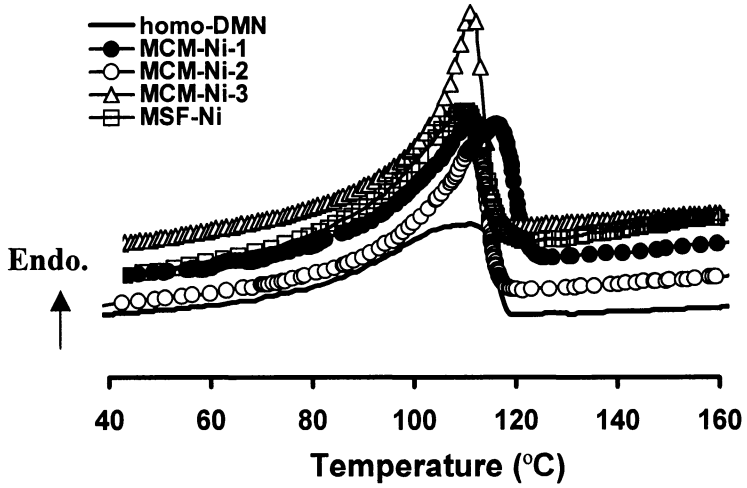

Figure 3.7 DSC thermograms of the polymers produced with homogeneous and supported catalysts at ethylene pressure of 200 psig and reaction temperature of 35 °C.

fraction of chain population was probably generated from the active sites extracted from the support during polymerization. The higher melting temperature was in the range of 113 ~ 128 °C and had no clear dependence on the reaction condition. This chain fraction was produced by the unleached active sites. The unleached active sites, due to the strong steric effects exerted by the support, exhibited lower chain-walking rates and therefore produced chains having lower branch density and thus higher melting point. Similar bimodal melting behavior was also observed with other supported systems.[17]

Table 3.7 Short chain branch densities (per 1000 carbons) for polyethylene produced at 100 psig and 55 °C.

Catalyst	Methyl	Ethyl	Propyl	Butyl	Pentyl	Hexyl+	Total
Homo-DMN	45.9	4.9	2.7	2.3	2.1	5.9	63.8
MCM-Ni-1	42.1	4.0	2.7	2.5	2.0	5.0	58.3
MCM-Ni-2	41.7	4.8	3.0	2.7	2.4	5.8	60.4
MCM-Ni-3	41.6	4.8	2.8	2.3	2.2	5.5	59.2
MSF-Ni	45.9	4.5	3.0	2.3	2.1	5.9	63.7

The bimodal melting behavior was not observed with the polymer samples prepared by MCM-Ni-2 and MCM-Ni-3 catalysts. These supports had shorter nanotube length and/or bigger pore size, and thus more significant leaching. The polymers produced by these two supported catalysts had similar thermograms as those with homogeneous catalysts, although the ^{13}C NMR analysis (see Table 3.7) showed that these samples had slightly lower short chain branch densities.

Despite the extraction of active sites during polymerization, morphological replication of the supports was observed in the produced polymers. Figure 3.8 shows some SEM pictures of samples prepared at 100 psig and 55 °C.

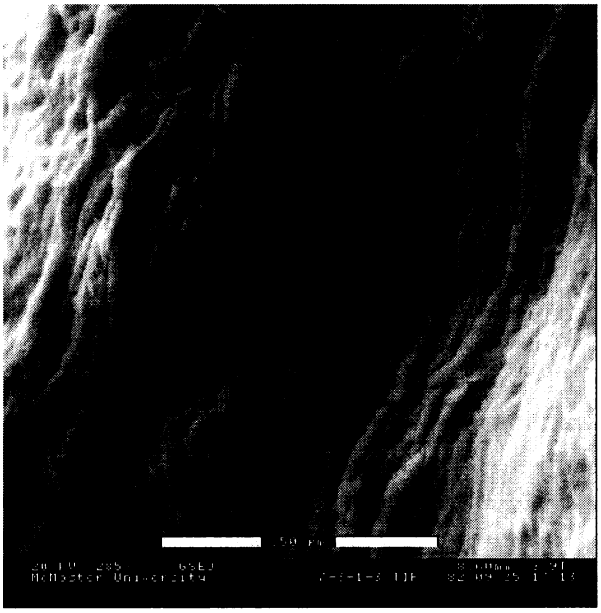

(a)

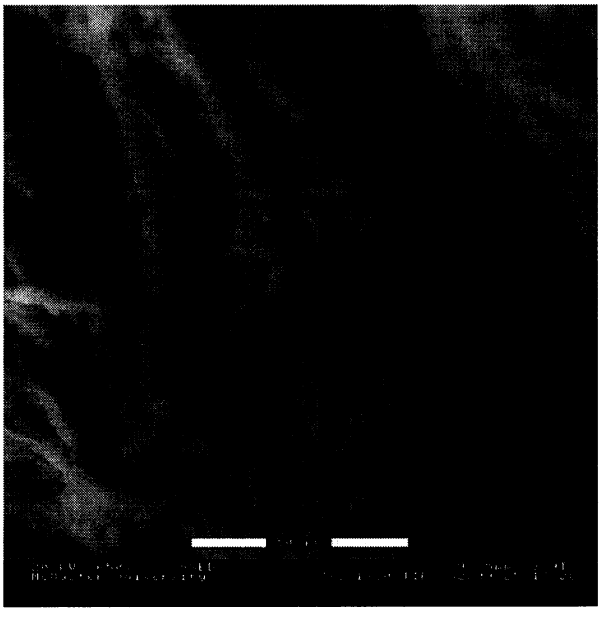

(b)

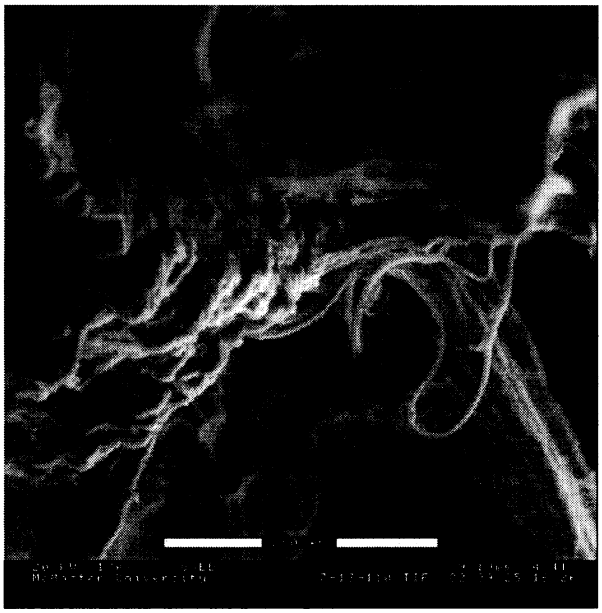

(c)

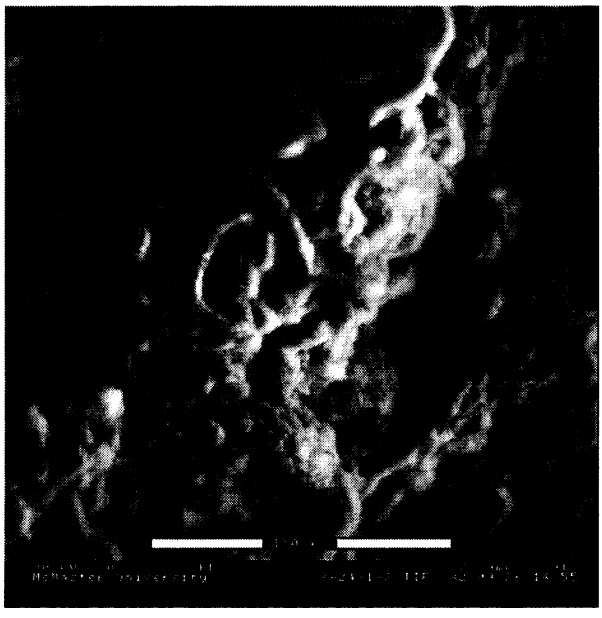

(d)

(e)

Figure 3.8 SEM photographs of the polymers produced at 100 psig and 55 °C: (a) Run 3 with MCM-Ni-1 (scale bar: 150 μm); (b) Higher magnification of (a) (scale bar: 50 μm); (c) Run 9 with MCM-Ni-2 (scale bar: 250 μm); (d) Run 15 with MCM-Ni-3 (scale bar: 150 μm); (e) Run 20 with MSF-Ni catalysts (scale bar: 250 μm).

The polymer particles have morphologies resembling their corresponding supports. These particles are totally different from the spherical morphologies produced with an in-situ supported DMN/MAO catalyst system reported in the literature.[17] However, there were no individual polymer particles found in all the samples produced in this work. The particles were all agglomerated together. Similar replications were also observed in the polymer samples produced under the conditions of 50 psig / 35 °C, 100 psig / 35 °C, and 200 psig / 55 °C with all the four supported catalyst systems.

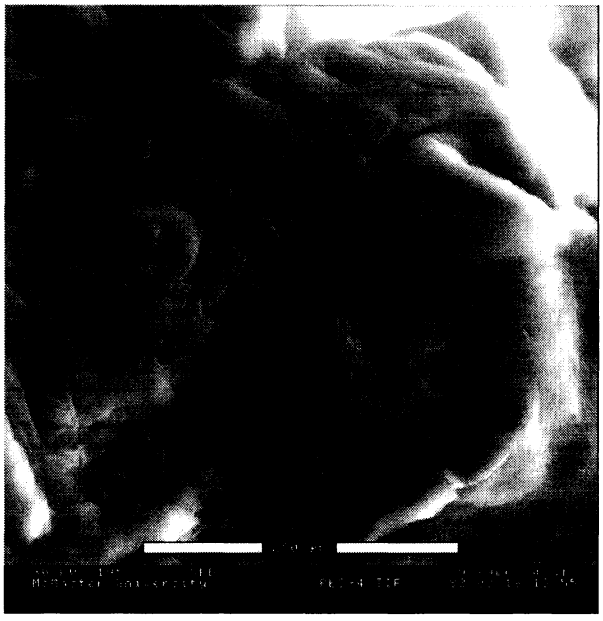

Figure 3.9 SEM photograph of the polymer produced in Run 21 with MSF-Ni catalyst (scale bar: 250 μm)

Figure 2.10 TEM photograph of the polymer produced in Run 21 with MSF-Ni catalyst (scale bar: 0.2 μm), showing a silica fragment (dark area).

In addition to the pore size and particle size, polymerization conditions also affected the chain structure. The bimodal melting behavior was observed for all the polymers with MSF-Ni except for Run 21. The Run 21 sample had a very similar thermogram as the homogeneous catalyst. A similar observation was made for MCM-Ni-1 in Run 6. These results suggest that active site extraction was more complete in these runs. Moreover, the polymer morphology was also very different. Figure 3.9 shows a SEM image of the polymer produced in run 21. There is no replication of the support morphology. Similar morphology was found for the polymer produced in Run 6. These exceptions may be related to the high polymer productivities due to higher ethylene concentrations at these conditions (200 psig/ 35 °C, 400 psig / 35 °C).

An important phenomenon in olefin polymerization with supported catalysts is the fragmentation of catalyst particle during polymerization due to the hydraulic force caused by fast polymer growth.[6d] The degree of fragmentation is related to the support structure and polymer productivity. The higher porosity and thinner pore wall of the support and the higher polymer productivity will make the catalyst readily undergo fragmentation. An EDX-TEM study was conducted on the polymer produced in Run 21. Irregular silica fragments with sizes around 1 μm were found widely dispersed in the polymer bulk. Figure 3.10 shows one TEM picture of a silica fragment.

3.5 Conclusion

Mesoporous particles, including MCM-41 and MSF, with different geometric parameters, such as pore size and particle size, were used as support for a nickel-Diimine catalyst (DMN, 1,4-bis(2,6-diisopropylphenyl)acenaphthene Diimine nickel(II) dibromide). This study showed that pretreating the supports

with MMAO prior to the DMN impregnation yielded high catalyst loading and high ethylene polymerization activity. The particle parameters strongly affect the catalyst impregnation. Ethylene polymerization was carried out with the particle-supported DMN catalysts. A significant reduction in catalyst activity was observed with the supported systems compared to their homogeneous counterparts. Extraction of the active site from the supports was observed during polymerization. The unleached active sites exhibited much lower chain walking ability and produced polymers with fewer short chain branches. This active site extraction was also related to the mesoporous particle structure and polymerization conditions. Replication of support morphology was found in the polymers produced at some conditions.

3.6 Reference

1. Kaminsky, W.; Arndt, M. *Adv. Polym. Sci.* **1997**, *127*, 143.
2. (a) Ittel, S. D.; Johnson, L. K.; Brookhart, M. *Chem. Rev.* **2000,** *100*, 1169. (b) Johnson, L. K.; Killian, C. M.; Brookhart, M. *J. Am. Chem. Soc.* **1995**, *117*, 6414. (c) Killian, C. M.; Tempel, D. J.; Johnson, L. K.; Brookhart, M. *J. Am. Chem. Soc.* **1996**, *118*, 11664. (d) Gates, D. P.; Svejda, S. A.; Oñate, E.; Killian, C. M.; Johnson, L. K.; White, P. S.; Brookhart, M. *Macromolecules* **2000**, *33*, 2320.
3. (a) McLain, S. J.; McCord, E. F.; Johnson, L. K.; Ittel, S. D.; Nelson, L. T. J.; Arthur, S. D.; Halfhill, M. J.; Teasley, M. F.; Tempel, D. J.; Killian, C.; Brookhart, M. S. *Polym. Prepr. (Am. Chem. Soc., Div. Polym. Chem.)* **1997**, *38*, 772. (b) Galland, G. B.; de Souza, R. F.; Mauler, R. S.; Nunes, F. F. *Macromolecules* **1999**, *32*, 1620. (c) Jurkiewicz, A.; Eilerts, N. W.; Hsieh, E. T. *Macromolecules* **1999**, *32*, 5471.

4. (a) Guan, Z.; Cotts, P. M.; McCord, E. F.; McLain, S. J. *Science* **1999**, *283*, 2059. (b) Cotts, P. M.; Guan, Z.; McCord, E.; McLain, S. *Macromolecules* **2000**, *33*, 6945.
5. (a) Pappalardo, D.; Mazzeo, M.; Pellecchia, C. *Macromol. Rapid Commun.* **1997**, *18*, 1017. (b) Simon, L. C.; Mauler, R. S.; de Souza, R. F. *J. Polym. Sci., Part A: Polym. Chem.* **1999**, *37*, 4656.
6. Some recent review papers about supported catalysts, see: (a) Ribeiro, M. R.; Deffieux, A.; Portela, M. F. *Ind. Eng. Chem. Res.* **1997**, *36*, 1224. (b) Abbenhuis, H. C. L. *Angew. Chem. Int. Ed.* **1999**, *38*, 1058. (c) Hlatky, G. G. *Chem. Rev.* **2000**, *100*, 1347. (d) Fink, G.; Steinmetz, B.; Zechlin, J.; Przybyla, C.; Tesche, B. *Chem. Rev.* **2000**, *100*, 1377.
7. (a) Kresge, C. T.; Leonowicz, M. E.; Roth, W. J.; Vartuli, J. C.; Beck, J. S. *Nature* **1992**, *359*, 710. (b) Beck, J. S.; Vartuli, J. C.; Roth, W. J.; Leonowicz, M. E.; Kresge, C. T.; Schmitt, K. D.; Chu, C. T. W.; Olson, D. H.; Sheppard, E. W.; McCullen, S. B.; Higgins, J. B.; Schlenker, J. L. *J. Am. Chem. Soc.* **1992**, *114*,10834.
8. (a) Huo, Q.; Zhao, D.; Feng, J.; Weston, K.; Buratto, S. K.; Stucky, G. D.; Schacht, S.; Schüth, F. *Adv. Mater.* 1997, *9*, 974. (b) Marlow, F.; McGehee, D.; Zhao, D.; Chmelka, B.; Stucky, G. *Adv. Mater.* **1999**, *11*, 632. (c) Marlow, F.; Spliethoff, B.; Tesche, B.; Zhao, D. *Adv. Mater.* **2000**, *12*, 961.
9. (a) Ko, Y. S.; Han, T. K.; Park, J. W.; Woo, S. I. *Macromol. Rapid Commun.* **1996**, *17*, 749. (b) Ko, Y. S.; Woo, S. I. *Macromol. Chem. Phys.* **2001**, *202*, 739.
10. (a) Tudor, J.; O'Hare, D. *Chem. Commun.* **1997**, 603. (b) O'Brien, S.; Tudor, J.; Maschmeyer, T.; O'Hare, D. *Chem. Commun.* **1997**, 1905.
11. (a) Van Looveren, L. K.; Geysen, D. F.; Vercruysse, K. A.; Wouters, B. H.; Grobet, P. J.; Jacobs, P. A. *Angew. Chem. Int. Ed.* **1998**, *37*, 517. (b) Van

Looveren, L. K.; De Vos, D. E.; Vercruysse, K. A.; Geysen, D. F.; Janssen, B.; Jacobs, P. A. *Catal. Lett.* **1998**, *56*, 53.

12. Rahiala, H.; Beurroies, I.; Eklund, T.; Hakala, K.; Gougeon, R.; Trens, P.; Rosenholm, J. B. *J. Catal.* **1999**, *188*, 14.
13. Kageyama, K.; Tamazawa, J.; Aida, T. *Science*, **1999**, *285*, 2113.
14. (a) Rao, R. R.; Weckhuysen, B. M.; Schoonheydt, R. A. *Chem. Commun.* **1999**, 445. (b) Weckhuysen, B. M.; Rao, R. R.; Pelgrims, J.; Schoonheydt, R. A.; Bodart, P.; Debras, G.; Collart, O.; Van Der Voort, P.; Vansant, E. F. *Chem. Eur. J.* **2000**, *6*, 2960.
15. Kaminsky, W.; Strűbel, C.; Lechert, H.; Genske, D.; Woo, S. I. *Macromol. Rapid. Commun.* **2000**, *21*, 909.
16. (a) Sugimura, K.; Yorozu, K.; Suzuki, Y.; Hayashi, T. JP Patent 09278821, April 8, 1996. (b) Sugimura, K.; Yorozu, K.; Suzuki, Y.; Hayashi, T. JP Patent 09278822, April 8, 1996. (c) Vaughan, G. A.; Canich, J. A. M.; Matsunaga, P. T.; Gindelberger, D. E.; Squire, K. R. WO Patent Application 9748736, June 17, 1996. (d) MacKenzie, P. B.; Moody, L. S.; Killian, C. M.; Lavoie, G. G. WO Patent Application 9962968, Jan 22, 1998.
17. Simon, L. C.; Patel, H.; Soares, J. B. P.; de Souza, R. F. *Macromol. Chem. Phys.* **2001**, *202*, 3237.
18. Preishuber-Pflugl, P., Brookhart, M. *Macromolecules* **2002**, *35*, 6074.
19. Bennett, A. M. A.; McLain, S. J. WO Patent Application 9856832, June 9, 1997.
20. (a) Mokaya, R.; Zhou, W.; Jones, W. *Chem. Commun.* **1999**, 51. (b) Cai, Q.; Lin, W.-Y.; Xiao, F.-S.; Pang, W.-Q.; Chen, X.-H.; Zou, B.-S. *Microporous and Mesoporous Mater.* **1999**, *32*, 1. (c) Sayari, A.; Liu, P.; Kruk, M.; Jaroniec, M. *Chem. Mater.* **1997**, *9*, 2499.
21. Dufrenne, N. G.; Blitz, J. P.; Meverden, C. C. *Microchem. J.* **1997**, *55*, 192.

22. (a) Soga, K.; Nakatani, H. *Macromolecules* **1990**, *23*, 957. (b) Soga, K.; Kaminska, M. *Makromol. Chem. Rapid Commun.* **1992**, *13*, 221.
23. Chien, J. C.; He, D. *J. Polym. Sci. Part A: Polym. Chem.* **1991**, *29*, 1603.
24. Karger J, Ruthven DM. Diffusion in Zeolite and other Microporous Solids. New York: Wiley, 1992 (chapter 11).
25. Liimatta, J. O.; Lőfgren, B.; Miettinen, M.; Ahlgren, M.; Haukka, M.; Pakkanen, T. T. *J. Polym. Sci., Part A: Polym. Chem.* **2001**, *39*, 1426.
26. Chen, E. Y.-X.; Marks, T. J. *Chem. Rev.* **2000**, *100*, 1391.
27. Sano, T.; Doi, K.; Hagimoto, H.; Wang, Z.; Toshiya, U.; Soga, K. *Chem. Commun.* **1999**, 733.

Chapter 4

Structure and Rheological Properties of Branched Polyethylenes Produced with Pd and Ni-Diimine Catalysts

This chapter is organized based on the paper published in *Macromolecules*, **2003**, *36*, 2194-2197 by Z. Ye and S. Zhu and the paper published in *Macromolecular Chemistry and Physics*, **2004**, *205*, 897-906 by Z. Ye, F. AlObaidi, and S. Zhu.

4.1 Abstract

Seven branched polyethylenes differing in chain topology and branch structure were synthesized with chain walking Pd-Diimine catalyst, [(ArN=C(Me)-C(Me)=NAr) $Pd(CH_3)(NCMe)]SbF_6$ (**1**), and Ni-Diimine catalyst, (ArN=C(An)-C(An)=NAr) $NiBr_2$ (**2**) /MMAO, respectively. In addition to polymer structural and topological characterizations with DSC, ^{13}C NMR, and GPC-VIS, the first extensive rheological study, employing steady-shear, creep-recovery, and dynamic oscillation tests, was conducted to examine and compare the melt rheological properties of this novel series of polymers. It was found that the change of chain topology from hyperbranched to linear structure dramatically affected the polymer flow behavior, flow activation energy, and dynamic moduli (G'(ω), G"(ω)). The two hyperbranched polymers (Samples 1 and 2) exhibited typical Newtonian flow behavior and extremely low viscosity owing to their compact globular structure. The other five polymers (Samples 3 ~ 7) with chain topology intermediate between hyperbranched and linear structures, however, were essentially viscoelastic materials containing chain entanglements. All the polymers obeyed the time-temperature superposition and exhibited enhanced flow

activation energy (43.8 ~ 57.2 kJ/mol) compared to HDPE and LLDPE. In the terminal region, these polymers had different dependencies of dynamic moduli (G'(ω), G"(ω)) on angular frequency (ω) and different master curves in the logG' vs. logG" plot depending on the chain topology and branching structure. The plateau modulus (G_N^0) at 60 °C and the average entanglement molecular weight (M_e) for Samples 6 and 7 were determined. The hyperbranched polymer (Sample 2) was also blended with more linear Sample 4 as a rheology modifier and was found to be able to significantly lower the viscosity of the blends.

Keywords: rheology, polyethylene, chain walking polymerization, chain topology, hyperbranched polymer, dynamic moduli, flow activation energy, Newtonian flow behavior, shear-thinning, chain entanglement, structure property relationship.

4.2 Introduction

The latest developments in catalysis of ethylene polymerization have offered unprecedented freedom in controlling polymer chain structure and tailoring material properties. With the homogeneous single-site catalysts, polymers of low polydispersity and uniform comonomer composition can be readily synthesized.[1] Furthermore, with the metallocene technologies (such as Dow Chemical's Insite Technology [2]), long chain branched (LCBed) polyethylenes, can be effectively produced through the incorporation of *in situ* produced or externally added macromonomers into the polymer backbone by homogeneous catalysts during ethylene polymerization. The presence of LCBing in the polymer chain can dramatically improve polymer rheological properties and enhance polymer processibility.[3] A large number of rheological investigations

have been carried out in literatures on LCBed polyolefins to investigate the effects of LCBing on polymer rheological properties.[4~8]

Alternative to metallocene catalysts, α-Diimine derived Ni/Pd catalysts are another family of single-site catalysts that have recently attracted significant attention from both industrial practitioners and academia.[9] Compared to metallocene catalysts, the uniqueness of this novel series of catalysts lies in their chain-walking mechanism (involving β-H elimination and readdition steps) exhibited during ethylene polymerization, which introduces a new route to produce branched polyethylenes directly from ethylene stock alone, that is, without comonomer addition. The polymers produced with these novel catalysts exhibit unique chain structure and topology, depending on the competition between chain walking and chain propagation processes. With Ni-Diimine catalysts, a series of short chain branched (SCBed) PEs (similar to LLDPE) with branch length ranging from methyl to hexyl and even higher and with various controllable branching densities can be produced. The SCB density in the polymers can be easily manipulated by varying the polymerization conditions, such as ethylene pressure and reaction temperature.[9] Pd-Diimine catalysts were found to have higher ability to control polymer chain topology owing to their much higher chain walking ability than Ni-Diimine catalysts. By regulating the competition between chain walking and chain propagation rates through reaction conditions, a series of polyethylenes with chain topologies ranging from hyperbranched dendritic to highly branched to linear can be effectively produced. Studies have shown these Pd-Diimine polyethylenes possess unique branch-on-branch chain structures with the branch content depending on the reaction conditions, such as ethylene pressure.[10] Ethylene polymerization with Pd-Diimine catalysts at high ethylene pressure results in polymers with predominantly linear chain topology with significant SCBs and a small number branch-on-branch structures. However, polymerization at low ethylene pressures

leads to compact hyperbranched polymers that have a much higher level of branch-on-branch structures. Studies have shown that these hyperbranched polymers produced at low pressure resemble dilute solution properties observed for dendritic polymers. From neutron scattering and AFM studies, it was also found that these polymers resembled the compact globular structure observed in dendritic polymers.[10,11]

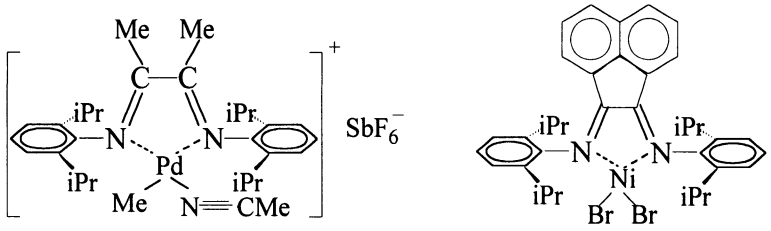

1 **2**

Scheme 4.1 Pd and Ni -Diimine catalysts used.

Rheological properties of polymers are very important factors determining the processibilities and end-use properties of polymer materials. The chain structure and topology of polymers determine the rheological properties of polymer materials. The branched polyethylenes produced with Pd- and Ni-Diimine catalysts represent a new series of polyethylenes and their unique branching structure and controllable chain topology are very different from those observed in commercial HDPE, LLDPE, and LDPE. Compared to the extensive rheological studies [4~8] reported in the literature on LCBed polyethylenes by metallocene technologies, little attention has been paid to the rheological properties of this novel series of polyethylenes, except for the investigations [10,11] on the unique chain structure and dilute solution properties of these polymers utilizing ^{13}C NMR, GPC-MALLS, and AFM techniques. In this chapter, an

extensive investigation on the rheological properties of this unique series of polyethylenes produced with Pd and Ni -Diimine catalysts, [(ArN=C(Me)-C(Me)=NAr)Pd(CH_3)(NCMe)]SbF_6 (Ar = 2,6-$(iPr)_2C_6H_3$) (**1**) and (ArN=C(An)-C(An)=NAr)$NiBr_2$(**2**)/MMAO (see Scheme 4.1), respectively, is presented and the dramatic effects of chain topology on polyethylene rheological properties are examined in detail.

4.3 Experimental Part

4.3.1 Materials

All manipulations involving air- and/or moisture-sensitive compounds were carried out in a N_2 filled drybox or using Schlenk techniques. The Diimine ligands, Pd-Diimine catalyst, [(ArN=C(Me)-C(Me)=NAr)Pd(CH_3)(NCMe)]SbF_6 (Ar = 2,6-$(iPr)_2C_6H_3$) (**1**), and Ni-Diimine catalyst precursor, (ArN=C(An)-C(An)=NAr)$NiBr_2$ (**2**), were all synthesized according to the literature procedures.[9b] Modified methylaluminoxane aluminum (MMAO-3A, 65.9 % methyl and 31.7 % isobutyl) was provided by Akzo-Nobel Corporation as 7.25 wt% aluminum in toluene. UHP N_2 (from Matheson Gas) and polymerization-grade ethylene (from Matheson Gas) were purified by passing through CuO, Ascarite, and 5A molecular sieves.

4.3.2 Ethylene Polymerizations with 1

The polymerization at ethylene pressure of 0.2 atm with **1** was conducted in a 500 ml glass reactor equipped with a magnetic stirrer. A stock solution of catalyst **1** in CH_2Cl_2 was prepared. A prescribed amount of CH_2Cl_2 was added to the dried reactor under N_2 atmosphere. The reactor was then sealed, heated to 35

°C with an oil bath, and the pressure was balanced to 0 atm (gauge pressure). Subsequently, the reactor was pressurized with ethylene to 0.2 atm (gauge pressure). After equilibrium for 10 minutes the polymerization was started by injecting a prescribed amount of catalyst stock solution into the reactor. Magnetic stirring was applied during polymerization. Throughout the reaction, reactor pressure was kept constant at 0.2 atm by continuously bubbling ethylene through a needle and the temperature was maintained at 35 °C by the oil bath. After 20 hours, the reactor was evacuated and a large amount of methanol was added to the mixture. Methanol was decanted off. The sticky polymer was re-dissolved in petroleum ether and was filtered through a short plug of neutral alumina and silica. The petroleum ether in the filtered solution was then evaporated and the viscous polymer oil was dried at 70 °C under vacuum for one week.

The polymerization at ethylene pressure of 1.0 atm with **1** followed the same procedure. The glass reactor containing a prescribed amount of CH_2Cl_2 was sealed, vacuumed, and then pressurized with ethylene. The reactor was subsequently heated to the reaction temperature with an oil bath. Ethylene pressure was balanced to 1.0 atm (absolute pressure). After the reactor mixture was equilibrated for 10 minutes, a certain amount of stock solution of catalyst **1** was injected to start polymerization. After a predetermined period of reaction time as reported in Table 1, the reactor was vented. The reaction mixture was then decanted to a large amount of methanol. The solvent was decanted off and the polymer was re-dissolved in petroleum ether. The polymer solution in ether was filtered through a plug filled with alumina and silica to remove catalyst residues. Finally the solvent in the filtered solution was evaporated and the resulting polymer was further dried at 70 °C under vacuum for one week.

The polymerization runs under ethylene pressure of 6.5 and 30 atm with **1** were carried out in a one-liter Autoclave stainless steel reactor. The reactor was

carefully cleaned with acetone, heated to 140 °C under vacuum for two hours, purged five times with UHP nitrogen, and then cooled down to room temperature. 300 ml CH_2Cl_2 and a certain amount of catalyst stock solution were added into the reactor under nitrogen protection. The mixture was stirred for ten minutes while being heated up to the reaction temperature. The reactor was then pressurized to the desired ethylene pressure to start polymerization. The reactor temperature was controlled by flowing water through internal cooling coil of the reactor. Mechanical stirring with a rate of 1000 rpm was applied throughout the polymerization. The reaction was terminated by venting the reactor after a predetermined period of time as shown in Table 1. The solvent in the mixture was evaporated and sticky polymer samples were recovered and re-dissolved in petroleum ether. The ether polymer solution was then filtered through a short alumina and silica plug to give a clear colorless solution. The solvent was evaporated to yield sticky amorphous solids, which were further dried at 70 °C under vacuum for one week.

4.3.3 Ethylene Polymerizations with 2/MMAO

Ethylene polymerization runs with **2**/MMAO were conducted with toluene as solvent under ethylene pressure of 1 atm in a 500 mL glass reactor equipped with a magnetic stirrer. A stock solution of catalyst precursor **2** in toluene was prepared. Under nitrogen atmosphere, prescribed amounts of toluene and MMAO solution were added to the dried reactor. The reactor was sealed and heated to the reaction temperature with an oil bath. It was then vacuumed and pressurized with ethylene to 1 atm (absolute pressure). After equilibrium for 10 minutes, the polymerization was started by injecting a prescribed amount of stock solution of **2** into the reactor. Magnetic stirring was applied throughout the polymerization. Ethylene pressure was kept constant at 1 atm throughout the reaction and the temperature was maintained by the oil bath. After the prescribed reaction time,

the reactor was evacuated and the mixture was added to a large amount of acidified methanol. The polymer was collected, washed with excessive methanol, and dried in vacuum oven at 70 °C overnight.

4.3.4 Preparation of Polymer Blends

The two dried polymers (Samples 2 and 3) with the prescribed weight ratios (total weight ~ 2 g) were mixed and dissolved in 20 ml of hexane. After stirred overnight at room temperature, the solvent in the mixture was evaporated. The resulting polymer blend was further dried in a vacuum oven at 70 °C for 2 days.

4.3.5 Polymer Characterizations

The glass transition temperatures of the produced polyethylenes were measured using a Thermal Analysis 2910 MDSC from TA Instruments in the standard DSC mode. UHP N_2 gas at a flow rate of 30 ml/min was purged through the calorimeter. The temperature and heat capacity for the instrument were initially calibrated with indium standard at the heating rate of 10 °C/min. The DSC cell loaded with polymer sample (about 20 mg) was first cooled to - 120 °C with liquid nitrogen. It was then heated to 50 °C at 10 °C/min to determine the glass transition temperature.

GPC-VIS (Gel Permeation Chromatography equipped with a Differential Refractive Index detector and an in-line capillary viscometer) measurements on polymer molecular weight (MW), molecular weight distribution (MWD), and intrinsic viscosity ([η]) were measured at 140 °C in 1,2,4-trichlorobenzene on a Waters Alliance GPCV 2000. In the system, four Waters Styragel HT 6E linear columns were used. The flow rate was 1.0 ml/min and the injection volume was

418.5 μL. The polymer concentrations in the solutions were in the range of 3-6 mg/mL. The data were collected every 0.1 second. The inter-detector volume between DRI detector and viscometer was determined to be 0.086 mL by averaging the retention time differences for polystyrene narrow standards. Polymer molecular weight and molecular weight distribution were calculated according to a universal calibration curve based on eleven polystyrene narrow standards with molecular weights ranging from 1.09×10^6 to 1000 g/mol.

75.4 MHz ^{13}C NMR analyses were conducted on a Bruker AV300 pulsed NMR spectrometer with Waltz-supercycle proton decoupling. Polymer samples 1 ~ 5 (see Table 1) prepared with catalyst **1** were dissolved in $CDCl_3$ in 10 mm NMR tubes with concentration about 20 wt% and the acquisitions were performed at 30 °C. Samples 6 and 7 (see Table 4.1) prepared with **2**/MMAO were dissolved in 1,2,4-trichlorobenzene and deuterated *o*-dichlorobenzene mixture (with a weight ratio of 9/4) in 10 mm NMR tubes with concentration about 20 wt% and the measurements were conducted at 120 °C. At least 4000 scans were applied for each acquisition to obtain a good signal-to-noise ratio. The assignment of the signals was referred to literature reports.

All rheological characterizations of the polymer melts were conducted on a Stresstech HR rheometer, which was calibrated with 1000 cp standard oil. For polymers prepared with **1**, a 25 mm parallel plate geometry with a gap size around 1 mm was applied for the measurements. The measurements were performed at regular 5 °C intervals within temperature range from 25 to 65 °C and at 10 °C intervals within temperature range from 65 to 115 °C. Temperature was maintained within ± 0.2 °C using an ETC-3 temperature control system and the measurements were done under N_2 blanket. The polymer samples were subject to steady shear, creep recovery, and small amplitude dynamic oscillation in the controlled-stress mode. In the steady shear mode, at least three orders of

magnitude of shear rates were covered. In the creep recovery experiments, the samples were subject to stress at time zero, and the compliance was monitored at constant stress for a certain period of time, then the applied stress was removed, and the relaxation behavior was recorded. This procedure was then repeated with different stresses. In the small amplitude dynamic oscillation mode, the frequency range covered 0.001 to 90 Hz. Strain sweeps were performed before frequency sweeps to establish the linear viscoelastic region. All the three measurements were conducted on the same loaded sample. At the end of the experiments, the sample was retested at 25 °C to confirm the stability of the sample during measurement. For all the samples, this difference did not exceed ± 5 %. For polymer samples prepared with **2**/MMAO, a 20 mm parallel plate geometry of a gap size around 1 mm was used for the measurements. The polymer samples were first compression-molded in a Carver Press at 150 °C into small disks with 20 mm in diameter and 1 mm in thickness. The rheological measurements were conducted in the small amplitude dynamic oscillation mode within the frequency range of 0.001 ~ 50 Hz. Strain sweeps were performed at 1 Hz before frequency sweeps to establish the linear viscoelastic region. The experiments were performed at regular 10 °C intervals within temperature range from 40 to 120 °C.

4.4 Results and Discussion

4.4.1 Polymer Synthesis and Characterization by ^{13}C NMR, GPC-VIS, and DSC

Seven polyethylene samples with different branching densities and chain topologies were prepared as shown in Table 4.1. The catalysts were chosen because of their ability to produce high molecular weight polyethylenes owing to

the presence of sterically bulky chelating Diimine ligands, which reduces the chain transfer reactions. From Table 4.1, **2**/MMAO exhibited activity several orders of magnitude higher than **1** toward ethylene polymerization at the same reaction condition. The activities of both catalysts were sensitive to reaction temperature. An increase in reaction temperature led to a reduction in the activity due to enhanced catalyst deactivation. The polymer samples exhibited different physical morphologies. Samples 1 ~ 3 were viscous oils. Samples 4 and 5 were sticky solids. Samples 6 and 7 were non-sticky elastomeric materials. All the polymers were amorphous materials and had glass transitional temperatures (T_g) at – 65 to – 57 °C, as reported in Table 4.1.

Table 4.1 Polymerization reaction conditions and polymer properties.[a]

Polymer Sample	Cat.	Catalyst amount (μmol)	Ethylene pressure (atm)	Temp (°C)	Time (hr)	Activity[c]	Mw[d] (kg/mol)	PDI[d]	[η][d] (dl/g)	Tg[e] (°C)
1	**1**	200	0.2	35	20	1.6	94	2.3	0.093	-67
2	**1**	100	1.0	35	18	7.1	161	2.1	0.14	-65
3	**1**	100	1.0	25	18	15.2	149	2.2	0.35	-65
4	**1**	100	6.5	25	19	37.2	165	2.7	0.54	-64
5	**1**	90	30.0	25	5	27.1	140	2.4	0.82	-63
6	**2**[b]	4	1.0	35	1	1325	191	2.7	1.38	-57
7	**2**[b]	4	1.0	55	1	875	162	2.7	1.31	-62

[a] Polymerization solvent: CH_2Cl_2 (200 ml) for Samples 1~3; CH_2Cl_2 (350 ml) for 4 and 5; toluene (200 ml) for 6 and 7.
[b] Activated with MMAO with Al/Ni = 1000 (molar).
[c] Activity calculated in kg PE /(mol of catalyst × time).
[d] From GPC-VIS measurement at 140 °C in 1,2,4-trichlorobenzene.
[e] From DSC measurement at 10 °C/min.

The polymers were characterized using ^{13}C NMR. A series of short chain branches with the branch length ranging from methyl to hexyl and higher could be observed from the ^{13}C NMR spectra. Table 4.2 lists the SCB distribution. In addition to the known branches, *sec*-butyl branches, the shortest branch-on-branch

structure generated via chain walking through tertiary carbons, could be seen from the resulting methyl and ethyl resonances centered at 19.5 and 11.7 ppm,[10a] respectively, in the ^{13}C NMR spectra. The percentages of methyl branches from *sec*-butyl end group in the total methyl branches are also listed in Table 4.2. All the seven polymer samples had very similar total branch density. However, the Pd-Diimine polymers (Samples 1 ~ 5) and those of Ni-Diimine (Samples 6 and 7) had different features in the SCB distribution. For the Pd-Diimine polymers, hexyl+ (about 33 % of the total branches) were the major branch type with methyl (31 % of the total branches) as the second, while in the Ni-Diimine polymers, the methyl branch was the dominant type (about 61 %) and the contribution from hexyl+ was minor (~ 10 %). In addition, the percentages of methyl branches on *sec*-butyl end group in the total methyl branches were much higher in the Pd-Diimine polymers (16.6 ~ 23.7 %) than in the Ni-Diimine polymers (3.6 ~ 5.4 %). These differences indicate that the Pd-Diimine catalyst had much longer walking distance than the Ni-Diimine catalyst.

Table 4.2 Polymer short chain branch distribution from ^{13}C NMR in number of branches per 1000 carbons.[a]

Sample	Me	Et	Pr	Bu	Am	Hex+	%B[b]	Total Branch
1	35.7	26.2	2.8	12.1	3.1	40.1	23.5	120
2	33.7	24.2	2.4	11.5	2.9	37.2	23.7	112
3	32.9	23.8	2.2	11.4	2.7	37.7	23.4	111
4	33.0	23.1	3.1	11.3	3.1	35.5	20.0	109
5	32.0	19.3	3.5	9.4	3.5	34.2	16.6	102
6	70.3	9.3	4.9	5.4	5.0	12.2	3.6	115
7	79.1	14.6	5.1	6.7	4.6	13.3	5.4	123

[a] ^{13}C NMR spectra for Samples 1 ~ 5 were obtained at 30 °C with $CDCl_3$ as solvent, the spectra for 6 and 7 were obtained at 120 °C with 1,2,4-trichlorobenzene and o-dichlorobenzene as solvent.

[b] Percentage of methyl from *sec*-butyl branches in the total methyl branches.

All the Pd-Diimine polymers exhibited very similar SCB density and distribution irrespective of their very different preparation conditions (temperature and pressure). A drastic change in the ethylene pressure from 1 to 30 atm at 25 °C only caused a slight decrease in the total SCB density of the Pd-Diimine polymers (Samples 3 versus 5). Comparing Samples 2 and 3, the temperature effect on branch density and distribution was also negligible with the Pd-Diimine catalyst. On the other side, an increase in temperature from 35 °C to 55 °C caused an obvious increase in the total branch density in the Ni-Diimine polymers (Samples 6 versus 7). Due to the inability of ^{13}C NMR technique to differentiate branches with branch length longer than hexyl, no direct information regarding chain topology could be obtained from polymer ^{13}C NMR spectra.

GPC-VIS (GPC coupled with an in-line viscometer) was used to determine polymer average molecular weight, molecular weight distribution, and intrinsic viscosity. By measuring the intrinsic viscosity ($[\eta]$) for each elution fraction with the in-line viscometer coupled with a DRI concentration detector, GPC-VIS determines the average molecular weight (M) for each fraction by referring to the universal calibration curve ($log([\eta]M) = f(t)$, in which M stands for average molecular weight and t stands for elution time) generated from narrow polystyrene standards based on the hydrodynamic volume theory. With the data from all of the elution fractions, polymer average molecular weights, polydispersities (PDI), and intrinsic viscosities were obtained. The GPC-VIS results are summarized in Table 4.1. The polymer samples had high and very close Mw. Their PDIs were also very similar and close to 2, indicating the single-site nature of the polymerization.

The GPC-VIS measurements also provided information about chain topology. Figure 4.1 shows the dependences of intrinsic viscosity on molecular

weight (Mark-Houwink plot) for these polymers with comparison to a linear HDPE sample (NIST 1475a).

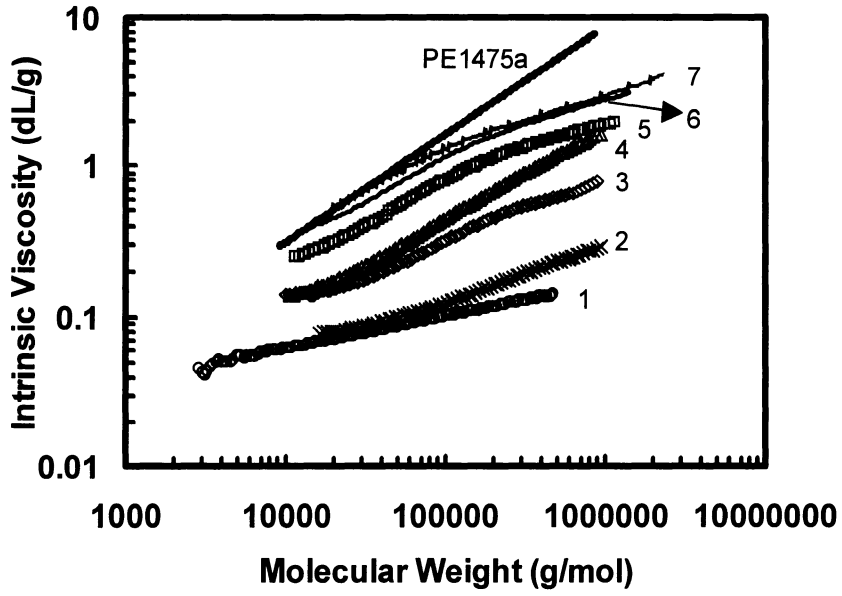

Figure 4.1 Intrinsic viscosity [η] vs. MW in TCB at 140 °C from GPC-VIS characterizations.

Polymer intrinsic viscosity is related to the dimension of chain coil following the Fox-Flory expression:[13]

$$[\eta] = \Phi \frac{R_g^3}{M} \tag{1}$$

where R_g is the polymer coil gyration radius and Φ is a constant. Polymers with different branch densities and topological structures exhibit different intrinsic viscosities. Among the seven samples, the Ni-Diimine polymers (Samples 6 and 7) had the highest intrinsic viscosities owing to their approximately linear chain topology. However, compared to the linear HDPE sample, due to the presence of

SCBes that reduce the polymer coil dimension at the same molecular weight, Samples 6 and 7 had lower intrinsic viscosities. All the Pd-Diimine polymers had lower intrinsic viscosities than the Ni-Diimine counterparts. Increasing the reaction pressure from 0.2 to 30 atm and decreasing the reaction temperature from 35 to 25 °C significantly increased the intrinsic viscosities for the Pd-Diimine polymers, suggesting the change of chain topology from hyperbranched dendritic to relatively linear structure. Different from the linear relationship between $log[\eta]$ and $logM$ in the Mark-Houwink plot seen in Figure 4.1 for the linear HDPE sample and reported in the literature [14] for metallocene LLDPE, the branched polymers prepared in this work exhibited somewhat curved lines at reduced slopes, i.e. lower α values in the Mark-Houwink equation.

4.4.2 Effect of Chain Topology on Polymer Flow Behavior

The seven polymers, which differed greatly in chain topology, exhibited very different flow behaviors. Figures 4.2 and 4.3 show, respectively, the melt viscosity curves for polymers 1 and 2 obtained from steady-shear measurements conducted in a broad range of shear rates and under various temperatures. These two viscous oil-like polymers, synthesized at low ethylene pressures (0.2 and 1.0 atm, respectively) and 35 °C with Pd-diimine catalyst **1**, displayed typical Newtonian flow behavior, i.e., the independence of viscosity on shear rate. Moreover, the viscosities for these two high-molecular-weight polymers were extremely low. At 25 °C they exhibited viscosities of only 25 and 43 Pa s, respectively, which are as low as that of liquid honey. Small amplitude dynamic oscillation tests were also performed in the linear viscoelastic region. It was found that the complex viscosity was equal to the steady-shear viscosity, in accordance with Cox-Merz rule [15], and independent of the frequency in the range studied. Typically Figure 4.5 shows the complex viscosity measured at 25 °C vs.

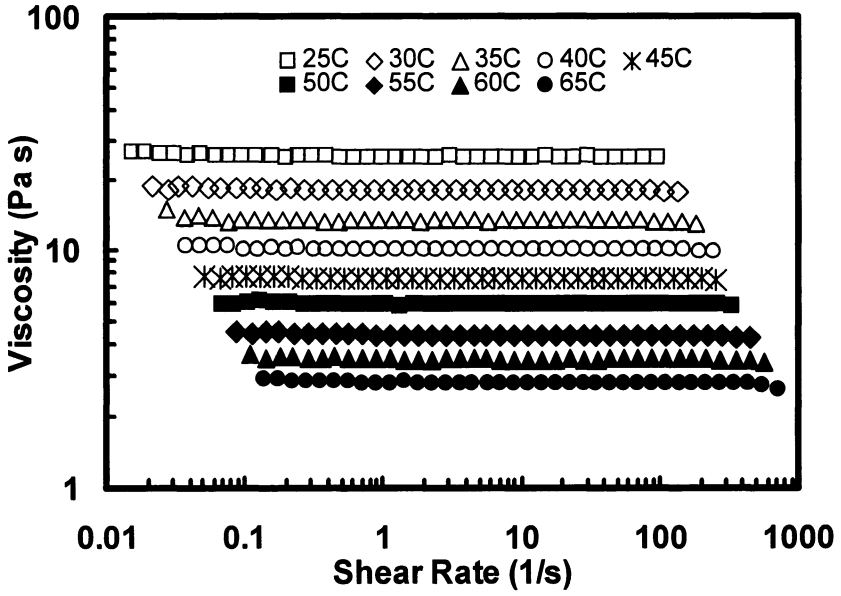

Figure 4.2 Steady-shear viscosity as a function of shear rate for polymer 1 measured at various temperatures.

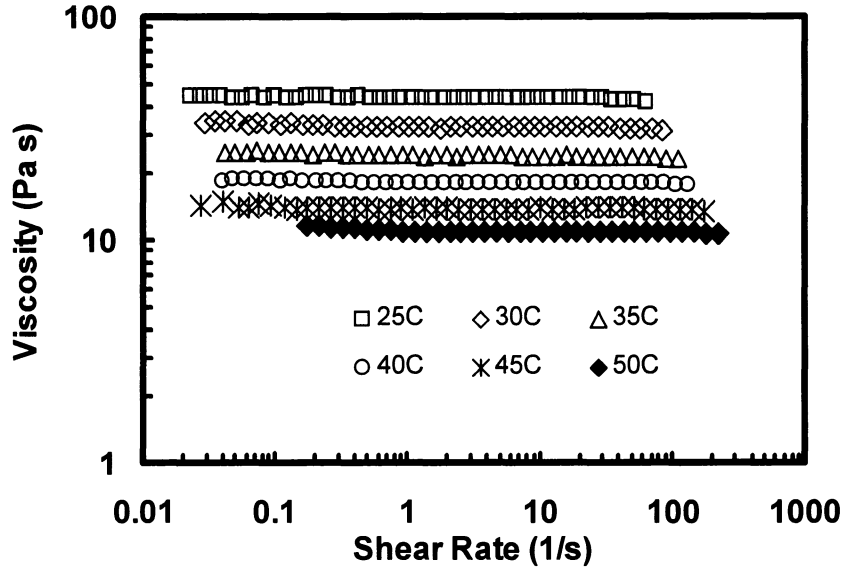

Figure 4.3 Steady-shear viscosity as a function of shear rate for polymer 2 measured at various temperatures.

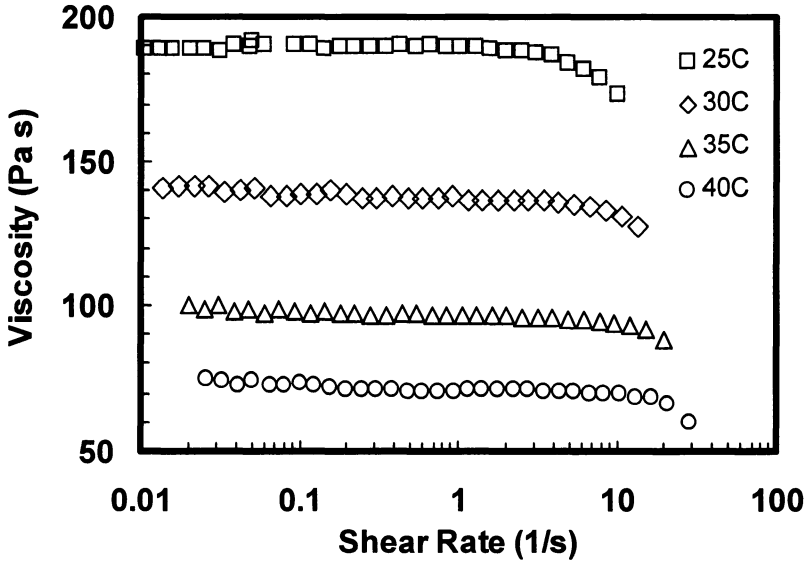

Figure 4.4 Steady-shear viscosity as a function of shear rate for polymer 3 measured at various temperatures.

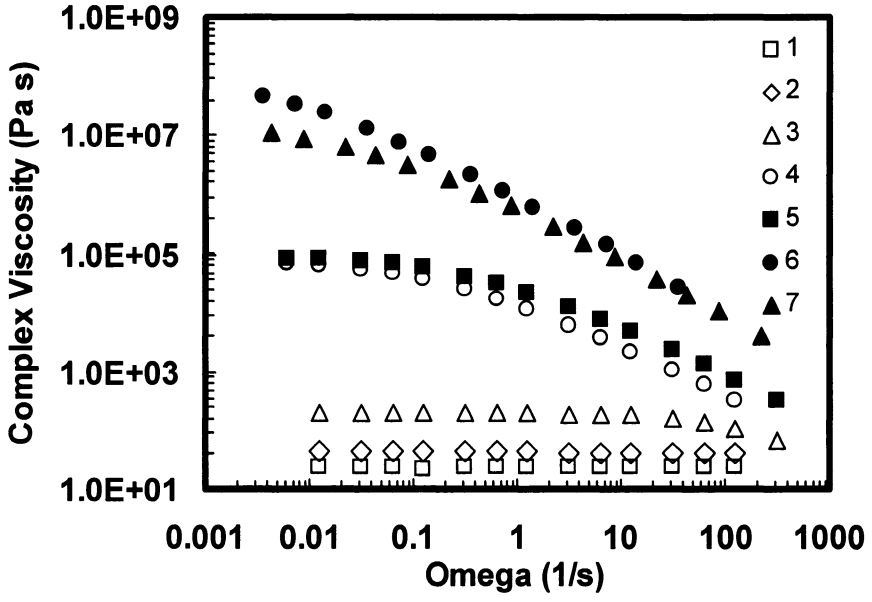

Figure 4.5 Complex viscosity as a function of angular frequency from dynamic oscillation measurements at 25 °C.

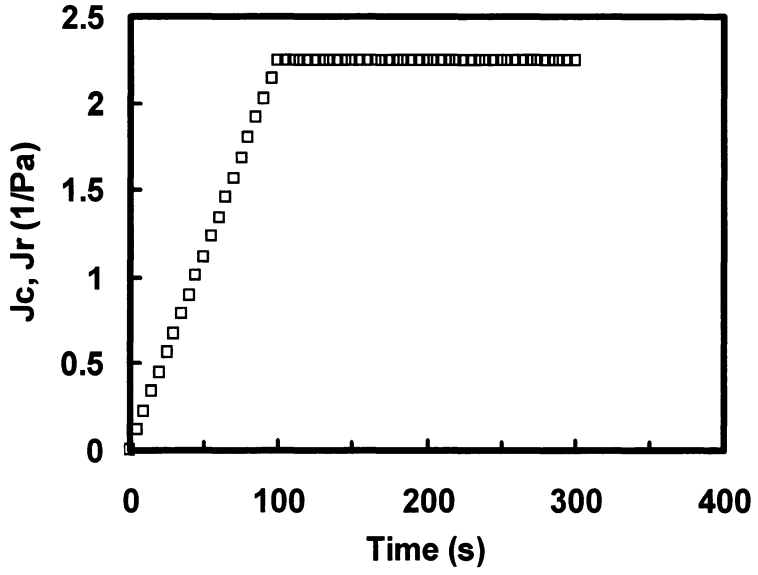

(a)

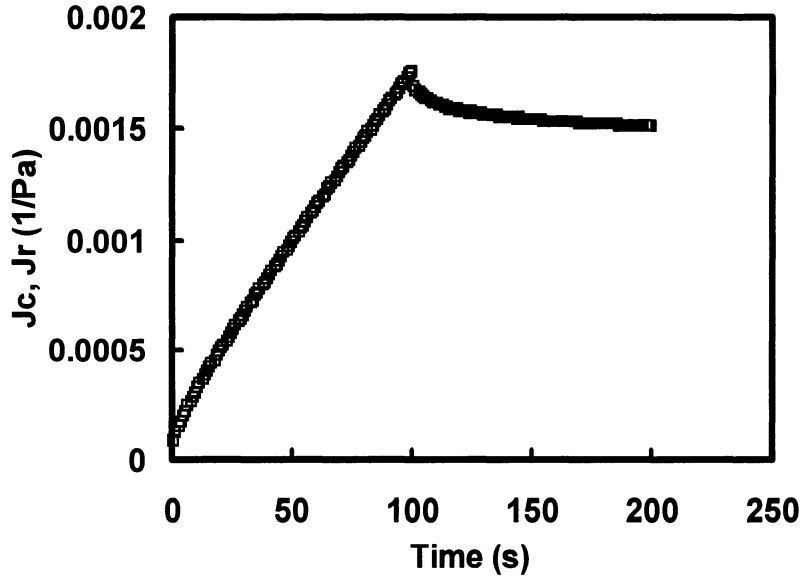

(b)

Figure 4.6 Compliance curve from creep-recovery test conducted at 25 °C with creep stress of 10 Pa for (a) polymer 2 and (b) polymer 4.

oscillation frequency. The polymers were also examined in creep-recovery tests and they both showed the ideal viscous behavior in the range of applied stresses and temperatures. Representatively Figure 6(a) shows a creep-recovery compliance curve conducted on polymer 2 at 25 °C under creep stress of 10 Pa. These unique rheological properties, which are characteristic of hyperbranched dendritic polymers [16], suggest that these two high MW polymer oils exhibited chain topology similar to that observed in hyperbranched dendritic polymers. In these polymers, the compact hyperbranched chain topology and surface congestion of the densely packed polymer molecules prevented chain entanglements between polymer molecules and thus led to the typical Newtonian flow behavior.[17]

For polymers 3 ~ 5 prepared with catalyst **1** at 25 °C under enhanced pressures and polymers 6 and 7 prepared with catalyst **2**, typical non-Newtonian shear-thinning behavior was observed in both steady-shear and dynamic oscillation measurements. Figure 4.4 shows the steady-shear viscosity vs. shear rate for polymer 3 at different measurement temperatures. Different from polymers 1 and 2, an obvious viscosity decrease can be seen at the high shear-rate end. In Figure 4.5, the different dependences of complex viscosity on oscillation frequency for the seven polymers at 25 °C are compared. Different from the constant viscosities for polymer 1 and 2 at different frequencies, a strong dependence of viscosity on the frequency can be found for polymers 3 ~ 7, showing the presence of chain entanglement in these polymers with relatively more linear chain topology. Furthermore, compared to polymer 3, polymers 4 ~ 7 exhibited more pronounced shear thinning, indicating the more chain entanglement involved in polymers with more linear chain topology. Creep-recovery tests were also conducted. Typically Figure 6(b) illustrates the creep-recovery compliance curve for polymer 4 at 25 °C under creep stress of 10 Pa,

which demonstrates clearly the viscoelastic nature of the polymer with chain entanglements.

A significant difference in the polymer zero-shear viscosities was also found in the seven polymers having quite similar average molecular weight but different chain topology and/or branching structures. Table 4.3 lists the polymer zero-shear viscosities obtained at 60 °C. The change of chain topology from hyperbranched dendritic to linear structure dramatically increased the zero-shear viscosity (more than 6 orders of magnitude). Comparing polymers 6 and 7 with polymers 4 and 5, the Ni-Diimine polymers exhibited much higher zero-shear viscosities than the Pd-Diimine polymers owing to their shorter average branch length and/or more linear chain topology.

Table 4.3 Polymer rheological parameters (T_{ref} = 60 °C).

Polymer	η_0[a] (Pa s)	λ[b] (s)	Ea (kJ/mol)	G_N^0 (MPa)	M_e (kg/mol)
1	3.5		46.4		
2	6.7		43.8		
3	26		47.0		
4	9.3×10^3	0.95	51.9		
5	7.9×10^3	0.30	57.2		
6	1.4×10^7	48.8	51.0	1.24	1.90
7	1.6×10^6	8.1	54.8	1.15	2.06

[a] zero shear viscosity, for polymers 1 ~ 3, it was the Newtonian viscosity data directly from the rheological tests; for polymers 4 ~ 5, it was obtained through fitting the viscosity data with Cross equation.

[b] Characteristic relaxation time, obtained through fitting the viscosity with Cross equation.

4.4.3 Time-Temperature Superposition and Flow Activation Energy

Time-temperature superposition was found to be valid for all the seven polymers in both steady shear and dynamic oscillation measurements despite of their very different chain topologies and flow behaviors. The temperature shift factor, a_T, was calculated according to

$$\eta_0(T) = a_T \eta_0(T_0) \tag{2}$$

where T_0 is an arbitrary reference temperature (here we chose 60 °C) and η_0 is the zero-shear viscosity. For Samples 1 ~ 3, the η_0 data were directly obtained from the frequency-independent Newtonian viscosities at low shear rates. For Samples 4 ~ 7, the η_0 values were inferred by fitting the complex viscosity curve with the Cross equation:[18]

$$\eta^*(\varpi) = \frac{\eta_0}{1+(\lambda\varpi)^n} \tag{3}$$

where λ is a characteristic relaxation time and n is a power law exponent. For the seven polymers, the dependences of a_T on temperature were all found to agree with the Arrhenius equation in the studied temperature range.

$$a_T = \exp\left[\frac{E_a}{R}\left(\frac{1}{T}-\frac{1}{T_0}\right)\right] \tag{4}$$

The flow activation energy E_a values are listed in Table 4.3.

The activation energy is a measure of temperature sensitivity for flow under shear and is affected by polymer chain topological structure and branch density for high MW polymers. Conventional HDPEs have activation energies of approximately 27 kJ/mol.[8a] For conventional LLDPEs, studies on ethylene-butene copolymers with different ethyl branch densities showed that E_a initially increases with the butene content and then levels off at about 33-34 kJ/mol for the butene contents between 7 wt% (corresponding to an ethyl branch density of 17.5 branches per 1000 carbons) and 25 wt% (62.5 branches per 1000 carbons).[6c] However, no studies on the effect of the length of short chain branches on activation energy of LLDPE have been reported. LDPE, due to the presence of

both SCBing and LCBing, typically exhibits E_a values of about 55 kJ/mol.[4b] For LCBed metallocene HDPE and LLDPE, E_a generally increases with long chain branching density (LCBD) and is usually between 30 and 65 kJ/mol depending on the LCBD.[4,6~8]

Compared to these well-studied polymers, the novel highly branched polymers reported here exhibited very unique activation energies. The hyperbranched Samples 1 and 2, which resembled the topology of hyperbranched dendritic polymers, had the E_a values of 46.4 and 43.8 kJ/mol, respectively. The change of chain topology from hyperbranched dendritic to relative linear structure caused a significant increase in E_a, with 47.0, 51.9, and 57.2 kJ/mol for Samples 3, 4, and 5, respectively. For the linear SCBed Ni-Diimine polymers 6 and 7, their activation energies tended to increase from 51.0 to 54.8 kJ/mol with the increase of total SCB densities from 115 to 123 branches per 1000 carbons. The high activation energies of these new polymers could be attributed to their very high branch densities at 102 ~ 123 branches per 1000 carbons. The presence of LCBing with branch length longer than entanglement can be ruled out based on the fact that all the polymers obeyed the time-temperature superposition, which is not valid for LCBed polymers.

4.4.4 Dynamic Moduli (G' and G")

Different dynamic moduli (G' and G") behaviors were observed for these polymers differing in chain topology and branching structure. Figures 7(a)-(e) show the G' and G" master curves for the five viscoelastic polymers (Samples 3 ~ 7) measured in the linear viscoelastic range of dynamic oscillation. For the purely viscous polymers (Samples 1 and 2), the dynamic oscillation tests showed that both polymers were essentially Newtonian, G' ~ 0 and G" ~ ω that agreed with the results obtained from the steady-shear and creep experiments.

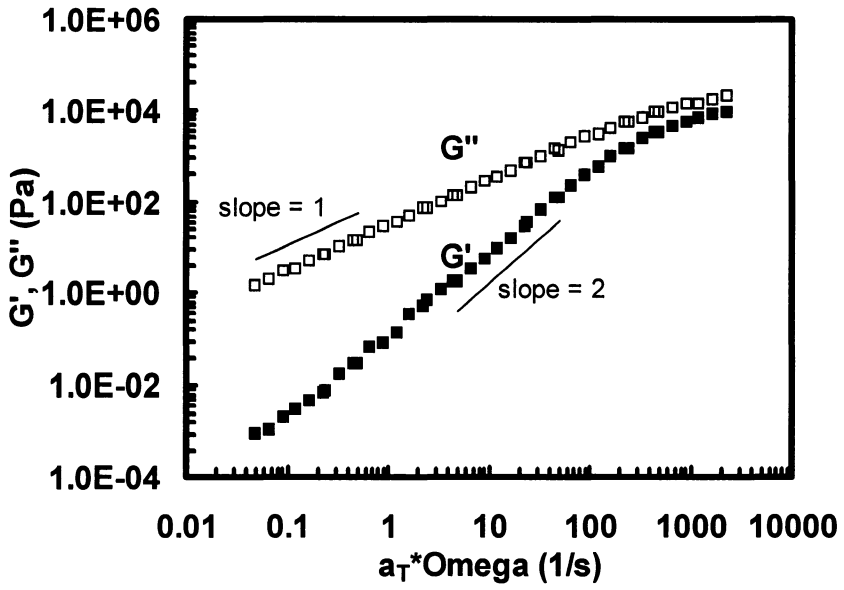
1.0E+06
1.0E+04
1.0E+02
1.0E+00
1.0E-02
1.0E-04
G', G" (Pa)
G"
G'
slope = 1
slope = 2
0.01
0.1
1
10
100
1000
10000
aT*Omega (1/s)

(a)

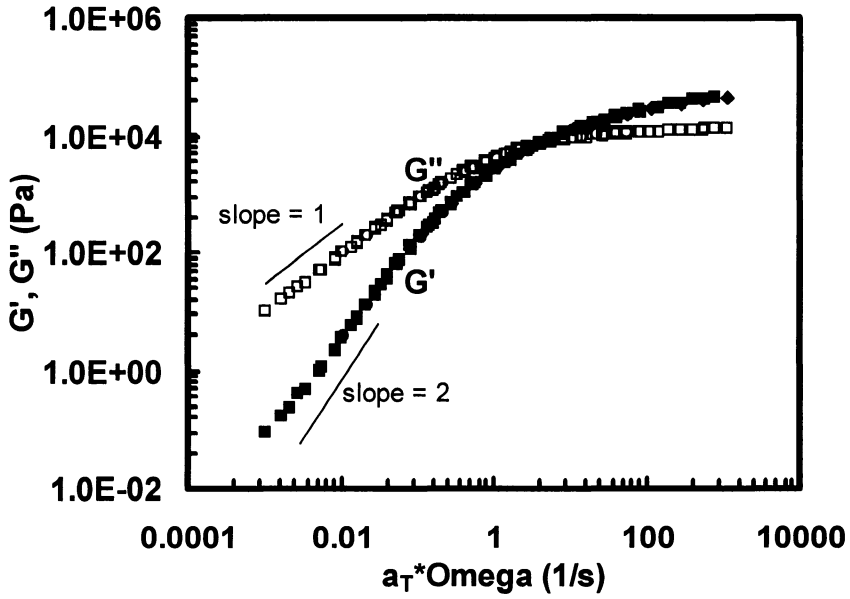
1.0E+06
1.0E+04
1.0E+02
1.0E+00
1.0E-02
G', G" (Pa)
G"
G'
slope = 1
slope = 2
0.0001
0.01
1
100
10000
aT*Omega (1/s)

(b)

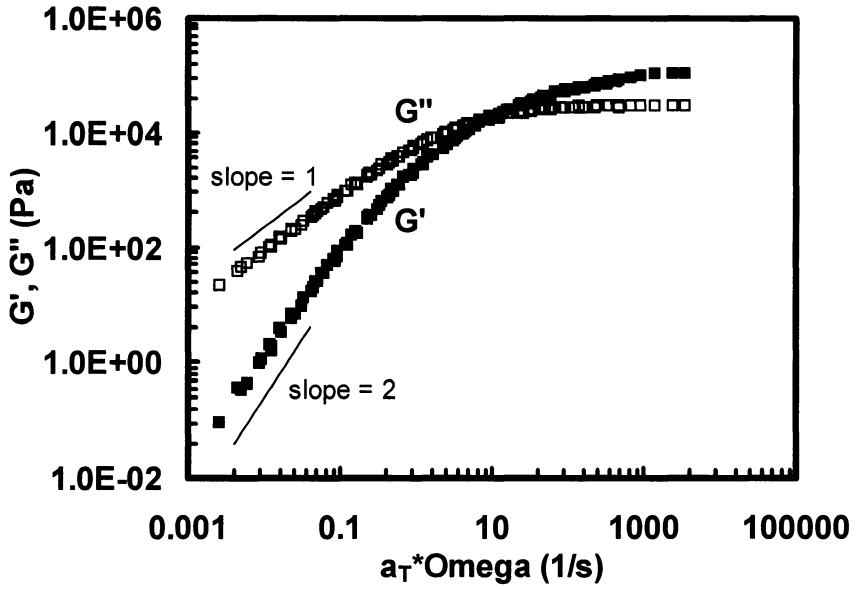
1.0E+06
1.0E+04
1.0E+02
1.0E+00
1.0E-02
G', G" (Pa)
G"
G'
slope = 1
slope = 2
0.001
0.1
10
1000
100000
aT*Omega (1/s)

(c)

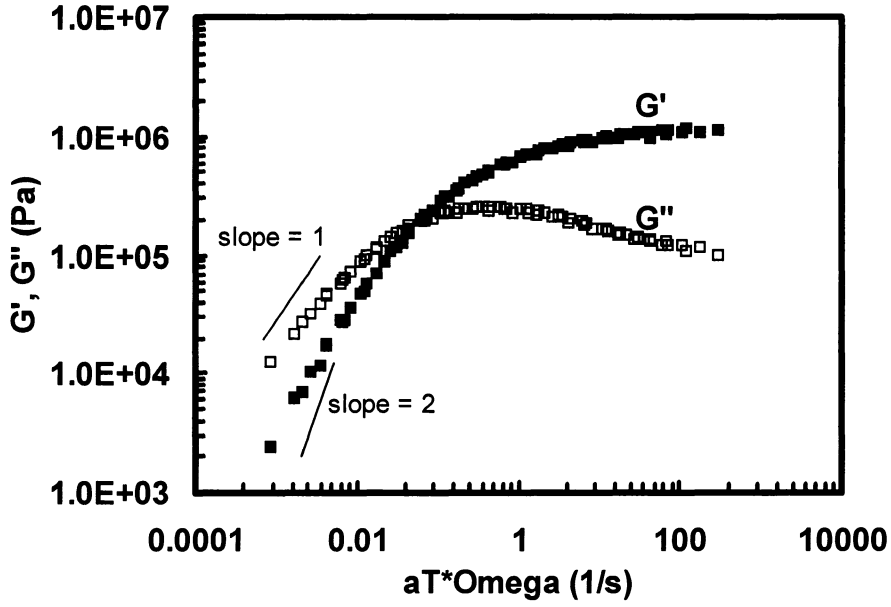
1.0E+07
1.0E+06
1.0E+05
1.0E+04
1.0E+03
G', G" (Pa)
G'
G"
slope = 1
slope = 2
0.0001
0.01
1
100
10000
aT*Omega (1/s)

(d)

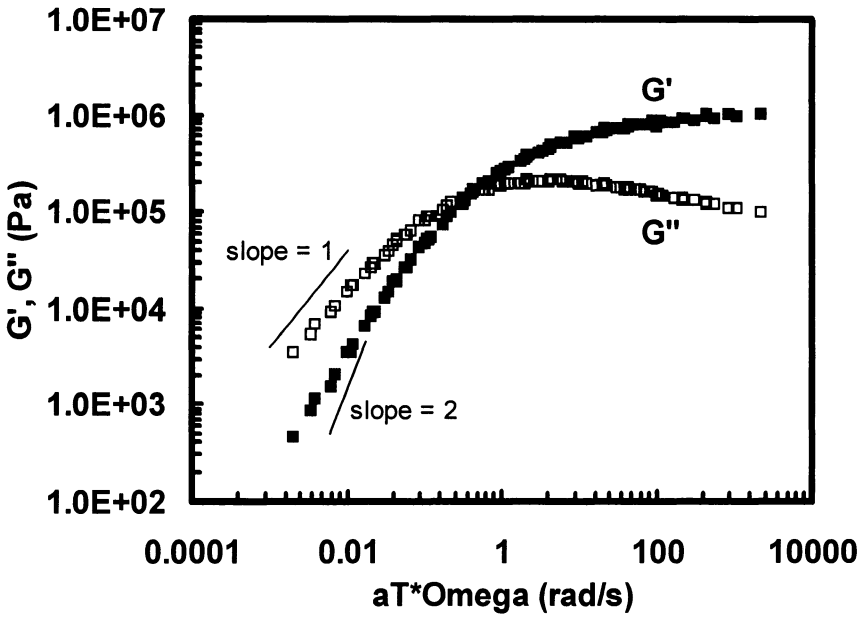

(e)

Figure 4.7 Master curves of storage modulus (G') and loss modulus (G") vs. angular frequency at the reference temperature T_0 = 60 °C for (a) Sample 3; (b) Sample 4; (c) Sample 5; (d) Sample 6; (e) Sample 7.

Figure 4.7(a) shows the G'(ω) and G"(ω) master curves for Sample 3. The G" was always dominant over the G' in the whole frequency range investigated and there was no cross between the two curves. This dynamic moduli behavior, observed by many investigators,[19] is unique for hyperbranched polymers and dendrimers, due to a lack of chain entanglements. The polymer melts were mainly viscous. In the studied frequency range, we had G" ~ ω and G' ~ $\omega^{1.9}$, close to the Rouse model's prediction (i.e., G" ~ ω and G' ~ ω^2) [20] in the terminal zone.

Different from Sample 3, there were crossovers between G'(ω) and G"(ω) in Sample 4 and 5, as shown in Figures 4.7(b) and 4.7(c). Their development into

rubbery plateau was evident, suggesting significant entanglements involved in these two polymers that have more linear chain topology. In the terminal region, their dependencies of moduli on frequency (G" ~ ω and G' ~ $\omega^{1.63}$ for Sample 4, G" ~ ω and G' ~ $\omega^{1.86}$ for Sample 5) were similar and showed some deviations in G' from the Rouse model.

There were also crossovers in Samples 6 and 7. However, the rubber plateau region was more pronounced in these two polymers, showing the presence of more chain entanglements. Figures 4.7(d) and 4.7(e) show the maximum values in the G"(ω) curves. The frequency dependencies of moduli in the terminal region (G" ~ $\omega^{0.79}$ and G' ~ $\omega^{1.18}$ for Sample 6; G" ~ $\omega^{0.87}$ and G' ~ $\omega^{1.21}$ for Sample 7) were more deviant from the prediction of the Rouse model.

4.4.5 Plateau Modulus (G_N^0) and Average Entanglement Molecular Weight (M_e)

The plateau modulus, G_N^0, is a characteristic parameter that is associated with the entanglement network and is related to the average entanglement molecular weight (M_e), which is defined as the average molecular weight between adjacent temporary entanglement points, in the form of

$$G_N^0 = \frac{\rho RT}{M_e} \tag{5}$$

where R is the universal gas constant (R = 8.314 J/(mol K)) and ρ is the polymer density at temperature T.[21] The G_N^0 value can be estimated from loss modulus data according to:

$$G_N^0 = \frac{2}{\pi}\int_{-\infty}^{\infty} G''(\omega)\, d\ln\omega \tag{6}$$

in which the integral extends only over the terminal peak of G"(ω).[21] Among the seven polymers, only those of Samples 6 and 7 could be calculated because the G"(ω) data of the other polymers did not extend beyond the G"(ω) maximum. Figure 4.8 shows G"(ω) vs. ln(ω) for the two polymers. Using the data points beyond the maxima of G"(ω), we extrapolated G"(ω) to zero linearly for high frequencies.[21] The values of G_N^0 obtained at 60 °C are listed in Table 3.

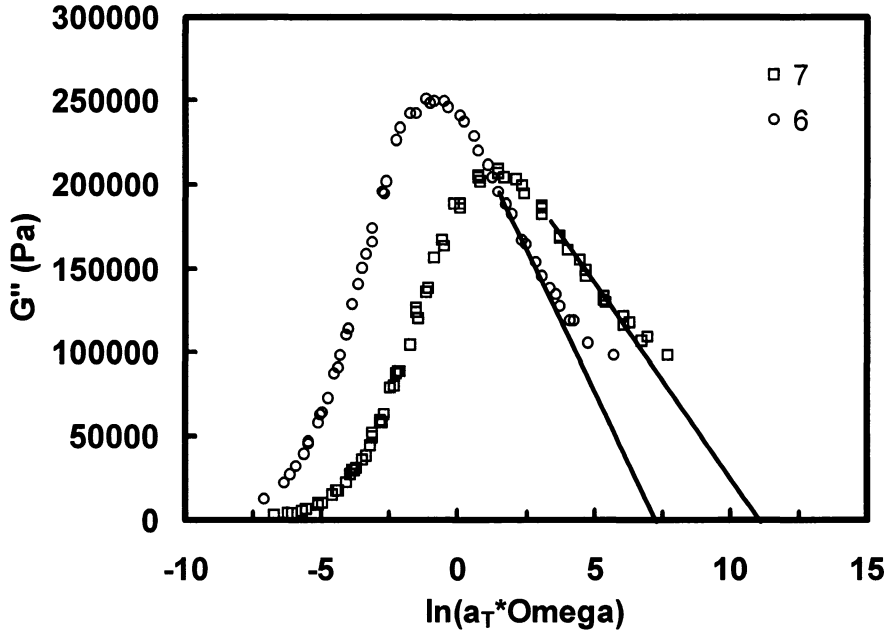

Figure 4.8 Loss moduli G"(ω) of Samples 6 and 7 vs. reduced angular frequency at the reference temperature T_0 = 60 °C.

The average entanglement molecular weight (M_e), which is independent of temperature, could be obtained using Eq.(5). Assuming a density of ρ = 850 kg/m^3 at T = 60 °C, we estimated $M_e = 1.90 \times 10^3$ g/mol for Sample 6 and $M_e = 2.06 \times 10^3$ g/mol for Sample 7. Although they must be regarded as an

approximate, these values were in agreement with but slightly higher than the M_e values reported for HDPE, ranging between 1250 and 1460 g/mol.[6b,22]

4.4.6 Log(G') vs. Log(G") plot

The log(G') vs. log(G") plot has been proven to be a useful tool to investigate the effects of LCBing and polydispersity on rheological properties.[4b] Both theoretical and experimental studies have shown that, for high MW polymer melts with narrow PDI, in the terminal region the log(G') vs. log(G") curve does not depend on MW and is only a very weak function of temperature. All the data measured at various temperatures and molecular weights can be described by a single master curve in the Log(G') vs. log(G") plot.[23] Experimental investigations have also shown that the SCB would not affect the master curve. However, any change in chain topology, such as LCBing, and PDI would lead to a significant deviation of data points from the master curve.[4b] In the terminal region, theoretical derivations [23] have shown that, for monodisperse linear polymers with $M > M_e$,

$$\log G' = 2\log G'' - \log(\rho RT / M_e) + \log(\pi^2/8) \qquad (7)$$

However, experimental studies [4b] have shown that linear HDPE and LLDPE with narrow PDI (PDI = 3) deviate from the above theoretical quadratic dependence of G' on G" and instead they follow

$$G' = 0.00541(G'')^{1.42} \qquad (8)$$

In this work, we investigated the differences in the log(G') ~ log(G") curves for the five viscoelastic polymers (Samples 3 ~ 7) that have different chain topologies and branch densities. Figure 4.9 shows the log(G') vs. log(G') master curves with the data points collected at several different temperatures. For

comparison, a straight line (the master curve for linear HDPE and LLDPE) based on Eq. 8 was also drawn.

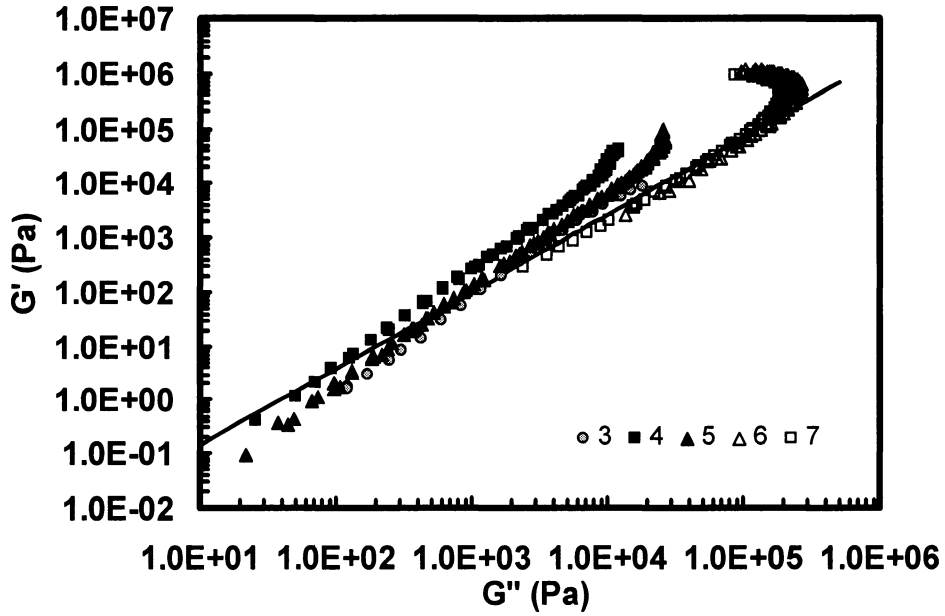

Figure 4.9 Storage modulus (G') vs. loss modulus (G") in the double logarithmic plots for viscoelastic polymers (Samples 3 ~ 7) measured at various temperatures.

There were several interesting features in this plot. For the Ni-Diimine polymers (Samples 6 and 7), their master curves were very close to those of HDPE and LLDPE despite their highly branched chain structure. This result suggests that the branch density as high as 123 branches per 1000 carbons did not change the linear chain topological characteristics of these two polymers. In contrast, the master curves of the Pd-Diimine polymers (Samples 3 ~ 5) all deviated from those of HDPE and LLDPE, suggesting that the chain topologies of these three polymers were essentially different from those of the Ni-Diimine polymers. The three curves were all parallel to each other with a slope of 1.78

(i.e., G' ~ (G")$^{1.78}$). The displacements of the three master curves were slightly different from each other. From Eq.(7), these differences might be caused by their different ρ/M_e values. Studies [17] on dendritic polymers have shown that, compared to their linear analogs, dendritic polymers exhibit much higher characteristic molecular weight (M_c), which is usually related to M_e in the form of $M_c = 2M_e$,[21] because of their compact dendritic structure. The differences in the chain topologies of the three polymers resulted in different M_e values and led to the different displacements for the log(G') vs. log(G") curves.

4.4.7 Rheological Properties for Blends of Samples 2 and 4

Owing to their unique molecular architectures and rheological properties, dendrimers and hyperbranched polymers are attractive candidates for applications as rheology modifiers in linear polymer processing.[16] When blended into linear polymers, these compact globular molecules would act as bearing balls, lubricate movements of linear polymer chains and, therefore, significantly reduce polymer melt viscosity. For this perspective, we investigated the effects of blending hyperbranched polymer on the viscosity reduction of linear polymers.

Hyperbranched Sample 2 was blended with Sample 4 that has more linear chain topology, at three weight percentages (10, 30, and 50 wt%) through a solution blending technique. Dynamic oscillation tests were conducted at 25 °C on the three blends. Figure 10(a) shows the complex viscosity curves for the three blends with a comparison to the two pure polymers. Figure 10(b) shows the effects of the Sample 2 percentage on the complex viscosity at angular frequency of 0.0063 s^{-1}. Increasing the Sample 2 percentage in the blend decreased the low frequency viscosity. This viscosity reduction was more significant when Sample 2 was lower than 30 wt% and in this range the viscosity was a linear function of the percentage of Sample 2.

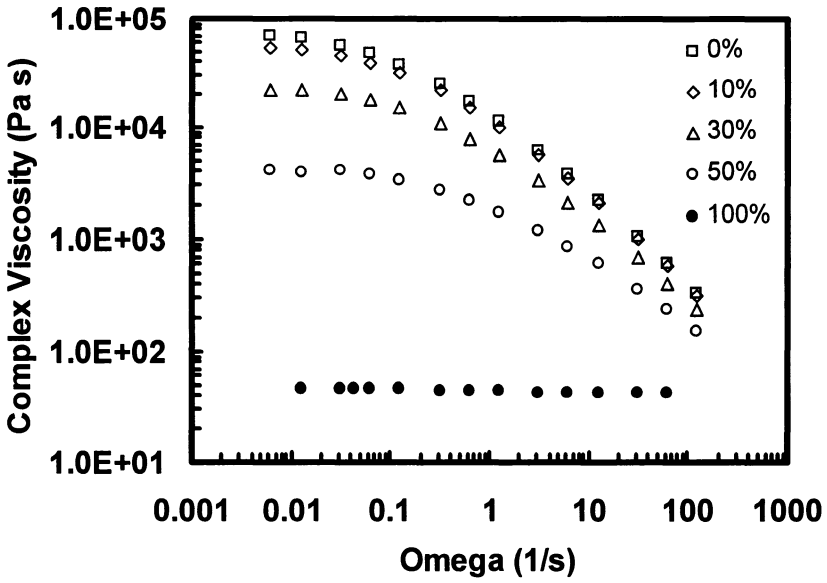

(a)

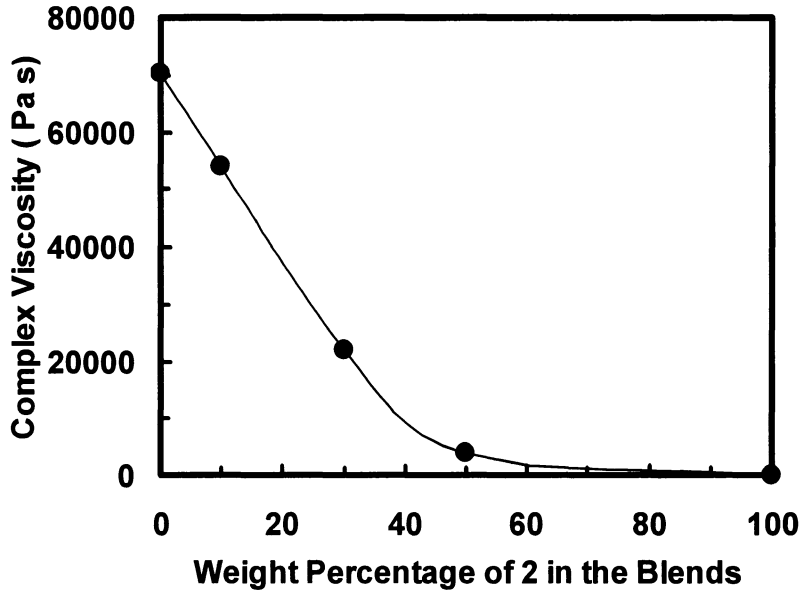

(b)

Figure 4.10 (a) Complex viscosity as a function of angular frequency from dynamic oscillation measurements for blends of Samples 2 and 4 at 25 °C: the effect of the weight percentage of Sample 2. (b) Complex viscosity of blends measured at angular frequency of 0.063 s^{-1} at 25 °C vs. the weight percentage of Sample 2 in the blend.

4.5 Conclusion

Seven branched polyethylenes of different chain topologies and branch densities were prepared with chain walking catalysts **1** and **2**/MMAO. The unique rheological properties of this novel series of polymers were first examined through extensive rheological characterizations utilizing steady shear, creep-recovery, and dynamic oscillation techniques. The effects of chain topology and branch structure on polymer flow behavior, flow activation energy, and dynamic moduli were elucidated in detail. The main findings from this work were as follows:

1. Chain topology greatly affected the polymer flow behavior. Hyperbranched polymers (Samples 1 and 2) exhibited typical Newtonian flow behavior, while the other polymers with chain topology intermediate between hyperbranched and linear structure showed non-Newtonian shear-thinning behavior due to the presence of chain entanglements.
2. Time-temperature superposition was valid for all the polymers. The temperature effect agreed to an Arrhenius equation. The polymers exhibited higher activation energy (E_a = 43.8 ~ 57.2 kJ/mol) than conventional HDPE and LLDPE. The activation energy tended to increase with the change of chain topology from hyperbranched to linear structure.
3. In the terminal region, different dependencies of dynamic moduli (G'(ω), G"(ω)) on angular frequency (ω) were found. The dependencies tended to be closer to those from theoretical prediction when the chain topology became less linear. The master curves in the log(G') vs. log(G") plot were also dependent on chain topology. For the Ni-dimine polymers (Samples 6 and 7), their master curves were very close to those of linear HDPE and LLDPE owing to their linear chain topology.

4. The plateau modulus at 60 °C and the entanglement molecular weight for Samples 6 and 7 were experimentally determined from the G"(ω) vs. ln(ω) curves. The M_e values were slightly higher than those of HDPE.
5. The blends of Samples 2 and 4 were rheologically characterized. The addition of hyperbranched polymer to linear polymer significantly reduced the viscosity of the blends.

4.6 References

1. Kaminsky, W.; Arndt, M. *Adv. Polym. Sci.* **1997**, *127*, 143.
2. Chum, P. S.; Kruper, W. J.; Guest, M. J. *Adv. Mater.* **2000**, *12*, 1759.
3. Gahleitner, M. *Prog. Polym. Sci.* **2001**, *26*, 895.
4. (a) Vega, J. F.; Munoz-Escalona, A.; Santamaria, A.; Munoz, M. E.; Lafuente, P. *Macromolecules* **1996**, *29*, 960. (b) Vega, J. F.; Santamaria, A.; Munoz-Escalona, A.; Lafuente, P. *Macromolecules* **1998**, *31*, 3639.
5. (a) Yan, D.; Wang, W.-J.; Zhu, S. *Polymer* **1999**, *40*, 1737. (b) Kolokda, E.; Wang, W.-J.; Zhu, S.; Hamielec, A. E. *Macromolecules* **2002**, *35*, 10062.
6. (a) Wood-Adams, P. M.; Dealy, J. M. *Macromolecules* **2000**, *33*, 7481. (b) Wood-Adams, P. M.; Dealy, J. M.; deGroot, A. W.; Redwine, O. D. *Macromolecules* **2000**, *33*, 7489. (c) Wood-Adams, P.; Costeux, S. *Macromolecules* **2001**, *34*, 6281.
7. (a) Shroff, R. N.; Mavridis, H. *Macromolecules* **1999**, *32*, 8454. (b) Shroff, R. N.; Mavridis, H. *Macromolecules* **2001**, *34*, 7362.
8. (a) Malmberg, A.; Kokko, E.; Lehmus, P.; Lőfgren. B.; Seppälä, J. V. *Macromolecules* **1998**, *31*, 8448. (b) Malmberg, A.; Gabriel, C.; Steffl, T.; Münstedt, H.; Lőfgren. B. *Macromolecules* **2002**, *35*, 1038.

9. (a) Ittel, S. D.; Johnson, L. K.; Brookhart, M. *Chem. Rev.* **2000**, *100*, 1169. (b) Johnson, L. K.; Killian, C. M.; Brookhart, M. *J. Am. Chem. Soc.* **1995**, *117*, 6414. (c) Tempel, D. J.; Johnson, L. K.; Huff, R. L.; White, P. S.; Brookhart, M. *J. Am. Chem. Soc.* **2000**, *122*, 6686.

10. (a) Guan, Z.; Cotts, P. M.; McCord, E. F.; McLain, S. J. *Science* **1999**, *283*, 2059. (b) Cotts, P. M.; Guan, Z.; McCord, E.; McLain, S. *Macromolecules* **2000**, *33*, 6945. (c) Guan, Z.; Cotts, P. M.; McCord, E. F. *Polym. Prepr.* **1998**, *39*, 402. (d) Guan, Z.; Cotts, P. M. *Polym. Mater. Sci. Eng.* **2001**, *84*, 382. (e) Guan, Z. *Chem. Eur. J.* **2002**, *8*, 3086.

11. (a) Plentz Menegetti, S.; Kress, J.; Lutz, P. J. *Macromol. Chem. Phys.* **2000**, *201*, 1823. (b) Lutz, P. J.; Plentz, Meneghetti, S.; Kress, J.; Lapp, A.; Duval, M. *Polym. Prepr.* **2000**, *41*, 1882.

12. Ye, Z.; Zhu, S. *Macromolecules* **2003**, *36*, 2194.

13. Flory, P. J.; Fox, T. G. *J. Am. Chem. Soc.* **1951**, *73*, 1904.

14. Sun, T.; Brant, P.; Chance, R. R.; Graessley, W. W. *Macromolecules* **2001**, *34*, 6812.

15. Cox, W. P.; Merz, E. H. *J. Polym. Sci.* **1958**, *28*, 619.

16. Hult, A.; Johansson, M.; Malmström, E. *Adv. Polym. Sci.* **1999**, *143*, 1.

17. Hawker, C. J.; Farrington, P. J.; Mackay, M. E.; Wooley, K. L.; Fréchet, J. M. J. *J. Am. Chem. Soc.* **1995**, *117*, 4409.

18. Cross, M. M. *J. Colloid Sci.* **1965**, *20*, 417.

19. (a) Jahromi, S.; Palmen, J. H. M.; Steeman, P. A. M. *Macromolecules* **2000**, *33*, 577. (b) Sendijarevic, I.; McHugh, A. J. *Macromolecules* **2000**, *33*, 590. (c) Kwak, S.-Y.; Ahn, D. U. *Macromolecules* **2000**, *33*, 7557. (d) Suneel, D.; Buzza, M. A.; Groves, D. J.; McLeish, T. C. B.; Parker, D.; Keeney, A. J.; Feast, W. J. *Macromolecules* **2002**, *35*, 9605.

20. Rouse, P. E. *J. Chem. Phys.* **1953**, *21*, 1272.

21. Graessley, W. W. *Adv. Polym. Sci.* **1974**, *16*, 1.

22. Rjau, V. R.; Rachapudy, H.; Graessley, W. W. *J. Polym. Sci., Polym. Phys. Ed.* **1979**, *17*, 1223.

23. Han, C. D. *J. Appl. Polym. Sci.* **1988**, *35*, 167.

Chapter 5

Synthesis of Ethylene-1-Hexene Copolymers from Ethylene Stock with Tandem Catalyst Systems

This chapter is organized based on the paper published in *Macromolecular Rapid Communication*, **2004**, *25*, 647-652 by Z. Ye, F. AlObaidi, and S. Zhu.

5.1 Abstract

This chapter reports and investigates the utilization of tandem catalyst systems for the synthesis of linear low density polyethylene with predominantly butyl branches from ethylene stock in a single reactor. The catalyst systems employed the tandem action between an ethylene trimerization catalyst, (η^5-$C_5H_4CMe_2C_6H_5$)$TiCl_3$ (**1**)/MMAO, and a copolymerization metallocene catalyst, [(η^5-C_5Me_4)$SiMe_2$(^{t}BuN)]$TiCl_2$ (**2**)/MMAO or *rac*-Me_2Si(2-MeBenz[*e*]Ind)$_2ZrCl_2$ (**3**)/MMAO. During the reaction, **1**/MMAO *in situ* generated 1-hexene with high activity and high selectivity by ethylene trimerization, while **2**/MMAO or **3**/MMAO copolymerized ethylene with the *in situ* produced 1-hexene to generate butyl branched polyethylene. By adjusting the ratio of the trimerization and copolymerization catalysts and/or changing the reaction temperature, a series of branched polyethylene grades with melting temperature from 60 °C to 127 °C and crystallinity from 7.6 % to 56.9 % were prepared.

Keywords: linear low density polyethylene (LLDPE), ethylene-1-hexene copolymer, binary catalyst system, trimerization, copolymerization, metallocene catalyst.

5.2 Introduction

Linear low-density polyethylene (LLDPE) is an important family of polyolefins. Compared to high density polyethylene (HDPE), due to controlled length and frequency of short chain branches, LLDPE exhibits lower melting point, low crystallinity, and low density, which effectively facilitate polymer processing and introduces favorable materials properties for a wide range of applications.[1]

LLDPE is conventionally produced by ethylene copolymerization with α-olefin comonomers, such as 1-butene, 1-hexene, and 1-octene, with classical Ziegler-Natta catalysts and/or recently developed single-site type catalysts. This conventional route is a two-stage operation, i.e., ethylene oligomerization to produce α-olefin followed by ethylene copolymerization with the α-olefin comonomer. Recently there has been a considerable amount of research interest in preparing LLDPE in a single stage with ethylene as the sole monomer stock in a single reactor.[2,3] Compared to the two-stage process, this single-stage route provides great advantages in process operation and cost saving.

Two different strategies have been explored in literatures for LLDPE production by a single-stage process with ethylene as the sole monomer. The first is to use Ni-Diimine type catalysts for ethylene polymerization. This new series of catalysts are able to produce short chain branches on polyethylene backbone through a chain-walking mechanism.[4] By a simple change of catalyst structure and reaction conditions such as ethylene pressure and reaction temperature, short chain branched polyethylenes of various branch densities can be effectively produced.[4,5] This strategy has been successfully realized in Dupont's Versipol process.[6] However, a main drawback of this process is its difficulty in controlling short chain branch length, which is a very important factor determining materials

properties. It has been shown that ethylene copolymers with 1-hexene or 1-octene have improved properties compared to ethylene-1-butene copolymer.[7] The PE products prepared with Ni-Diimine catalyst mainly constitute methyl branches, about 70 % of the total branches.[8] Their materials properties are close to those of ethylene-propylene copolymers, which limits their applications as LLDPE.

The other alternative strategy employs the tandem action of binary catalyst systems for ethylene polymerization.[2,3] One catalyst produces short/long-chain 1-alkene through ethylene oligomerization/polymerization. The other catalyst component copolymerizes ethylene with the *in situ* produced 1-alkene to produce branched chains. A simple change in the ratio of two catalysts can adjust the branching amount in the product.[2,3] A suitable selection of the catalyst type for 1-alkene generation can efficiently control the branch length by tailoring the 1-alkene length. The advantages of easy operation and cost effectiveness make this binary catalyst approach a promising route to LLDPE production.

The selection of catalysts for a tandem system is critical in order to have successful tandem action and a number of factors need to be considered. These factors include (1) compatibility of the catalysts; (2) reactivity and kinetic behavior of the catalysts at the same reaction condition; (3) ability of 1-alkene incorporation; (4) diffusion of 1-alkene in reaction system.[2] Fortunately, the latest developments in homogeneous single-site metallocene and late transitional metal catalysts provide us with unprecedented freedom in selecting suitable combinations of catalysts. Some successful examples have been reported in literatures. Bazan and coworkers [9a] demonstrated the synthesis of butene-ethylene and hexene-butene-ethylene copolymers by the binary tandem system of {[(η^5-C_5Me_4)$SiMe_2$(^{t}BuN)]TiMe}{$MeB(C_6F_5)_3$} / [$(C_6H_5)_2PC_6H_4C(OB(C_6F_5)_3)O$-$\kappa^2$P,O]Ni($\eta^3$-$CH_2CMeCH_2$), in which the single-site Ni catalyst produced 1-butene and 1-hexene by ethylene dimerization and trimerization, while the Ti

catalyst copolymerized ethylene with the *in situ* produced 1-butene and/or 1-hexene. Other systems producing branched polyethylenes with various branch lengths were also reported. Bazan and coworkers reported the production of branched polyethylenes with some combinations of the catalysts $(C_5H_5BOEt)_2ZrCl_2$/MAO, $[(\eta^5\text{-}C_5Me_4)SiMe_2(^tBuN)]TiCl_2$/MAO, $[(2\text{-}ArN{=}C(Me))_2C_5H_3N]FeCl_2$/MAO, $Me_2SiInd_2ZrCl_2$/MAO, and $EtInd_2ZrCl_2$/MAO.[9b,9c] In a recent work,[9d] they reported a triple tandem catalyst system, comprising of $\{[(\eta^5\text{-}C_5Me_4)SiMe_2(^tBuN)]TiMe\}\{MeB(C_6F_5)_3\}$, $[(C_6H_5)_2PC_6H_4C(OB(C_6F_5)_3)O\text{-}\kappa^2P,O]Ni(\eta^3\text{-}CH_2C_6H_5)$, and $\{(H_3C)C[N(C_6H_5)]C[O\text{-}B(C_6F_5)_3][N(C_6H_5)]\text{-}\kappa^2N,N\}Ni(\eta^3\text{-}CH_2C_6H_5)$. Dupont researchers [10] also reported in several patents the production of branched PE with binary systems consisting of the tridentate bisiminepyridine iron and metallocene catalysts. More recently, Marks et al. [11] studied the tandem catalytic system of $[(\eta^5\text{–}3\text{-}EtInd)SiMe_2(^tBuN)]ZrMe_2/[(\eta^5\text{-}C_5Me_4)SiMe_2(^tBuN)]TiMe_2$ activated with a binuclear cocatalyst, $[Ph_3C^+]_2[1,4\text{-}(C_6F_5)_3BC_6F_4B(C_6F_5)_3^{-2}]$, for the synthesis of branched polyethylene. Significantly more homogeneous polyethylene samples were produced with the binuclear catalyst than with mononuclear activators. In above systems, 1-alkene monomers with Schultz-Flory chain length distribution were produced and *in situ* copolymerized with ethylene to produce branched polyethylenes with various branch lengths.

The tandem catalyst systems were also reported for the production of long chain branched polymers. Soares et al reported a binary metallocene system $\{[(\eta^5\text{-}C_5Me_4)SiMe_2(^tBuN)]TiMe\}\{MeB(C_6F_5)_3\}$ combined with $Et[Ind]_2ZrCl_2$/MAO for the production of long chain branched polyethylene.[12]

However, all the above reported systems produced either mainly short ethyl-branched ethylene-butene copolymers or polymer mixtures of linear PEs and branched PEs with very complex branch structures due to the generation of 1-

alkenes with broad chain length distribution. Here we report the first tandem systems, comprising of a cyclopentadienyl-arene titanium catalyst, [(η^5-$C_5H_4CMe_2C_6H_5$)]$TiCl_3$ (**1**)/MMAO, and a metallocene catalyst, [(η^5-C_5Me_4)$SiMe_2$(^{t}BuN)]$TiCl_2$ (**2**)/MMAO or *rac*-Me_2Si(2-MeBenz[*e*]Ind)$_2ZrCl_2$ (**3**)/MMAO (see Scheme 5.1), to prepare butyl branched ethylene-1-hexene copolymers, which are usually more expensive and have significantly improved physical properties compared to ethylene-1-butene copolymers.[7] The cyclopentadienyl-arene titanium catalyst trimerized ethylene into 1-hexene with high activity and high selectivity while the metallocene catalyst simultaneously copolymerized ethylene with the *in situ* produced 1-hexene. The polymer samples produced in this work are very pure in terms of branch type with butyl branch > 98 %.

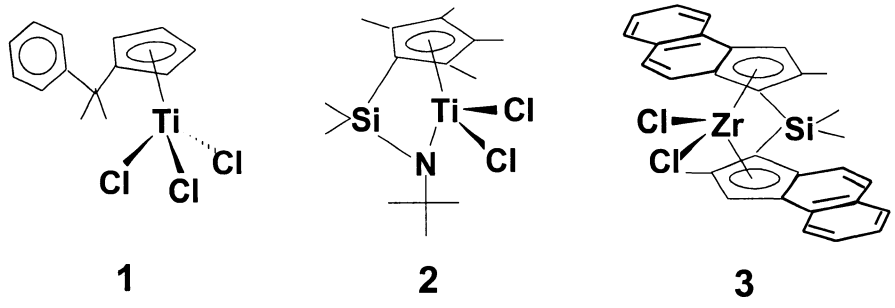

1 2 3

Scheme 5.1 The catalysts applied in this work.

5.3 Experimental Part

5.3.1 Materials

Toluene (anhydrous grade, from Aldrich) was refluxed over metallic sodium with benzophenone as indicator and distilled under nitrogen atmosphere

prior to use. UHP nitrogen (from Vitale Air) and polymerization-grade ethylene (from Matheson Gas) were purified by passing through CuO, ascarite, and 5A molecular sieves. The cocatalyst, modified methylaluminoxane aluminum (MMAO-3A), was provided by Akzo-Nobel Corporation as 7.25 wt% aluminum in toluene. The cyclopentadienyl-arene titanium catalyst precursor (**1**), was synthesized according to the literature procedure.[13] The constrained geometry catalyst precursor, $[(\eta^5\text{-}C_5Me_4)SiMe_2(^tBuN)]TiCl_2$ (**2**), was purchased from Boulder Scientific Company and used as received. The zirconocene catalyst precursor, *rac*-$Me_2Si(2\text{-}MeBenz[e]Ind)_2ZrCl_2$ (**3**), was donated from Mitsubishi Chemical and used as received. Handling of the air and/or moisture sensitive materials was all conducted in a nitrogen-filled dry-box or under nitrogen protection.

5.3.2 Polymer Synthesis

(a) Ethylene Trimerization with 1/MMAO at 1 atm Ethylene Pressure

The trimerization was carried out in a 500 mL glass reactor equipped with a magnetic stirrer under atmospheric ethylene pressure. Toluene and MMAO were introduced into the reactor under nitrogen protection. The reactor was evacuated, pressurized with ethylene, and then placed into an oil bath set at the operating temperature. After equilibrium for 10 minutes, a prescribed amount of toluene stock solution of **1** was injected to start trimerization. The reaction temperature and ethylene pressure was kept constant throughout the trimerization process. Magnetic stirring was applied. After 1 hour, the reactor was vented. The trimerization product was collected for GC-MS analysis. Polymer byproduct was collected, washed with acidified methanol, and then dried.

(b) Ethylene Polymerization with Tandem 1/2/MMAO System under 1 atm Ethylene Pressure

A procedure similar to the above trimerization process was applied. The prescribed amount of each catalyst (both **1** and **2**) stock solution in toluene was injected simultaneously to initiate the concurrent trimerization and polymerization. The reaction temperature and ethylene pressure were kept constant throughout the reaction. Magnetic stirring was applied. After 1 hr, the reaction was quenched by injecting 20 ml methanol and venting the reactor. The polymer produced was collected, washed with an excessive amount of methanol, and then dried.

(c) Ethylene Copolymerization with Trimerization Product Directly Prepared with 1/MMAO

In a 500 mL glass reactor equipped with a magnetic stirrer, prescribed amounts of toluene and MMAO were added under nitrogen protection. The reactor was evacuated, pressurized with 1 atm ethylene, and then placed into an oil bath set at 25 °C. After equilibrium catalyst **1** stock solution was injected to start the trimerization process. After 1 hour of trimerization, stock solution of catalyst **2** was injected into the reactor to initiate the copolymerization process. In the whole process, ethylene pressure (1 atm) and reaction temperature (25 °C) were stabilized. After 1 hour, the reactor was vented and 20 mL acidified methanol solution was injected to terminate the copolymerization process. The polymer was collected, washed with a large amount of methanol, and dried.

(d) Ethylene Copolymerization with Distilled Trimerization Product Prepared with 1/MMAO

In a 500 mL glass reactor equipped with a magnetic stirrer, prescribed amounts of toluene and MMAO were added under nitrogen protection. Subsequently the reactor was evacuated, pressurized with 1 atm ethylene, and then placed into an oil bath set at 25 °C. After equilibrium catalyst **1** stock solution was injected to start the trimerization process. After 1 hour, the reactor was vented. The trimerization reaction mixture was then distilled under nitrogen protection to recover 1-hexene and most of the toluene. The collected distillate and a prescribed amount of MMAO were then added into a 500 mL glass reactor under nitrogen atmosphere. Again the reactor was evacuated, pressurized with 1 atm ethylene, and placed into an oil bath set at 25 °C. After equilibrium stock solution of catalyst **2** was added to start the copolymerization. After 1 hour, the reactor was vented and acidified methanol was added. The polymer was collected, washed with methanol, and then dried.

5.3.3 Polymer Characterizations

The GC-MS analysis was conducted on a Micromass GCT time of flight mass spectrometer attached to an Agilent HP6890 GC to determine the 1-hexene and C10 alkene concentrations in the trimerization product. The polymer melting point (T_m) was measured using Thermal Analysis 2910 MDSC from TA Instruments in the standard DSC mode. UHP N_2 gas at a flow rate of 30 ml/min was purged through the calorimeter. A refrigerated cooling system (RCS) with the cooling capacity to 220 K was attached to the DSC cell. The temperature and heat capacity of the instrument were initially calibrated with indium standard at the heating rate of 10 °C/min. The polymer sample (about 5 mg) was first heated to 180 °C at the rate of 10 °C/min to remove thermal history. It was then cooled down to 20 °C at 10 °C/min. A second heating cycle was used for the acquisition of the DSC thermogram at the scanning rate of 10 °C/min. The peak temperature with the highest endotherm was chosen as the melting point. Polymer molecular

weight (MW) and molecular weight distribution (MWD) were measured at 140 °C in 1,2,4-trichlorobenzene using Waters Alliance GPCV 2000 with DRI detector coupled with an in-line capillary viscometer. The polymer molecular weights were calculated according to a universal calibration curve based on 11 polystyrene standards with molecular weights ranging from 1.09×10^6 to 2500 g/mol. The 75.4 MHz ^{13}C NMR analyses were conducted on a Bruker AV300 pulsed NMR spectrometer at 120 °C. The polymer samples were dissolved in 1,2,4-trichlorobenzene and deuterated *o*-dichlorobenzene (weight ratio of 9/4) mixture in 10 mm NMR tubes with a concentration about 20 wt%. Waltz-supercycle decoupling was used to remove ^{13}C - ^{1}H couplings. At least 2500 scans were applied for each acquisition to obtain a good signal-to-noise ratio. Polymer chemical shift assignments and calculations followed ASTM D5017-91 method.[14]

5.4 Results and Discussion

5.4.1 Reactivities of Individual Catalysts

The reactivity profiles for individual catalysts are important parameters for designing a binary catalyst system. It not only provides a guideline to determine the ratio of catalysts used, but also sets a baseline to evaluate possible interactions of the two catalysts. Detailed ethylene trimerization and polymerization with individual precursors **1**, **2**, and **3** activated with MAO have been reported in the literatures,[13,15,16] respectively. In this part, we report the performance of the individual catalysts conducted under our experimental conditions.

Table 5.1 lists two runs of ethylene trimerization with **1**/MMAO under ethylene pressure of 1 atm. The system is highly active (with 1-hexene

Table 5.1 Ethylene trimerization with **1**/MMAO.[a]

Run	Temp (°C)	1-hexene[b] (g)(wt%)	C10[b] (g)(wt%)	PE (g)(wt%)	Prod.[c]	PE properties				
						M_w[d] (K)	PDI[d]	T_m[e] (°C)	ΔH_m[e] (J/g)	χ_c[f] (%)
1	25	1.3 (76)	0.2 (12)	0.2 (12)	0.065	241.7	8.7	127.5	121.4	41.9
2	45	0.4 (71)	0.06 (11)	0.1 (18)	0.020	837.6	11.3	129.3	128.4	44.3

[a] Other reaction conditions: solvent, toluene; total volume, 150 mL; ethylene pressure, 1 atm; **1** amount, 20 μmol; Al/Ti = 1000 (molar); reaction time, 1 hr.
[b] Determined from GC-MS.
[c] 1-hexene productivity in (kilograms of 1-hexene)/(mmol Ti hr)
[d] Determined from GPCV measurement at 140 C in 1,2,4-trichlorobenzene.
[e] Determined from DSC measurement.
[f] Crystallinity based on H_m = 290 J/g for a perfect PE crystal.

Table 5.2 Ethylene polymerization with individual **2**/MMAO and **3**/MMAO catalysts.[a]

Run	Reaction conditions				Polymer (g)	Prod.[b]	Polymer properties				
	Catalyst and amount	[Al]/[M]	Temp (°C)	Time (min)			M_w[c] (K)	PDI[c]	T_m[d] (°C)	ΔH_m[d] (J/g)	χ_c[e] (%)
3	2, 15 μmol	1000	25	60	2.60	0.173	386.4	11.9	135.1	164.2	56.6
4	2, 25 μmol	700	45	60	4.69	0.188	147.2	6.7	134.1	199.9	68.9
5	3, 0.1 μmol	21900	25	20	3.23	96.9	500.7	11.7	133.9	138.4	47.7

[a] Other reaction conditions. Solvent, toluene; total volume, 150 mL; ethylene pressure, 1 atm.
[b] Polymer productivity in (kilograms of PE produced)/(mmol M hr).
[c] From GPCV measurement in 1,2,4-trichlorobenzene at 140 C.
[d] From DSC measurement.
[e] Crystallinity based on H_m = 290 J/g for a perfect PE crystal.

productivity up to 65 g/(mmol Ti bar hr)) and highly selective (with 1-hexene selectivity up to 76 %) for ethylene trimerization. In addition to 1-hexene produced, C10 alkene fractions (~ 10 wt%) mainly in the form of incorporable 5-methylnon-1-ene[13] were also produced and they were the concomitant

cotrimerization products of two ethylene units with one 1-hexene unit. A small amount of high molecular weight PE byproduct was also produced. These PE byproducts had high melting points, melting enthalpies, and crystallinities as shown in Table 5.1. ^{13}C NMR analysis of the PE byproduct in Run 1 showed a very low level of 1-hexene incorporation (1-hexene molar percentage = 0.99 % in the copolymer). GPCV analyses showed that these polymers have high molecular weight and broad molecular weight distribution.

2/MMAO and **3**/MMAO were chosen in this work as the catalysts for copolymerization because of their high ability of comonomer incorporation.[9,16] Table 5.2 lists the results of ethylene polymerization with the individual catalysts. **2**/MMAO appeared to be very stable and facile for ethylene polymerization and it was active throughout the 1-hour reaction time at both 25 °C and 45 °C. In contrast, **3**/MMAO was over 500 times more active than **2**/MMAO. The highest exotherm was immediately observed when the polymerization started. All the polymers produced with the individual catalysts exhibited typical thermal properties of homo PEs, such as high melting temperature (130 ~ 135 °C) and high crystallinity (47 ~ 69 %). Broad molecular weight distributions were observed for these homo polymers. This broadening in MWD has been observed in previous investigations [11,15] and is believed to be caused by the heterogeneity of physical states in the polymerization system due to PE precipitation, instead of by the heterogeneity of active sites.

Before the application of the tandem catalyst systems for the ethylene polymerization, two conventional step-wise ethylene copolymerization runs (Runs 6 and 7 in Table 5.3) with the trimerization product from Run 1 in Table 5.1 were conducted using **2**/MMAO. In Run 6, right after ethylene trimerization with **1**/MMAO for 1 hr, **2** was directly injected into the reactor to start the

Table 5.3 Sequential two-step copolymerizations of ethylene with trimerization products from **1**/MMAO in Run 1 with **2**/MMAO system.[a]

Run	Reaction conditions			Polymer (g)	Polymer properties					
	2 amount (μmol)	[Al]/[M]	Temp (°C)		Hexene[b] (%)	M_w[c] (K)	PDI[c]	T_m[d] (°C)	ΔH_m[d] (J/g)	χ_c[e] (%)
6	15	1000	25	2.40	11.8	109	4.2	48.6, 126.9[f]	39.4	13.6
7	15	1000	25	3.50	10.4	96	2.7	99.1	44.5	15.3

[a] Other conditions: solvent, toluene; total volume, 150 mL.
[b] 1-Hexene molar percentage in the copolymer from ^{13}C NMR measurement.
[c] Determined by GPCV.
[d] Measured by DSC.
[e] Crystallinity based on H_m = 290 J/g for a perfect PE crystal.
[f] Higher melting peak was from a small amount of polymer byproduct produced by **1**/MMAO.

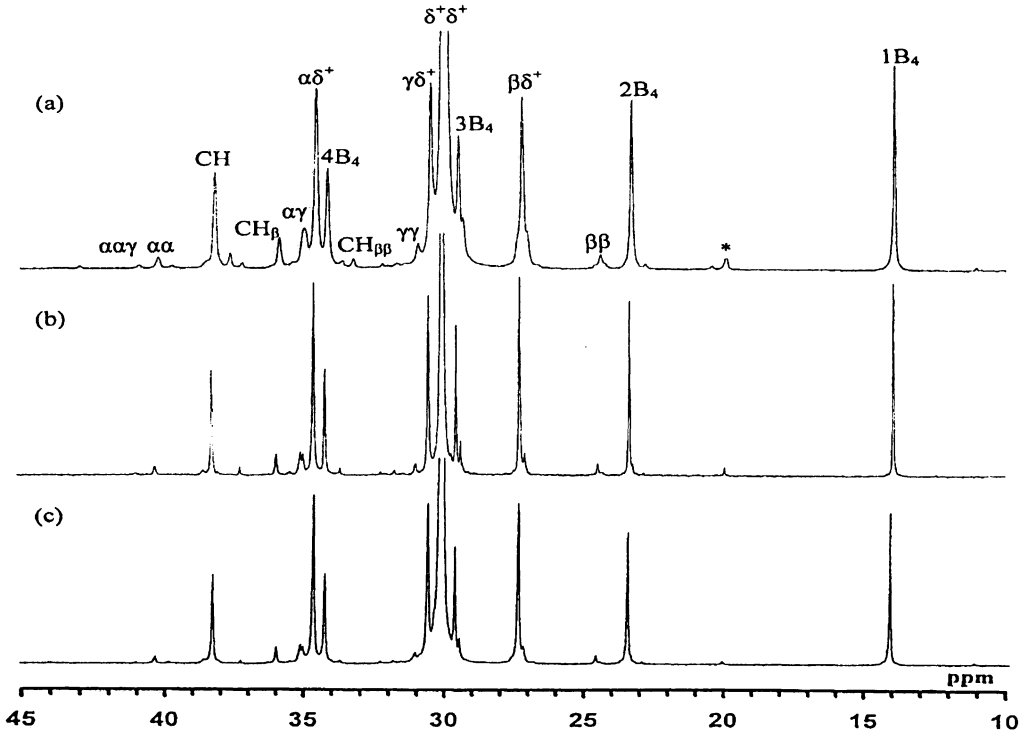

Figure 5.1 ^{13}C NMR spectra of the polymers produced in (a) Run 6, (b) Run 7 and (c) Run 11.

copolymerization of ethylene with the 1-alkenes produced in the trimerization. In Run 7, the trimerization product in toluene solution after 1 hr reaction time was first distilled under atmospheric pressure to purify 1-hexene from the C10 fraction that has higher boiling point and then ethylene copolymerization with the purified 1-hexene in toluene was conducted using **2**/MMAO.

As shown in Run 7 in Table 5.3, the presence of the comonomer obviously enhanced polymer productivity. This activity enhancement could be attributed to a decrease in crystallinity and therefore an increase in solubility of the branched polymer produced, which improved the diffusion of monomers into active sites.[15] Compared to homo PE, the DSC analysis showed a significant decrease in the melting point and crystallinity (T_m = 99.1 °C and χ_c = 15.3 %), of the copolymer, indicating the presence of short chain branches.

The ^{13}C NMR spectra of the copolymers (Figure 5.1(a) and (b)) suggest that the polymers are typical butyl-branched ethylene-1-hexene copolymers with 1-hexene molar percentage around 10 %. From Figure 5.1(a), in addition to butyl branches, in the copolymer produced in Run 6 the 5-methyl-heptyl branches resulted from the incorporation of copolymerizable 5-methylnon-1-ene were seen from the methyl branch resonance centered at 20.0 ppm. The 5-methyl-heptyl branches counted for ~ 10 % of the total branches in the copolymer, which was consistent with the 5-methylnon-1-ene content in the trimerization product. However, from Figure 5.1(b) the percentage of 5-methyl-heptyl branches in the Run 7 sample was much lower (~ 4 %) due to the purification of 1-hexene by distillation

Figure 5.2 compares the molecular weight distribution curves for the copolymer from Run 7 and the homopolymer from Run 3. Lower weight-average molecular weight was observed for the copolymer because of the comonomer

incorporation. The copolymer also exhibited narrower MWD (PDI = 2.7), showing the improvement of homogeneity due to the enhanced solubility of copolymer.

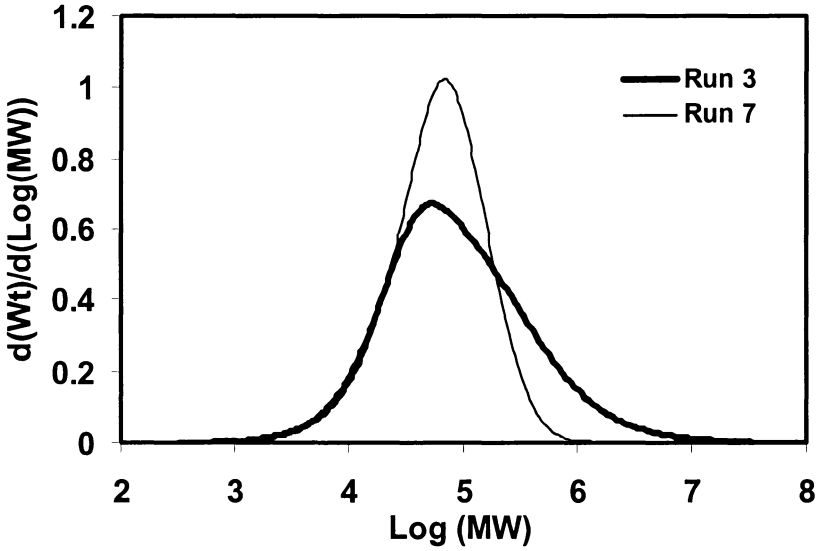

Figure 5.2 Molecular weight distributions of the polymer samples produced in Runs 3 and 7.

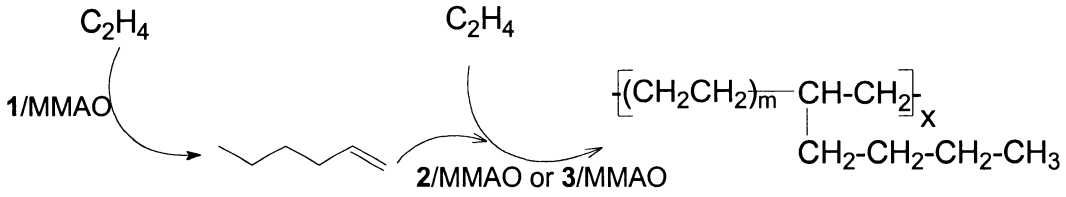

Scheme 5.2 The strategy for the tandem catalyst system for producing ethylene-1-hexene copolymers.

5.4.2 Ethylene Polymerization with the Tandem 1/2/MMAO System

A tandem action of the 1-hexene generation catalyst, **1**/MMAO, and the copolymerization catalyst, **2**/MMAO or **3**/MMAO, in a single reactor should lead to the production of ethylene-1-hexene copolymer from ethylene. The overall strategy of the tandem catalyst systems is presented in Scheme 5.2. The two catalysts were simultaneously added into the reactor to start the concurrent trimerization and copolymerization processes.

The results of ethylene copolymerization with the **1**/**2**/MMAO system are presented in Table 5.4. For the runs at the same reaction temperature, the amount of **2** was kept constant, while the amount of **1** was changed to investigate its effect on polymer properties and polymerization behavior.

Table5.4 Ethylene polymerization with the tandem **1**/**2**/MMAO system.[a]

Run	Reaction conditions			Polymer (g)	Polymer properties					
	1:**2**:Al	**2** amount (μmol)	Temp (°C)		M_w[b] (K)	PDI[b]	hexene[c] (%)	T_m[d] (°C)	ΔH_m[d] (J/g)	χ_c[e] (%)
8	1:3:4000	15	25	2.29	100.3	3.3	3.0	113.6	99.6	34.3
9	2:3:4000	15	25	2.49	160.0	4.3	5.1	91.8	81.2	28.0
10	3:3:4000	15	25	3.19	117.8	2.8	6.9	80.8, 126.1[f]	53.6	18.5
11	6:3:4000	15	25	3.13	99.2	3.2	9.5	60.0, 127.3[f]	22.0	7.6
12	1.5:5:4000	25	45	3.26	75.1	3.7	-	127.0	164.9	56.9
13	3:5:4000	25	45	3.98	57.2	4.3	-	126.5	156.1	53.8
14	5:5:4000	25	45	4.10	40.7	2.9	2.3	124.2	129.6	44.7
15	10:5:4000	25	45	4.23	40.2	2.6	-	121.7	117.6	40.6

[a] Other reaction conditions. Solvent, toluene; total volume, 150 ml; ethylene pressure, 1 atm; time, 1 hr.
[b] From GPCV measurement.
[c] Molar percentage of 1-hexene in the copolymer determined from ^{13}C NMR.
[d] From DSC measurement.
[e] Crystallinity based on H_m = 290 J/g for a perfect PE crystal.
[f] Higher melting peak was from a small amount of polymer byproduct produced by **1**/MMAO

From Table 5.4, for a given amount of **2**, an increase of the **1/2** molar ratio led to an increase in the polymer productivity. This can be attributed to two factors. One is due to an increased amount of polymer byproducts formed by **1**/MMAO. The other is because of the enhancement of homogeneity due to the increase of polymer solubility.

DSC, ^{13}C NMR, and GPCV were used to analyze the polymer properties. From these analytical results, it can be found that a successful tandem action between the two catalysts was achieved. Figure 5.3 compares the DSC thermograms of the polymers produced at different **1/2** molar ratios but the same concentration of **2** at 25 °C. An increase of **1/2** ratio from 0 to 2 effectively decreased the melting point from 135.1 °C to 60.0 °C and reduced the crystallinity from 56.6 % to 7.6 % due to an increased amount of 1-hexene generated by **1**/MMAO in the binary system.

Surprisingly and interestingly, for the copolymers produced in the concurrent trimerization and polymerization processes with the tandem catalytic system, ^{13}C NMR analyses showed that butyl branches were > 98 % of the total branches and the amount of 5-methyl-heptyl branches was negligible (< 2 %) in all the copolymers investigated. Figure 5.1(c) shows the ^{13}C NMR spectrum of a typical polymer produced in Run 11 in Table 5.4 with the tandem system. In the polymerization runs with the tandem catalytic system, 1-hexene was *in situ* generated and simultaneously consumed. Therefore, the 1-hexene concentration was lower than that in trimerization at the same condition, where the 1-hexene content was accumulated. This reduced 1-hexene concentration minimized the product of ethylene/1-hexene cotrimerization and thus resulted in a lower 5-methyl-heptyl branch content in the copolymer.

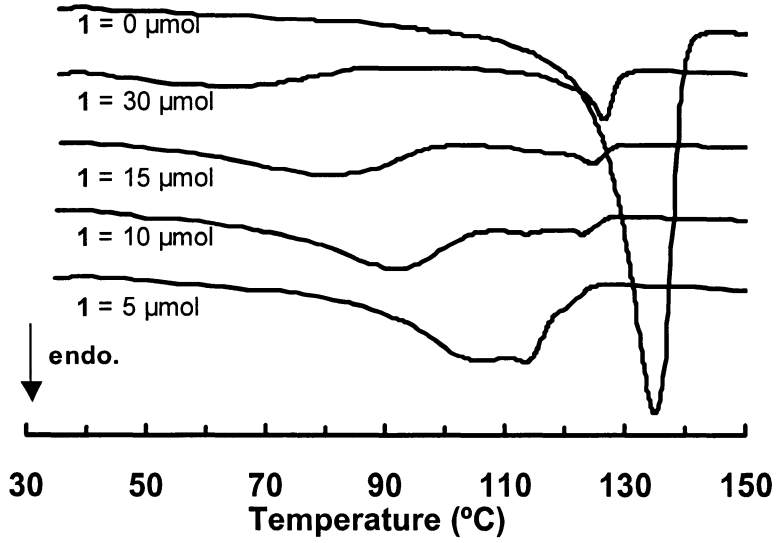

Figure 5.3 DSC thermograms of the polymers produced with the **1**/**2**/MMAO system at 25 °C. The concentration of **1** varied, while that of **2** remained the same at 15 μmol.

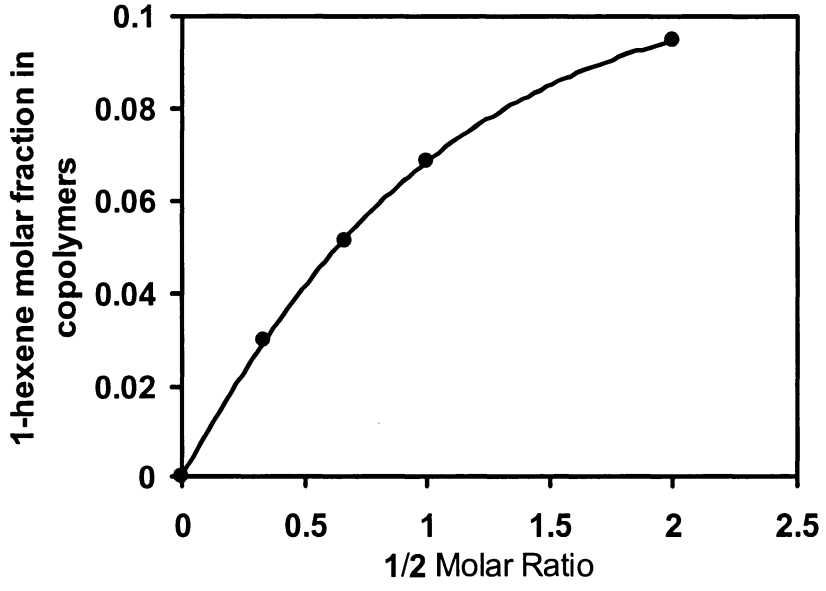

Figure 5.4 Effect of **1**/**2** ratio on 1-hexene molar fraction in the copolymers at 25 °C. The concentration of **1** remained 15 μmol.

Figure 5.4 shows the dependence of 1-hexene molar fraction in the copolymer on the ratio of **1/2**. By adjusting the molar ratio of **1/2**, a series of copolymer samples with molar fraction of 1-hexene ranged from 0.03 to 0.10 were obtained at this reaction temperature. The GPCV analysis showed that the copolymers had lower weight-average molecular weights than the homo polymers produced with **2**/MMAO at the same condition. The MWD of the copolymers are narrower than the homo polymer. However, the polydispersity values of 2.8 ~ 4.3 were observed. This might be caused by the polymer byproduct produced with **1**/MMAO.

Another feature of these copolymers is their broad melting endotherm. As shown in Figure 5.3, very broad and even multi-modal melting behavior were observed. The melting peak centered at 126 °C can be attributed to the polymer byproduct produced by **1**/MMAO. The intensity of the peak increased with an increase of the **1/2** ratio. The broad melting endotherm indicated broad distribution of comonomer composition. It can be attributed to the unsteady concentration of 1-hexene in the reaction system. During the reaction, 1-hexene is generated by **1**/MMAO and is *in situ* consumed by **2**/MMAO. Its concentration depends on both the generation rate and the consumption rate. When the rate of generation is much faster than that of consumption, the system is 1-hexene abundant. The copolymers with high 1-hexene fraction can be produced. When the rate of consumption is much faster than that of generation, the system is 1-hexene starving, the copolymer would contain less comonomer. The kinetic behaviors of the two catalysts are the factors that determine the product composition.

The tandem action was also observed in the polymerization at 45 °C with the **1/2**/MMAO system. Figure 5.5 compares the DSC thermograms of the copolymers produced at different **1/2** ratios at this temperature. An increase in the

1/2 ratio resulted in a decrease in the melting point and crystallinity. However, compared to 25 °C, the polymers exhibit much higher melting point (121 ~ 127 ° C) and crystallinity (40.6 ~ 56.9 %). This difference can be attributed to a much lower trimerization productivity of **1**/MMAO at higher temperature due to the enhanced catalyst deactivation.

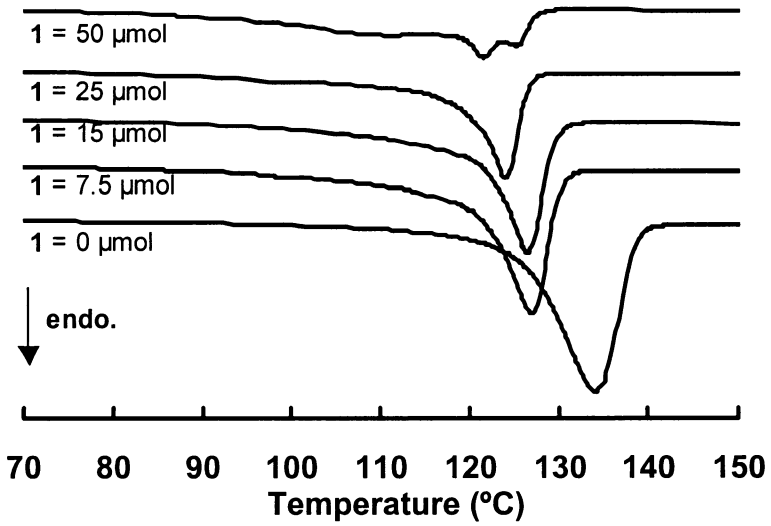

Figure 5.5 DSC thermograms for the polymers produced with **1/2**/MMAO system at 45 °C. The concentration of **1** varied, while that of **2** remained the same at 25 μmol.

5.4.3 Ethylene Polymerization with the Tandem 1/3/MMAO System

Table 5.5 summarizes the results of ethylene copolymerization with the **1/3**/MMAO system. Considering the much higher activity of **3**/MMAO than **1**/MMAO and **2**/MMAO, we used high **1/3** ratios (50 ~ 200) in order to balance

Table 5.5 Ethylene polymerization with binary **1**/**3**/MMAO system. [a]

Run	Reaction conditions				Polymer (g)	Polymer properties				
	1:**3**:Al	**3** amount (μmol)	Temp (°C)	Time (min)		M_w[b] (K)	PDI[b]	T_m[c] (°C)	ΔH_m[c] (J/g)	χ_c[d] (%)
16	5:0.1:16400	0.1	25	20	3.43	862.6	12.5	121.0	114.4	39.4
17	10:0.1:21900	0.1	25	20	1.92	540.7	10.9	111.7	89.7	30.9
18	20:0.1:21900	0.1	25	20	2.24	299.8	6.9	104.5	80.9	27.9
19	20:0.2:21900	0.2	25	20	3.08	333.9	4.2	105.0	68.6	23.7

[a] Other reaction conditions: Solvent, toluene; total volume, 150 mL; ethylene pressure, 1 atm.
[b] From GPCV measurement.
[c] From DSC measurement.
[d] Crystallinity based on H_m = 290 J/g for a perfect PE crystal.

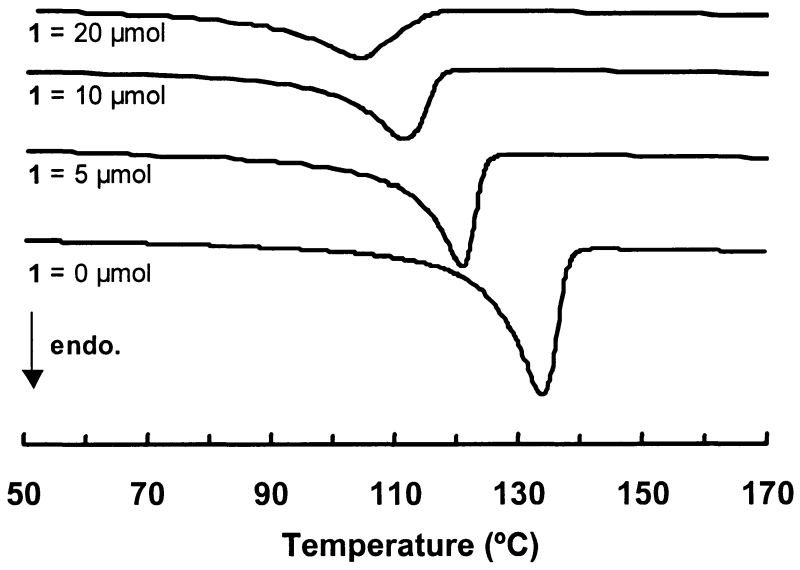

Figure 5.6 DSC thermograms for the polymers produced with **1**/**3**/MMAO system at 25 °C. The concentration of **1** varied, while that of **3** amount remained the same at of 0.1 μmol.

the rate of trimerization and that of polymerization. As shown in Table 5.5, at a low **1/3** ratio (Run 16), the binary tandem system produced more polymer materials than homopolymerization (Run 5 in Table 5.3) due to the improvement of homogeneity. However, a further increase in the **1/3** ratio reduced the amount of polymer, suggesting the interaction between the two types of active sites at the higher **1/3** ratios.

Figure 5.6 shows the DSC thermograms of the copolymers produced at the same **3** concentration but different **1/3** ratios. An increase in the **1/3** ratio resulted in a decrease of the melting point and crystallinity. Compared to the copolymers produced with the **1/2** system at the same amount of **1**, the copolymers produced with this system had lower 1-hexene incorporation. This difference was attributed to the different kinetic behaviors of **2**/MMAO and **3**/MMAO.

5.5 Conclusion

The binary tandem catalyst systems, **1/2**/MMAO and **1/3**/MMAO, were used to synthesize ethylene-1-hexene copolymers from ethylene stock in a single reactor. By varying catalyst ratio, reaction temperature, and the catalyst combination, polyethylene materials with different melting points and crystallinities were obtained. Compared to other tandem systems reported in the literature, the systems reported in this work represent the first tandem catalyst systems that are capable of producing LLDPE samples with predominantly butyl branches.

5.6 Reference

1. Peacock, A. J. *Handbook of Polyethylene: Structures, Properties, and Applications*, Marcel Dekker, New York, 2000.
2. Komon, Z. J. A.; Bazan, G. C. *Macromol. Rapid Commun.* **2001**, *22*, 467.
3. de Souza, R. F.; Casagrande Jr., O. L. *Macromol. Rapid Commun.* **2001**, *22*, 1293.
4. (a) Ittel, S. D.; Johnson, L. K.; Brookhart, M. *Chem. Rev.* **2000**, *100*, 1169. (b) Johnson, L. K.; Killian, C. M.; Brookhart, M. *J. Am. Chem. Soc.* **1995**, *117*, 6414.
5. Ye, Z.; Alsyouri, H.; Zhu, S.; Lin, Y. S. *Polymer* **2003**, *44*, 969.
6. Johnson, L. K.; Killian, C. M.; Brookhart, M. US Patent 96/23010, **1996**.
7. James, D. E. "Linear low density polyethylene", in *Encyclopedia of Polymer Science and Engineering* Mark, H. F.; Bikales, N. M.; Overberger, C. G.; Menges, G. Eds., Wiley Interscience, New York, 1985, Vol. 6, p. 429.
8. Galland, G. B.; Souza, R. F. de; Mauler, R. S.; Nunes, F. F. *Macromolecules* **1999**, *32*, 1620.
9. (a) Komon, Z. J. A.; Bu, X.; Bazan, G. C. *J. Am. Chem. Soc.* **2000**, *122*, 1830. (b) Barnhart, R. W.; Bazan, G. C. *J. Am. Chem. Soc.* **1998**, *120*, 1082. (c) Quijada, R.; Rojas, R.; Bazan, G.; Komon, Z. J. A.; Mauler, R. S.; Galland, G. B. *Macromolecules* **2001**, *34*, 2411. (d) Komon, Z. J. A.; Diamond, G. M.; Leclerc, M. K.; Murphy, V.; Okazaki, M.; Bazan, G. C. *J. Am. Chem. Soc.* **2002**, *124*, 15280.
10. (a) Bennett, A. M. A. US Patent Application 729305, **2000**. (b) Bennett, A. M. A. US Patent Application 729286, **2000**. (c) Bennett, A. M. A.; Coughlin, E. B.; Citron, J. D.; Wang, L. US Patent Application 945861, **2001**.
11. Abramo, G. P.; Li, L.; Marks, T. J. *J. Am. Chem. Soc.* **2002**, *124*, 13966.

12. Beigzadeh, D.; Soares, J. B. P.; Duever, T. A. *Macromol Rapid Commun* **1999**, *20*, 541.
13. (a) Deckers, P. J. W.; Hessen, B.; Teuben, J. H. *Angew. Chem. Int. Ed.* **2001**, *40*, 2516. (b) Deckers, P. J. W.; Hessen, B.; Teuben, J. H. *Organometallics* **2002**, *21*, 5122.
14. ASTM D 5017-96, "Determination of Linear Low Density Polyethylene (LLDPE) Compositions by Carbon-13 Nuclear Magnetic Resonance", in 1998 Annual Book of ASTM Standards, Vol 08.03, 1998, p.286.
15. Shiono, T.; Moriki, Y.; Ikeda, T. *Macromol. Chem. Phys.* **1997**, *198*, 3229.
16. Schneider, M.J.; Suhm, J.; Mülhaupt, R.; Prosenc, M.-H.; Brintzinger, H.-H. *Macromolecules* **1997**, *30*, 3164.

Chapter 6

Synthesis of Branched Polypropylene with Isotactic Backbone and Atactic Side Chains by Binary Iron and Zirconium Single-Site Catalysts

This chapter is based on the paper published in *Journal of Polymer Science, Part A: Polymer Chemistry*, **2003**, *41*, 1152-1159 by Z. Ye and S. Zhu.

6.1 Abstract

This chapter reports the use of a binary single-site catalyst system for synthesizing comb-branched polypropylene samples having isotactic polypropylene backbones and atactic polypropylene side chains from propylene feedstock. This catalyst system consisted of the bisiminepyridine iron catalyst $[(2\text{-ArN=C(Me)})_2C_5H_3N]FeCl_2$ (Ar = $2,6\text{-}C_6H_3(Me)_2$) (**1**) and the zirconocene catalyst *rac*-$Me_2Si(2\text{-MeBenz}[e]Ind)_2ZrCl_2$ (**2**). The former *in situ* generated 1-propenyl ended atactic polypropylene macromonomer, while the latter incorporated the macromonomer into the copolymer. The effects of reaction conditions, such as catalyst addition procedure and molar ratio of **1/2** on the branching frequency were studied. Copolymer samples having branching density up to 8.6 aPP side chains per 1000 iPP monomer units were obtained. The branched copolymers were characterized by ^{13}C NMR and DSC.

Keywords: Binary catalyst system, single-site type catalysts, tandem action, propylene polymerization, branching, high impact polypropylene.

6.2 Introduction

Metallocene technology has a tremendous impact on polyolefin industry. It provides unprecedented flexibility in polymer design.[1] One of the most unique developments in this technology is the preparation of long-chain-branched polyolefins by using homogeneous metallocene catalysts capable of incorporating *in situ* produced or externally added vinyl-ended macromonomer during olefin polymerization.[2-5] The presence of LCBing in a polymer product can significantly improve the material processability and increase its melt strength.[6] Moreover, for isotactic polypropylene, a recent study by Kolodka et al. has shown that grafting rubbery poly(ethylene-co-propylene) side chains onto plastic isotactic polypropylene backbone can improve the polymer impact strength.[7]

Binary catalyst systems are effective and promising for one-step production of short- and/or long-chain-branched polyethylene in a single reactor with ethylene as the sole monomer.[8] The overall strategy of this technique employs a tandem action of two single-site catalysts. In this catalytic system, one catalyst produces vinyl-ended long- and/or short-chain 1-alkenes by ethylene polymerization and/or oligomerization; the other catalyst component polymerizes ethylene and incorporates the *in situ* produced 1-alkenes into growing polyethylene chains. A simple change in the ratio of the two catalysts can adjust the branching level in the copolymer.[8]

There are some successful examples reported for the production of branched polyethylenes in the literature using binary tandem catalyst systems.[9-12] And in Chapter 5, the tandem systems for the production of ethylene-1-hexene copolymers were investigated. However, no work has been reported about the synthesis of branched/grafted polypropylenes with the binary catalytic system, although there are some reports [13] about the use of binary metallocene systems for

production of stereo-block polypropylene, which allowed chain transfers to occur between catalysts of different stereoselectivities during chain formation and was very different from the point of view involved here. In this chapter we report the synthesis of isotactic polypropylene grafted with atactic polypropylene side chains using the binary catalyst system of the bisiminepyridine iron catalyst [(2-ArN=C(Me))$_2$C$_5$H$_3$N]FeCl$_2$ (**1**) /MMAO combined with the zirconocene catalyst *rac*-Me$_2$Si(2-MeBenz[*e*]Ind)$_2$ZrCl$_2$ (**2**) /MMAO. The **1**/MMAO catalyst was chosen because of its highly selective production of vinyl-ended polypropylene macromonomer during propylene polymerization and its easy adjustment on macromonomer molecular weight by changing the bulkiness of the tridentate pyridine-bis(imine) ligand.[14] The zirconocene catalyst was selected based on its high ability to copolymerize propylene macromonomer with propylene.[4,5] The branched polymer produced in this work is expected to improve polymer rheological property and mechanical impact.

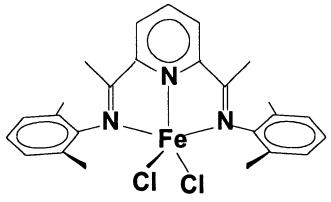

1

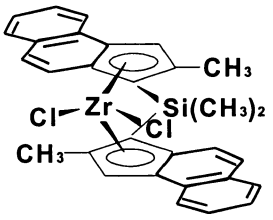

2

Scheme 6.1 The catalysts used in this work.

6.3 Experimental Part

6.3.1 Materials

Toluene (anhydrous grade, from Aldrich) was refluxed over metallic sodium with benzophenone as indicator and distilled under nitrogen atmosphere prior to use. Polymerization grade propylene (from Matheson Gas) was purified by passing it through CuO, Ascarite, and 5A molecular sieves. The cocatalyst, modified methylaluminoxane aluminum (MMAO-3A), was provided by Akzo-Nobel Corporation as 7.25 wt% aluminum in toluene. The bisiminepyridine iron catalyst precursor, $[(2\text{-ArN=C(Me)})_2C_5H_3N]FeCl_2$ (Ar = 2,6-$C_6H_3(Me)_2$) (**1**), was synthesized according to the literature procedure.[14] The zirconium catalyst precursor, *rac*-$Me_2Si(2\text{-MeBenz}[e]Ind)_2ZrCl_2$ (**2**), was donated from Mitsubishi Chemical Company and used as received. Handling of the air and/or moisture sensitive material was all conducted in a nitrogen-filled drybox or under nitrogen protection.

6.3.2 Propylene Homopolymerization

The polymerization was carried out in a 500 mL glass reactor at 25 °C under atmospheric propylene pressure. Toluene (200 mL) and MMAO were introduced into the reactor under nitrogen atmosphere. The reactor was evacuated and then pressurized with propylene. The reaction was initiated by injecting catalyst precursors. Propylene pressure and reaction temperature were kept constant throughout the polymerization. The reaction was quenched with acidified methanol. For the reactions with catalyst **1**/MMAO, the atactic polypropylene was isolated by evaporation of the solvent and dissolution of the remaining in hexane followed by washing with a large amount of acidified methanol to remove any remaining aluminum salts. For the polymerization using **2**/MMAO, the polymer produced was filtered and washed with a large amount of methanol.

6.3.3 Propylene Copolymerization

The copolymerization was conducted in a flame-dried 500 mL glass reactor under atmospheric propylene pressure at 25 °C. Toluene of 200 ml and a prescribed amount of MMAO were added into the reactor under nitrogen atmosphere. The reactor was then vacuumed and pressurized with propylene. Two catalyst addition methods were applied. In Method (a), toluene slurry of **1** and toluene solution of **2** were added into the reactor simultaneously. In Method (b), toluene slurry of **1** was injected into the reactor to produce and accumulate atactic polypropylene macromonomers. After a certain period of reaction time, toluene solution of **2** was injected to initiate the copolymerization. The reaction temperature and propylene pressure were kept constant during the whole reaction period. After a certain period of copolymerization time, the reaction was quenched by turning off the propylene feed and venting the reactor. The polymer mixture was filtered to separate the soluble atactic polypropylene macromonomer from the insoluble isotactic polypropylene. The copolymer from the filter residue was washed with acidified methanol and dried under vacuum. The solvent in the filtrate was evaporated and the atactic polypropylene was recovered, dissolved in hexane, washed with acidified methanol, and then dried under vacuum.

6.3.4 Polymer Characterizations

The polymer melting point (T_m) was measured using Thermal Analysis 2910 MDSC from TA Instruments in the standard DSC mode. UHP N_2 gas at a flow rate of 30 ml/min was purged through the calorimeter. A refrigerated cooling system (RCS) with the cooling capacity to 220 K was attached to the DSC cell. The temperature and heat capacity for the instrument were initially calibrated with indium standard at the heating rate of 10 °C/min. The polymer sample (about 5 mg) was first heated to 180 °C at the rate of 10 °C/min to remove

thermal history. It was then cooled down to 0 °C at 5 °C/min. A second heating cycle was used for the acquisition of the DSC thermogram at the scanning rate of 10 °C/min. Polymer molecular weight (MW) and molecular weight distribution (MWD) were measured at 140 °C in 1,2,4-trichlorobenzene using Waters Alliance GPCV 2000 with DRI detector coupled with an in-line capillary viscometer. The polymer molecular weight was calculated according to a universal calibration curve based on polystyrene standards. ^{1}H and ^{13}C NMR analyses were conducted on a Bruker AV300 pulsed NMR spectrometer. ^{1}H NMR analysis for atactic polypropylene macromonomer was conducted at 30 °C with deuterated chloroform as solvent. For ^{13}C NMR analysis, the polymer samples were dissolved in 1,2,4-trichlorobenzene and deuterated *o*-dichlorobenzene mixture in 10 mm NMR tubes with concentration about 20 wt%. Waltz-supercycle decoupling was used to remove ^{13}C-^{1}H couplings. At least 3000 scans were applied for each acquisition to obtain a good signal-to-noise ratio.

6.4 Results and Discussion

6.4.1 Propylene Polymerization with Individual Catalysts

The detailed work on propylene polymerization with **1** or **2** catalyst system has been reported in the literature.[14,15] The propylene polymerization with these catalyst systems was also conducted in this work under the conditions of 1 atm propylene pressure and 25 °C to evaluate their performances and to provide guidance for designing the binary catalyst system. Table 6.1 summarizes the propylene polymerization with these individual catalysts. Compared to **2**/MMAO system, **1**/MMAO had much lower activities toward propylene polymerization, suggesting a higher level of **1** needed in the binary system to match the reactivity of **2**/MMAO. The polypropylene samples produced with **1**/MMAO were viscous

oil-like materials due to their low polymer molecular weight (~ 3.0 kg/mol) and atactic nature.

Table 6.1 Propylene polymerization with individual catalysts.[a]

Run	Cat.	[Al]/[Cat.]	[Cat.] (μM)	Time (min)	Polymer Produced (g)	Polymer Properties		
						M_w[b] (kg/mol)	PDI[b]	T_m[c] (°C)
1	**1**	1000:1	75	120	3.9	3.2	1.3	-
2	**1**	1000:1	75	30	1.5	3.0	1.2	-
3	**2**	15000:1	5	45	10.6	532.3	2.5	154.6

[a] Other reaction conditions: solvent, toluene 200 mL; propylene pressure, 1atm; reaction temperature, 25 °C.
[b] Determined by GPCV.
[c] Peak melting point from DSC measurements.

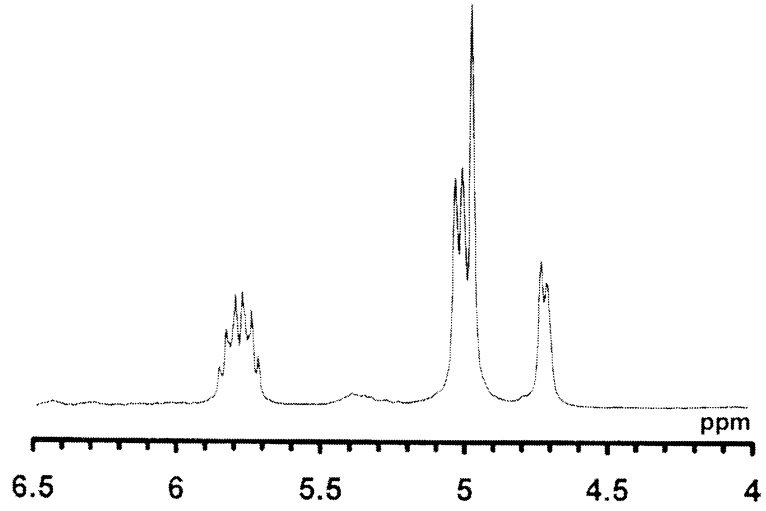

Figure 6.1 ^{1}H NMR spectrum of aPP produced in Run 1.

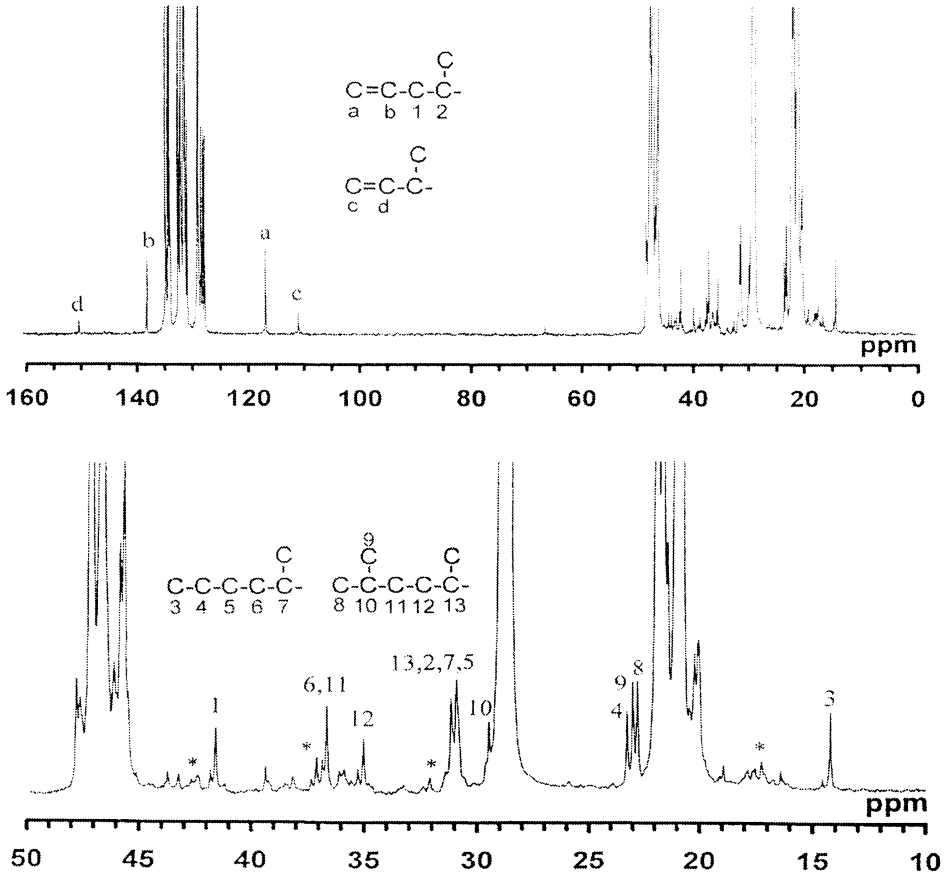

Figure 6.2 ^{13}C NMR spectrum of aPP produced in Run 1.

The bisiminepyridine series of iron catalysts were reported to exhibit a unique 2,1 chain propagation mechanism, leading to the exclusive formation of 1-propenyl end groups following β-H elimination/abstraction and chain transfer.[14] Figure 6.1 shows the ^{1}H NMR spectrum of the polypropylene produced with **1**/MMAO at our condition (Run 1 in Table 6.1). The resonances of vinyl protons are shown at 5.0 and 5.8 ppm. The resonances of vinylidene protons around 4.8 ppm are weak. The presence of the two types of unsaturated end groups is also evident in the ^{13}C NMR spectrum of the polymer as shown in Figure 6.2. The relative intensity of the vinyl and vinylidene groups indicates that the majority of

unsaturation is vinyl group (about 77 mol%). The formation of the vinylidene group was not reported in the work by Brookhart et al.[14] Its presence in our samples is probably due to the increased 1,2 propylene insertion followed by β-H elimination at the reaction condition. The 1,2 error insertion can be confirmed from the signals with asterisks near 16.0–18.5 ppm, 30.5–33.0, 34.5–38.5 ppm, and 41.0–44.0 ppm in the ^{13}C NMR spectrum shown in Figure 6.2. These regioerror signals are split into broad peaks due to stereo irregularity nature of the polymer chain.

From Figure 6.2, two types of saturated end groups, n-butyl and 3-methyl-butyl, can be identified. The formation of these chain ends was elucidated in the work by Brookhart et al.[14] From the ^{13}C NMR spectrum, the unsaturated end groups exhibit intensity close to that of the saturated end groups. The number-average molecular weight calculated from the ^{1}H NMR by assuming one polymer chain has one unsaturated end group is very close to the one measured by GPCV. These results suggest that an individual polypropylene chain bear one unsaturated end group, either 1-propenyl or vinylidene. The methyl resonance in the ^{13}C NMR indicates that the polypropylene produced with **1**/MMAO is atactic with [mmmm] = 29 %.

6.4.2 Propylene Polymerization with Binary 1/2/MMAO System

The tandem action of the macromonomer-forming catalyst, **1,** and the copolymerizing catalyst, **2**, in a single reactor leads to the formation of branched isotactic polypropylene from propylene. The overall strategy for the tandem catalyst system is presented in Scheme 6.2.

Two catalyst addition methods were applied for the propylene polymerization with the binary catalyst system in this work. In Method (a), after

the reactor was filled with certain amounts of toluene and MMAO, purged and pressurized with propylene, prescribed amounts of toluene solution or slurry of **1** and **2** were added into the reactor simultaneously. In Method (b), the reactor was first charged with prescribed amounts of toluene and MMAO, purged and pressurized with propylene, before toluene slurry of **1** was injected into the reactor. After a certain period of reaction time, toluene solution of **2** was added. In both methods, the molar concentration of **1** was higher than **2**, in order to compensate its lower activity toward propylene polymerization. After a certain reaction time, the polymer mixture was filtered and washed with heated toluene several times to separate the toluene-soluble atactic polypropylene produced with **1**/MMAO from the insoluble isotactic polypropylene produced with **2**/MMAO. Table 6.2 summarizes the polymerization runs and the properties of polymers produced.

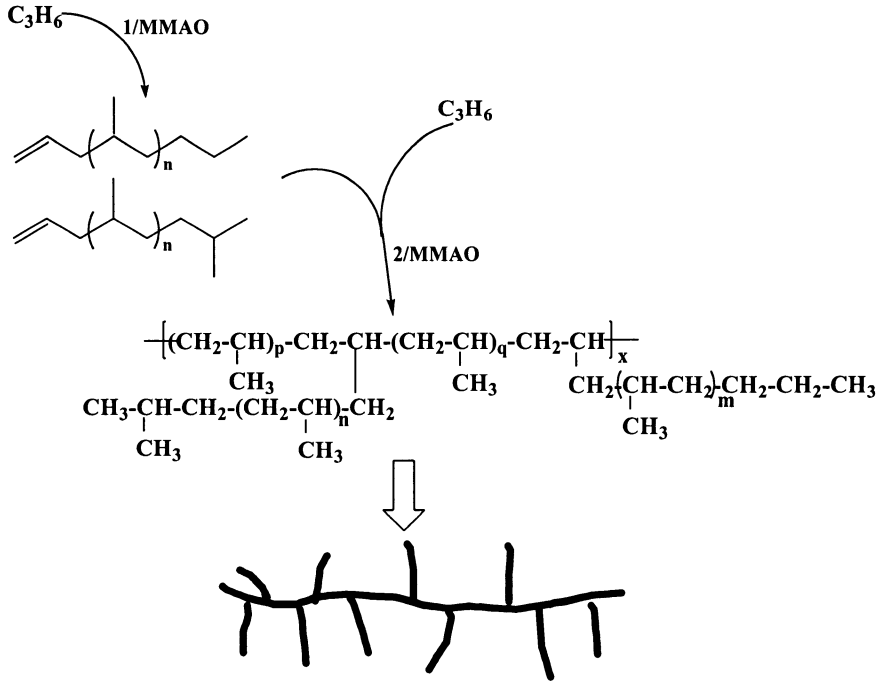

Scheme 6.2 Strategy for the binary system for branched polypropoylenes.

It is of interest to see that the catalyst addition method greatly affected the performance of the binary catalyst system. For the reactions with Method (a), no tandem action between **1** and **2** was observed. The polymer product was a mixture of homo isotactic polypropylene and atactic polypropylene produced by **2**/MMAO and **1**/MMAO, respectively. No grafting of atactic polypropylene side chains onto isotactic polypropylene backbone was found. Take Runs 4 and 5 in Table 2 as example. Catalysts **1** and **2** were added into reactor simultaneously. The DSC analyses showed that the toluene-insoluble polymer part exhibited a melting point as high as that of homo isotactic polypropylene produced with **2**/MMAO (Run 3 in Table 6.1). Moreover, ^{13}C NMR spectra of the toluene-insoluble polymer parts (Figure 6.3(b)) were identical to that of high molecular weight homo isotactic polypropylene,[4] no new peaks were observed in addition to the resonances due to methylene, methyl, methine cabons of iPP and regioerror carbons. The toluene-soluble atactic polypropylenes produced in these two runs exhibited similar M_w and PDI compared to the homo atactic polypropylene prepared with **1**/MMAO. ^1H NMR showed these atactic polypropylenes exhibited similar unsaturated end groups as shown in Figure 1. The inefficient grafting with Method (a) can probably be related to diffusion limitations on the propylene macromonomer in the system. During polymerization, the isotactic polypropylene produced will precipitate out around active sites of **2**, form a barrier to the diffusion of propylene macromonomer into the active sites and thus inhibit the branching.

In contrast, when Method (b) was applied, significant incorporation of atactic polypropylene macromonomer was observed. Compared to Method (a), this method introduces aPP macromonomers around the active sites of **2** before the formation and precipitation iPP, which allows the copolymerization to occur.

In Table 6.2 (Runs 6 ~ 10), the polymerization with Method (b) and the polymer properties were summarized. ^{13}C NMR was used to investigate the branched copolymer structure in detail. In Figure 6.3, the ^{13}C NMR spectrum of branched iPP copolymer produced in Run 6 is illustrated together with those of homo iPP in Run 4 and aPP macromonomer in Run 1. In addition to the resonances of methylene, methyl and methine carbons of iPP and regioerror carbons, the carbons of n-butyl and 3-methyl butyl end groups can be observed, whereas those of 1-propenyl groups disappear. Moreover, new resonances appear at around 31.7 and 44.5 ppm, which are attributed to the conjunction methine and methylene carbons, respectively, of aPP macromonomer in the branched copolymer. The methylene carbons of the conjunction parts are split into several peaks due to the stereoirregularity in the aPP macromonomer chain end. The assignment of these chemical shifts were reported and confirmed by Shiono et al..[4] Based on the relative intensity of resonances of the conjunction carbons in the ^{13}C NMR spectrum, the branching density of aPP macromonomer in the iPP copolymer was calculated and reported in Table 6.2. The branching density as high as 8.6 aPP side chains per 1000 iPP monomer units was obtained.

The DSC analyses of the branched copolymer showed that melting points (T_m) of these polymers were lower than that of iPP produced with individual **2**/MMAO. Moreover, the melting point of the copolymer decreases with the increase of the branching density.

From Table 6.2, the branching density of aPP macromonomer in the copolymer is dependent on the addition time of catalyst **2** and also on the molar ratio of **1**/**2**. Comparing Run 6 with 7 and Run 8 with 9, an increase in the interval between the additions of **1** and **2** could significantly increase the branching density of aPP in the copolymer due to the higher aPP concentration accumulated in the system before the addition of **2**. Similarly, as shown in Runs 9

and 10, for a given concentration and addition time of **2**, an increase in the ratio of **1/2** leads to a reduction in the copolymer melting point, indicating an increase in the branching density. This is because of the higher macromonomer concentration in the system due to a higher amount of active sites by **1**/MMAO. The iPP copolymer produced exhibited similar molecular weight compared to the homo polymer produced with **2**/MMAO.

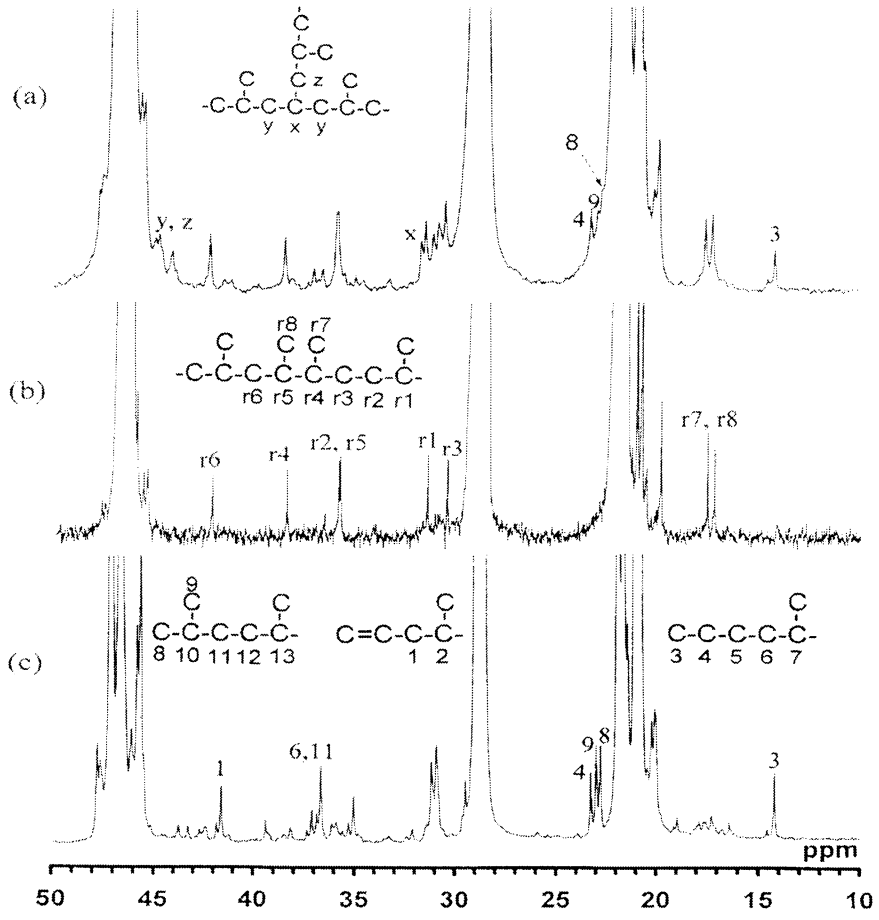

Figure 6.3 ^{13}C NMR spectra of PP copolymer and homo polymers: (a) branched iPP copolymer in Run 6, (b) iPP homo polymer in Run 4, and (c) aPP in Run 1.

Table 6.2 Propylene polymerization with binary **1/2** catalysts.[a]

Run	Zr:Fe:Al	[Zr] (μm)	Addition Time of **2** [b] (min)	Copolym Time[c] (min)	Polymer Produced (g)		Polymer Properties					
					a-PP[d]	i-PP[e]	a-PP[d]		i-PP[e]			
							M_w[f] (kg/mol)	PDI[f]	M_w[f] (kg/mol)	PDI[f]	Grafting Density[g]	T_m[h] (°C)
4	1:15:15000	5	0	60	4.3	4.4	3.4	1.3	548.8	2.5	0	155.1
5	2:15:15000	10	0	60	4.6	13.9	3.6	1.3	387.8	4.0	0	155.0
6	2:15:15000	10	90	90	4.0	1.5	3.6	1.3	631.8	2.7	8.4	144.4
7	2:15:15000	10	30	90	5.1	0.9	3.6	1.4	564.7	2.5	1.7	148.6
8	3:15:15000	15	120	60	5.3	13.8	3.3	1.3	447.3	2.3	8.6	145.6
9	3:15:15000	15	30	60	3.5	11.8	3.1	1.3	395.2	2.4	ND[i]	149.7
10	3:5:15000	10	30	60	1.3	15.6	3.0	1.3	514.4	2.3	ND[i]	153.5

[a] Other reaction conditions: solvent, toluene 200 mL; propylene pressure, 1atm; reaction temperature, 25 °C.
[b] Time interval between the additions of **1** and **2**.
[c] Polymerization time after the addition of **2**.
[d] Atactic polypropylene produced by **1**/MMAO.
[e] Grafted isotactic propylene.
[f] By GPCV vs. polystyrene standards at 140 °C.
[g] Number of grafted a-PP side chains per 1000 isotactic PP monomer units calculated based on ^{13}C NMR data.
[h] Peak melting point from DSC measurements.
[i] Not determined.

6.5 Conclusion

Through the tandem action of the bisiminepyridine iron catalyst, [(2-ArN=C(Me))$_2$C$_5$H$_3$N]FeCl$_2$ (Ar = 2,6-C$_6$H$_3$(Me)$_2$), and the zirconocene catalyst, *rac*-Me$_2$Si(2-MeBenz[*e*]Ind)$_2$ZrCl$_2$, the comb-branched polypropylene products having isotactic PP backbones and atactic PP side chains were synthesized. The former catalyst generated aPP macromonomer chains *in situ*, while the latter polymerized the macromonomer with propylene and formed iPP backbones. The samples having branching density up to 8.6 aPP side chains per 1000 iPP monomer units were prepared. The branching density was determined by the ratio of the two catalysts as well as the catalyst addition procedure. Increasing the ratio of iron/zirconium increased the branching level. The time interval between catalyst additions also had a significant effect on branching density.

6.6 Reference

1. (a) Alt, H. G.; Köppl, A. *Chem. Rev.* **2000**, *100*, 1205. (b) Coates, G. W. *Chem. Rev.* **2000**, *100*, 1223. (c) Resconi, L.; Cavallo, L.; Fait, A.; Piemontesi, F. *Chem. Rev.* **2000**, *100*, 1253. (d) Imanishi, Y.; Naga, N. *Prog. Polym. Sci.* **2001**, *26*, 1147.
2. (a) Wang, W.-J.; Yan, D.; Zhu, S.; Hamielec, A. E. *Macromolecules* **1998**, *31*, 8677. (b) Wang, W.-J.; Zhu, S.; Park, S.-J. *Macromolecules* **2000**, *33*, 5770.
3. Malmberg, A.; Liimatta, J.; Lehtinen, A.; Löfgren, B. *Macromolecules* **1999**, *32*, 6687.
4. Shiono, T.; Azad, S. M.; Ikeda, T. *Macromolecules* **1999**, *32*, 5723.
5. Weng, W.; Hu, W.; Dekmezian, A. H.; Ruff, C. J. *Macromolecules* **2002**, *35*, 3838.

6. Yan, D.; Wang, W.-J.; Zhu, S. *Polymer* **1999**, *40*, 1737.
7. Kolodka, E.; Wang, W.-J.; Zhu, S.; Hamielec, A. E. *Macromol. Rapid Commun.* **2002**, *23*, 470.
8. (a) Komon, Z. J. A.; Bazan, G. C. *Macromol. Rapid Commun.* **2001**, *22*, 467. (b) de Souza, R. F.; Casagrande Jr., O. L. *Macromol. Rapid. Commun.* **2001**, *22*, 1293.
9. (a) Komon, Z. J. A.; Bu, X.; Bazan, G. C. *J. Am. Chem. Soc.* **2000**, *122*, 1830. (b) Barnhart, R. W.; Bazan, G. C. *J. Am. Chem. Soc.* **1998**, *120*, 1082. (c) Quijada, R.; Rojas, R.; Bazan, G.; Komon, Z. J. A.; Mauler, R. S.; Galland, G. B. *Macromolecules* **2001**, *34*, 2411.
10. (a) Bennett, A. M. A. U.S. Patent Application 729305 to DuPont, priority date Dec 4, 2000. (b) Bennett, A. M. A. U.S. Patent Application 729286 to DuPont, priority date Dec 4, 2000. (c) Bennett, A. M. A.; Coughlin, E. B.; Citron, J. D.; Wang, L. U.S. Patent Application 945861 to DuPont, priority date Sept 4, 2001.
11. Abramo, G. P.; Li, L.; Marks, T. J. *J. Am. Chem. Soc.* **2002**, *124*, 13966.
12. Beigzadeh, D.; Soares, J. B. P.; Duever, T. A. *Macromol. Rapid Commun.* **1999**, *20*, 541.
13. (a) Lieber, S.; Brintzinger, H. H. *Macromolecules* **2000**, *33*, 9192. (b) Chien, J. C. W.; Iwamoto, Y.; Rausch, M. D.; Wedler, W.; Winter, H. H. *Macromolecules* **1997**, *30*, 3447.
14. Small, B. L.; Brookhart, M. *Macromolecules* **1999**, *32*, 2120.
15. Stehling, U.; Diebold, J.; Kirsten, R.; Röll, W.; Brintzinger, H. H.; Jüngling, S.; Mülhaupt, R.; Langhauser, F. *Organometallics* **1994**, *13*, 964.

Chapter 7

Synthesis and Rheological Properties of Long-Chain-Branched Isotactic Polypropylenes Prepared by Copolymerization of Propylene and Non-Conjugated Dienes

This chapter is based on a paper accepted for publication in *Industrial & Engineering Chemistry Research* by Z. Ye, F. AlObaidi, and S. Zhu.

7.1 Abstract

Long chain branched isotactic polypropylenes (LCBed PP) were synthesized by copolymerizing propylene with a small amount of non-conjugated α,ω-diene (1,9-decadiene or 1,7-octadiene) using the catalyst system of *rac*-Me_2Si(2-MeBenz[*e*]Ind)$_2ZrCl_2$(MBI)/MMAO. In this approach, the LCB structures were introduced by the incorporation of *in situ* generated macromonomers with pendant 1-octenyl or 1-hexenyl groups during the polymerization. A detailed study on the effects of diene concentration on polymer properties was conducted. Polymer chain microstructures were characterized by ^{13}C NMR, GPCV, and DSC. In the propylene/1,9-decadiene copolymerization, a series of LCBed polymer samples with the long chain branch density (LCBD) of up to 0.53 branches per 1000 carbons were produced with the diene concentrations of 0.177 ~ 3.54 mmol/L at 40 °C and 25 °C. A diene concentration of 35.4 mmol/L yielded cross-linked polymer gels. In the copolymerization of propylene and 1,7-octadiene, in addition to a small fraction of LCB structures produced, a cyclic seven-member ring structure was observed due to the cyclo-addition of 1,7-octadiene. The cyclization significantly

decreased the LCBD in the polymers. A small amplitude oscillatory shear flow measurement was conducted to evaluate the rheological properties of the LCBed polymers. Compared to the linear samples prepared at the same polymerization conditions, the LCBed polymers exhibited enhanced low-frequency complex viscosity, improved shear-thinning, increased dynamic moduli, and reduced phase angle. The samples also showed thermorheological complexity and enhanced activation energy at low frequencies. These particular properties are related to the LCB in the polymers and become more significant with the increase of LCBD. The LCBed polypropylenes were also blended with the counterpart linear samples and demonstrated the improvement of rheological properties.

Keywords: Long chain branching, polypropylene, α,ω-diene, copolymerization, metallocene catalyst, rheology, structure-property relation.

7.2 Introduction

Metallocene technology has significantly impacted polyolefin industry.[1] The homogeneous single site catalysts not only enable the production of polyolefins with narrow molecular weight distribution (MWD), narrow chemical composition distribution (CCD) and precisely controlled polymer stereoregularity, but also allow the introduction of long chain branches (LCBs) during the olefin polymerization by incorporating *in situ* generated or externally added vinyl-ended macromonomers.[2] The presence of LCBs in polymers dramatically influences the viscoelastic properties of polyolefins.[3] Numerous studies have shown that an extremely low level of LCBs can significantly enhance polymer melt strength, increase zero-shear viscosity, and improve shear-thinning, as a result, improve the processibility of metallocene polymers of narrow MWD.[4-11] Given these unique features and innovative superiorities, LCBed polyolefins have become one of the

major themes in recent polyolefin research. Extensive studies have been conducted in the literature in the areas of synthesis and rheological characterization of LCBed polyolefins, especially polyethylenes.[12-26]

Isotactic polypropylene (iPP) is one of the leading and fast growing polyolefins in terms of both production and application owing to its excellent materials properties, such as high melting point, high tensile strength, stiffness, and excellent chemical resistance.[27] However, in spite of their desirable properties, linear polypropylenes exhibit relatively low polymer melt strength, which limits applications in some important fabrications, such as thermoforming, foaming, extrusion coating, and blow molding. In addition, the processibility is also an issue for linear metallocene polypropylenes of narrow MWD. Owing to its unique characteristics in improving polymer rheological properties, LCB has long been recognized as an ideal solution to improving PP melt strength and processibility while maintaining other desirable properties.

Several different approaches have been explored in the literature to produce LCBed polypropylenes. Some of these approaches employed post-reactor technologies such as high-energy electron beam radiation,[28] peroxide curing,[29] and grafting.[30] These methods are either quite inconvenient or complex due to the added treatment step, the involved reaction mechanism and complicated polymer structure produced. Other approaches utilized in-reactor metallocene copolymerization of propylene with *in situ* generated or externally added macromonomers. Shiono et al. reported the synthesis of isotactic polypropylene grafted with atactic polypropylene side chains by the copolymerization of propylene and atactic polypropylene macromonomer which was previously synthesized with $Cp^*_2ZrCl_2$/MAO catalyst system.[12] Weng et al. explored the copolymerization of propylene with isotactic polypropylene and polyethylene macromonomers prepared in a previous reactor.[13] Recently,

Kolodka et al. reported the use of poly(ethylene-co-propylene) macromonomer for the copolymerization.[24] And in Chapter 6 we studied a binary catalyst system for producing isotactic polypropylene grafted with atactic polypropylene.[31] All these methods require extra steps of macromonomer synthesis and/or macromomer removal in order to obtain pure LCBed samples.

Compared to the above multi-step in-reactor processes, the concise and straightforward single-step propylene copolymerization with *in situ* generated vinyl-functionalized macromonomer is more desirable for the production of LCBed polymers. This strategy requires a catalyst capable of generating vinyl-functionalized chains and incorporating the macromonomers during polymerization. This strategy has been successfully applied to the preparation of LCBed polyethylenes. The β-hydride elimination that yields vinyl-ended polymer chains is the predominant mechanism of chain termination in metallocene catalyzed ethylene polymerization.[32] Nevertheless, for propylene polymerization, this strategy has limited applicability due to the existence of various chain insertion (1,2-insertion and 2,1-insertion) and termination mechanisms (such as β-H elimination, β-methyl elimination, chain transfer to H_2 and aluminum) that result in various chain end moieties.[33] So far only one example has been reported in the literature utilizing this strategy for LCBed isotactic polypropylene.[14]

The copolymerization of ethylene or propylene with a non-conjugated α,ω-diene, such as 1,9-decadiene, is another important *in situ* in-reactor method for LCBed polyolefins.[34] The diene monomers copolymerize with propylene and become pendant vinyl moieties that are further incorporated into growing chains to form H-type LCBed polymers. A very small amount of diene can introduce a significant level of LCBs.[34] Compared to the previous *in situ* methods, this method suits most catalyst systems and appears to be more efficient and commercially feasible for the production of LCBed polypropylenes. Some systematic investigations have been carried out for ethylene copolymerization

with non-conjugated α,ω-dienes for LCBed polyethylenes.[34-39] However, although there are some reports [40-46] in the literature about the copolymerization of propylene with non-conjugated dienes, few detailed fundamental studies have been conducted for the copolymerization and evaluation of the effects of LCB on rheological properties. This chapter reports a systematic study on the copolymerization of propylene with 1,9-decadiene (DD) and 1,7-octadiene (OD) with *rac*-Me_2Si(2-MeBenz[*e*]Ind)$_2ZrCl_2$ (MBI)/MMAO catalyst system, and the characterization of microstructure and rheological properties of the obtained LCBed PP samples.

7.3 Experimental Part

7.3.1 Materials

Toluene (anhydrous grade, from Aldrich) was refluxed over metallic sodium with benzophenone as indicator and distilled under nitrogen atmosphere prior to use. Polymerization grade propylene (from Matheson Gas) was purified by passing it through CuO, Ascarite, and 5A molecular sieves. The cocatalyst, modified methylaluminoxane (MMAO-3A), was provided by Akzo-Nobel Corporation as 7.25 wt% aluminum in toluene. The zirconium catalyst precursor, *rac*-Me_2Si(2-MeBenz[*e*]Ind)$_2ZrCl_2$ (MBI), was donated from Mitsubishi Chemical Company and used as received. 1,7-Octadiene and 1,9-decadiene were purchased from Aldrich and were dried with 5A molecular sieve. Handling of the air and/or moisture sensitive materials was all conducted in a nitrogen-filled glove box or under nitrogen protection.

7.3.2 Polymer Synthesis

All the polymerization runs were carried out in a 500 mL glass reactor equipped with a magnetic stirrer under atmospheric propylene pressure. Inside a nitrogen-filled glove box, prescribed amounts (reported in Table 1) of toluene, MMAO, and diene were introduced into the oven-dried reactor. The reactor was sealed, evacuated, and then pressurized with propylene. An oil bath was used to set up the reaction temperature. After 10 min equilibrium, the polymerization was initiated by injecting 0.5 μmol of stock solution of the zirconium catalyst precursor MBI. Magnetic stirring was applied during the reaction. Propylene pressure and reaction temperature were kept constant throughout the polymerization. After a prescribed period of reaction time, the polymerization was quenched by injecting 20 mL acidified methanol. The produced polymer was filtered, washed with a large amount of methanol, and then dried in a vacuum oven overnight.

7.3.3 Polymer Characterizations

The polymer melting point (T_m) was measured using a Thermal Analysis 2910 MDSC from TA Instruments in the standard DSC mode. UHP N_2 gas at a flow rate of 30 ml/min was purged through the calorimeter. A refrigerated cooling system (RCS) with the cooling capacity to 220 K was attached to the DSC cell. The temperature and heat capacity for the instrument were initially calibrated with indium standard at the heating rate of 10 °C/min. The polymer sample (about 5 mg) was first heated to 180 °C at the rate of 10 °C/min to remove thermal history. It was then cooled down to 30 °C at 10 °C/min. A second heating cycle was used for the acquisition of the DSC thermogram at the scanning rate of 10 °C/min. Polymer molecular weight (MW) and molecular weight distribution (MWD) were measured at 140 °C with 1,2,4-trichlorobenzene as solvent using Waters Alliance GPCV 2000 with DRI detector coupled with an in-line capillary viscometer. The polymer molecular weight was calculated

according to a universal calibration curve based on polystyrene standards. ^{13}C NMR analyses were conducted on a Bruker AV300 pulsed NMR spectrometer at 120 °C. The polymer samples were dissolved in 1,2,4-trichlorobenzene and deuterated *o*-dichlorobenzene mixture (weight ratio of 9/4) in 10 mm NMR tubes with concentration about 20 wt%. Waltz-supercycle decoupling was used to remove ^{13}C-^{1}H couplings. Around 5000 scans were applied for each acquisition to obtain a good signal-to-noise ratio.

7.3.4 Rheological Measurements

All melt rheological measurements of the polymer samples were conducted on a Stresstech HR rheometer in the stress-controlled oscillation mode with a 20 mm parallel plate geometry at a gap size of around 1.0 mm. Before the measurements, the polymer samples were stabilized with 5000 ppm Irganox 1010 antioxidant supplied from Ciba-Geigy Canada. Acetone as a solvent for the stabilizer was used to assist the mixing with the reactor powder of polypropylene. The solvent was evaporated under vacuum at 75 °C for overnight. For the preparation of polymer blends, the fine polymer powders were mixed at room temperature, added with antioxidant, and then melt-blended in an ATLAS Laboratory Mixing Molder at 190 °C under shear for 5 minutes. The antioxidant-conditioned polymer powders were then pelletized and compression-molded in a Carver Press at 190 °C into small disks with 20 mm in diameter and 1 mm in thickness. The rheological measurements were conducted in the frequency range of 0.002 ~ 50 Hz. Strain sweeps were performed at 1 Hz before frequency sweeps to establish the linear viscoelastic region. The experiments were performed at regular 10 °C intervals within temperature range from 170 to 240 °C. Temperature was maintained within ± 0.2 °C using an ETC-3 temperature control system and the measurements were all conducted under N_2 atmosphere. At the end of the experiment, the sample was retested at 190 °C to confirm the stability

of the sample during the measurement. For all the samples, this difference did not exceed ± 5 %.

7.4 Results and Discussion

7.4.1 Copolymerization of Propylene with 1,9-Decadiene and 1,7-Octadiene

In the copolymerization of propylene with non-conjugated α,ω-diene for the production of LCBed propylene, the proper selections of diene type and copolymerization catalyst are vital for desirable polymer microstructure and LCB efficiency. Some dienes experience intramolecular cyclo-addition during copolymerization.[34] The cyclic ring structures have been observed in the copolymerization of propylene with 1,5-hexadiene or 1,7-octadiene using various metallocene catalyst systems.[41,44] It has been shown that the cyclization selectivity of dienes depends on catalyst system and length and concentration of α,ω-diene.[41,44] Different metallocene catalysts lead to different cyclization selectivities with the same diene comonomer. However, no correlation between catalyst structure and cyclization selectivity has been established. The length of diene affects the cyclization selectivity. Studies [41,42] have shown that higher α,ω-dienes have lower cyclization selectivity (e.g. 1,9-decadiene < 1,7-octadiene < 1,5-hexadiene). The cyclo-addition of dienes in copolymerization has provided a novel route to synthesize ring structure featured polyolefins, which have enhanced glass transition temperature and improved transparency.[41] However, the objective of this study is to produce LCBed polypropylenes. The formation of ring structures is to be minimized because the cyclization consumes pendant vinyl moieties and thus decrease the LCB efficiency. Therefore, 1,9-decadiene was selected in this work, and 1,7-octadiene was used for a comparison purpose.

A zirconocene catalyst, *rac*-Me_2Si(2-MeBenz[*e*]Ind)$_2ZrCl_2$ (MBI), was selected as the copolymerization catalyst due to its excellent combination of high activity, isoselectivity, and ability of comonomer/macromonomer incorporation.[12] The copolymerization runs were carried out in toluene at 1 atm propylene pressure and 25 and 40 °C, respectively. Table 7.1 summarizes the polymerization conditions and results.

Table 7.1 Polymerization reaction conditions and results.[a]

Polymers	Diene	Diene conc. (mmol/L)	Temp (°C)	Time (hr)	Polymer (g)	Activity (kg PP/(mol Zr h))
PP1	no diene	0	40	30	8.3	33 200
PP2	DD	0.354	40	30	8.1	32 400
PP3	DD	1.06	40	30	8.4	33 600
PP4	DD	1.77	40	30	8.1	32 400
PP5	DD	3.54	40	30	8.2	32 800
PP6[b]	DD	35.4	40	30	6.9	27 600
PP7	OD	1.77	40	30	8.6	34 400
PP8	OD	3.54	40	30	8.3	33 200
PP9[b]	OD	35.4	40	30	6.1	24 400
PP10	no diene	0	25	30	4.8	19 200
PP11	DD	0.177	25	30	4.9	19 600
PP12	DD	0.354	25	30	4.7	18 800
PP13	DD	1.06	25	30	4.8	19 200

[a] Other polymerization conditions: Solvent, toluene; total volume, 150 mL; Propylene pressure, 1 atm; MBI catalyst, 0.5 μmol; Al(MMAO)/Zr (molar) = 15,000.
[b] Formation of polymer gels.

The proper selection of diene concentration in the polymerization is another important factor that affects the polymer microstructure and properties. Too low diene concentration results in linear polypropylene chains or chains that have too few LCBs to have significant improvement in rheological properties. On the other side, too high diene concentration leads to the formation of undesirable polymer gels. There is an operating window for the optimum concentration of diene. From a practical point of view, it is desirable to use a minimum dosage of

diene that can effectively produce LCBed PP with improved rheological properties because of the high cost of α,ω-dienes.

To identify the operating window of diene concentration, two polymerization runs, PP6 and PP9 in Table 7.1 were first carried out at 40 °C with DD and OD, respectively, at the diene concentration of 35.4 mmol/L (corresponding to 1.0 ml DD and 0.8 ml OD). Severe gelation was observed in both runs. No precipitation of fine white polypropylene powder was observed and the systems remained transparent. The viscosity of the polymerization mixture increased dramatically with the reaction time. After 30 minutes, the systems became jelly-like. All the solvent was absorbed in the network of polymer gels.

These two runs provided a guideline for the selection of proper diene concentration. In the subsequent runs, much lower diene concentrations were employed to avoid the gelation problem. The concentration was varied in the range of 0.177 ~ 3.54 mmol/L. Table 7.1 shows that, at these low diene concentrations, the polymerization activities were independent of the diene concentration at both temperatures and similar to that of the propylene homopolymerization. However, due to the diffusion limitations caused by polymer gels, the activities of the PP6 and PP9 runs were lower.

7.4.2 Characterization of LCBed PP by ^{13}C NMR, GPCV and DSC

Table 7.2 summarizes all the characterization results. ^{13}C NMR was used to study the microstructure of LCBed PPs. Figure 7.1 shows the spectra of PP5, PP8, and PP1 for a comparison purpose. Three types of diene microstructures in the propylene/diene copolymers were identified and reported in literatures: cyclic ring (cyclo-addition of diene), pendant vinyl group (one vinyl moiety

incorporated), and long chain branch (both vinyl moieties incorporated). The OD copolymers, PP7 and PP8, contained both seven-member ring, evident from resonances centered at 26.6, 36.8, 37.0 and 41.8 ppm,[41] and the LCB structure from the resonance at 43.9 ppm.[47] There was no pendant vinyl signal (1-hexenyl) observed in the olefin region of ^{13}C NMR spectrum in both samples. The spectra permitted us to estimate the content of incorporated diene and the respective percentages of ring and LCB structures. The calculated results are summarized in Table 7.2. Increasing the diene concentration in the polymerization stock from 1.77 to 3.54 mmol/L led to an increase in the overall percentage of diene in copolymer, the cyclization selectivity of diene (the percentage of diene incorporated through cyclization in the overall incorporated diene), and the LCBD (defined as the number of LCB structures per 1000 carbons).

For the propylene/DD copolymers, the pendant 1-octenyl structure was found only in the sample of PP5 (evident from the resonances at 114.5 and 139.5 ppm in the ^{13}C NMR spectrum), which was synthesized at a higher diene concentration. The other propylene/DD copolymers (except for the cross-linked sample of PP6 that was not measured by ^{13}C NMR due to its solubility problem) produced at both temperatures contained no 1-octenyl groups. The peaks at 43.9 and 33.9 ppm in Figure 7.1(b) were attributed to the α carbons and methine branching carbons, respectively, from both LCB and 1-octenyl structures. These resonances together with those of 1-octenyl structures in the olefinic region allowed us to quantitatively determine the overall amount of incorporated DD and the respective percentages of the 1-octenyl and LCB structures in the overall incorporated dienes as shown in Table 7.2. No signal of incorporated diene was observed with about 5000 scans in the samples PP2 and PP11 synthesized at very low diene concentrations due to the limited sensitivity of the NMR. Increasing the diene concentration led to an increase in the LCBD. The effect of temperature on the LCB formation was not conclusive. Different from the OD copolymers,

Table 7.2 Polymer characterization results by GPCV, DSC, and ^{13}C NMR.

Polymer	M_n[a] (kg/mol)	M_w[a] (kg/mol)	PDI[a]	T_m[b] (C)	ΔH_m[b] (J/g)	incorporated diene in copolymer[c] (mol %)	Incorporated diene			LCBD[g]
							Pendant vinyl[d] (%)	Cyclization selectivity[e] (%)	LCB selectivity[f] (%)	
PP1	91.4	224.6	2.5	152.5	90.4	0	0	0	0	0
PP2	86.2	264.0	3.1	152.1	83.4	n.o.	n.o.	n.o.	n.o.	n.o.
PP3	110.0	879.2	8.0	149.3	73.3	0.061	0	0	100	0.20
PP4	95.4	1257.5	13.1	150.4	80.8	0.083	0	0	100	0.28
PP5	122.5	1752.0	14.3	148.2	84.6	0.30	47	0	53	0.53
PP6	n.d.	n.d.	n.d.	114.0	45.0	n.d.	n.d.	n.d.	n.d.	n.d.
PP7	88.1	264.7	3.0	151.3	76.9	0.10	0	71	29	0.10
PP8	100.7	339.4	3.4	149.0	85.9	0.25	0	83	17	0.14
PP9	n.d.	n.d.	n.d.	120.4	47.7	n.d.	n.d.	n.d.	n.d.	n.d.
PP10	210.0	545.9	2.6	153.4	96.7	0	0	0	0	0
PP11	123.2	678.8	5.5	152.6	59.5	n.o.	n.o.	n.o.	n.o.	n.o.
PP12	144.8	1378.3	9.5	152.9	86.3	0.041	0	0	100	0.14
PP13	232.6	2533.6	10.9	152.2	78.7	0.056	0	0	100	0.19

[a] From GPCV measurement at 140 °C in 1,2,4-trichlorobenzene.
[b] From DSC measurements.
[c] mol% of incorporated diene in copolymer = the number of incorporated diene monomer units / the total number of monomeric units × 100; calculated from ^{13}C NMR.
[d] % pendant vinyl = the number of pendant vinyl groups / the total number of incorporated diene units × 100; observed only in PP5.
[e] % cyclization selectivity = the number of rings / the total number of incorporated diene units × 100, for propylene/OD copolymers only.
[f] % LCB selectivity = the number of LCB units / the total number of incorporated diene units × 100.
[g] Long chain branching density (LCBD) defined as the number of LCB structures per 1000 carbons as determined from ^{13}C NMR spectra.
n.d. = not determined. n.o. = not observed.

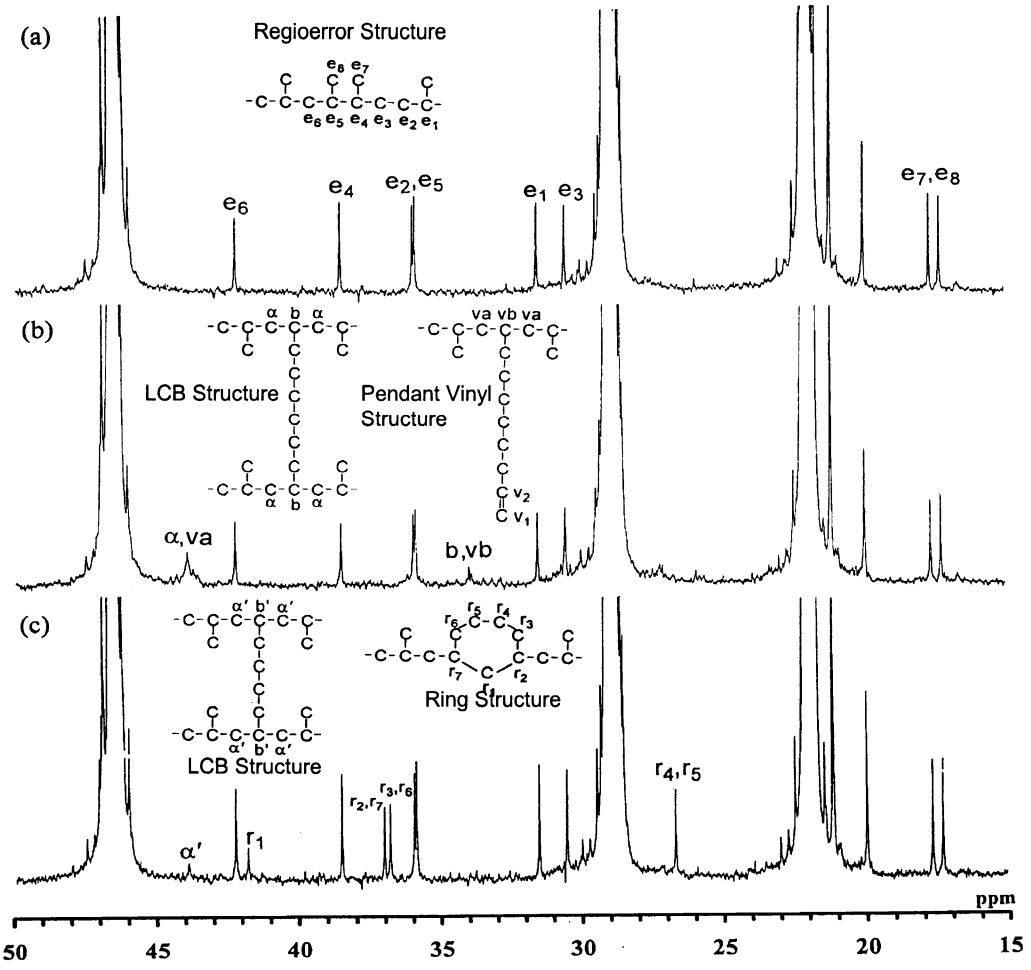

Figure 7.1 ^{13}C NMR spectrum of (a) linear polymer PP1; (b) LCBed propylene/DD copolymer PP5; (c) LCBed propylene/OD copolymer PP8.

there was no nine-member ring structure in the propylene/DD samples (note: the cross-linked sample PP6 was not analyzed). According to Arnold et al.[44] the absence of this nine-member ring structure in propylene/DD copolymers is because (1) the nine-member ring has lower stability than the seven-member counterpart formed in OD copolymers and (2) the movement of pendant vinyl moiety towards the catalytic center is slower than propylene insertion.

All the polymer samples except for the cross-linked PP6 and PP9 were soluble in 1,2,4-trichlorobenzene at 140 °C. Table 7.2 also summarizes the GPCV characterization results. The addition of a very small amount of diene significantly changed the polymer molecular weight distribution. Figure 7.2(a) shows the MWD curves for the copolymers produced with different DD concentrations at 40 °C. Compared to the homo-polymer PP1, all the LCBed samples showed a tail in the high MW end. This tail became a shoulder and the MWD turned to be very broader at high LCBD. Many studies [8,19,34,46] have shown that the LCBed polymer fractions usually reside in the high MW end and these small fractions of LCBed polymers play a decisive role in improving rheological properties. The number average MW (M_n) was not much affected by the diene incorporation. However, the weight-average MW (M_w) increased dramatically with the increase of DD concentration. A polydispersity index (M_w/M_n) as high as 14.3 was observed in PP5. Similar results were reported for the LCBed polyethylenes prepared by the copolymerization of ethylene/diene.[34] Figure 7.2(b) shows the MWD curves for propylene/DD copolymers produced at 25 °C. Compared to the polymers produced at 40 °C, these polymers had higher MWs due to a reduced rate of chain termination. Similar effects of diene concentration on average MWs and MWD as those at 40 °C were observed.

Figure 7.2(c) shows the MWD curves for the propylene/OD copolymers produced at 40 °C together with a DD copolymer, PP4, for the comparison. In contrast to the DD copolymers, the variation of OD concentration only slightly changed the average MWs and MWD curve. The M_n still remained relatively constant, but the increase in M_w and MWD broadening were milder. A polydispersity index of 3 was found for PP7 in contrast to that of 13.1 for PP4 prepared at the same condition but with DD. This drastic difference can be attributed to the formation of seven-member ring structure in the OD copolymers

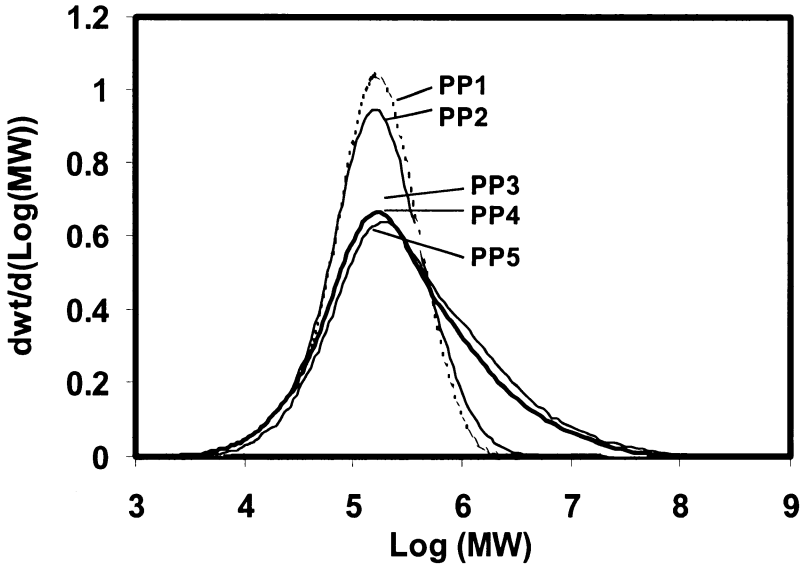
1.2
1
0.8
0.6
0.4
0.2
0
dwt/d(Log(MW))
PP1
PP2
PP3
PP4
PP5
3
4
5
6
7
8
9
Log (MW)

(a)

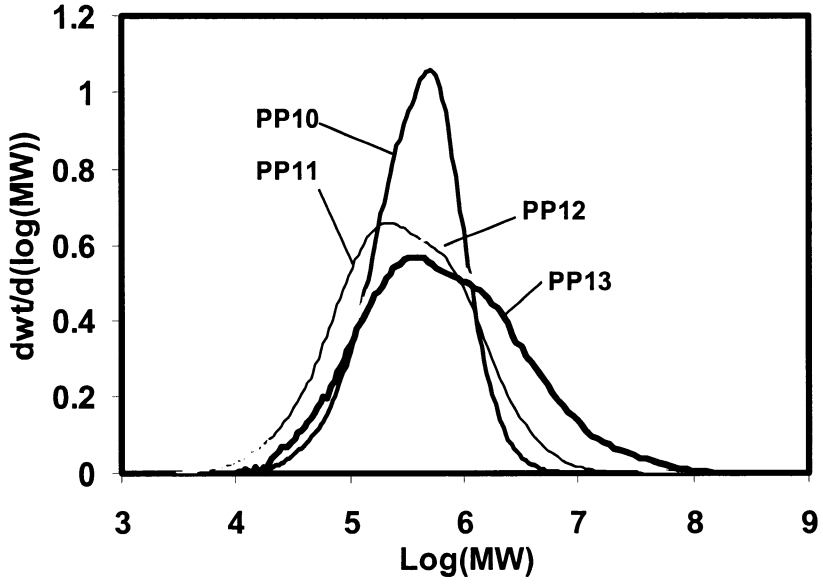
1.2
1
0.8
0.6
0.4
0.2
0
dwt/d(log(MW))
PP10
PP11
PP12
PP13
3
4
5
6
7
8
9
Log(MW)

(b)

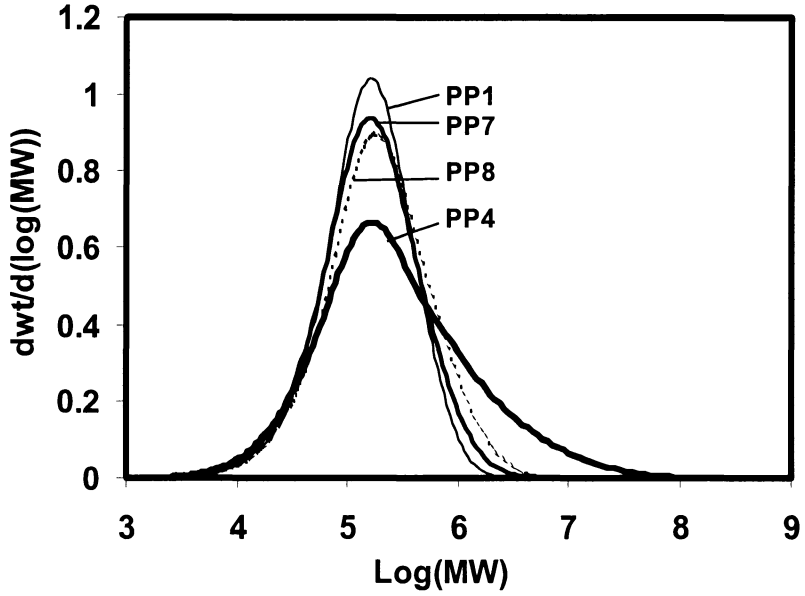

(c)

Figure 7.2 The effect of diene concentration on molecular weight distribution for (a) the propylene/DD copolymers prepared at 40 °C, (b) the propylene/DD copolymers prepared at 25 °C, and (c) the propylene/OD copolymers prepared at 40 °C (also compared to PP4).

that consumed pendant vinyl moieties and resulted in polymers having lower LCBD.

The DSC results, including melting point, T_m, and melting enthalpy, ΔH_m, are also reported in Table 7.2. Despite the significant difference in MWD, owing to the very small amount of diene incorporation, these LCBed polymers exhibited very similar T_m and ΔH_m. The increase of LCBD only very slightly decreased the polymer melting point. This result suggests that the slight LCBing in these polymers did not have an undesired effect on the crystal forming process. The cross-linked samples PP6 and PP9, analyzed by DSC, had very low melting point and melting enthalpy.

7.4.3 Effects of Diene Incorporation on Rheological Properties of LCBed Polypropylene Melts

Figure 7.3(a) compares the complex viscosity versus angular frequency curves measured at 190 °C for the samples of PP1 ~ PP4. The incorporation of very small amount of DD (up to 0.083 %) significantly changed the complex viscosity curve due to the formation of LCB structure and the increased M_w. Compared to the linear polymer, PP1, the LCBed polymers, PP2 ~ PP4, exhibited much higher viscosity in the low frequency region. The rheological analysis showed enhanced viscosity of PP2 over PP1 of similar M_w and elucidated the presence of LCB structures in PP2 that was not detected in the ^{13}C NMR measurement due to sensitivity. This result indicates that at this polymerization condition LCBed polymer chains can be efficiently generated with a DD concentration as low as 0.354 mmol/L. Due to the much higher LCBD, the melt of PP5 was very elastic and behaved like a cross-linked polymer gel. The polymer melt was almost non-flowable and was difficult to be molded into disk-like samples for the rheological measurement.

Figure 7.3(b) shows the frequency dependency of phase angle measured at 190 °C for PP1 ~ PP4. A drastic difference in the phase angle curves was observed for the LCBed polypropylenes. The LCBed polymers exhibited reduced phase angles compared to the linear counterpart. The increase of LCBD also changed the shape of the phase angle curves. A plateau started to appear and the frequency range for this plateau increased with the increase of LCBD. This unique behavior was also observed in LCBed polyethylenes prepared by metallocene catalysts in several investigations.[10,21] The plateau is characteristic of polymer gel materials. Garcia-Franco et al.[21] demonstrated that the LCBed polymers exhibit physical gel-like behavior and can be studied with rheological theories proposed for polymer gels.

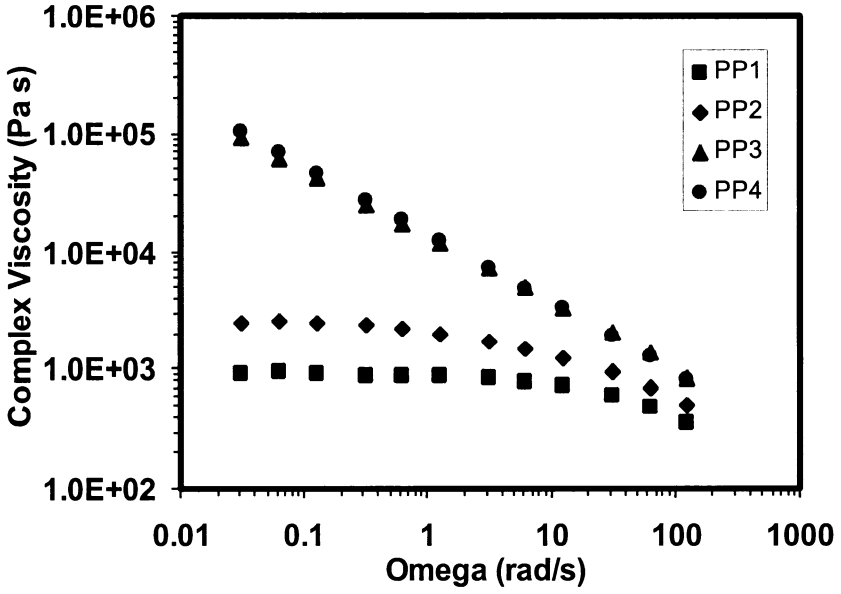

(a)

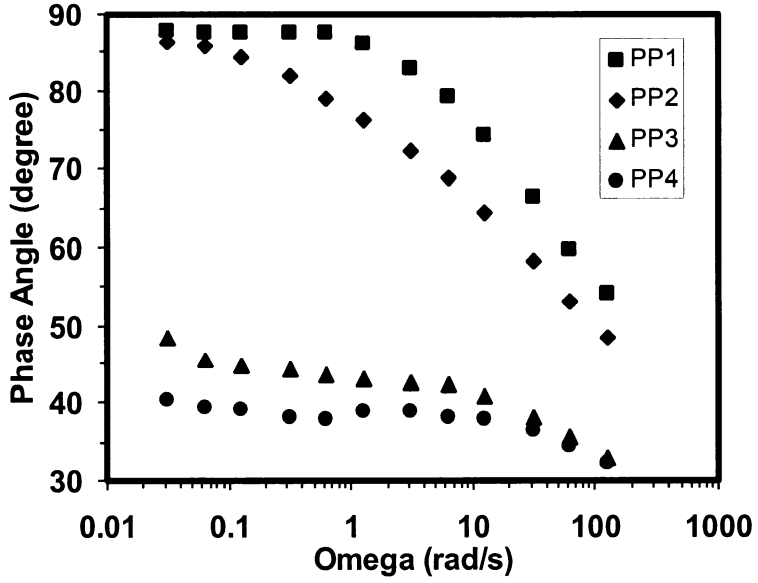

(b)

Figure 7.3 (a) Complex viscosity and (b) phase angle vs angular frequency measured at 190 °C for the propylene/DD copolymers prepared at 40 °C with various diene concentrations.

Figures 7.4(a) ~ (c) show the angular frequency dependence of dynamic moduli at 190 °C for PP1 ~ PP4. Increasing the LCBD significantly increased both G' and G" and therefore improved the polymer melt strength. For PP1 and PP2, the contribution of G" was greater than that of G' in the whole studied frequency range. No crossover of the G'-G" moduli was found. For PP3, however, a crossover was observed at a low angular frequency of 0.063 rad/s and the contribution from G' was dominant over a wide range of frequencies. For PP4 in Figure 7.4(c), G' was always larger than G" in the whole studied range of frequencies. Similar changes were observed in other studies,[16,25] and it suggested that highly LCBed polymers resemble the rheological behavior characteristic of crosslinked or partially crosslinked polymers.

LogG' vs logG" plot has been proven to be a useful tool to investigate the effects of LCBing and polydispersity on rheological properties.[5,6] For high MW polymer melts with narrow PDI, the logG' vs logG" curve does not depend on MW and is only a very weak function of temperature. All the data measured at various temperatures and molecular weights can be described by a single master curve. For the linear polyethylenes of narrow MWD, the correlation was found to be:[5,6] $G' = 0.00541(G")^{1.42}$. Figure 7.5 compares the logG' vs logG" curves for PP1 ~ PP4. Our PP1 (PDI = 2.5) data fit $G' = 0.00079(G")^{1.65}$. An up-shift from the linear sample PP1 was evident for the LCBed samples PP2 ~ PP4 in the plot. With the increase of LCBD, the shift became more significant.

For the LCBed polymers prepared at 25 °C with DD, the rheological characterization was conducted for PP11 only. Similar to PP5, the melts of PP12 and PP13 were highly elastic and gel-like even though they were soluble in 1,2,4-trichlorobenzene at 140 °C. These samples could not be molded into disks for the rheological measurements. They were press-molded under 5000 pounds of

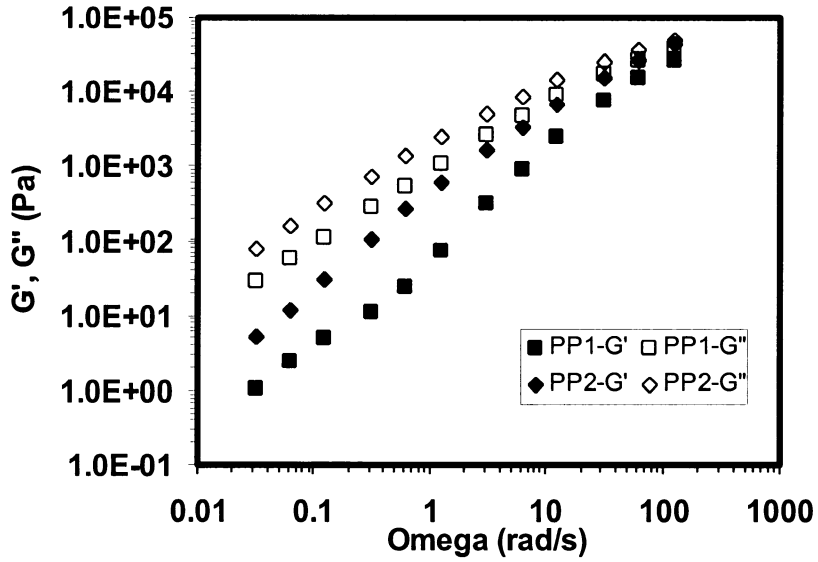
1.0E+05
1.0E+04
1.0E+03
1.0E+02
1.0E+01
1.0E+00
1.0E-01
G', G" (Pa)
0.01
0.1
1
10
100
1000
Omega (rad/s)
PP1-G'
PP1-G"
PP2-G'
PP2-G"

(a)

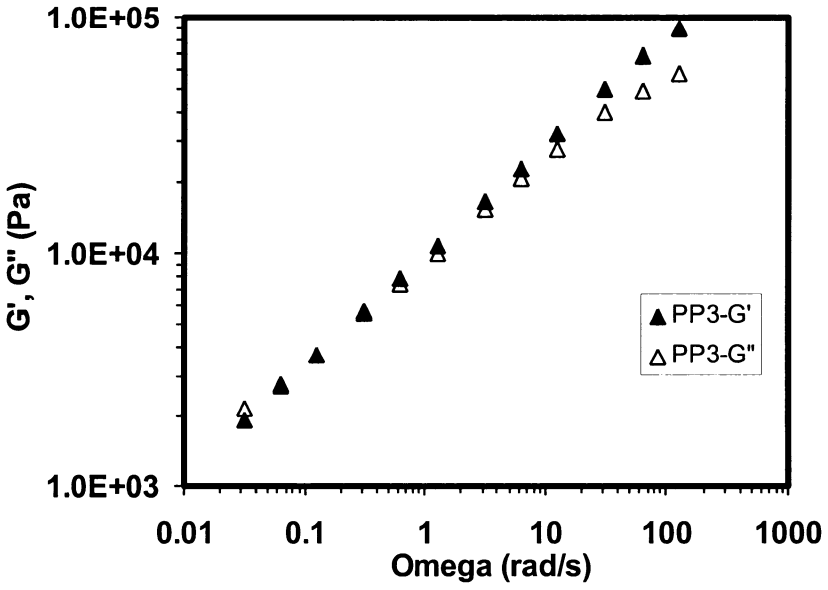
1.0E+05
1.0E+04
1.0E+03
G', G" (Pa)
0.01
0.1
1
10
100
1000
Omega (rad/s)
PP3-G'
PP3-G"

(b)

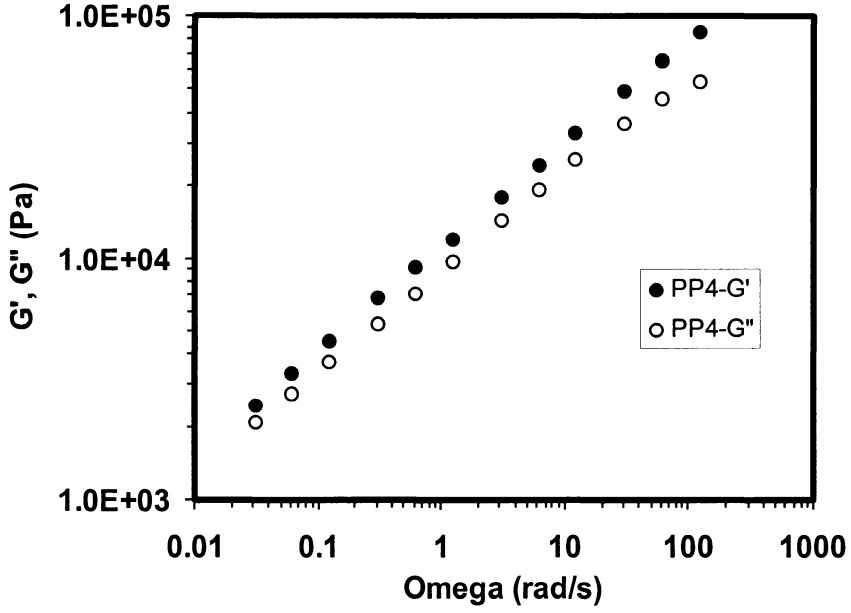

(c)

Figure 7.4 Dynamic moduli (G', G") vs angular frequency measured at 190 °C for the propylene/DD polymers prepared at 40 °C with different diene concentrations: (a) PP1 and PP2; (b) PP3; (c) PP4.

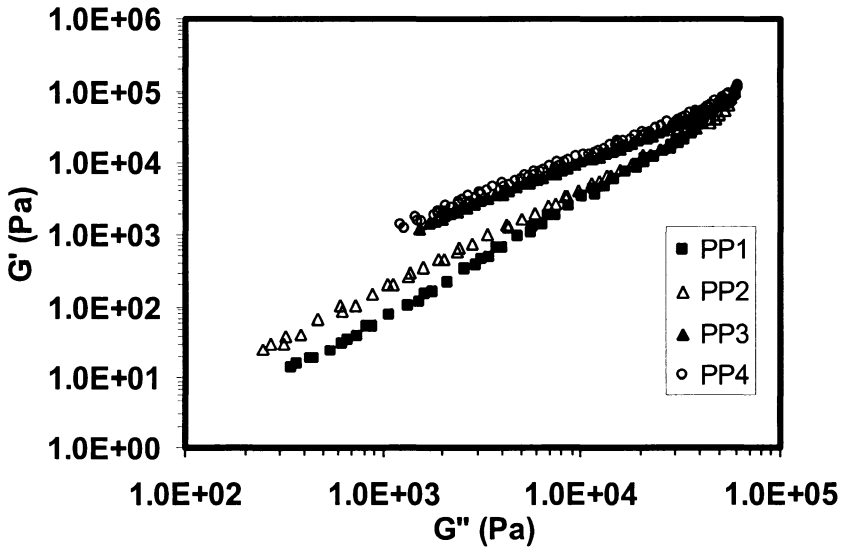

Figure 7.5 LogG' vs logG" measured at 190 °C for the propylene/DD polymers prepared at 40 °C with different diene concentrations.

pressure in the Carver Press at 190 °C for 5 minutes. However, the samples contracted and tended to return to their original shapes upon the removal of the pressure. These samples required long relaxation time to have permanent deformation. For the LCBed polymers, the relaxation time is a function of MW, LCBD, and branch length.[11] Although PP12 and PP13 had lower LCBD than PP4, their higher MW and expected higher branch length gave them longer relaxation time and made them harder to be rheologically analyzed. Compared to the linear PP10, the LCBed PP11 exhibited different rheological behaviors shown in Figures 7.6(a) ~ (d). The presence of LCB, even at a level too scarce to be detected by ^{13}C NMR, gave a significant effect on rheological properties.

The rheological properties for the propylene/OD copolymers, PP7 and PP8, are shown in Figures 7.7(a) ~ (d) together with a DD copolymer PP4 for comparison. Referred to the linear polymer PP1, significant changes in the rheological properties, such as enhanced complex viscosity, improved shear thinning, reduced phase angle, increased dynamic moduli, and up-shifted logG' vs logG" curve, were also seen in these two samples. These changes are typical of LCB polymers and are consistent with the increase of LCBD. However, the cyclo-addition of OD significantly decreased the LCBD in OD copolymers. Therefore, compared to the DD copolymer PP4 that was prepared with the same diene concentration, PP7 exhibited weaker effects on the rheological properties.

The diene concentration in copolymerization is a key parameter that determines rheological and end-use properties of LCBed polymers: too little giving no improvement in rheological properties, too much leading to gelation. From the above rheological analyses, for the propylene/DD copolymerization at 40 °C, a diene concentration in the range of 0.354 ~ 1.77 mmol/L is suitable for the production of processable LCBed PP. However, at 25 °C a diene

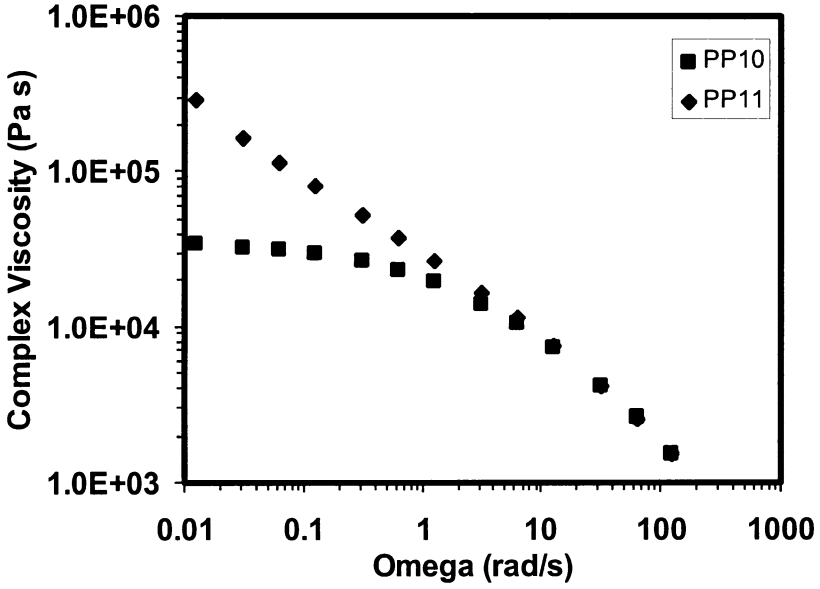
1.0E+06
1.0E+05
1.0E+04
1.0E+03
Complex Viscosity (Pa s)
0.01
0.1
1
10
100
1000
Omega (rad/s)
PP10
PP11

(a)

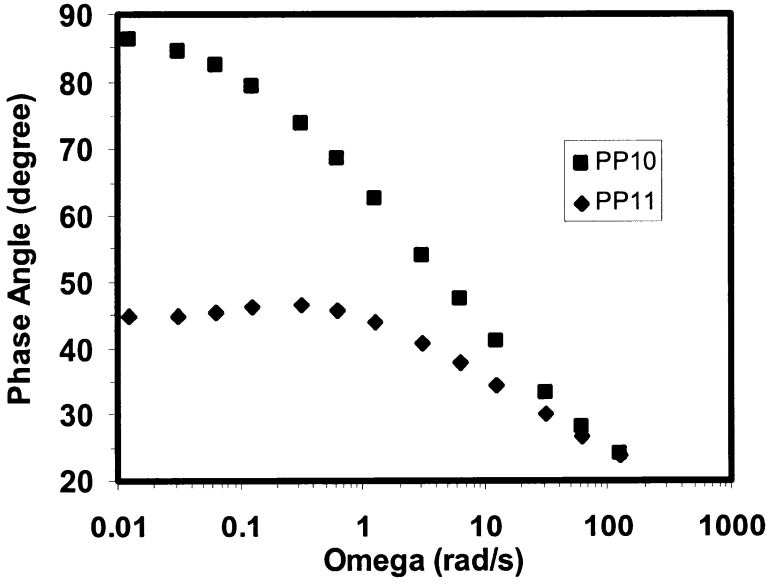
90
80
70
60
50
40
30
20
Phase Angle (degree)
0.01
0.1
1
10
100
1000
Omega (rad/s)
PP10
PP11

(b)

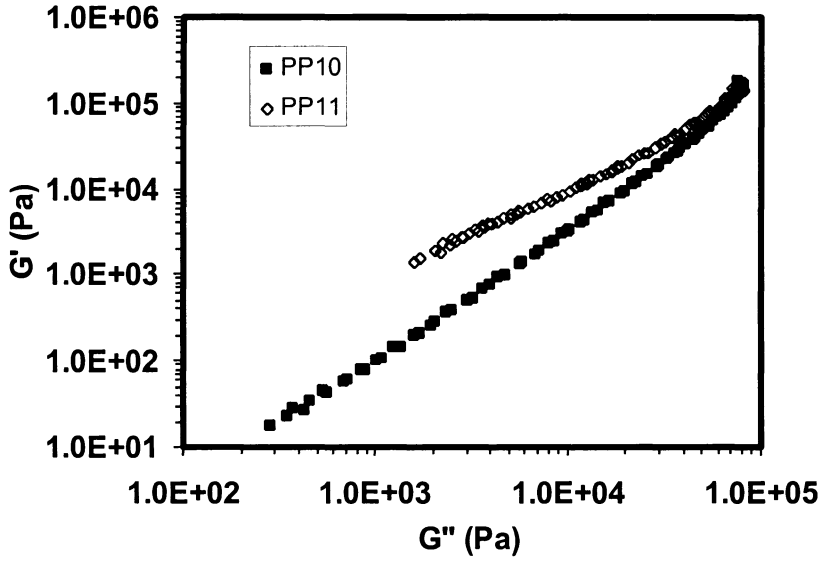

(c)

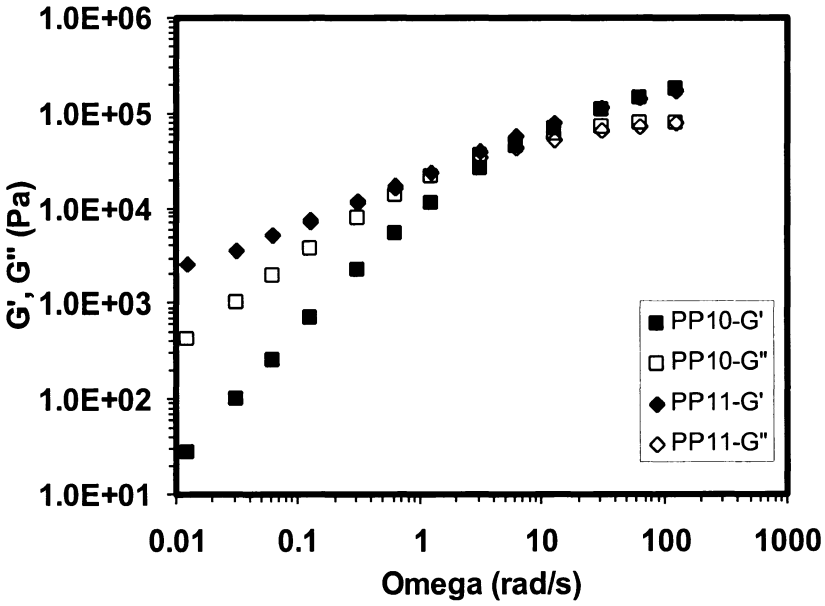

(d)

Figure 7.6 (a) Complex viscosity vs angular frequency, (b) phase angle vs angular frequency, (c) dynamic moduli vs angular frequency measured at 190 °C, and (d) logG' vs logG" for linear PP10 and LCBed PP11 prepared at 25 °C.

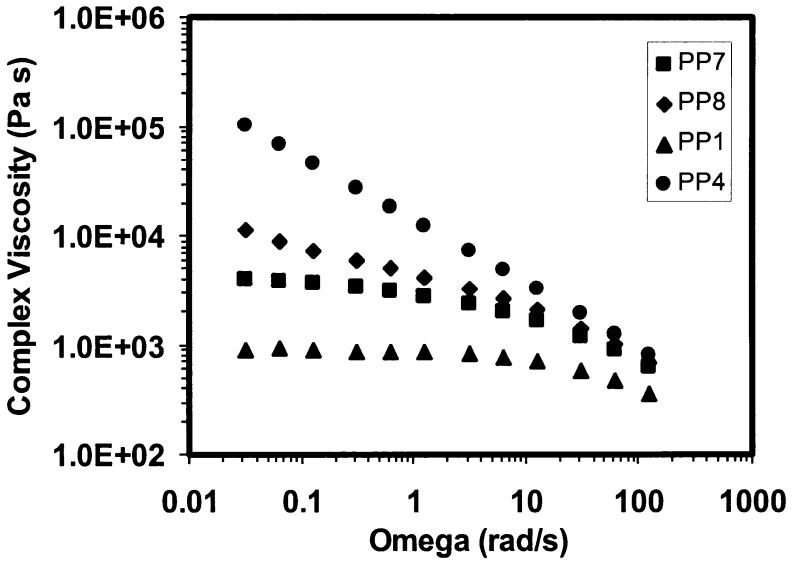
1.0E+06
1.0E+05
1.0E+04
1.0E+03
1.0E+02
Complex Viscosity (Pa s)
0.01
0.1
1
10
100
1000
Omega (rad/s)
PP7
PP8
PP1
PP4

(a)

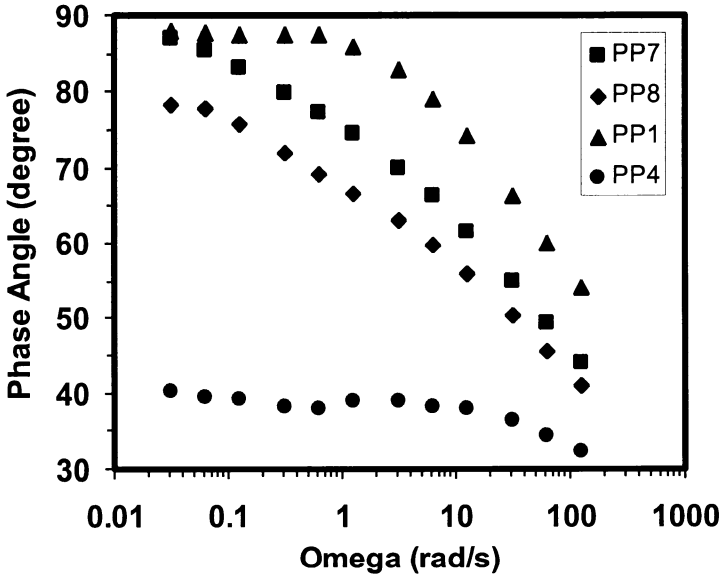
90
80
70
60
50
40
30
Phase Angle (degree)
0.01
0.1
1
10
100
1000
Omega (rad/s)
PP7
PP8
PP1
PP4

(b)

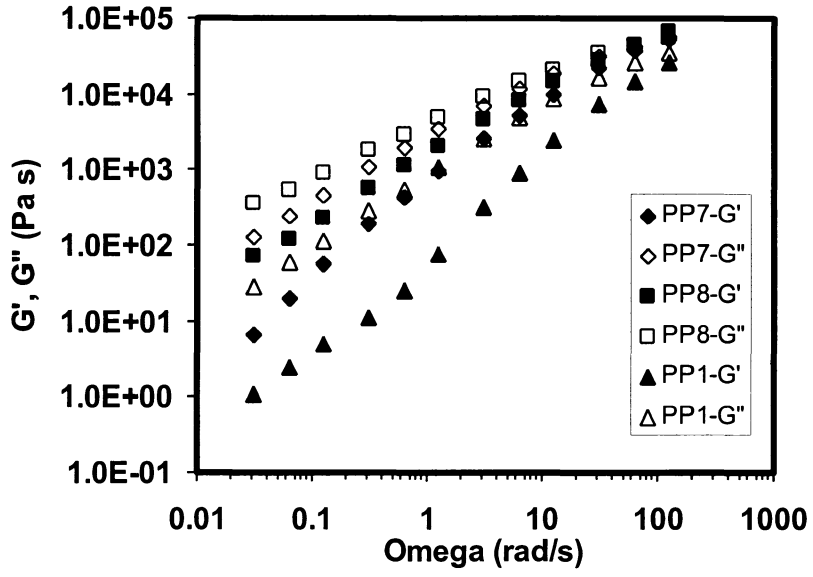

(c)

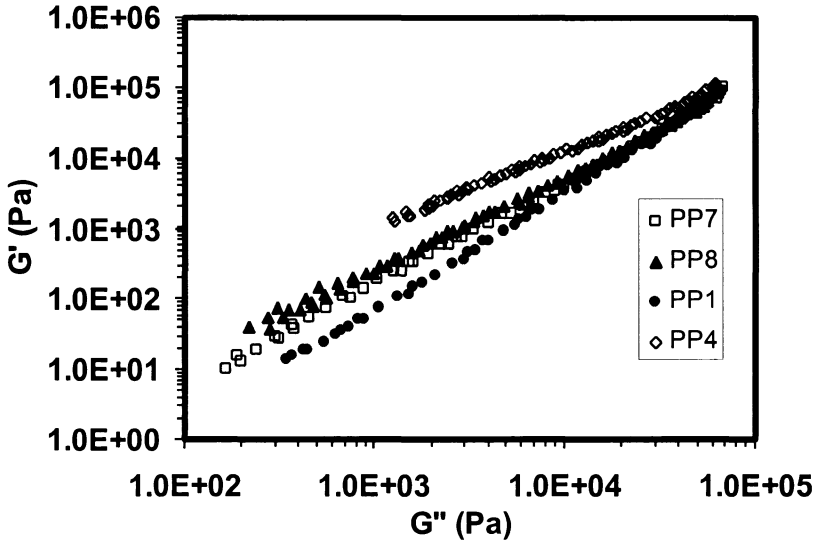

(d)

Figure 7.7 (a) Complex viscosity vs angular frequency, (b) phase angle vs angular frequency, (c) dynamic moduli vs angular frequency measured at 190 °C, and (d) logG' vs logG" for the propylene/1,7-octadiene polymers prepared at 40 °C and the comparison with PP4.

concentration can be lowered to 0.177 mmol/L for the LCBed PP. For the propoylene/OD copolymerization at 40 °C, the cyclo-addition reduces the LCB selectivity and thus higher diene concentration (typically 1.77 ~ 3.54 mmol/L) is needed.

7.4.4 Thermorheological Complexity and Spectra of Flow Activation Energy

LCBing significantly affects the rheological behaviors of polymer melts through its effects on the chain relaxation process. Linear polymers obey the time-temperature superposition principle and are thermorrheologically simple. However, LCBed polymers do not obey the superposition principle due to constraints imposed by branching points on chain relaxation, and are thermorheologically complex. Van Gurp's plot (phase angle versus logG*) has been shown to be useful for evaluating the thermorheological complexity of LCBed polymers.[6,10,26] The phase angle versus logG* data measured at different temperatures should fall into a single smooth line for thermorheological simple materials. The Van Gurp's plots for PP1 ~ PP4 at five temperatures are shown in Figure 7.8(a). For the linear PP1 it gave a smooth line. The PP2 ~ PP4 samples appeared to be complex. The higher the LCBD, the more significant the complexity became. The Van Gurp's plots for PP7 and PP8, PP10 and PP11 are shown in Figures 7.8(b) and 7.8(c), respectively. All these data confirmed the presence of LCB in the propylene/diene copolymers.

Thermorheological complexity of LCBed polymers can also be elucidated by examining the frequency dependence of activation energy in the time shift factor a_T of $G'(T,\omega)$ referred to an arbitrary temperature T_0. The temperature dependence of a_T for rheologically simple polymers, at temperatures well above

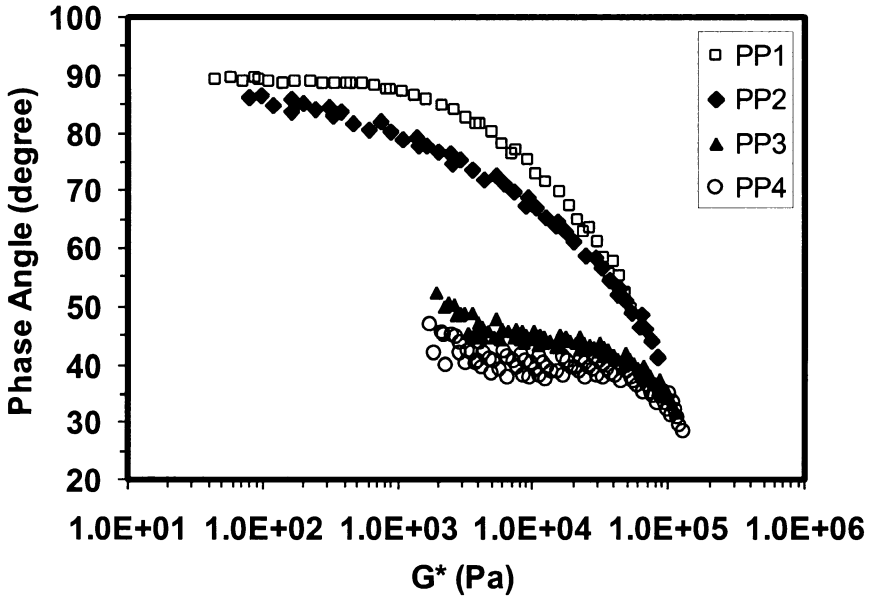
100
90
80
70
60
50
40
30
20
Phase Angle (degree)
1.0E+01 1.0E+02 1.0E+03 1.0E+04 1.0E+05 1.0E+06
G* (Pa)
PP1
PP2
PP3
PP4

(a)

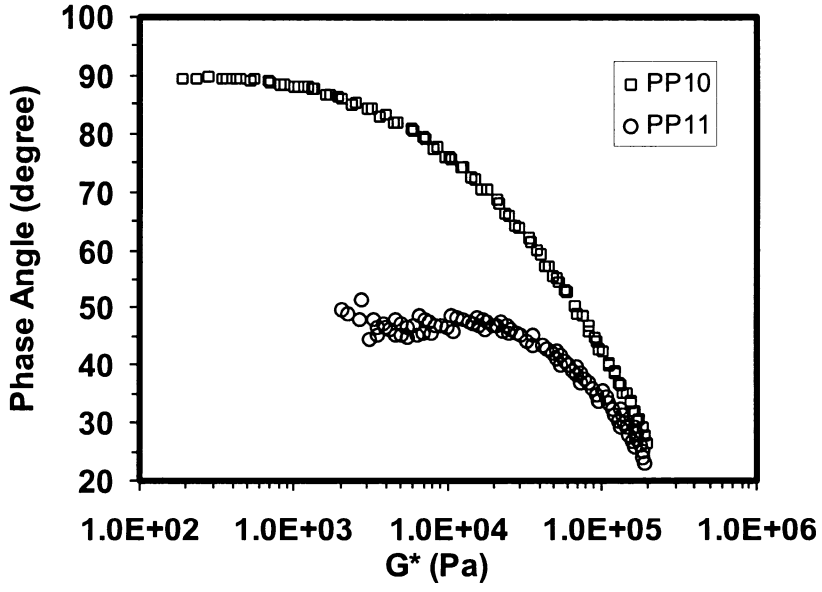
100
90
80
70
60
50
40
30
20
Phase Angle (degree)
1.0E+02 1.0E+03 1.0E+04 1.0E+05 1.0E+06
G* (Pa)
PP10
PP11

(b)

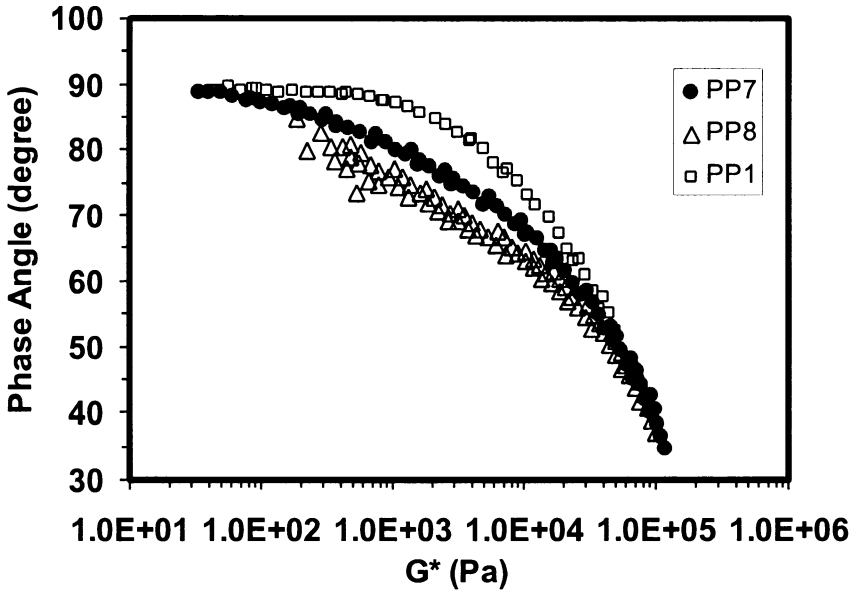

(c)

Figure 7.8 Van Gurp's plot for (a) propylene/DD polymers prepared at 40 °C, (b) propylene/DD polymers prepared at 25 °C, and (c) propylene/OD polymers prepared at 40 °C.

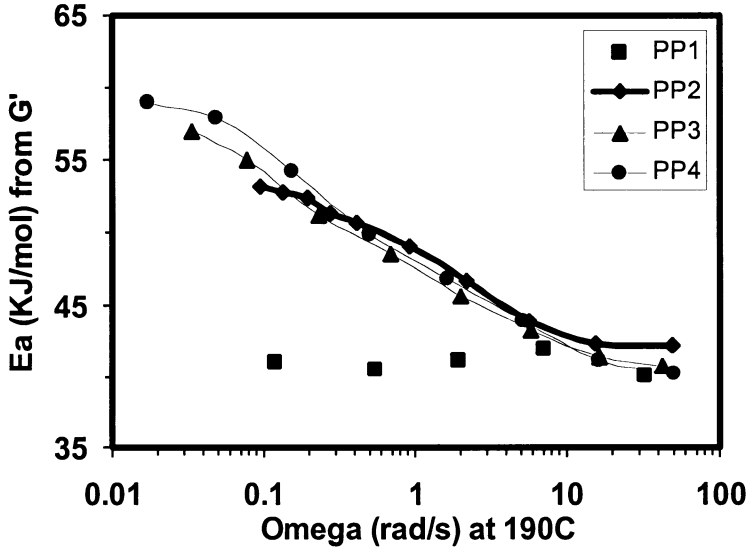

(a)

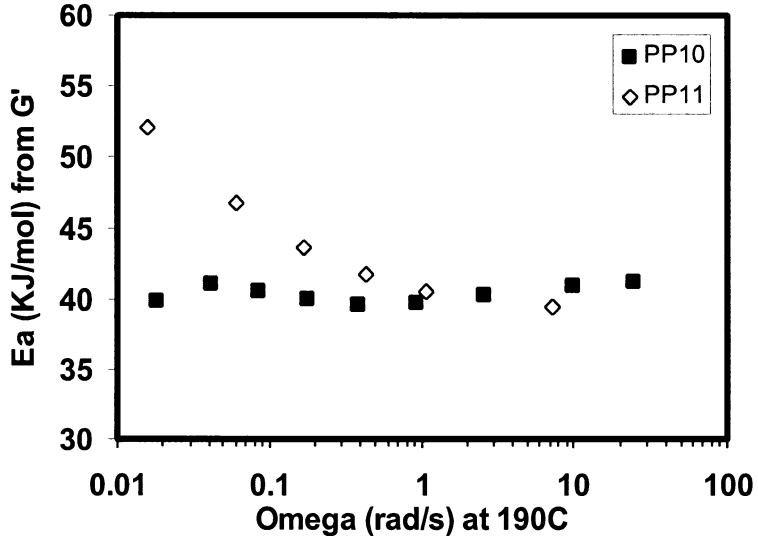

(b)

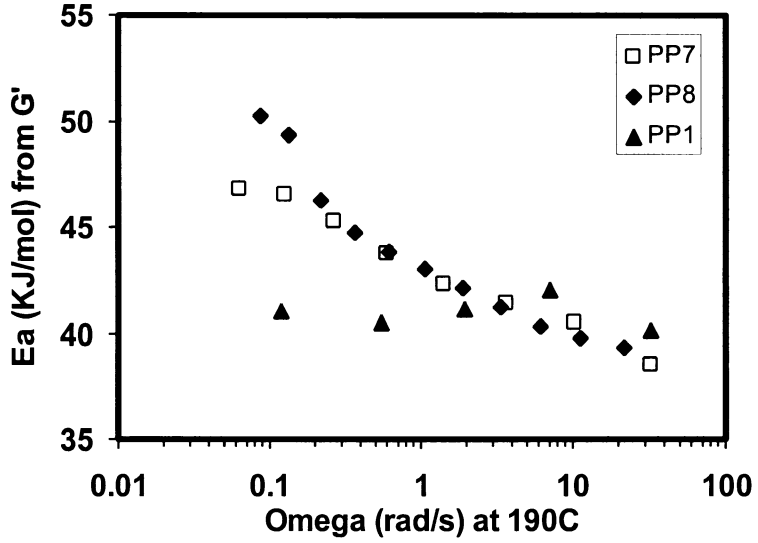

(c)

Figure 7.9 The activation energy spectra (referenced to 190 °C) for (a) propylene/1,9-decadiene polymers prepared at 40 °C, (b) propylene/1,9-decadiene polymers prepared at 25 °C, and (c) propylene/1,7-octadiene prepared at 40 °C.

the glass transition temperatures (T_g), often follows an Arrhenius relation. The flow activation energy E_a, which is a measure of temperature sensitivity, is given by

$$a_T = \exp\left[\frac{E_a}{R}\left(\frac{1}{T} - \frac{1}{T_0}\right)\right]$$

Viscoelastic behaviors of thermorheological complex polymers do not follow this simple relation. These polymers do not have a single activation energy but exhibit shear dependent temperature sensitivity.[15,18]

Figures 7.9(a) ~ (c) show the activation energy spectra referenced at 190 °C for the LCBed samples with the corresponding linear counterparts. These spectra were plotted based on the experimental storage moduli (G' vs ω) according to the method outlined by Wood-Adams et al.[18] Figure 7.9(a) compares the activation energy spectra for the polymers synthesized at 40 °C with different DD concentrations. For the linear thermorheologically simple sample, PP1, the activation energy remained constant (about 40.5 kJ/mol, similar to the reported value for linear iPP [48]) over a broad range of frequencies. However, the behaviors for the thermorheologically complex LCBed polymers (PP2 ~ PP4) were very different. At the low frequencies, high activation energies of 54 ~ 59 kJ/mol were observed. With the increase of the frequency, the activation energy gradually decreased and reached a final plateau of about 40.5 kJ/mol at the high frequency region. The low-frequency activation energy varied from sample to sample and tended to increase with the increase of LCBD while the plateau value at the high frequency for the LCBed polymers was similar to that of the linear sample. Similar observations were found in Figures 7.9(b) and 7.9(c) for the samples prepared at other reaction conditions.

7.4.5 Melt Rheological Properties of Blends of Linear and LCBed Polypropylenes

LCBed polymers can be used as rheology modifier for their linear counterparts. Blending a small amount of LCBed polymer into linear polymer can enhance melt strength and improve shear-thinning property. Linear HDPE and LLDPE have been blended with LDPE that has LCB structures to yield controlled rheological properties. The novel LCBed PP synthesized in this work may also serve as rheology modifier for linear PP. For this perspective, the rheological properties of several linear/LCBed PP blends were examined.

The linear PP1 and LCBed PP4 prepared at the same temperature and propylene pressure were melt-blended at 190 °C under shear with three different PP4 fractions: 10, 30 and 50 wt%, respectively. Figures 7.10(a) ~ (c) compare the rheological properties of these blends to the pure linear sample. The low-frequency complex viscosity was significantly increased and the shear thinning performance was improved. With the increase of the weight percentage of PP4 in the blend, the viscosity increase and shear thinning improvement became more significant. The Van Gurp's plot illustrated the thermorheological complexity and the reduction of phase angle of the polymer blends. There was also up-shift of the logG' vs logG" curves. The temperature dependence of the blends at different frequencies was calculated. Typically in Figure 11(d) the activation energy spectrum for the blend with 30 wt% of PP4 is shown. The activation energies for the three blends of 10, 30, and 50 wt% PP4 at the low frequency of 0.02 rad/s were 43, 46, and 51 kJ/mol, respectively.

The LCBed PP5 that had LCBD higher than PP4 could not be prepared for the rheological characterization due to its extremely long relaxation time. Here we blended it with the linear PP1 with 30 wt% PP5. The blend became moldable. The rheological characterization was conducted for this blend and was compared to the PP1/PP4 blend. Figures 7.11(a) ~ (d) show these comparisons. The

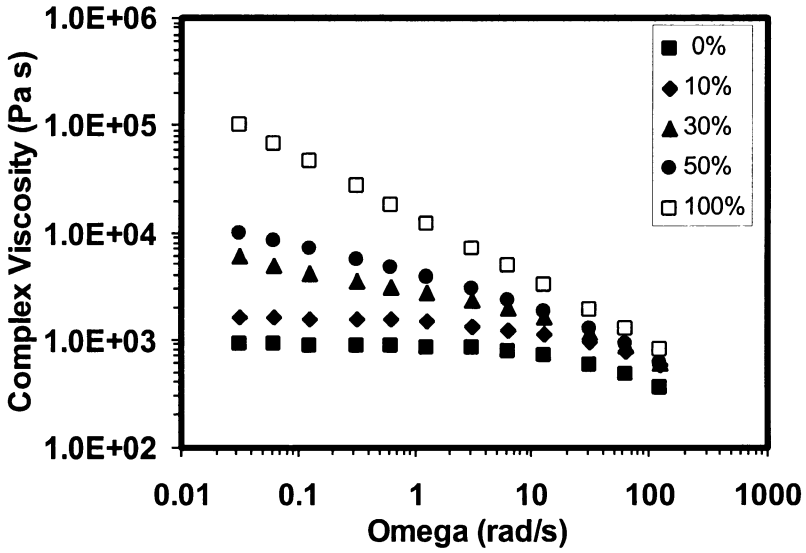
Complex Viscosity (Pa s)
1.0E+06
1.0E+05
1.0E+04
1.0E+03
1.0E+02
0.01
0.1
1
10
100
1000
Omega (rad/s)
0%
10%
30%
50%
100%

(a)

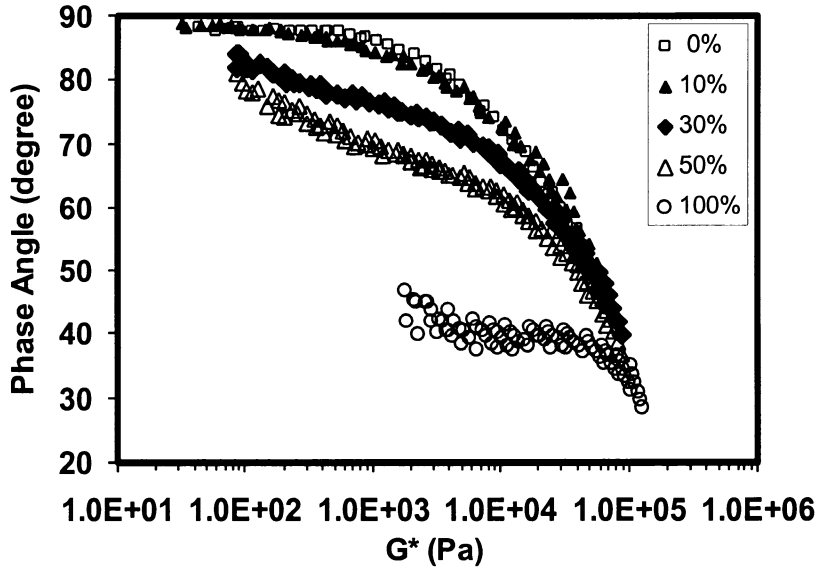
Phase Angle (degree)
90
80
70
60
50
40
30
20
1.0E+01
1.0E+02
1.0E+03
1.0E+04
1.0E+05
1.0E+06
G* (Pa)
0%
10%
30%
50%
100%

(b)

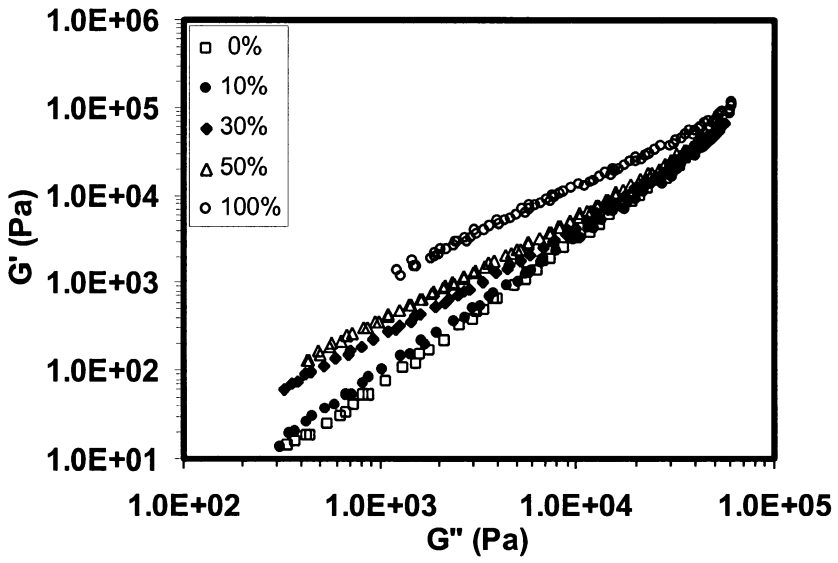

(c)

Figure 7.10 (a) Complex viscosity vs angular frequency measured at 190 °C, (b) Van Gurp's plot, and (c) logG' vs logG" for the blends of PP1/PP4 with different compositions.

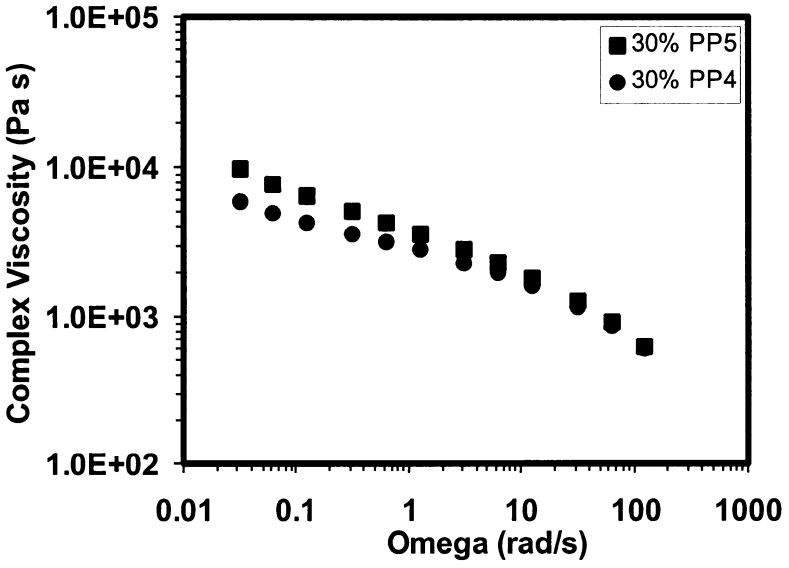

(a)

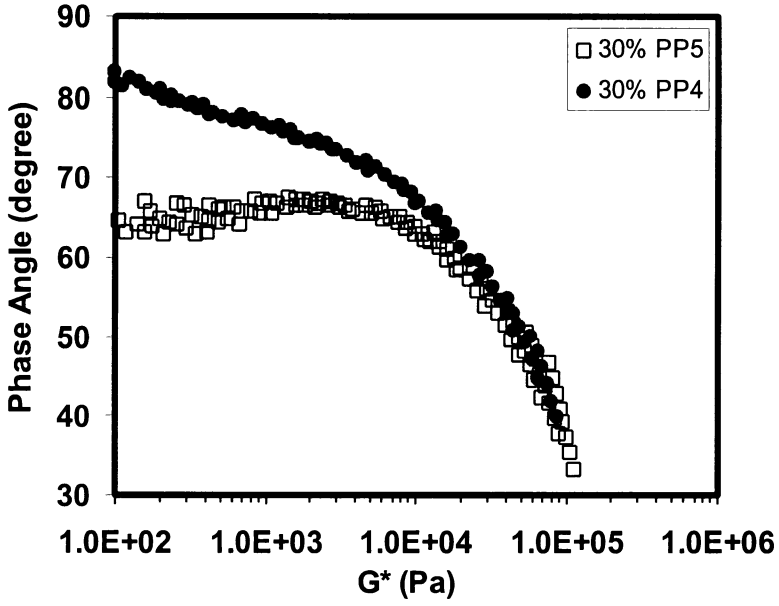
90
80
70
60
50
40
30
Phase Angle (degree)
30% PP5
30% PP4
1.0E+02
1.0E+03
1.0E+04
1.0E+05
1.0E+06
G* (Pa)

(b)

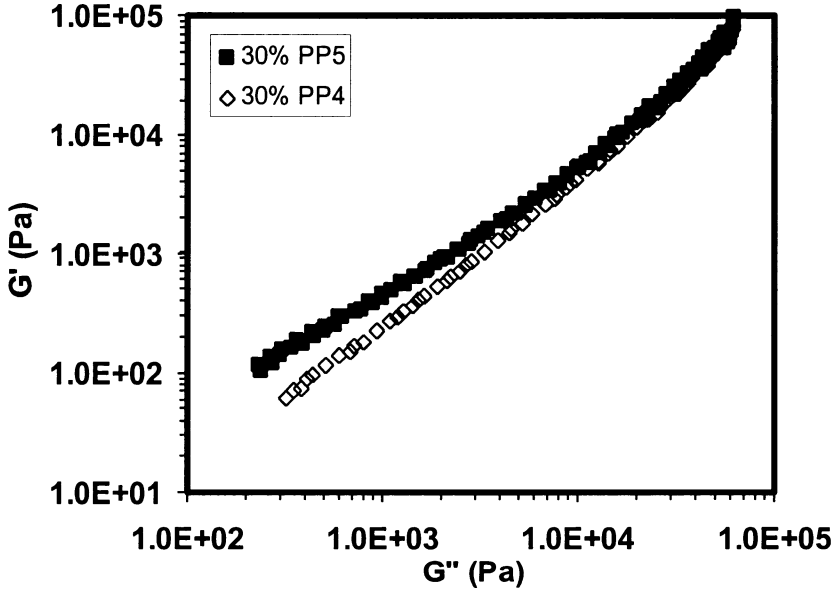
1.0E+05
1.0E+04
1.0E+03
1.0E+02
1.0E+01
G' (Pa)
30% PP5
30% PP4
1.0E+02
1.0E+03
1.0E+04
1.0E+05
G" (Pa)

(c)

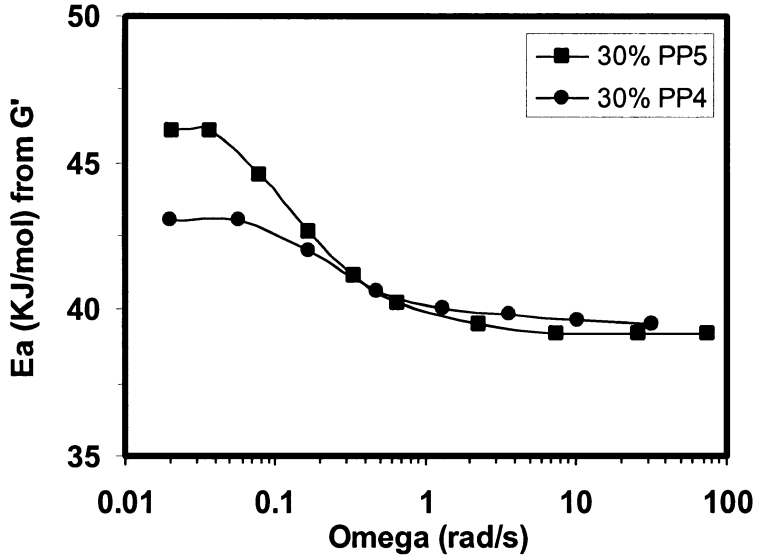

(d)

Figure 7.11 (a) Complex viscosity vs angular frequency measured at 190 °C, (b) Van Gurp's plot, (c) logG' vs logG", and (d) Activation energy spectra (referenced to 190 °C) for the blends of PP1/PP5 and PP1/PP4 with the PP1 fraction of 70 wt%.

PP1/PP5 exhibited even higher complex viscosity and higher activation energy at low frequency, more shear-thinning and thermorheological complexity,and higher activation energy at low frequencies due to the higher LCBD in the PP5 sample.

7.5 Conclusions

LCBed PP samples were prepared by propylene copolymerization with a small amount of 1,9-decadiene (DD) or 1,7-octadiene (OD), using the catalyst system of *rac*-Me_2Si(2-MeBenz[*e*]Ind)$_2ZrCl_2$ (MBI)/MMAO. A systematic

investigation on the polymer synthesis, polymer structure characterization, and rheological properties was conducted. The main findings were as follows:

(1) In the copolymerization of propylene/DD, DD monomers were incorporated as pendant 1-octenyl groups, which were further incorporated into polymer chains to produce LCBed polypropylenes. Increasing the DD concentration from 0.177 to 3.54 mmol/L yielded LCBed PPs of LCBD up to 0.53 branches per 1000 carbons. The polymerization activity and polymer thermal properties were independent of the diene concentration. Increasing the diene concentration did not change the M_n value, but significantly increased the M_w and thus PDI.

(2) In the copolymerization of propylene/OD, the formation of seven-member ring structures by cyclo-addition of OD significantly decreased the amount of LCB structures in the polymer. The diene concentration was varied between 1.77 and 3.54 mmol/L. Higher diene concentration led to higher LCBD. However, at the same diene concentration, LCBD of OD copolymer was much lower than in that of DD counterpart. The increase in diene concentration only slightly increased the polymer Mw and PDI while the Mn remained constant.

(3) The LCB structures in the copolymers enhanced low-frequency viscosity, improved shear thinning, reduced phase angle, and increased low-frequency activation energy. The rheological studies also showed that, during the copolymerization, a DD concentration as low as 0.177 mmol/L at 25 °C and 0.354 mmol/L at 40 °C was adequate to produce polymer samples with significantly improved rheological properties.

(4) Adding the LCBed PP to linear PP significantly modified the rheological properties of the polymer blends. The LCBed PP produced in this work could serve as rheology modifier for the linear PP.

7.6. Reference

1. Resconi, L.; Cavallo, L.; Fait, A.; Piemontesi, F. *Chem. Rev.* **2000**, *100*, 1253.
2. Chum, P. S.; Kruper, W. J.; Guest, M. J. *Adv. Mater.* **2000**, *12*, 1759.
3. Gahleitner, M. *Prog. Polym. Sci.* **2001**, *26*, 895.
4. Vega, J. F.; Munoz-Escalona, A.; Santamaria, A.; Munoz, M. E.; Lafuente, P. *Macromolecules* **1996**, *29*, 960.
5. Vega, J. F.; Santamaria, A.; Munoz-Escalona, A.; Lafuente, P. *Macromolecules* **1998**, *31*, 3639.
6. Vega, J. F.; Fernández, M.; Santamaria, A.; Munoz-Escalona, A.; Lafuente, P. *Macromol. Chem. Phys.* **1999**, *200*, 2257.
7. Yan, D.; Wang, W.-J.; Zhu, S. *Polymer* **1999**, *40*, 1737.
8. Shroff, R. N.; Mavridis, H. *Macromolecules* **1999**, *32*, 8454.
9. Wood-Adams, P. M.; Dealy, J. M.; deGroot, A. W.; Redwine, O. D. *Macromolecules* **2000**, *33*, 7489.
10. Malmberg, A.; Gabriel, C.; Steffl, T.; Münstedt, H.; Lőfgren. B. *Macromolecules* **2002**, *35*, 1038.
11. Lohse, D. J.; Milner, S. T.; Fetters, L. J.; Xenidou, M.; Hadjichristidis, N.; Mendelson, R. A.; Garcia-Franco, C. A.; Lyon, M. K. *Macromolecules* **2002**, *35*, 3066.
12. Shiono, T.; Azad, S. M.; Ikeda, T. Macromolecules 1999, *32*, 5723.
13. Weng, W.; Markel, E. J.; Dekmezian, A. H. *Macromol. Rapid Commun.* **2001**, *22*, 1488.
14. Weng, W.; Hu, W.; Dekmezian, A. H.; Ruff, C. J. *Macromolecules* **2002**, *35*, 3838.
15. Carella, J. M.; Gotro, J. T.; Graessley, W. W. *Macromolecules* **1986**, *19*, 659.

16. Malmberg, A.; Kokko, E.; Lehmus, P.; Lőfgren. B.; Seppälä, J. V. *Macromolecules* **1998**, *31*, 8448.
17. Malmberg, A.; Liimatta, J.; Lehtinen, A.; Lőfgren. B. *Macromolecules* **1999**, *32*, 6687.
18. Wood-Adams, P.; Costeux, S. *Macromolecules* **2001**, *34*, 6281.
19. Wood-Adams, P. M.; Dealy, J. M. *Macromolecules* **2000**, *33*, 7481.\
20. Shroff, R. N.; Mavridis, H. *Macromolecules* **2001**, *34*, 7362.
21. Garcia-Franco, C. A.; Srinivas, S.; Lohse, D. J.; Brant, P. *Macromolecules* **2001**, *34*, 3115.
22. Hadjichristidis, N.; Xenidou, M.; Iatrou, H.; Pitsikalis, M.; Poulos, Y.; Avgeropoulos, A.; Sioula, S.; Paraskeva, S.; Velis, G.; Lohse, D. J.; Schulz, D. N.; Fetters, L. J.; Wright, P. J.; Mendelson, R. A.; Garcia-Franco, C. A.; Sun, T.; Ruff, C. J. *Macromolecules* **2000**, *33*, 2424.
23. Wang, W.-J.; Yan, D.; Zhu, S.; Hamielec, A. E. *Macromolecules* **1998**, *31*, 8677.
24. Kolokda, E.; Wang, W.-J.; Zhu, S.; Hamielec, A. E. *Macromolecules* **2002**, *35*, 10062.
25. Villar, M. A.; Failla, M. D.; Quijada, R.; Mauler, R. S.; Vallés, E. M.; Galland, G. B.; Quinzani, L. M. *Polymer* **2001**, *42*, 9269.
26. Walter, P.; Trinkle, S.; Suhm, J.; Mäder, D.; Friedrich, C.; Műlhaupt, R. *Macromol. Chem. Phys.* **2000**, *201*, 604.
27. Moore, Jr., E. P.; Larson, G. A. In *Polypropylene Handbook*; Moore, Jr., E. P., Ed.; Hanser: Munich, 1996.
28. Scheve, B. J.; Mayfield, J. W.; DeNicola, Jr., A. J. U.S. Patent 5, 731, 362, 1998.
29. Graebling, D. *Macromolecules* **2002**, *35*, 4602.
30. Lu, B.; Chung, T. C. *Macromolecules* **1999**, *32*, 8678.
31. Ye, Z.; Zhu, S. *J. Polym. Sci., Part A: Polym. Chem.* **2003**, *41*, 1152.

32. Stehling, U.; Diebold, J.; Kristen, R.; Roll, W.; Brintzinger, H. H.; Jungling, S.; Mülhaupt, R.; Langhauser, F. *Organometallics* **1994**, *13*, 964.
33. Weng, W.; Markel, E. J.; Dekmezian, A. H. *Macromol. Rapid Commun.* **2000**, *21*, 1103.
34. Kokko, E.; Pietikäinen, P.; Koivunen, J.; Seppälä, J. V. *J. Polym. Sci., Part A: Polym. Chem.* **2001**, *39*, 3805.
35. Pietikäinen, P.; Starck, P.; Seppälä, J. V. *J. Polym. Sci., Part A: Polym. Chem.* **1999**, *37*, 2379.
36. Pietikäinen, P.; Väänänen, T.; Seppälä, J. V. *Eur. Polym. J.* **1999**, *35*, 1047.
37. Pietikäinen, P.; Seppälä, J. V.; Ahjopalo, L.; Pietilä, L.-O. *Eur. Polym. J.* **2000**, *36*, 183.
38. Naga, N.; Imanishi, Y. *Macromol. Chem. Phys.* **2002**, *203*, 2155.
39. Williamson, A.; Fink, G. *Macromol. Chem. Phys.* **2003**, *204*, 1178.
40. Hackmann, M.; Repo, T.; Jany, G.; Rieger, B. *Macromol. Chem. Phys.* **1998**, *199*, 1511.
41. Naga, N.; Shiono, T.; Ikeda, T. *Macromolecules* **1999**, *32*, 1348.
42. Kim, I.; Shin, Y. S.; Lee, J. K. *J. Polym. Sci., Part A: Polym. Chem.* **2000**, *38*, 1590.
43. Walter, P.; Trinkle, S.; Lilge, D.; Friedrich, C.; Mülhaupt, R. *Macromol. Mater. Eng.* **2001**, *286*, 309.
44. Arnold, M.; Bornemann, S.; Schimmel, T.; Heinze, T. *Macromol. Symp.* **2002**, *181*, 5.
45. Agarwal, P. K.; Weng, W.; Mehta, A. K.; Dekmezian, A. H.; Chang, M.; Chudgar, R. K.; Davey, C. R.; Lin, C. Y.; Chen, M. C.; Richeson, G. C. U.S. Patent Application 2002/0013440 A1, Jan 31, 2002.
46. Agarwal, P. K.; Somani, R. H.; Weng, W.; Mehta, A.; Yang, L.; Ran, S.; Liu, L.; Hsiao, B. S. *Macromolecules* **2003**, *36*, 5226.
47. Soga, K.; Uozumi, T.; Park, J. R. *Makromol. Chem.* **1990**, *191*, 2853.

48. Eckstein, A.; Suhm, J.; Friedrich, C.; Maier, R.-D.; Sassmannshausen, J.; Bochmann, M.; Műlhaupt, R. *Macromolecules* **1998**, *31*, 1335.

Chapter 8

Significant Research Contributions and Recommendations for Future Developments

8.1 Significant Research Contributions of Thesis Work

With a main theme in developing new polymers or new processes for olefin polymerization, this thesis reports the synthesis and characterization of a novel series of polyolefins by olefin polymerization with various single-site catalysts. The unique structures and superior properties of these polymers were systematically characterized and correlated. A number of significant contributions to the polyolefin research areas have been made in this thesis work. These contributions are respectively summarized as follows.

In Chapter 2, polyethylene fibers were synthesized by ethylene extrusion polymerization with MCM-41 supported titanocene catalyst. This work is the first extensive study on the morphological and mechanical properties of this novel series of fibrous materials. It has been clearly shown in this work that PE fibrous materials produced with this nano-fabrication technique exhibit three levels of hierarchical morphological structures: nanofibrils, microfibers, and microfiber aggregates and/or bundles. Mechanical studies have shown that the microfibers exhibit high tensile strength (0.3 ~ 1.0 GPa) due to the presence of extended-chain crystalline structure along the axial direction of fibres.

In Chapter 3, the first investigation of the effects of internal structure of mesoporous particles on impregnation of a Ni-diimine catalyst was conducted. It was found that both nanotube diameter and length could significantly affect the

loading of MMAO and Ni-diimine catalyst. For large-sized MAO molecules, the nanotube diameter is the main constraining factor, while, for comparatively smaller Ni-diimine catalyst, the effect of nanotube length is more significant. These catalysts impregnated on different mesoporous supports were also found to exhibit different polymerization activities. The nanotube length of supports plays a decisive role. Longer nanotubes lead to lower polymerization activity.

In Chapter 4, the rheological properties of a novel series of branched polyethylenes prepared with Pd and Ni –diimine catalysts were presented. For the fist time, from a rheological point of view, it was shown that the novel polyethylenes prepared with Pd diimine catalysts at low ethylene pressures have a dendritic chain topology. These novel dendritic PEs exhibit extremely low melt viscosity and typical Newtonian flow behavior. Polymers with various chain topologies were also prepared and the effects of chain topology on polymer melt rheological properties were elucidated.

In Chapter 5, the first tandem catalytic system for an efficient production of ethylene-1-hexene copolymers directly from ethylene monomer was designed and investigated. Butyl-branched copolymers with a broad range of branch densities were effectively produced using the tandem catalytic system. Compared to the step-wise copolymerization procedures for LLDPE production, this tandem catalyst method is advantageous and convenient.

In Chapter 6, a binary catalyst system was developed and used for the synthesis of branched polypropylenes with an isotactic backbone and atactic side chains. The unique polymers produced would exhibit enhanced impact properties compared to isotactic PP, which has low impact strength. By controlling reaction conditions and catalyst ratios, branched PPs with various densities of atactic PP branches could be produced.

In Chapter 7, a unique series of long chain branched isotactic polypropylenes were synthesized by propylene copolymerization with non-conjugated dienes. Compared to reactive extrusion methods widely used for the production of long chain branched PP, the convenience and effectiveness of this *in situ in-reactor* approach makes it very promising for the synthesis of isotactic polypropylenes with enhanced melt strength. In this work, PPs with various long chain branch densities and thus controllable melt rheological properties were effectively prepared and characterized.

8.2 Recommendations for Future Research

The novel polymers synthesized and/or developed in this thesis have very good potentials for future explorations and commercial applications. Some suggestions for future research and development are provided in the following section.

8.2.1 Supported Tandem Catalyst Systems and Continuous Processes for LLDPE Production from Ethylene Monomer Stock

The success and convenience of tandem catalytic systems for the synthesis of LLDPE from ethylene has been demonstrated in Chapter 5 and in literatures. Currently all investigations on tandem catalyst systems have been on unsupported homogeneous systems and conducted through semi-batch processes. In order to pursue the perspective of industrial applications, developments of supported tandem catalyst systems and continuous polymerization processes are highly needed. By controlling reaction conditions, catalyst combinations and ratios, and adjusting reactor residence times in slurry or solution continuous polymerization reactors, polyethylenes with narrow MWD and CCD and with controllable SCB

densities can be continuously produced. The success of supported systems and continuous processes will be of significant academic importance and industrial interests.

8.2.2 Continuous Ethylene Extrusion Polymerization with Catalysts Coated on Mesoporous Membranes

The semibatch process for PE fiber production by extrusion polymerization with mesoporous particle supported catalysts is quite inconvenient and costly. It is highly desirable to develop continuous extrusion polymerization process using reactive mesoporous membranes coated with ethylene polymerization catalysts. The membranes are required to have parallel nanotube structures similar to that of mesoporous particles (MCM-41 and MSF). By feeding ethylene at one side of the membrane, high strength polyethylene fiber is expected to be obtained from the other side of membrane, which is further connected to fiber spinning and drawing facilities. This would represent the main research thrust in this direction.

8.2.3 Processing of LCBed PP Prepared by Propylene Copolymerization with Non-Conjugated Dienes

LCBed PP has enhanced melt strength, which makes them desirable in such processing applications as thermoforming, foaming, extrusion coating, and blow molding. In Chapter 7, the LCBed PPs were produced by copolymerization of propylene with non-conjugated dienes and rheologically characterized. However, the processing behavior of this novel series of polymers, which is very important for commercial applications, has not been investigated. It is of practical value and industrial significance to study the processing of these polymers. Work

in this direction would help build a bridge between polymer synthesis and polymer processing.

Appendix

ESR Study on Reduction of Constrained Geometry Catalyst Systems

This appendix is based on the paper published in *Journal of Applied Polymer Science*, **2003**, *89*, 2474-2482 by Z. Ye, W.-J. Wang, and S. Zhu.

A.1 Abstract

The reduction of a constrained geometry catalyst ($CGCTiMe_2$) activated with a series of cocatalysts including modified methylaluminoxane (MMAO), tris(pentafluorophenyl) borane ($B(C_6F_5)_3$), and combined $B(C_6F_5)_3$/MMAO, was experimentally investigated using an on-line electron spin resonance spectroscopy (ESR) technique. The effects of the solvent type, cocatalyst/catalyst ratio, and temperature on the reduction were examined. In the $CGCTiMe_2$/MMAO system, increasing Al/Ti molar ratio from 20 to 250 significantly increased the Ti(III) content. Adding trimethylaluminum (TMA) to the system lowered the Ti(III) content. Three trivalent Ti species: **Ti(a)** (g = 1.972), **Ti(b)** (g = 1.992, α(H) = 7.4 G), and **Ti(c)** (g = 1.995) were observed. In the $CGCMe_2/B(C_6F_5)_3$ system, only one trivalent Ti species (g = 1.988) was observed. The $CGCTiMe_2/B(C_6F_5)_3$ system was more stable to reduction than the $CGCTiMe_2$/MMAO system.

Keywords: ESR, metallocene, constrained geometry catalyst, reduction, olefin polymerization, transition metal chemistry.

A.2 Introduction

Metallocene-based coordination catalysts have a significant impact on polyolefin industries.[1] An important development in the technology is the constrained-geometry catalyst (CGC),[2-8] $(Cp^*SiR_2NR)MX_2$, where Cp* = tetramethylcyclopentadienyl , R = alkyl, M = Group 3 or 4 transition metal, and X = CH_3 or Cl (e.g. Scheme 1). The CGC system, amongst the first commercialized single-site catalysts,[9] is able to produce a new family of polyethylene with long chain branching.[10-12] This exceptional characteristic provides polymers with the combination of good processibility and desirable strength properties. Meanwhile, the CGC system is remarkably stable even at high polymerization temperatures (> 140 °C). Also it was reported that the reduction of titanium CGCs by methylaluminoxane (MAO) was less significant than other titanocenes.[13]

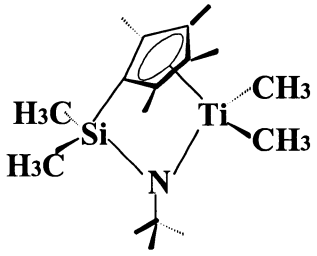

1

Scheme A.1 Structure of Constrained Geometry Catalyst.

Study on catalyst reduction is very important for elucidating the active site structure and for understanding the reaction mechanism and kinetics in catalyst polymerization. In this regard, electron spin resonance (ESR) technique appears to be a useful tool for investigating catalyst reduction in the polymerization of olefin [14-17] and that of sydiotactic styrene [18-23]. On-line monitoring the

paramagnetic trivalent Ti(III) or Zr(III) signals provides both qualitative and quantitative information about reduction mechanism and kinetics. In olefin polymerization, some studies showed that tetravalent cationic metallocene complexes are the active sites for olefin monomers and are reduced to inactive paramagnetic trivalent complexes during polymerization.[14-17] The reduction is believed to be due to a reductive decomposition of electron deficient bridging complex of catalyst and cocatalyst by ejecting non-bridged alkyl groups.[14,15] In an early study on homogeneous Cp_2TiCl_2/AlR_xCl_{3-x} system, Olivé et al [14] proposed that reduction was from a bimolecular second-order mutual deactivation of two Ti(IV) active sites. On the other side, the attribution of active sites in half-sandwich metallocene catalysts for syndiotactic styrene polymerization remains to be a controversy. It used to be believed that reduced trivalent cationic complexes were the active sites based on the correlations between polymerization kinetic data and ESR work.[18-22] However, other studies observed none or very weak ESR signals attributed to trivalent complexes, showing no correlation with the polymerization data.[23]

As an important catalyst system, CGC has attracted lots of research efforts. However, to the best of our knowledge, a systematical reduction study on this catalyst system has not been reported. In this work, we utilized an on-line ESR technique to experimentally investigate the reduction of the $CGCTiMe_2$ (**1**) catalyst activated with different cocatalyst systems, including modified MAO (MMAO), $B(C_6F_5)_3$, and combined MMAO/$B(C_6F_5)_3$ cocatalyst systems.

A.3 Experimental Part

A.3.1 Materials

CGC catalyst precursor, $[C_5Me_4(SiMe_2N^tBu)]TiMe_2$ (Me: methyl, ^{t}Bu: isobutyl, C_5: cyclopentadiene), and borane cocatalyst, $B(C_6F_5)_3$, were provided by Dow Chemical and Boulder Scientific, respectively. Modified methylaluminoxane, MMAO-3A with 65.9 % methane and 31.7 % isobutane, supplied by Akzo-Nobel Corporation as 6.68 wt% aluminum in heptane and 11.6 % in toluene was used as the MAO source in the experiments. Trimethylaluminum (TMA) was provided by Aldrich Chemical as 2 mol/L solution in toluene. The catalysts and cocatalysts were used as received. Anhydrous grade toluene and heptane supplied by Aldrich Chemical were refluxed over sodium with benzophenone as indicator for 48 hours and distilled out before use. All the manipulation of catalyst and cocatalyst solutions and ESR samples were conducted in a controlled nitrogen drybox or under nitrogen protection.

A.3.2 ESR Sample Preparation and Analysis

Screw-capped ESR sample tubes were used in this work. The samples were prepared as follows. In a drybox, a proper amount of solvent was added into the ESR tube by a syringe. A prescribed amount of cocatalyst solution (MMAO or $B(C_6F_5)_3$) was then added to the tube. For the mixed cocatalyst systems (MMAO/TMA, MMAO/ $B(C_6F_5)_3$), MMAO solution was added first, followed by the addition of a certain amount of TMA or $B(C_6F_5)_3$ solution by syringe. The ESR tube was then capped and wrapped with Parafilm. The sample was then transferred to an Aldrich AtmosBag filled with UHP nitrogen. A desired amount of the catalyst precursor solution was finally added prior to ESR measurement.

The ESR measurements were conducted at different temperatures using a Bruker EP072 X-band ESR spectrometer equipped with a temperature control unit. Spin concentration calibrations at different temperatures were carried out

using standard TEMPO solutions (10^{-5} ~ 10^{-3} molar) for quantitatively determining the Ti(III) concentration. The magnetic field was calibrated with DPPH. The ESR measurement conditions were: magnetic modulation frequency 100 kHz, intensity 20 dB, central magnetic field 3400 G, swift range 600 G, receive gain 2×10^{-4}, and modulation amplitude 5 G. Bruker WinEPR SimFonia (version 1.25) software was used to simulate the experimental spectrum.

A.4 Results and Discussion

A.4.1 MMAO as Cocatalyst

MAO is one of the most commonly used cocatalysts for metallocene polymerization of olefins monomers. However, conventional MAO has a low solubility in aliphatic solvents as well as poor storage stability in solution. Modified MAO (MMAO) prepared by controlled hydrolysis of TMA and TiBA has higher solubility and better storage stability in solvent than MAO for olefin polymerization.[1h] In this work, MMAO was used as MAO source.

The Ti(IV) reduction in the $CGCTiMe_2$/MMAO system with different Al/Ti ratios was carried out in toluene at various temperatures. Figure A.1(a) shows a set of experimental ESR spectra at different aging times and 100 °C with an original $CGCTiMe_2$ concentration of 5×10^{-4} mol/L and Al/Ti molar ratio of 100. The ESR spectra collected after 2 min reaction with Al/Ti molar ratios ranging from 20 to 2000 are presented in Figure A.2. Three Ti(III) paramagnetic signals can be resolved by a computer simulation: two singlets **Ti(a)** (g = 1.972), **Ti(c)** (g = 1.995), and one doublets **Ti(b)** (g = 1.992, α(H) = 7.4 G). The simulated signals and their combined resulting spectra with relative intensities of the three individual signals are also included in Figure A.1(b) and A.1(c),

(a)

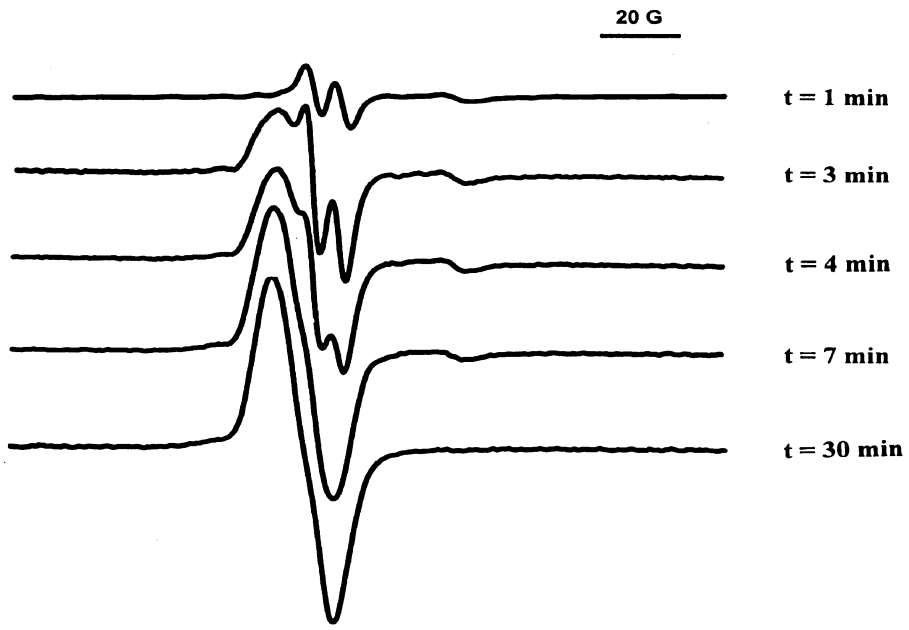

(b)

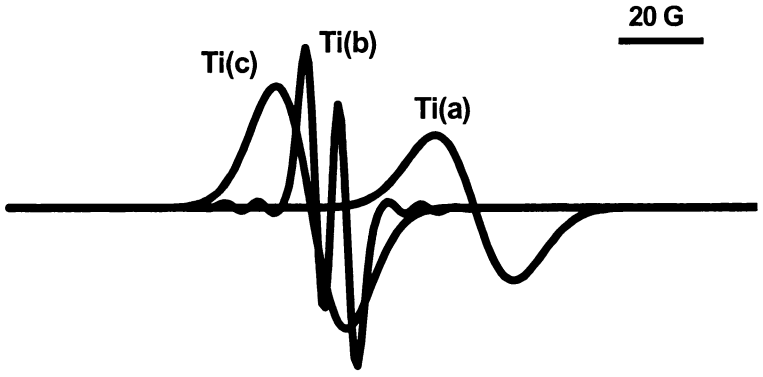

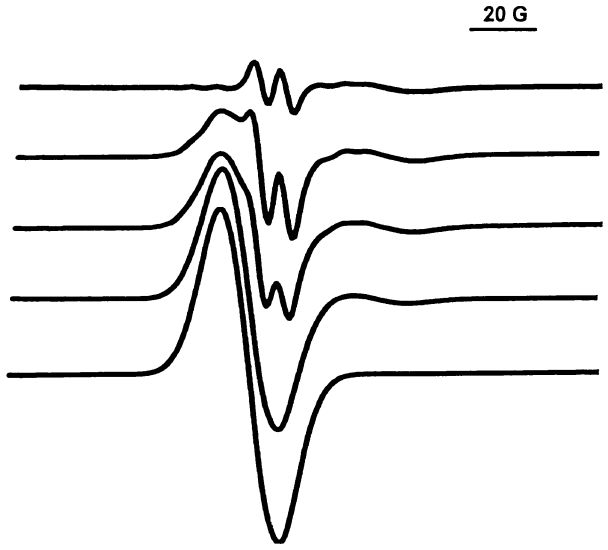

Figure A.1 (a) ESR spectra (from 3300 G to 3480 G) recorded at different times during the reduction of the CGCTiMe$_2$/MMAO system in toluene with $[Ti]_0 = 5 \times 10^{-4}$ M, Al/Ti = 100 (molar), and T = 100 °C. (b) The computer simulated **Ti(a)**, **Ti(b)**, **Ti(c)** signals. (c) Computer simulated spectra parallel to (a).

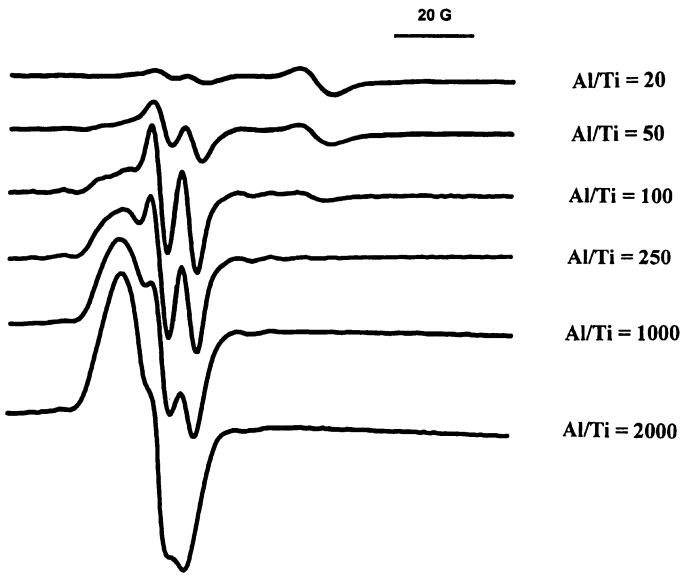

Figure A.2 ESR spectra (from 3340 G to 3460 G) recorded at T = 100 °C for the CGCTiMe$_2$/MMAO system in toluene with $[Ti]_0 = 5 \times 10^{-4}$ M and different Al/Ti molar ratios.

respectively. The singlet **Ti(c)** and doublet **Ti(b)** overlap with each other. There are some satellite lines in **Ti(b)** attributed to the α(Ti) = 8.2 G hyperfine interaction with ^{47}Ti (7.28 % abundance, I = 5/2) and ^{49}Ti (5.51 % abundance, I = 7/2). These lines, though weak due to signal overlap, are observable in Figure A.1. The integral intensity of the satellite lines constituted about 12.8 % of the total area, corresponding to the natural abundance of ^{47}Ti and ^{49}Ti. No resolvable hyperfine splitting was found with **Ti(a)** and **Ti(c)** signals.

The intensities of the three paramagnetic signals varied with the aging time. At the beginning of aging, only **Ti(a)** and **Ti(b)** were observed (see Figure A.1). The intensity of **Ti(b)** then increased and that of **Ti(a)** decreased gradually. In about 2 min, a new signal **Ti(c)** appeared. The **Ti(c)** signal gained its intensity quickly and gradually overlaid **Ti(b)** signal. In 30 min, **Ti(a)** signal disappeared and **Ti(b)** was overwhelmed by **Ti(c)**. Applying a further derivative to the shown spectra gave an evidence for the existence of **Ti(b)** through aging time. The intensities of the three Ti(III) signals also changed with the Al/Ti molar ratio. The signal **Ti(a)** was present in the initial period of reaction with the Al/Ti molar ratios lower than 250. At high Al/Ti molar ratios (> 250), only **Ti(b)** and **Ti(c)** were observable. The variation of the relative intensities of these signals with the Al/Ti molar ratio in Figure A.2 followed the same manner as with the aging time in Figure A.1(a). Similar changes in spectra with time and Al/Ti ratio were also observed in a half sandwich metallocene trichloride/MAO system by Chien et al.[15]

In the CGCTiMe$_2$/MMAO system, there could be four CGCTiMe$_2$/MMAO complexes as shown in Scheme A.2: weak complex of CGCTiMe$_2$ with MMAO (**2**), binuclear cationic ion pair (**3** and **4**) and monomeric cationic ion pair (**5**). The existence of these four species is dependent on the Al/Ti ratio. These species have been elucidated by detailed ^{13}C and ^{1}H NMR studies on

dialkyl metallocence/MAO systems.[24] Because binuclear cationic ion pairs **3** and **4** are quite stable, the reduction is mainly due to the elimination of non-bridged methyl group from complexes **2** and **5**. The NMR studies showed that weak complexes of metallocene/MAO were only present at low Al/Ti ratios.[24] Note that **Ti(a)** was also present only at low Al/Ti ratios. **Ti(a)** is therefore believed to be a reduction product from the weak complex of $CGCTiMe_2$ with MMAO (**2**). In the $CpTiCl_3$/MAO system by Chien et al.[15] a similar assignment was proposed for the trivalent Ti species formed at low Al/Ti ratio. The NMR studies on metallocene dialkyl/MAO systems also showed that the concentration of monomeric ion pair increased with the Al/Ti ratio and that it was the major complex at high Al/Ti ratios. In this work, **Ti(c)** was the dominant signal in the ESR spectra and its intensity increased with the time and Al/Ti ratio. This parallelism leads us to assign **Ti(c)** as a reduction product from the monomeric cationic ion (**5**). The structures of **Ti(a)** and **Ti(c)** are proposed in Scheme A.3. **Ti(b)** is a trivalent titanium hydride with g = 1.992, $\alpha(H)$ = 7.4 G, and $\alpha(Ti)$ = 8.2 G. The g and $\alpha(H)$ values of this species are very similar to the previously reported trivalent Ti hydrides in the $CpTiCl_3$/MAO (g = 1.989, $\alpha(H)$ = 7.4 G; g = 1.995, $\alpha(H)$ = 4.5 G),[15] $CpTi(OBu)_3$/MAO (g = 1.989, $\alpha(H)$ = 7.0 G),[19] $Cp^*TiMe_3/B(C_6F_5)_3$ (g = 1.994, $\alpha(H)$ = 8.4 G),[23d] and SiO_2 supported $CpTiCl_3$/MAO (g = 1.989, $\alpha(H) \cong 7.4$ G) system.[21a] . Its $\alpha(Ti)$ value is also very similar to the reported Ti(III) hydrides in $CpTiCl_3$/MAO ($\alpha(Ti)$ = 8 G)[15] and $CpTi(OBu)_3$/MAO ($\alpha(Ti) \cong 7$ G) systems.[19]. These similarities suggest the assignment of titanium hydride. This **Ti(b)** species, shown in Scheme A.3, is probably a further reaction product of **Ti(a).** Titanium hydrides with similar structures were also proposed in the $CpTiCl_3$/MAO and $CpZrCl_3$/MAO systems.[15]

The effects of the Al/Ti molar ratio on the reduction of $CGCTiMe_2$/MMAO/toluene system are shown in Figures A.3 and A.4. The

reduction occurred with a relatively high initial rate, but slowed down quickly with the Ti(III) concentration being leveled off after about 5 min of reaction. Increasing the Al/Ti molar ratio increased the reduction rate as well as the final Ti(III) concentration, particularly in the ratio range of 20-250 as shown in Figure A.4. This is probably due to the increasing concentrations of **5** with the increase of Al/Ti ratios. However, further increase of the Al/Ti ratio from 250 had little effect on the reduction behavior.

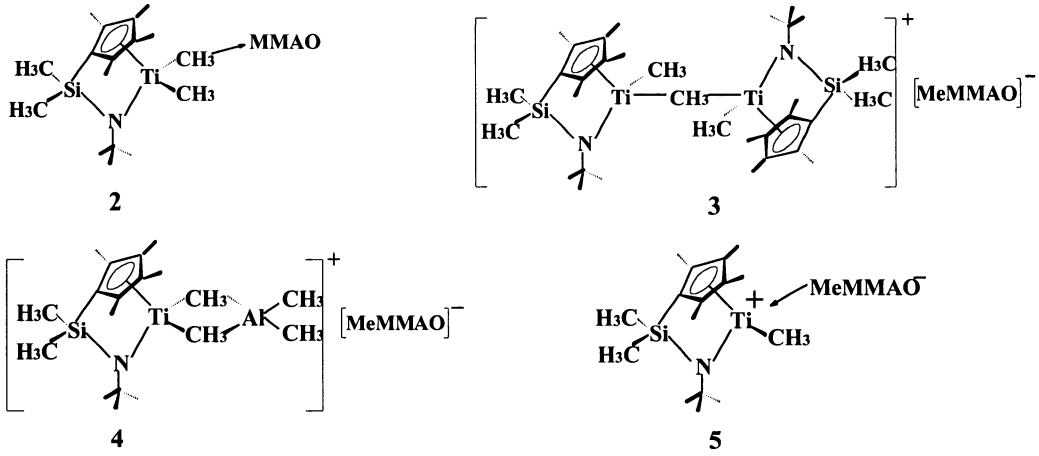

2 3 4 5

Scheme A.2 Proposed complexes in CGCTiMe$_2$/MMAO system.

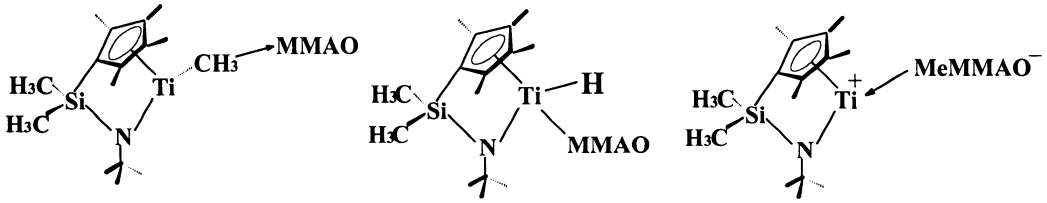

Ti(a) Ti(b) Ti(c)

Scheme A.3 Proposed reduction products in CGCTiMe$_2$/MMAO system.

MAO is an efficient cocatalyst for metallocene polymerization. It is prepared by a controlled hydrolysis of TMA with hydrated metal salts. Studies showed that free and associate TMA exist in the MAO solution. Polymerization studies were also conducted to examine the roles of TMA in catalysis.[25] In this work, the effect of TMA on the $CGCTiMe_2$/MMAO reduction was conducted. A series of catalyst toluene solutions with $[Ti]_0 = 5 \times 10^{-4}$ M, Al(MMAO)/Ti = 500 (molar) and different [TMA]/[MMAO] ratios were prepared and investigated at 100 °C. The ESR spectra showed the same three signals as in the $CGCTiMe_2$/MMAO/toluene system. The changes of Ti(III) concentration with time are presented in Figure A.5. Increasing the [TMA]/[MMAO] ratio decreased the Ti(III) concentration. This can be attributed to the coordination of TMA with the monomeric cationic ion pair (**5**) to form the methyl bridged binuclear complexes $[CGCTi(\mu\text{-}Me)_2AlMe_2]^+[MeMMAO]^-$ (**4**), which is stable towards reduction and inactive for polymerization. The higher the [TMA]/[MMAO] ratio, the more **5** species were converted into **4**, and the lower the Ti(III) concentration. This result may have implication of lower activities with TMA addition in metallocene/MMAO systems.

The solvent effect on the $CGCTiMe_2$/MMAO reduction was also investigated, toluene and heptane were used. Figure A.6 shows the ESR spectra for the $CGCTiMe_2$/MMAO/heptane system. Different from the $CGCTiMe_2$/MMAO/ toluene system, the spectrum shows a three-line overlapping signal. But similar to the $CGCTiMe_2$/MMAO/toluene system, the spectrum changed with the aging time and Al/Ti molar ratio. Figure A.7 shows the change of Ti(III) concentration with time in both heptane and toluene solutions. About 60 % of the original Ti(IV) was reduced to Ti(III) in toluene in 10 min. However, in heptane only 10 % original Ti(IV) was reduced to Ti(III).

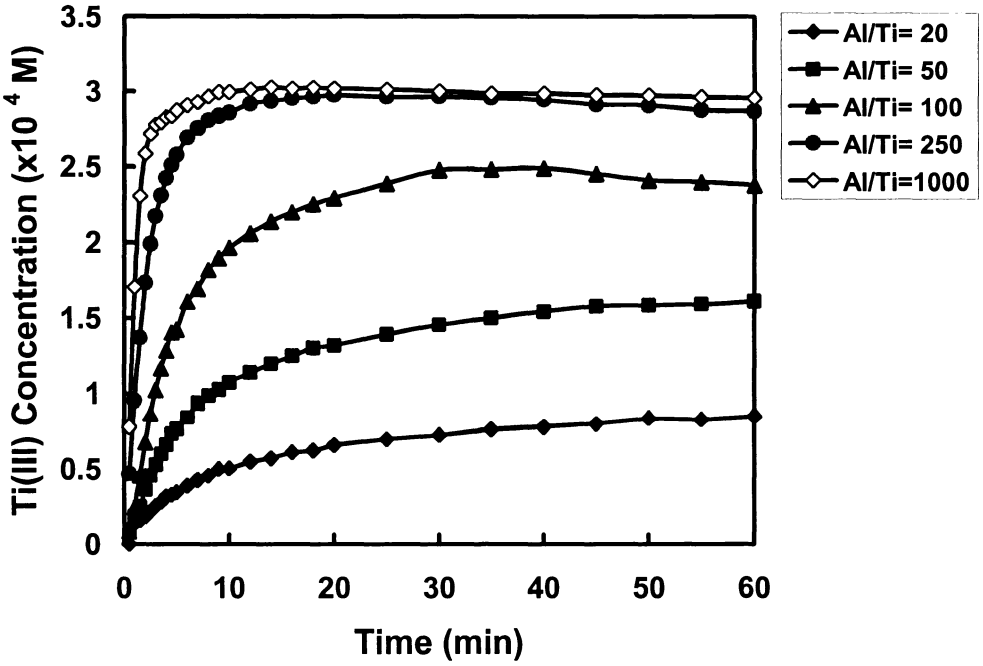

Figure A.3 Ti(III) concentration versus time for the $CGCTiMe_2$/MMAO system with different Al/Ti molar ratios at $[Ti]_0 = 5 \times 10^{-4}$ M and T = 100 °C in toluene.

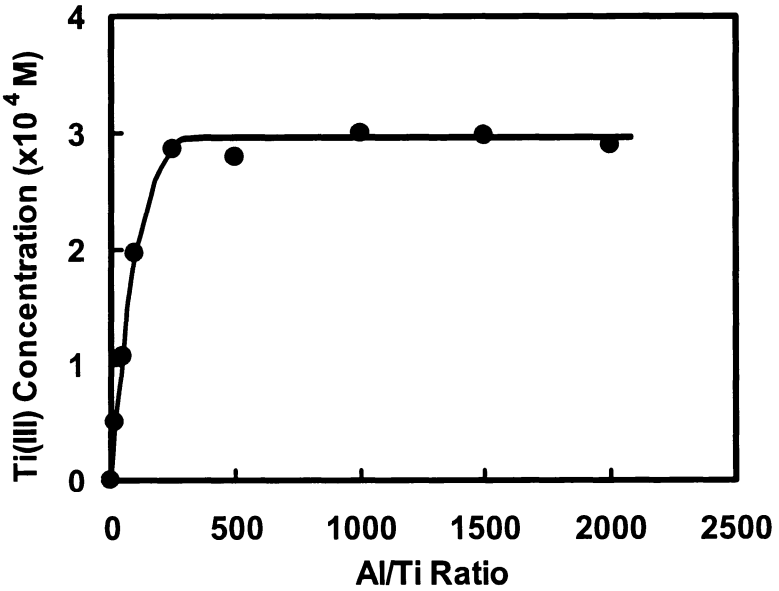

Figure A.4 Ti(III) concentration versus Al/Ti molar ratio for the $CGCTiMe_2$/MMAO system with $[Ti]_0 = 5 \times 10^{-4}$ M , t = 10 min and T = 100 °C in toluene.

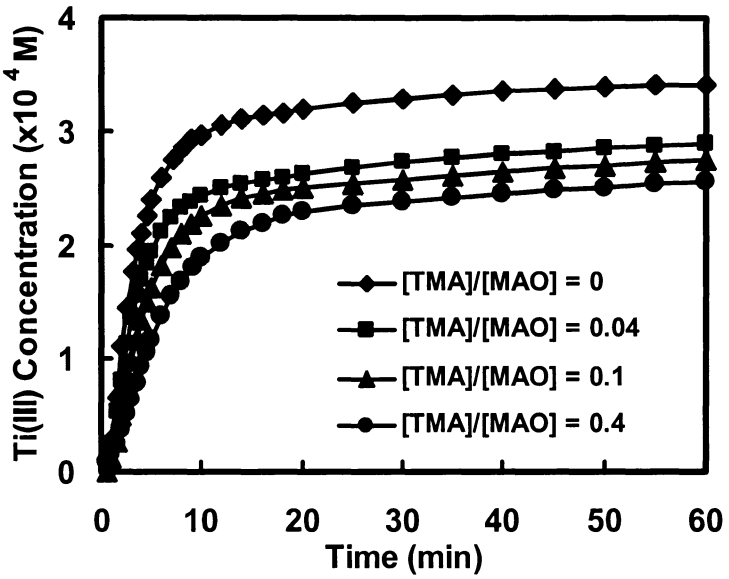

Figure A.5 Ti(III) concentration versus time for the $CGCTiMe_2$/MMAO/TMA system in toluene with different [TMA]/[MMAO] (molar Al) ratios at $[Ti]_0 = 5 \times 10^{-4}$ M, Al(MMAO)/Ti = 500 (molar) and T = 100 °C.

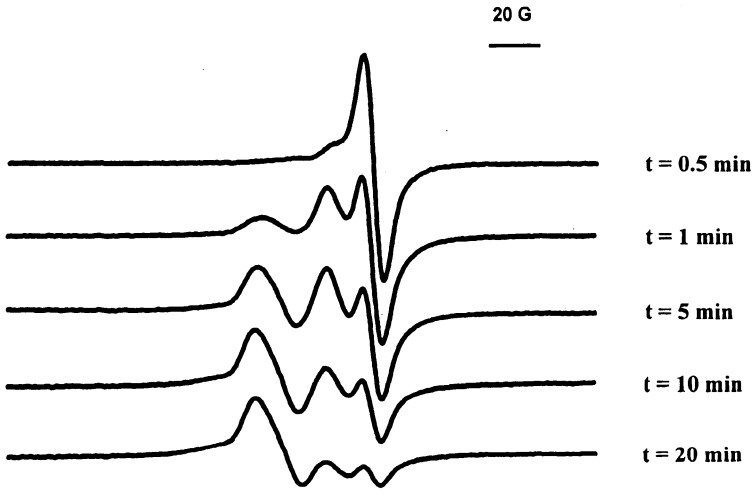

Figure A.6 ESR spectra (from 3270 G to 3500 G) recorded after different aging times for the $CGCTiMe_2$/MMAO system in heptane with $[Ti]_0 = 5 \times 10^{-4}$ M, Al/Ti = 300 (molar) and T = 100 °C.

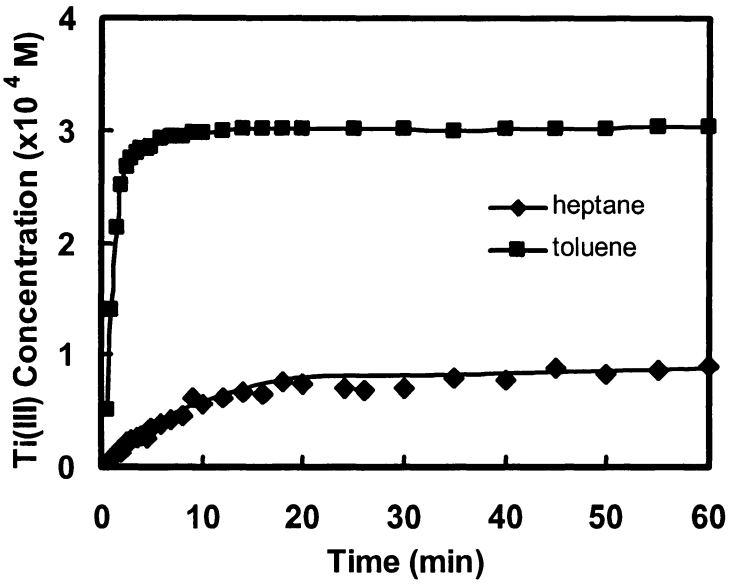

Figure A.7 Ti(III) concentration versus time for the $CGCTiMe_2$/MMAO system in different types of solvent with $[Ti]_0 = 5 \times 10^{-4}$ M, Al/Ti = 1500 (molar) and T = 80 °C.

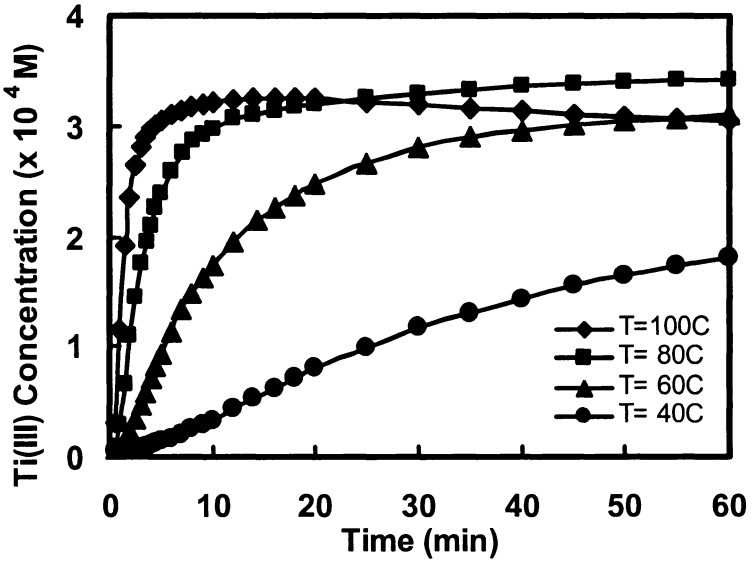

Figure A.8 Ti(III) concentration versus time for the $CGCTiMe_2$/MMAO system at different temperatures with $[Ti]_0 = 5 \times 10^{-4}$ M and Al/Ti =500 (molar) in toluene.

One possible explanation of this phenomenon is the solvent coordination effect on the reduction of Ti(IV) complexes. Solvent coordination with cationic metallocene species is an important interaction for such complexes as $[Cp^*ZrMe_2]^+[MeB(C_6F_5)]_3^-$. The complex acts as a toluene adduct both in solution and in solid state.[26] The coordination effect of arene with the constrained geometry Zr cation $[CGCZrMe]^+$ was observed from both analytical and spectroscopic evidences.[27] Toluene is a coordinating solvent and heptane is a non-coordinating solvent. In our system, when toluene coordinates with the Ti(IV) complexes, it destabilizes the titanium-methyl bond in complexes **2** and **5,** leading to an easier breakup of the titanium-methyl bond and thus generate more Ti(III) species. Moreover, solvent coordination will also change the unpaired spin density around the Ti(III) nucleus and cause the change of ESR signal.

Figure A.8 shows the effect of temperature on the $CGCTiMe_2$/MMAO/toluene reduction with an original $CGCTiMe_2$ concentration of 5×10^{-4} M and [Al]/[Ti] molar ratio of 500. High temperature accelerated the reduction.

A.4.2 $B(C_6F_5)_3$ as Cocatalysts

Different from MAO type of cocatalysts, perfluoroaryl boranes and borates react with metallocene compounds and yield an isolable and characterizable catalyst system.[1h] Many studies on this isolated complex have been carried out to elucidate this highly efficient catalytic system, especially for ethylene and α-olefin copolymerizations.[28]

The reaction of $CGCTiMe_2$ with $B(C_6F_5)_3$ generates the monomeric cationic species $[CGCTiMe]^+[MeB(C_6F_5)]_3^-$ (**6** in Scheme A.4). Studies also

showed that with 2:1 ratio of $CGCTiMe_2/B(C_6F_5)_3$ in toluene, the dinuclear species $[CGCTiMe(\mu\text{-}Me)MeTiCGC]^+$ $[MeB(C_6F_5)_3]^-$ (**7** in Scheme A.4), in equilibrium with the monomeric species, was also generated.[28]

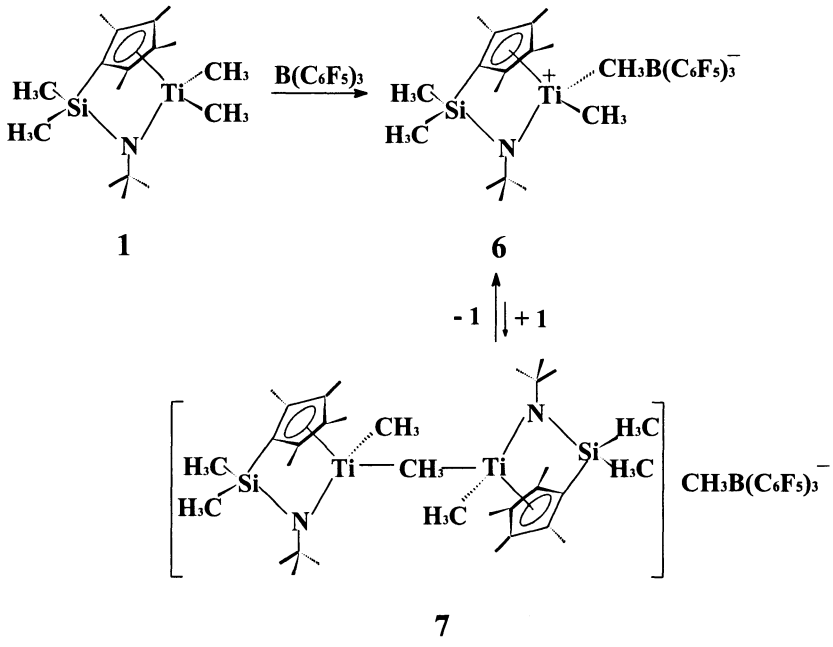

Scheme A.4 Formation of complexes in $CGCTiMe_2/B(C_6F_5)_3$ system.

The ESR spectrum for equal-molar $CGCTiMe_2$ and $B(C_6F_5)_3$ with $[Ti]_o = 2 \times 10^{-2}$ M in toluene after 20 min at 100 °C exhibited a singlet **Ti(d)** centered at g = 1.988, as shown in Figure A.9. There were also some additional resonances at the shoulders of the singlet. These additional signals, also observed in the 2×10^{-2} M $CGCTiMe_2$/toluene without $B(C_6F_5)_3$, were probably due to Ti(III) alkoxides and/or other products arising from oxygen traces and impurities in the ESR tube at this high initial titanium concentration. The singlet is attributed to the

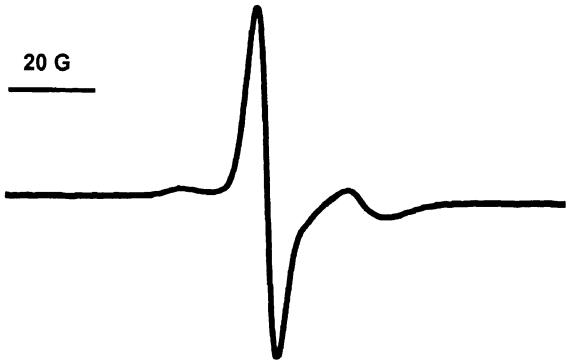

Figure A.9 ESR spectrum for the $CGCTiMe_2/B(C_6F_5)_3$ system in toluene recorded at $[Ti]_0 = 2 \times 10^{-2}$ M, B/Ti = 1.0 (molar), t = 20 min, and T = 100 °C.

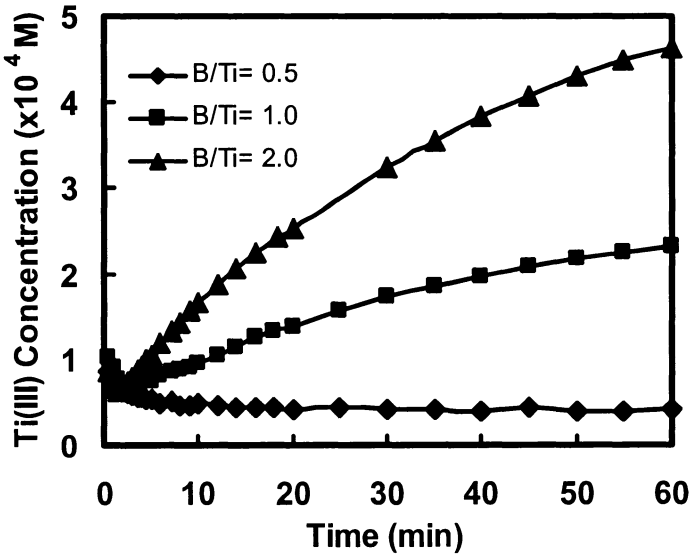

Figure A.10 Ti(III) concentration versus time for the $CGCTiMe_2/B(C_6F_5)_3$ system in toluene with different B/Ti molar ratios at $[Ti]_0 = 2 \times 10^{-2}$ M and T = 100 °C.

Ti(III)species produced by the reductive methyl group elimination from the monomeric cationic species **6**. Its structure is proposed in Scheme A.5. The intensity of this signal increased with the reduction time (Figure A.10).

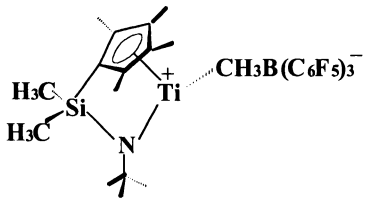

Ti(d)

Scheme A.5 Proposed structure of reduction product **Ti(d)**.

For comparisons, a parallel ESR experiment under the same conditions but at 2:1 CGCTiMe$_2$ and B(C_6F_5)$_3$ molar ratio showed no Ti(III) species produced even after an hour of reaction, except for the shoulder signals from impurities. It is known that at this B/Ti ratio, there existed a large amount of species **7**. This result indicated that the dinuclear species are quite stable towards reduction.

Figure A.10 shows the Ti(III) concentration as a function of reduction time for the CGCTiMe$_2$/B(C_6F_5)$_3$/toluene system at 100 °C with different B/Ti molar ratios. It can be seen that after an hour reaction only about 1 % of Ti(IV) was reduced to Ti(III) at B/Ti = 1, compared to the 60 % for the CGCTiMe$_2$/MMAO at Al/Ti = 500 and the same temperature. Also the reduction rates were much slower than the CGCTiMe$_2$/MMAO/toluene system. These results indicated that the monomeric cationic center **6** is much more stable than **5**. Increasing the B/Ti molar ratio increased the Ti(III) concentration, due to the higher concentrations of **6** at the higher B/Ti ratios.

To investigate the temperature effect on the reduction, a series of samples with $[Ti]_0 = 2 \times 10^{-2}$ M and B/Ti = 1 (molar) at temperatures 40 °C, 60 °C, 80 °C, and 100 °C were analyzed. Unlike the $CGCTiMe_2$/MMAO system, no detectable signal was observed when the reaction temperature was lower than 80 °C.

The solvent coordination also affected the reduction of the $CGCTiMe_2/B(C_6F_5)_3$ system. Two samples with $[Ti]_0 = 2 \times 10^{-2}$ M and B/Ti ratio =1.0 (molar), but in different solvents (toluene and heptane) were prepared and investigated at 80 °C. For the sample with heptane, no paramagnetic signal, except for those from impurities, was observed even after one hour of reaction. However, for the sample in toluene, the **Ti(d)** signal was detected after 5 min and its intensity increased with the aging time.

A.4.3 $B(C_6F_5)_3$/MMAO as Combined Cocatalyst System

The $CGCTiMe_2/B(C_6F_5)_3$ system is very active for olefin polymerization. However, its high sensitivity towards trace impurities usually requires an addition of aluminum alkyls or MAO in polymerization. In this work, the reduction of $CGCTiMe_2$ with the combined cocatalyst system $B(C_6F_5)_3$/MMAO was also studied.

The ESR spectra of the Ti(III) species in this mixed cocatalyst system were the same as in the $CGCTiMe_2$/MMAO/toluene system. Figure A.11 shows the effect of B/Ti molar ratio on the reduction with $[Ti]_0 = 5 \times 10^{-4}$ M and Al/Ti = 20 (molar). Compared to the $CGCTiMe_2$/MMAO system (B/Ti = 0 in Figure 11), the Ti(III) concentrations were lower. Increasing the B/Ti molar ratio led to a lower Ti(III) concentration. This is due to the formation of the monomeric cationic ion

pair $[CGCTiMe]^+[MeB(C_6F_5)_3]^-$(**6**), which is more stable than **2** and **5** towards reduction.

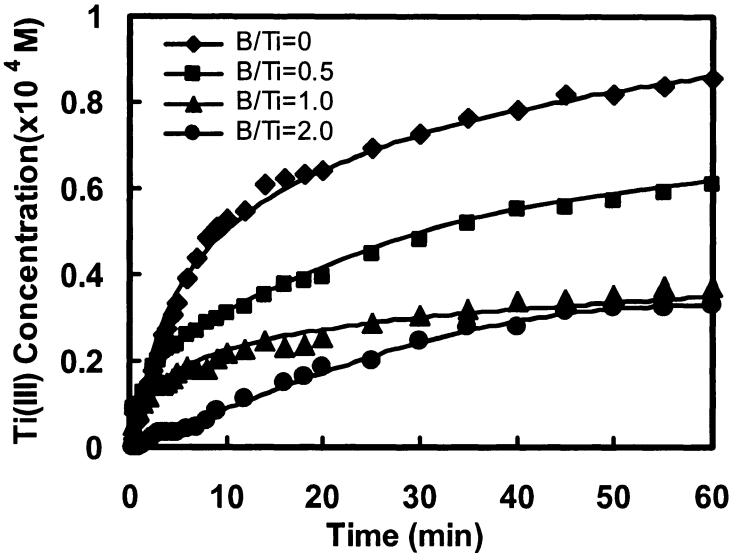

Figure A.11 Ti(III) concentration versus time for the $CGCTiMe_2/B(C_6F_5)_3$/MMAO system in toluene with different B/Ti molar ratios at $[Ti]_0 = 5 \times 10^{-4}$ M, Al/Ti = 20 (molar), and T = 100 °C.

A final point worth mentioning is that the activity of metallocene-type catalysts in olefin polymerization is well known to increase with the cocatalyst/catalyst ratio followed by leveling off. However, in this investigation, it is shown that the concentration of the inactive Ti(III) species also increases with the Al/Ti or B/Ti ratio. This apparent contradiction is caused by a confusion of the activation/deactivation process. MAO or $B(C_6F_5)_3$ as a cocatalyst is required to activate the catalyst $CGCTiMe_2$, i.e., to generate the active species **5** or **6**. Higher Al/Ti or B/Ti ratio yields higher active site concentration and thus higher

polymerization rate. On the other side, higher active site concentration also induces higher reduction (deactivation) rate, giving higher Ti(III) concentration.

A.5 Conclusion

In this work, the reduction of $CGCTiMe_2$ activated with three different cocatalyst systems (MMAO, $B(C_6F_5)_3$, and combined $B(C_6F_5)_3$/MMAO) was investigated using an on-line ESR technique. In the $CGCMe_2$/MMAO system, three trivalent titanium species were generated from the reductive elimination of methyl group in the $CGCTiMe_2$/MMAO weak complex (**2**) and in the monomeric cationic pair (**5**). The solvent coordination of toluene made Ti(IV) complex more facile to reduction. The Ti(III) concentration increased with the Al/Ti molar ratio from 20 - 250 and leveled off after Al/Ti = 250. The reduction rate increased with temperature and Al/Ti molar ratio. Adding TMA to the system lowered the Ti(III) concentration due to the production of stable heterogeneous dinuclear species $[CGCTi(\mu\text{-}Me)_2AlMe_2]^+[MeMAO]^-$ (**4**).

In the $CGCMe_2/B(C_6F_5)_3$ system, only one Ti(III) species was observed. It was the reductive product of $[CGCTiMe]^+[MeB(C_6F_5)_3]^-$ (**6**). The Ti(III) concentration increased with the B/Ti molar ratio because higher B/Ti molar ratio generated higher **6** content. The results indicated that the binuclear cationic ion pair $[CGCTiMe(\mu\text{-}Me)MeTiCGC]^+[MeB(C_6F_5)_3]^-$ (**7**) was stable to reduction. The $CGCTiMe_2/B(C_6F_5)_3$ system was much more stable to reduction compared to the $CGCTiMe_2$/MMAO system due to the higher stability of $[CGCTiMe]^+[MeB(C_6F_5)_3]^-$ (**6**).

A.6 Reference

1. (a) Kaminsky, W.; Arndt, M. *Adv. Polym. Sci.* **1997**, *127*, 144. (b) Bochmann, M. *J. Chem. Soc., Dalton Trans.* **1996**, 255. (c) Brintzinger, H.-H.; Fischer, D.; Mulhaupt, R.; Rieger, B.; Waymouth, R. M. *Angew. Chem., Int. Ed. Engl.* **1995**, *34*, 1143. (d) Marks, T. J. *Acc. Chem. Res.* **1992**, *25*, 57. (g) Jordan, R. F. *Adv. Organomet. Chem.* **1991**, *32*, 325. (h) Chen, E. Y.-X.; Marks, T. J. *Chem. Rev.* **2000**, *100*, 1391.
2. Stevens, J. C.; Timmers, F. J.; Wilson, D. R.; Schmidt, G. F.; Nickias, P. N.; Rosen, R. K.; Knight, G. W.; Lai, S. Eur. Pat. No. 416815, August 13, 1997.
3. Canich, J. A. M. Eur. Pat. No. 788521, December 23, 1998.
4. Devore, D. D.; Timmers, F. J., Hasha, D. L.; Rosen, R. K.; Marks, T. J.; Deck, P. A.; Stern, C. L. *Organometallics* **1995**, *14*, 3132.
5. Shapiro, P. J.; Cotter, W. D.; Schaefer, W. P.; Labinger, J. A.; Bercaw, J. E. *J. Am. Chem. Soc.* **1994**, *116*, 4623.
6. Shapiro, P. J.; Bunel, E.; Schaefer, W. P.; Bercaw, J. E. *Organometallics* **1990**, *9*, 867.
7. Lai, S.; Wilson, J. R.; Knight, G. W.; Stevens, J. C. U. S. Patent No. 5278272, January 11, 1994.
8. Nickias, P. N.; Devore, D. D.; Timmers, F. J.; Rosen, R. K.; Mussell, R. D. U. S. Patent No. 5347024, September 13, 1994.
9. Lindsay, K. F. *Mod. Plast.* **1993** (Oct.), 82.
10. Chum, P. S.; Kao, C. L.; Knight, G. W. *Plast. Eng.* **1995** (June), 21.
11. Wang, W.-J.; Yan, D.; Charpentier, P. A.; Zhu, S.; Hamielec, A. E.; Sayer, B. G. *Macromol. Chem. Phys.* **1998**, *199*, 2409.
12. Yan, D.; Wang, W.-J.; Zhu, S. *Polymer* **1999**, *40*, 1737
13. McKnight, A. L.; Masood, M. A.; Waymouth, R. M.; Straus, D. A. *Organometallics* **1997**, *16*, 2879.

14. Olivé, G. H.; Olivé, S. *Angew. Chem., Int. Ed. Engl.* **1967**, *6*, 790.

15. Bueschges, U.; Chien, J. C. W. *J. Polym. Sci., Polym. Chem. Ed.* **1989**, *27*, 1525.

16. Cam, D.; Sartori, F.; Maldotti, A. *Macromol. Chem. Phys.* **1994**, *195*, 2817.

17. Huang, Y. H.; Yu, Q.; Zhu, S.; Rempel, G. L.; Li, L. *J. Polym. Sci., Polym. Chem. Ed* **1999**, *37*, 1465.

18. (a) Grassi, A.; Pellecchia, C.; Oliva, L. *Macromol. Chem. Phys.* **1995**, *196*, 1093. (b) Grassi, A.; Zambelli, A.; Laschi, F. *Organometallics* **1996**, *15*, 480. (c) Grassi, A.; Lamberti, C.; Zambelli, A.; Mingozzi, I. *Macromolecules* **1997**, *30*, 1884. (d) Grassi, A.; Saccheo, S.; Zambelli, A. *Macromolecules* **1998**, *31*, 5588.

19. Chien, J. C. W.; Salajka, Z.; Dong, S. *Macromolecules* **1992**, *25*, 3199.

20. Yim, J. – H.; Chu, K. – J.; Choi, K. – W.; Ihm, S. – K. *Eur. Polym. J.* **1996**, *32*, 1381.

21. (a) Xu, J.; Zhao, J.; Fan, Z.; Feng, L. *Macromol. Rapid Commun.* **1997**, *18*, 875. (b) Xu, J.; Zhao, J.; Fan, Z.; Feng, L. *Eur. Polym. J.* **1999**, *35*, 127.

22. Huang, Y. H.; Wang, W. - J.; Zhu, S.; Rempel, G. L. *J. Polym. Sci., Polym. Chem. Ed.* **1999**, *37*, 3385.

23. (a) Kucht, H.; Kucht, A.; Chien, J. C. W.; Rausch, M. D. *Appl. Organomet. Chem.* **1994**, *8*, 393. (b) Ewart, S. W.; Sarsfield, M. J.; Jeremic, D.; Tremblay, T. L.; Williams, E. F.; Baird, M. C. *Organometallics* **1998**, *17*, 1502. (c) Ewart, S. W.; Sarsfield, M. J.; Williams, E. F.; Baird, M. C. *J. Organomet. Chem.* **1999**, *579*, 106. (d) Williams, E. F.; Murray, M. C.; Baird, M. C. *Macromolecules* **2000**, *33*, 261.

24. (a) Tritto, I.; Li, S.; Sacchi, M. C.; Zannoni, G. *Macromolecules* **1993**, *26*, 7111. (b) Tritto, I.; Donetti, R.; Sacchi, M. C.; Locatelli, P.; Zannoni, G. *Macromolecules* **1997**, *30*, 1247. (c) Babushkin, D. E.; Semikolenova, N. V.; Zakharov, V. A.; Talsi, E. P. *Macromol. Chem. Phys.* **2000**, *201*, 558.

25. (a) Reddy, S. S.; Shashidhar, G.; Sivaram, S. *Macromolecules* **1993**, *26*, 1180. (b) Giannetti, E.; Nicoletti, G.; Mazzocchi, R. *J. Polym. Sci., Polym. Chem. Ed.* **1985**, *23*, 2117. (c) Chien, J. C. W.; Wang, B.-P. *J. Polym. Sci., Polym. Chem. Ed.* **1988**, *26*, 3089. (d) Cam, D.; Giannini, U. *Makromol. Chem.* **1992**, *193*, 1049.

26. (a) Gillis, D. J.; Tudoret, M.-J.; Baird, M. C. *J. Am. Chem. Soc.* **1993**, *115*, 2543. (b) Lancaster, S. J.; Robinson, O. B.; Bochman, M.; Coles, S. J.; Hursthouse, M. B. *Organometallics* **1995**, *14*, 2456.

27. Jia, L.; Yang, X.; Stern, C. L.; Marks, T. J. *Organometallics* **1997**, *16*, 842.

28. Chen, Y.-X.; Marks, J. *Organometallics* **1997**, *16*, 3649.